TUM School of Natural Sciences
Technical University of Munich

TUM

Innovative Synthesis of Carbon Fiber Precursors and Epoxy Thermosets: Advances Towards Sustainable Fiber Composite Materials

Jonas Martin Breitsameter

Vollständiger Abdruck der von der TUM School of Natural Sciences der Technischen Universität München zur Erlangung eines

Doktors der Naturwissenschaften (Dr. rer. nat.)

genehmigten Dissertation.

Vorsitz: Prof. Dr.-Ing. Kai-Olaf M. Hinrichsen

Prüfer der Dissertation:

1. Prof. Dr. Dr. h. c. Bernhard Rieger
2. Prof. Dr. Thomas Brück

Die Dissertation wurde am 10.07.2023 bei der Technischen Universität München eingereicht und durch die TUM School of Natural Sciences am 06.11.2023 angenommen.

"Chemistry is necessarily an experimental science: its conclusions are drawn from data, and its principles supported by evidence from facts."

Michael Faraday

Acknowledgments

Table of contents

List of abbreviations

Abbreviations for formula signs

$\bar{X}_n$	Degree of polymerization	[–]
$\dot{\gamma}$	Shear rate	s^{-1}
η	Dynamic viscosity	mPa s
ν	Kinematic viscosity	cSt
ρ	Density	$kg\,m^{-3}$
D_{50}	Median particle size distribution of 50 %	µm
dn/dc	Refractive index increment	$mL\,g^{-1}$
M_n	Molecular weight	$g\,mol^{-1}$
p	Conversion	%
T_g	Glass transition temperature	°C
T_m	Melting point	°C
$T_{5\%}$	Temperature of 5 % weight-loss	%
$Đ$	Polydispersity index	[-]
IE	Initiator efficiency	%
St	Stokes	$10^{-4}m^2/s$

General abbreviations

(Z)-DATP	(Z)-1-(dimethylamino)-1-trimethylsiloxy-1-propene
12-HSA	12-Hydroxystearic acid

9/10-HSA	9/10-Hydroxystearic acid
*m*CPBA	*meta*-Chloroperoxybenzoic acid
sym-col	*sym*-Collidine
AHIBC	Allyl-7-methyl-1,3-dioxo-1,3,3a,4,7,7a-hexahydroisobenzo-furan-4-carboxylate
AIBN	Azobisisobutyronitrile
Bn	Benzyl-group
Boc	*tert*-Butoxycarbonyl protecting group
BPA	Bisphenol A
CF	Carbon fiber
CLA	Conjugated linoleic acid
Cp	Cyclopentadienyl
Cp*	1,2,3,4,5-Pentamethylcyclopentadienyl
DECP	Diethyl chlorophosphate
DMAc	*N,N'*-Dimethylacetamide
DMDO	Dimethyldioxirane
DMF	*N,N*-Dimethyl formamide
DMMA	Dimethyl metharcrylamide
DMSO	Dimethyl sulfoxide
ECH	Epichlorohydrin
EVO	Epoxidized vegetable oil
GTP	Group-transfer polymerization

HM	High modulus
HT	High tensile strength
IM	Intermediate modulus
LM	Low modulus
MCBz	Methacryloyl carbazole
NBS	*N*-Bromosuccinimide
PAM	Polymer-analogous modification
PO	Propylene oxide
REM	Rare earth metal
REM	Raster electron microscopy
S_N2	Second-order nucleophilic substitution
SKA	Silyl ketene acetal
TACHC	Triallyl-6-methylcyclohex-4-ene-1,2,3-tricarboxylate
TAG	Triacylglyceride
Tf	Trifluoromethanesulfonate
TFA	Trifluoroacetic anhydride
TfOH	Trifluoromethanesulfonic acid
TMS	Trimethylsilyl
UHM	Ultra high modulus

Abbreviations for methods

ATR-FTIR	Attenuated total reflection fourier transformed infrared
DFT	Density functional theory

DMA   Dynamic mechanical analysis

DSC   Differential scanning calorimetry

ESI HRMS   Electron-spray high resolution ionization mass spec-
                                trometry

GC-MS   Gas chromatographic-mass spectrocscopy

GPC   Size exclusion gel permeation chromatography

NMR   Nuclear magnetic resonance

TGA   Thermogravimetric analysis

Abbreviations for monomers, polymers, epoxy resins, and hardeners

*t*BuA   *tert*-Butyl acrylate

ACN   Acrylonitrile

Bn$_2$AA   *N,N'*-Dibenzyl acrylamide

Boc$_2$AA   *N,N'*-Di(*tert*-Butoxycarbonyl)-acrylamide

CAE   Cycloaliphatic epoxy resin

DDS   Diaminodiphenyl sulfone

DESA   9,10-12,13-Diepoxystearic acid

DESMe   9,10-12,13-Diepoxy methylstearate

DETA   Diethylene triamine

DGEBA   Diglycidyl ether of bisphenol A

DGEBF   Diglycidyl ether of bisphenol F

DMAA   *N,N'*-Dimethylacrylamide

EGCHC   1,2-Epoxy-6-methyl-triglycidyl-3,4,5-cyclohexanetricarboxylate

ELO	Epoxidized linseed oil
IPD	Isophorone diamine
MA	Methyl acrylate
Me-12-HSA	Methyl-12-hydroxystearate
Me-9/10-HSA	Methyl-9/10-hydroxystearate
MMA	Methyl methacrylate
MTHPA	Methyltetrahydrophtalic anhydride
PA	Phtalic anhydride
PAA	Polyacrylamide
PAN	Polyacrylonitrile
PBn$_2$AA	Poly(*N,N'*-dibenzyl acrylamide)
PBoc$_2$AA	Poly(*N,N'*-diboc acrylamide)
PMA	Polymethyl acrylate
PVA	Polyvinyl aclohol
TA	Tannic acid
TGDDM	*N,N,N',N'*-Tetragylcidyl-4,4'-diaminodiphenylmethane
TMSAA	*N*,O-Bis(trimethylsilyl)-acrylamide

List of publications

1. Reinhardt, N.*, <u>Breitsameter, J. M.*</u>, Drechsler, K. and Rieger, B., Fully Bio-Based Epoxy Thermoset Based on Epoxidized Linseed Oil and Tannic Acid, *Macromolecular Materials and Engineering*, **2022**, 307, 12, 2200455. *These authors contributed equally.*

2. <u>Breitsameter, J. M.*</u>, Reinhardt, N.*, Feigel, M., Hinrichsen, O., Drechsler, K. and Rieger, B., Synthesis of a sustainable and bisphenol A-free epoxy resin based on sorbic acid and characterization of the cured thermoset, *Macromolecular Materials and Engineering*, **2023**, 308, 9, 2300068. *These authors contributed equally.*

Publications beyond the scope of this thesis:

Kränzlein, M.*, Pongratz, S.*, Bruckmoser, J., Bratić, B., <u>Breitsameter, J. M.</u> and Rieger, B., Polyester synthesis based on 3-carene as renewable feedstock, *Polymer Chemistry*, **2022**, 13, 3729–3732. *These authors contributed equally.*

Feigel, M.*, <u>Breitsameter, J. M.*</u>, Rieger, B. and Hinrichsen, O., Kinetic Modeling of the Synthesis Path for the Production of a Sustainable Epoxy Resin, *Industrial & Engineering Chemistry Research*, **2023**, 62, 34, 13389–13400. *These authors contributed equally.*

Feigel, M., <u>Breitsameter, J. M.</u>, Rieger, B. and Hinrichsen, O., Bridging the Gap from Laboratory to Production: Kinetic Modelling-Guided Process Development for a Novel Epoxy Resin, *Industrial & Engineering Chemistry Research*, **2023**, under review.

Conference contributions:

Breitsameter, J. M. and Rieger, B., Combining group-transfer polymerization with polymer-analogous reactions – introducing precision polymerization to poly(acrylonitrile), The International Chemical Congress of Pacific Basin Societies, **2021**, Hawaii, Honolulu, USA, poster presentation.

Breitsameter, J. M., Reinhardt, N., Drechsler, K., and Rieger, B., Tannic acid and epoxidized linseed oil as promising components for high-performance, bio-based epoxy thermoset, Bordeaux Polymer Conference, **2022**, Bordeaux, France, poster presentation.

Abstract

The present work investigates approaches to developing innovative starting materials for the components of high-performance carbon fiber composites concerning their environmental impact.

Concerning carbon fibers, polymer analog approaches to the synthesis of the commonly used precursor polyacrylonitrile are investigated. The concept of polymer analog conversions provides access to polymers or polymer properties that are not directly accessible from the monomer. In the case of polyacrylonitrile, for example, catalytically controlled polymerization or the use of greener starting materials can be addressed this way. A promising polymer-analogous synthesis pathway could be found starting with the catalytic polymerization of methyl acrylate and proceeding *via* intermediate polyacrylamide. In addition to scaling up this reaction sequence to a multigram scale, the monomers *N*,*N'*-dibenzylacrylamide, *N*,*N'*-di(*tert*-butoxycarbonyl)acrylamide and *N*,*O*-bis(trimethylsilyl)acrylamide are also identified as potential candidates for polymerization and conversion towards polyacrylonitrile. The studies focus on the controlled polymerization of these molecules with the help of rare-earth-based organometallic catalyst systems as well as the polymer analogous cleavage of the protecting groups known from the synthesis of smaller organic molecules. In addition, the polymer-analogously produced polyacrylonitrile will be investigated in collaboration with the Fraunhofer Institute for Applied Polymer Research concerning process capability in converting carbon fibers.

For the thermoset matrix surrounding the fiber in composite materials, the use of unsaturated triglycerides as epoxy resins is investigated. The epoxidized vegetable oils are cured in combination with tannic acid as a curing agent resulting in a fully bio-based thermoset with excellent mechanical properties such as a flexural modulus of 2986 MPa and a high glass transition temperature of 147 °C. Processability and homogeneous curing are ensured by fine grinding of the tannic acid. The molecular

properties of the curing agent, such as high aromaticity and associated interactions, allow the system to be used as a bio-based alternative to petrochemical epoxy resins in high-performance applications.

Furthermore, the synthesis of a novel molecule 1,2-epoxy-6-methyl-triglycidyl-3,4,5-cyclohexanetricarboxylate (EGCHC), highly functionalized with epoxide groups, is presented. The molecule is prepared in a four-step reaction sequence starting from the esterification of sorbic acid with allyl alcohol, with these starting materials being potentially bioavailable or derived from biogenic resources. The synthesis proceeds *via* a Dials-Alder reaction followed by further allylation and epoxidation of the introduced double bonds. The first three reaction steps are characterized by high atomic efficiency and low solvent consumption. The resin that was reacted with standard amine-based curing agents shows high tensile moduli and strengths, which can compete with conventional bisphenol-A-based systems.

Lastly, a study is being conducted on the synthesis of fatty acid-based lubricants, so-called estolides. For this purpose, the monomer methyl 10-hydroxystearate is first synthesized and purified from oleic acid and then reacted in a catalytic polycondensation reaction. The focus is on the relationship between conversion, viscosity, and reaction time to achieve a defined target viscosity. The estolide samples are purified and analyzed for their thermal properties.

Overall, besides the biogenic fatty acid-based estolides, promising approaches towards bio-based and more sustainable carbon fiber composites are demonstrated, which convince by hitherto unachieved high (thermo)mechanical properties.

Zusammenfassung

Die vorliegende Arbeit untersucht Möglichkeiten, innovative und hinsichtlich der Umweltbilanz sinnvolle Ausgangsmaterialen der Komponenten für performante Kohlefaserverbundmaterialien zu erschließen.

Die Kohlefasern betreffend werden polymeranaloge Ansätze zur Synthese der gängigen Vorgängerverbindung Polyacrylnitril untersucht. Das Konzept der polymeranalogen Umwandlung bietet Zugang zu Polymeren oder Polymereigenschaften, welche nicht direkt vom Monomer zugänglich sind. Im Falle von Polyacrylnitril sind so zum Beispiel die vom Monomer bisher nicht mögliche katalytisch-kontrollierte Polymerisation oder die Verwendung grünerer Ausgangsmaterialien adressierbar. Es konnte ein vielversprechender polymeranaloger Syntheseweg beginnend bei der katalytischen Polymerisation von Methylacrylat gefunden werden, der über Zwischenstufe Polyacrylamid verläuft. Neben der Skalierung dieser Reaktionssequenz in den Multigrammaßstab werden auch die Monomere N,N'-Dibenzylacrylamid, N,N'-Di($tert$-butoxycarbonyl)acrylamid und N,O-Bis(trimetylsilyl)acrylamid als potentielle Kandidaten für die Polymerisierung und Umwandlung hin zu Polyacrylnitril identifiziert. Der Fokus dieser Studien liegt auf der kontrollierten Polymerisation der Monomere mit Hilfe von seltenerd-basierten organometallischer Katalysatorsysteme sowie der polymeranalogen Abspaltung der aus der für die Synthese kleinerer organischer Moleküle bekannten Schutzgruppen. Zusätzlich soll das polymer-analog hergestellte Polyacrylnitril in Zusammenarbeit mit dem Fraunhofer Institut für Angewandte Polymerforschung hinsichtlich auf die Prozessfähigkeit in der Umwandlung zu Carbonfasern untersucht werden.

Für die in Verbundmaterialien die Faser umgebende Duroplastenmatrix wird die Verwendung von ungesättigten Triglyceriden als Epoxidharz untersucht. Die epoxidierten Pflanzenöle werden in Verbindung mit Tanninsäure gehärtet was zu einem vollständig biobasierten Duroplast mit hervorragenden mechanischen Eigenschaften wie etwa

ein Biegemodul von 2986 MPa und eine hohe Glasübergangstemperatur von 147 °C führt. Die Prozessierbarkeit und homogenen Aushärtung wird über das feine Vermahlen der Tanninsäure gewährleistet. Die molekularen Eigenschaften des Härters wie die hohe Aromatizität und die damit verbundenen Wechselwirkungen erlauben die Verwendung des Systems als biobasierte Alternative zu petrochemischen Epoxidharzen in Hochleistungsanwendungen.

In einer weiteren Untersuchung wird die Synthese eines neuartigen, hoch mit Epoxidgruppen funktionalisierten Moleküls 1,2-Epoxy-6-methyl-triglycidyl-3,4,5-cyclohexantricarboxylat (EGCHC) präsentiert. Das Molekül wird in einer vierstufigen Reaktionssequenz ausgehend von der Veresterung von Sorbinsäure mit Allylalkohol hergestellt, wobei diese Ausgangsmaterialien potenziell bioverfügbar sind oder aus biogenen Stoffen gewonnen werden können. Die weitere Synthese verläuft über eine Diels-Alder Reaktion gefolgt von einer weiteren Allylierung und der Epoxidierung der eingeführten Doppelbindungen, wobei die ersten drei Reaktionsschritte eine hohe Atomeffizienz und einen niedrigen Lösungsmittelbedarf aufweisen. Das mit aminischen Standardhärtern umgesetzte Harz zeigt hohe Zugmodule und -Festigkeiten, welche mit konventionellen Bisphenol-A basierten Systemen konkurrieren kann.

Zuletzt wird eine Studie zur Synthese von fettsäurebasierten Schmierstoffen, sogenannte Estolide durchgeführt. Hierzu wird zunächst das Monomer Methyl-10-hydroxystearat aus Ölsäure synthetisiert und aufgereinigt und dann in einer katalytischen Polykondensationsreaktion umgesetzt. Das Augenmerk der Untersuchungen liegt auf der Beziehung zwischen Umsatz, Viskosität und der Reaktionsdauer, um eine definierte Zielviskosität zu erreichen. Die Estolidproben werden aufgereinigt und hinsichtlich ihrer thermischen Eigenschaften analysiert.

Alles in einem werden neben den auf biogenen Fettsäuren basierten Estoliden vielversprechende Ansätze hin zu biobasierten und nachhaltigeren Kohlefaserverbundmaterialien präsentiert, welche durch bisher unerreicht hohe (thermo)mechanische Kennwerte überzeugen.

1 Introduction

Fossil raw materials are currently the primary source of organic carbon processed in the chemical industry. Since this resource took millions of years to form and is therefore finite, renewable base chemicals are increasingly becoming the focus of industrial and scientific research. Biologically available carbon is mostly bound in complex, heterogeneous materials and occurs in the form of carbohydrates, proteins, lignin, or fats.[1] For use as basic chemicals, these complex molecules must be broken down into smaller building blocks. For example, ethanol can be obtained from starch *via* fermentation, which can then be converted into the industrially important starting materials ethylene, acetaldehyde, or acetic acid. An example product of the biological fermentation of carbohydrates is lactide which can be polymerized into polylactic acid. The polyester is already produced on a large scale (190,000 tons in 2019) and finds wide application as a low-carbon emission polymer.[2–4]

Another valuable feedstock currently explored is the use of triglycerides for the production of surfactants, lubricants, or as a monomer source for polymer synthesis. The main source of vegetable oils is currently palm oil, which was produced in 76 million tons in the harvesting period of 2019/20.[5,6] Although vegetable oils are renewable resources, vast areas of land are required for cultivation, which harms biodiversity.

An alternative triglyceride source in the future could be oil-forming microalgae or yeast cultures. Microalgae, for example, are capable of producing up to 70 % of their dry mass in oils. Promising properties include faster growth than terrestrial plants, and verticalization makes cultivation possible in a small area. Conversely, oleaginous yeasts can convert complex sugars into lipids, making them available for

oil production.[7,8] Glycerol, which is found in triglycerides, also has the potential to be used as a base chemical for the synthesis of more complex molecules.[9]

In the present work, new possibilities for the direct utilization of biobased oils and fatty acids are investigated. Parts of the work deal with an alternative synthetic route to polyacrylonitrile with biological carbon content as precursor material to carbon fibers starting from biobased glycerol. Furthermore, the synthesis of epoxy resins starting with biologically available unsaturated oils and fatty acids towards duroplasts with preferably high (thermo)mechanical properties is investigated. Finally, the synthesis of biobased lubricants (estolides) from hydroxylated fatty acids is part of the work.

2 Theoretical background

2.1 Carbon fibers

Carbon fibers (CF) increasingly receive attention for their outstanding mechanical properties. Compared to traditional materials like steel or aluminum, CFs offer, for example, higher tensile strength and elasticity with lower component weight due to the lower density. This makes CFs an ideal material for lightweight construction in aviation, wind energy, or sport goods (compare Figure 2.1a).[10,11] As shown in Figure 2.1b, the demand for CFs increased steadily, almost tripling from about 33 kt in 2010 to 92 kt in 2021.[12] Global developments such as the growth of renewable energies (especially wind energy) or the need for pressure vessels for the storage of hydrogen will very likely ensure that this trend continues.[13,14]

2.1.1 Polyacrylonitrile fiber spinning

Historically, CFs were produced from rayon as a precursor. Today, the CF market is dominated by polyacrylonitrile (PAN) fibers and petroleum pitch-based fibers, which account for only a small share.[16,17] PAN can be polymerized from acrylonitrile (ACN) radically from solution or by suspension polymerization (Scheme 1). Suitable solvents need to be polar molecules to interact with the nitrile groups of PAN and thus break dipole-dipole interactions. Such highly polar solvents are N,N-dimethyl formamide (DMF), dimethyl sulfoxide (DMSO), or concentrated solutions of $ZnCl_2$

(a)

(b)
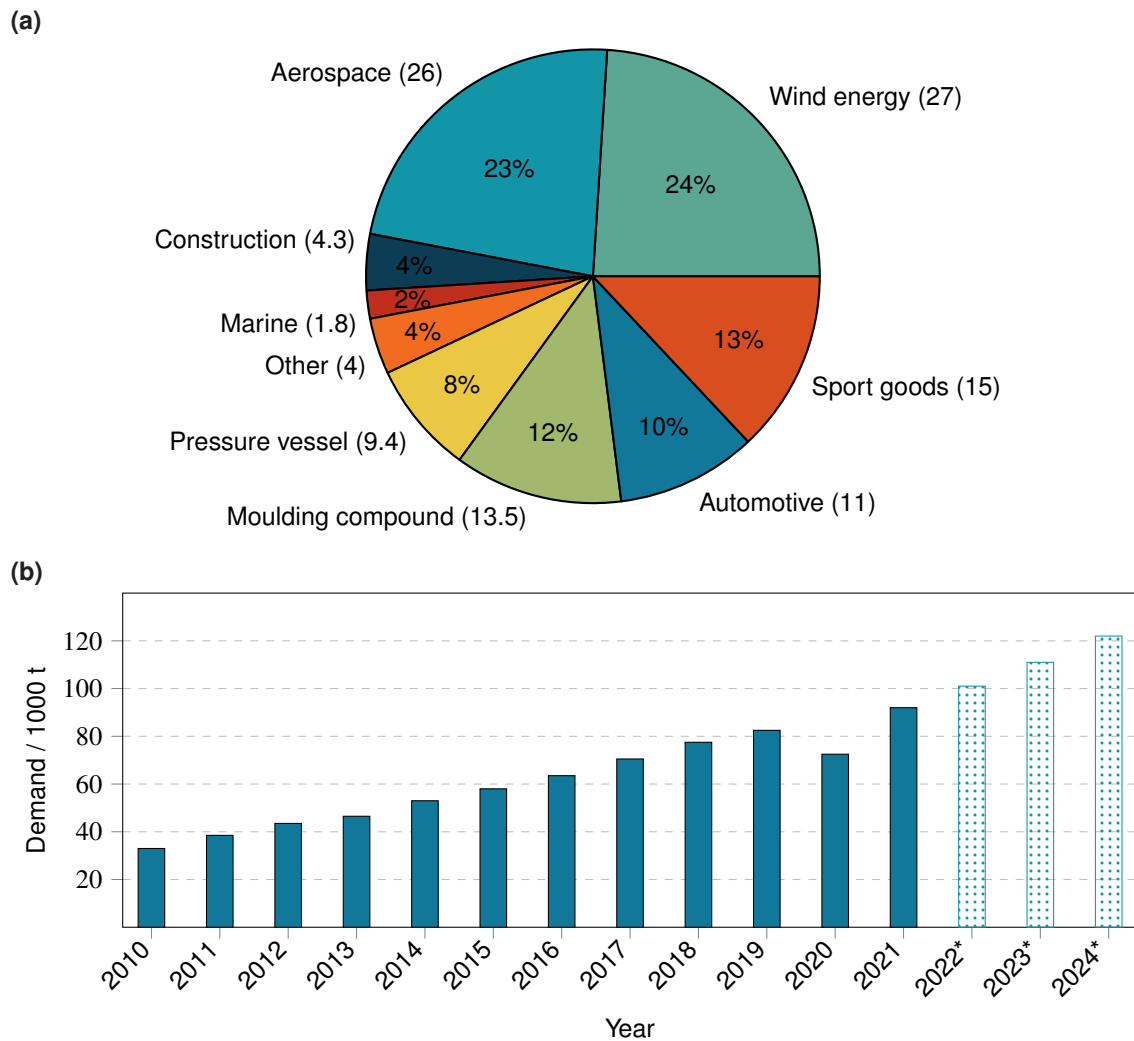
Figure 2.1: a) Global carbon fiber demand by application (Kilotonnes) in the year 2020. Adapted from Zhang *et al.*[15] b) Global CF demand in kilo tonnes by year, *estimations. Adapted from Sauer *et al.*[12]
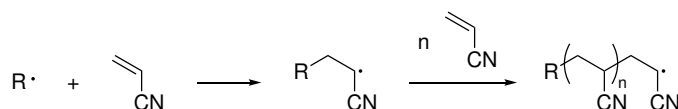
Scheme 1: Radical polymerization of AN, R· represents a radical.

and NaSCN.[18,19] The polyaddition reaction is started by a radical initiator such as peroxides, persulfates, azo compounds, or redox systems.[16,20]

The resulting white solid PAN is then converted into fibers by spinning techniques whereby wet spinning has been established as the standard method. For this, a dope solution containing 10 to 20 % PAN precursor is prepared in a mixture of DMF and water, DMSO and water, or similar solvents. As shown in Figure 2.2, the dope solution is then first filtrated and then pumped through the spinneret into a precipitation bath containing a nonsolvent. Here, the previously dissolved polymer coagulates forming fibers. The coagulation rate can be controlled by the concentration of the nonsolvent (typically water). However, slower coagulation is preferred to avoid surface irregularities.[20] All in all, spinning PAN for conversion into high-performance CF is a complex process with many variables:[11]

- molecular weight
- molecular weight distribution
- purity of the spin dope
- concentration of polymer in solution
- temperature of the solution
- spinneret geometry
- composition of the coagulation medium
- elongation rate (stress) applied during coagulation

2.1.2 Stabilization and carbonization

The next step after PAN-fiber-spinning towards the CF is the so-called "stabilization"-process. Here, a thermally induced cyclization reaction converts the polymer into heteroaromatic structures. Although this cascade of complex cyclization reactions
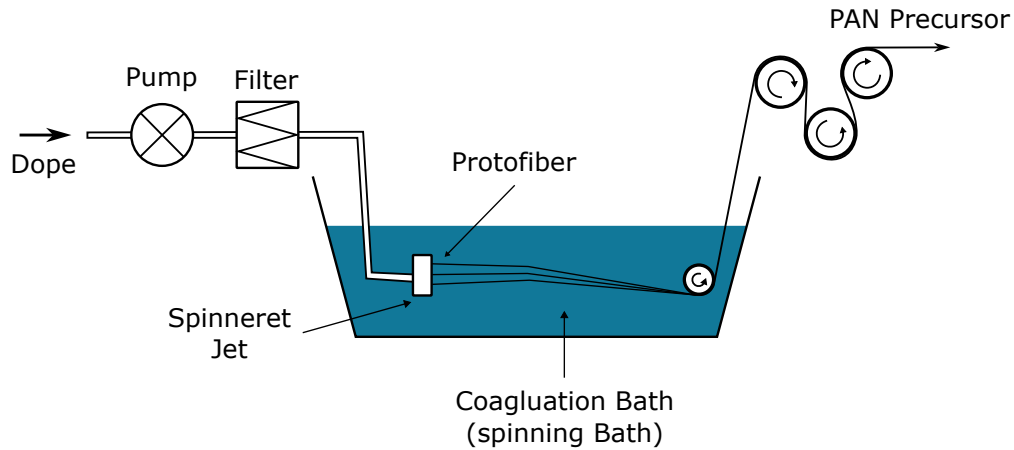
Figure 2.2: Schematic of wet spinning process. Adapted from Khayyam *et al.*[21]

can proceed in the absence of oxygen, it is carried out in the presence of oxygen to produce high-quality CFs.[22]

Over the last decades, the stabilization process has been heavily studied, and various structures shown in Figure 2.3 have been proposed. Houtz suggested a mechanism that leads to an *N*-heteroaromatic cyclic structure in 1950 (Figure 2.3a).[23] In the late 1950s, a polyimine cyclic structure was stated by Burlant *et al.*, La Combe, and Grassie *et al.* (Figure 2.3b).[24–26] Schurz observed discoloration effects while heating carbon fibers and proposed a crosslinking mechanism between neighboring chains resulting in azomethine crosslinks as shown in Figure 2.3c.[27] Standage *et al.* found oxidation occurring in an oxygen-containing atmosphere, leading to epoxide formation (Figure 2.3d).[28] Another oxygen-involving ladder structure was stated by Watt forming carbonyl substructures (Figure 2.3e).[29] Takahagi *et al.* performed x-ray photoelectron spectroscopy and found a ladder structure consisting of 40 % acridone ring, 30 % naphthyridine ring, 20 % hydronaphthyridine ring, and 10 % others (Figure 2.3f).[30] The stabilization process is very exothermic in the presence of oxygen. The thermal energy thus generated must necessarily be controlled to maintain an intact CF.[31,32]

To improve the properties of PAN-based CF, PAN is commercially produced not as a homopolymer but as a copolymer. The reasons for this are either to enhance processability or to optimize the stabilization reaction. As can be seen in Table 2.1, various acrylates are used, which have different influences depending on the side
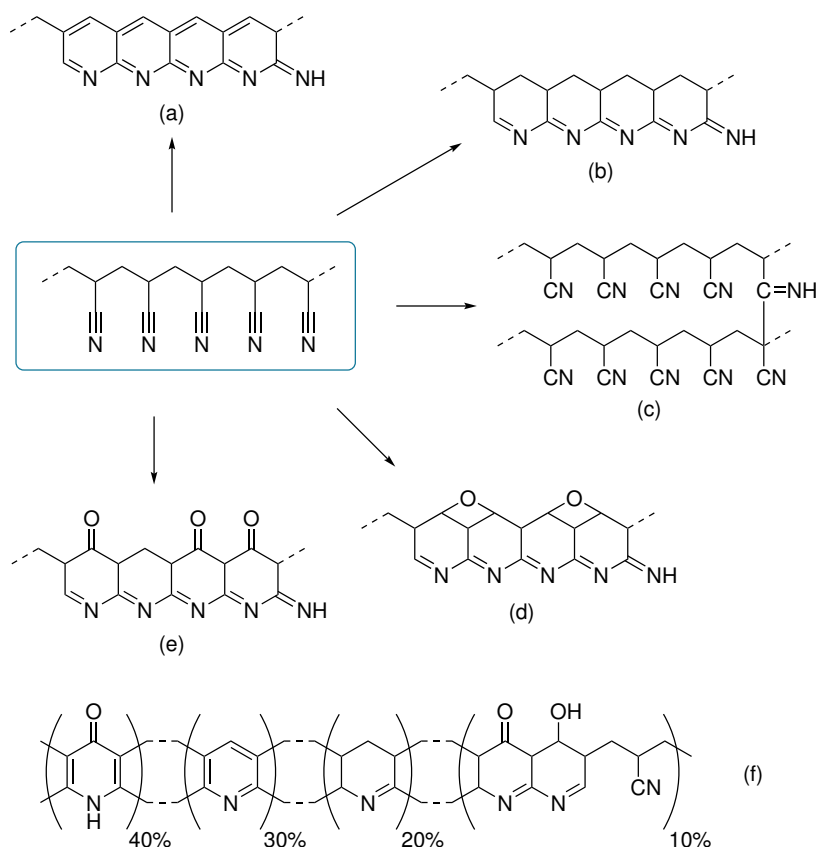
Figure 2.3: Model reaction paths of the stabilization reaction of PAN. Adapted from Huang.[16] Sources: a) Houtz[23], b) Burlant *et al.*, La Combe, Grassie *et al.*[24–26], c) Schurz[27], d) Standage *et al.*[28], e) Watt *et al.*[29], f) Takahagi *et al.*[30]

group. Most present comonomers in literature are itaconic acid and methyl acrylate (MA).

Acidic comonomers act as catalysts for stabilization and lower the onset temperature. Additionally, the temperature range of the exothermic process is broadened which makes it more controllable.[22] Acrylic esters provide better processability during the PAN-spinning and improve the orientation of the polymer chains.[35] Acrylamide and vinyl bromide both also speed up the stabilization process but are not used as often.[20,34]

After stabilizing the PAN fiber, a second processing step is necessary to obtain CF. In this, the cyclized fiber undergoes heating from low to high (1600 °C) temperatures. This causes crosslinking between the fiber strands and condensation reactions to result in graphite-type carbon layers (see Scheme 2). Further graphitization proceeds

Table 2.1: Effects of different comonomers on PAN-based CFs.
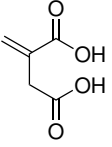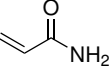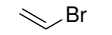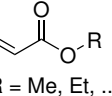
Comonomer	Structure	Property improvement
Itaconic acid		Lower stabilization temperatures, more moderate stabilization pace[33]
Acrylamide		Speeds up stabilization pace[34]
Vinyl bromide		Stabilization time shortened[16,20]
Acrylic esters	R = Me, Et, ...	Improve orientation of polymer during spinning, higher drawing rates[22]

Table 2.2: Classification of carbon fibers IUPAC.[36–38]

Classification	Tensile modulus / GPa	Tensile strength / MPa	Elongation at brak / %
UHM (Ultra high modulus)	> 600[37]	> 2,500[38]	–
HM (High modulus)	> 300[37]	> 2,500[38]	< 1[36]
IM (Intermediate modulus)	278–350[37]	> 3,500[38]	> 1[36]
LM (Low modulus)	< 100[37]	< 3,500[38]	–
HT (High tensile)	150–300[37]	> 3,000[36]	1.5–2[36]

by healing defects when heating above 1600 to 1800 °C up to 3000 °C resulting in the final CF.[22]

Again, during the carbonization/graphitization process, many parameters, such as heating rates, directly influence the quality of the CF. As can be seen in Table 2.2, different quality CFs are classified in terms of mechanical properties such as the tensile elastic modulus and tensile strength: ultra high-modulus (UHM), high-modulus (HM), intermediate-modulus (IM), low modulus (LM), and high tensile strength (HT). This opens up a broad spectrum of mechanical properties with tensile strengths from 3500 MPa up to 7000 MPa combined with stiffnesses between 230 GPa up to almost 600 GPa and an elongation at break of 1 to 2 %.[17,36]
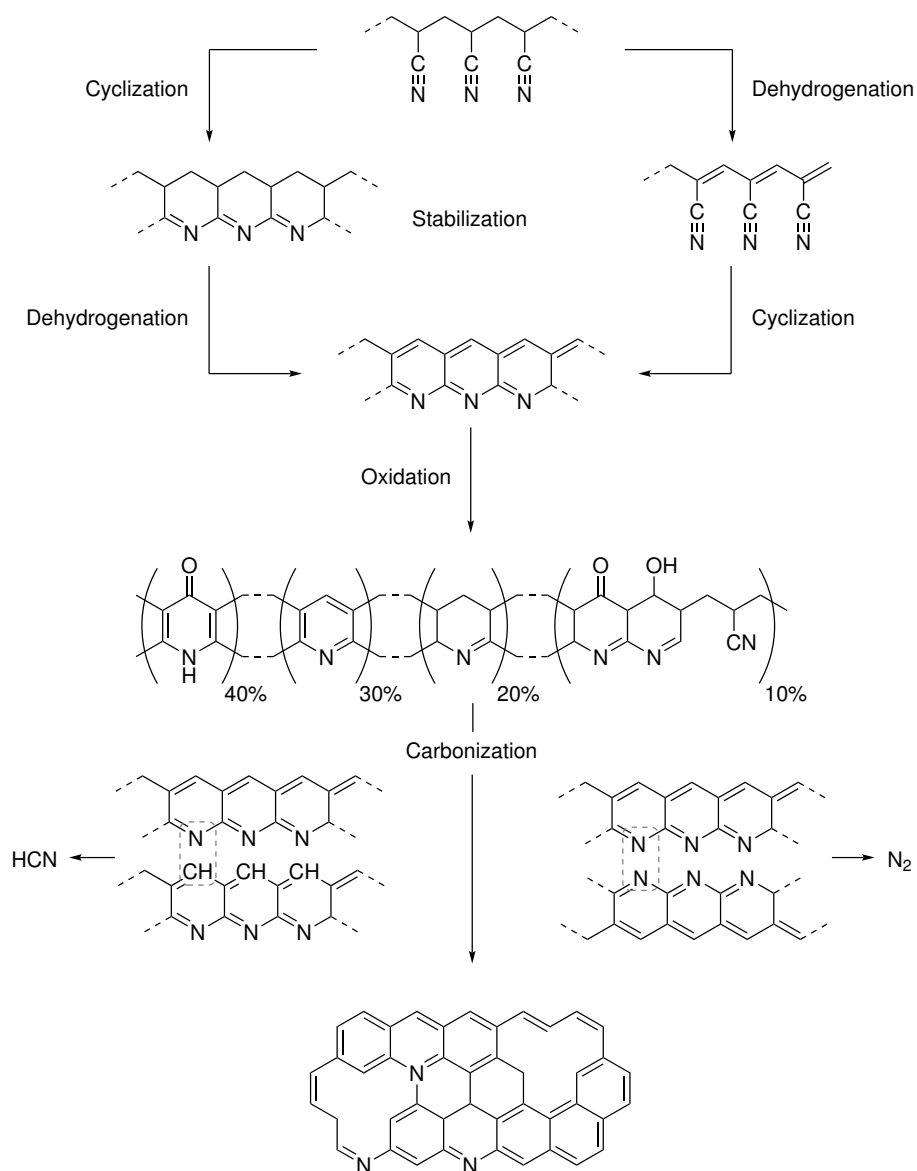
Scheme 2: Mechanisms of the stabilization chemistry and subsequent pyrolytic carbonization (structure of the stabilized PAN according to Takahagi.[30]) Adapted from Fitzer *et al.* and Frank *et al.*[22,32]

(a)

$$2 \text{ Propene} + 2\,NH_3 + 3\,O_2 \xrightarrow[\text{450 °C, 1.5 bar}]{\text{catalyst}} 2 \text{ ACN} + 6\,H_2O$$

(b)

$$\text{Propene} + O_2 \longrightarrow \text{Acrolein} + H_2O$$

(c)

$$\text{Propene} + NH_3 + 9/4\,O_2 \longrightarrow \text{Acetonitrile} + 1/2\,CO_2 + 1/2\,CO + 3\,H_2O$$

(d)

$$\text{Acrolein} + NH_3 + 1/2\,O_2 \longrightarrow \text{ACN} + 2\,H_2O$$

(e)

$$\text{ACN} + 2\,O_2 \longrightarrow CO_2 + CO + HCN + H_2O \quad \text{Hydrocyanic acid}$$

(f)

$$\text{CN} + 3/2\,O_2 \longrightarrow CO_2 + HCN + H_2O$$
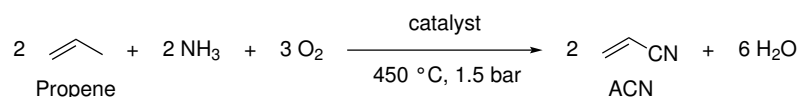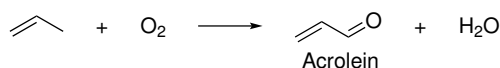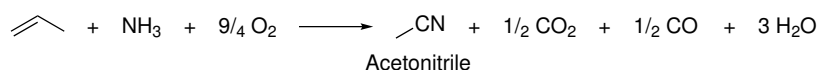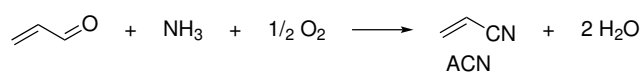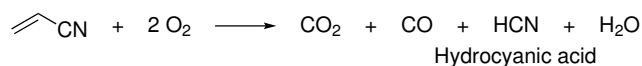
Scheme 3: Ammoxidation reaction of propene to ACN (a) and five possible side reactions forming acrolein (b), acetonitrile (c), hydrocyanic acid (e, f) or converting acrolein to ACN (d).[42]

2.1.3 Alternative feedstocks for carbon fibers

Over 90 % of the carbon fibers commercially available on the market are produced starting from PAN.[39] 90 % of the worldwide used ACN originates from the Sohio Acrylonitrile Process which converts propylene to ACN *via* a catalytic ammoxidation reaction using bismuth molybdate-based catalysts (see Scheme 3).[40,41] The process also involves five side reactions forming the by-products acrolein (Scheme 3b), acetonitrile (Scheme 3c), hydrocyanic acid (Scheme 3e and Scheme 3f) as well as the reaction of acrolein to the desired product ACN (Scheme 3d).[42]

Mainly for sustainability reasons, some effort is being put into finding alternative routes to ACN, leaving fossil-based propene as starting material behind.[43–45] In fact, the beginnings of CF production were based on rayon, a starting material derived from the biopolymer cellulose.[46] A second biopolymer that could possibly be used as a CF precursor is lignin.[47] It is abundant as waste material in the paper industry; however, as with rayon, the problem is that the mechanical properties of the CF cannot

(a)

(b)

(c)
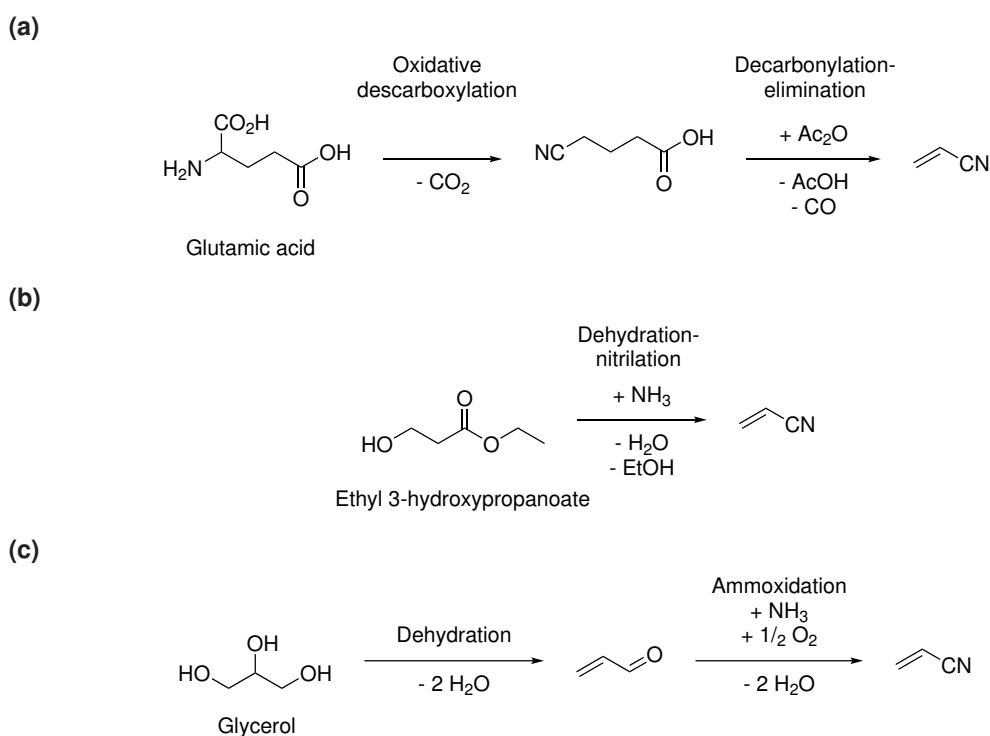
Scheme 4: ACN from a) glutamic acid,[49] b) ethyl 3-hydroxypropanoate,[41] and c) glycerol.[44,45]

keep up with those made from PAN.[47] Therefore, research is focusing on bio-based molecules that can be converted into ACN.[48] The most important studies are shown in Scheme 4. Biomolecules such as glutamic acid or ethyl 3-hydroxypropanoate (3-HP) were identified as possibly renewable feedstock,[41,49] but most routes are described starting from glycerol.[48]

For glutamic acid (Scheme 4a), first, an oxidative decarboxylation step is necessary, which is followed by a palladium-catalyzed decarbonylation-elimination reaction using acetic anhydride. The most significant disadvantage of this synthesis route is the low yields: while the first stage results in 70 % isolated product in the second stage only 17 % could be gained, which results in an overall yield of 12 %.[49]

More promising is the approach of Karp *et al.* They used 3-HP produced from biomass sugars by bacteria and successfully converted ACN in a one-step process (Scheme 4b). The authors proposed a reaction pathway in which the starting material

is dehydrated to ethyl acrylate, which is then converted to acrylamide and subsequently to ACN. The yields reached in this TiO_2-catalyzed process of over 90 % also make the process potentially competitive with the existing Sohio process.[41]

The usage of glycerol as starting material for the conversion into ACN is widely investigated. Synthesis usually includes the dehydration of glycerol to acrolein followed by an ammoxidation to ACN (Scheme 4). Here, different strategies are pursued: one-step,[44] two-step,[45] and three-step with a purification of the intermediary formed acrolein which can achieve yields of 60 %.[43] Guerrero-Perez and Banares describe a one-step ammoxidation of glycerol to ACN using an Nb-doped $VbSO_4$ catalyst.[44] This reaction was carried out at 400 °C in an atmosphere of 25 % oxygen, 8.6 % ammonia, and 66.4 % helium and resulted in a selectivity of 58 % for ACN with a conversion of 83 % glycerol. At first glance, this method represents a promising approach for ACN synthesis from biomass. However, deactivation processes due to the unwanted formation of polyaromatics and PAN significantly reduces the activity of the catalysts after only two hours. A two-step process in a tandem reactor, published by Liebig *et al.*, showed very useful results for the conversion of glycerol to acrolein with a WO_3/TiO_2 catalyst in the presence of oxygen at 280 °C.[45] However, ammoxidation of acrolein on FeSb-based mixed oxides revealed poor selectivities and yields of ACN. A subsequent process with an additional purification step of acrolein was able to achieve slightly improved values.[43] Nevertheless, problems are evident due to the short lifetimes of the catalysts for dehydration and the deactivation of the catalysts for the second step causing unreacted glycerol. Moreover, studies on the Sohio process show that not acrolein but the allyl radical formed on the surfaces of the commercial catalysts from propylene is the preferred precursor molecule for ACN production and leads to better yields.[50,51]

In summary, the heterogeneously catalyzed synthesis of ACN from biogenic glycerol, with its harsh conditions and moderate yields, is not the final and best route for the conversion of CF production to bio-based resources. Therefore, it is worthwhile to focus on alternative monomers produced from biogenic glycerol, which could be

converted into PAN after successful polymerization with so-called polymer analogous reactions, obviating the need for laborious purification of toxic ACN.

2.1.4 Polymer analogous route to polyacrylonitrile

Polymer-analogous modifications (PAM) refer to the process of chemically modifying polymers to improve their properties and performance. PAMs aim to tailor the properties of polymers for specific applications, such as increased strength, biological compatibility, or surface modifications.

Probably one of the first PAM was the nitration of cellulose by Braconnot in 1833 through the exposure of cellulose with sulfuric acid and nitric acid (Scheme 5a). This resulted not only in the development of gun cotton a few years later, but also paved the way of synthetic fibers called rayon with similar properties to natural silk.[52,53] Another early example of PAMs can be found in the vulcanization of natural rubber displayed in Scheme 5b. In 1839, Charles Goodyear found that sticky natural rubber could be converted into a highly elastic material by the addition of sulfur and heat treatment. This led to the development of the rubber industry, which is still utilized in *e.g.* car tire production.[54,55] PAM evolved steadily, and very many examples of it can be found both in literature and technically implemented.

A technologically relevant example is the halogenation of polymers (Scheme 5c). By adding bromine to polybutadiene gives the polymer material flame-retardant properties.[56] Also industrially widely applied is the basic saponification of polyvinyl acetate to polyvinyl alcohol (PVA, Scheme 5d). This particular reaction is interesting since direct polymerization of PVA from the monomer is not possible because of keto-enol tautomerism of the vinyl alcohol monomer.[57] Another substitution method is the fluorination of various kinds of polymers with gaseous F_2. This allows the functionalization of a polymeric surface to obtain typical properties of fluoropolymers such as polytetrafluoroethylene, which show high chemical stability and thermostability. Only the upper surface is modified with this procedure, leaving the bulk properties

(a)

(b)

(c)

(d)
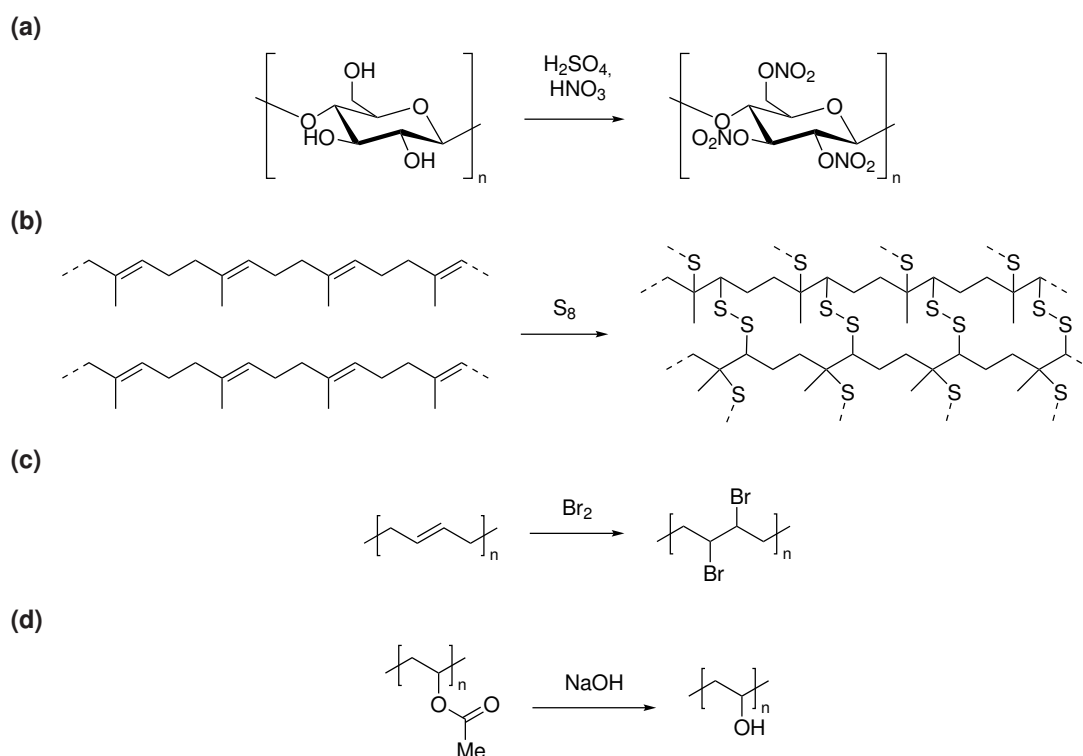
Scheme 5: a) Nitration of cellulose, b) vulcanization of natural rubber with sulfur (idealized crosslinking), c) bromination of polybutadiene, d) saponification of polyvinyl acetat to polyvinyl alcohol

unchanged, cutting production costs compared to manufacturing fluoropolymers from the respective monomer.[58]

Preliminary work at the WACKER-Chair of Macromolecular Chemistry resulted in a PAM synthesis pathway to PAN that skips polymerization starting from ACN. As shown in Scheme 6, the implementation of different, for the use as a precursor for CF typical comonomers is also achievable since synthesis starts from polymethyl acrylate (PMA). MA was polymerized anionically by *n*-butyl lithium at −78 °C, achieving comparatively low molar masses below 30 kg mol^{-1} and a PDI of 1.6. The first synthesis step towards homopolymeric polyacrylamide (PAA) or polyacrylamide-*co*-methylacrylate in controllable amounts proceeds *via* pressurizing dissolved PMA with 8 bar ammonia at 60 °C. A 2:1 mixture of thf and methanol was found to be best suited to dissolve both the polymer and the ammonia and allowed the reaction to succeed. The rate of the amidation reaction is influenced by the molecular weight of the polymer on the amidation reaction, which means that lower molecular weight
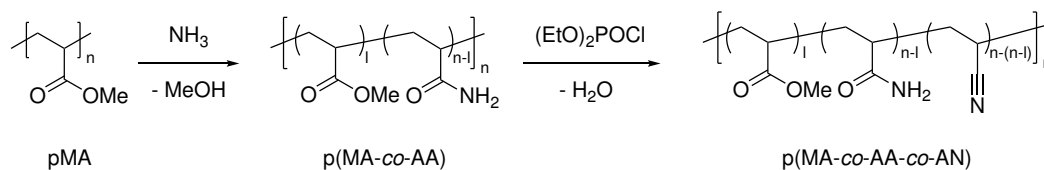
Scheme 6: Polymer-analogous conversion of poly methyl acrylate to poly acrylonitrile *via* poly acrylamide.

PMA (M_n = 3.4 kg mol^{-1}) reaches an amidation degree of 50 % after one day while the higher weight PMA with a M_n of 22.0 kg mol^{-1} reaches the same degree of amidation after three days. Because of the high oxophilicity of phosphorus reactants like diethyl chlorophosphate (DECP) can be used for the dehydration from PAA to PAN. This way, terpolymers consisting from methyl acrylate, acrylamide, and acrylonitrile are accessible depending from the degree of amidation in the first step and the stoichiometry of the dehydrating reagent in the second step.[59,60]

2.1.5 Conversion of glycerol into acrylate monomers

Acrylic acid is thus a promising candidate for the polymer analogous conversion towards PAN. It can be produced from glycerol using a two-step, wet-chemical synthesis. The deoxydehydration of glycerol to allyl alcohol is carried out almost quantitatively using formic acid with a direct distillation of the product (Table 2.3).[61]

Allyl alcohol, which can be ammoxidized heterogeneously in turn to ACN,[62] can be oxidized by several different methods summarized in Table 2.3. Traditionally, oxidation reactions were often performed using manganese or chromium as oxidizing agents.[63,64]. The use of chromium(III) oxide is also reported by Goldschmidt *et al.* combined with copper(II) oxide at high temperatures in 1934.[65] Mannam *et al.* found a route under mild conditions with *tert*-butyl hydroperoxide and catalytic amounts of copper(I) chloride in very high yields.[66] There are also various publications using supported ruthenium(IV) oxide or cerium(IV) oxide catalysts which work in combination with oxygen.[67,68] Wang *et al.* reported the successful conversion of allyl alcohol to acrylic acid using a chromium/molybdenum polyoxymetalate in a reaction with CO_2.

Table 2.3: Synthesis routes from glycerol to acrylic acid or its ester derivatives.
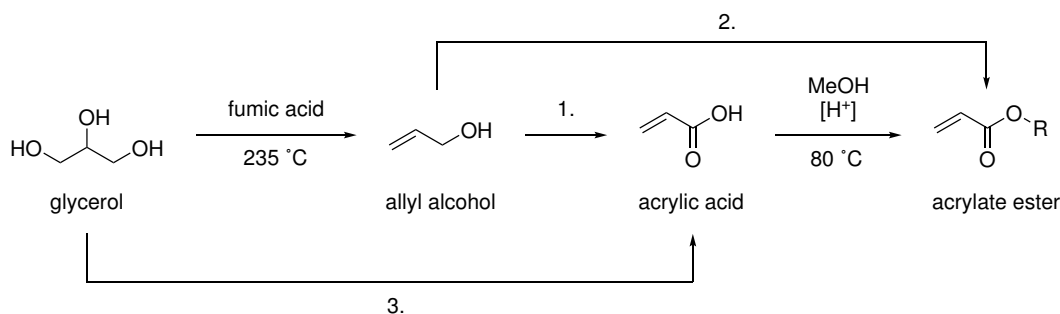
Step	Conditions	Reference
1.	CuO/Cr$_2$O$_3$, water at 300 °C	Goldschmidt et al.[65]
	CuCl, tBuOOH (5 M in decane), r.t.	Mannam et al.[66]
	RuO$_2$ on ZSM-5 zeolite, O$_2$, 80 °C, 840 mbar	Qian et al.[67]
	gold nanoparticle-supported CeO$_2$ catalyst, O$_2$	Kim et al.[68]
	(NH$_4$)$_3$[CrMo$_6$O$_{18}$(OH)$_6$] / DMSO / CO$_2$	Wang et al.[73]
2.	gold nanoparticles/SiO$_2$, O$_2$, MeOH, 6 bar, 130 °C	Oliveira et al.[69]
3.	1. formic acid, 2. Mo–V–W–O, O$_2$, 340 °C	Li et al.[61]

There is also an one-step directly from allyl alcohol to the methyl ester of acrylic acid catalyzed by gold nanoparticles with O$_2$ in methanol.[69]

Here, advantages are revealed in the reaction process compared with the conventional route from glycerol to ACN via the intermediate acrolein, which in some cases requires extreme conditions with high temperatures. In addition, both the intermediate acrolein and the end product are highly toxic, whereas in the polymer-analog synthesis route to PAN, no isolated acrylonitrile is produced, and the acrylic acid is much safer to handle.[70] The carboxylic acid group can be readily esterified with various alcohols under acid catalysis, opening up the application of various polymerization techniques.[71,72] While acrylic acid can be polymerized radically, its esters also allow the application of anionic and catalytic methods.

2.2 Monomer scope for polymer analogous modifications

As already seen in Section 2.1.1, vinyl monomers such as ACN can be prepared by free radical polymerization. Despite there are radical polymerization techniques that allow controlling both molecular weight and molecular weight distribution, anionic or coordinative anionic (catalytic) methods provide a more extensive and even more precise toolbox towards tailored macromolecular properties.[74] In terms of monomers, here the focus is on a palette of vinyl compounds, including the acrylate MA, but also derivatives of acrylamide which shall be used as alternative starting material for the PAM towards PAN.

(a)

Methyl acrylate
(MA)

N,N-Dibenzyl
acrylamide
(Bn₂AA)

N,N-Di(*tert*-Butoxycarbonly)-
acrylamide
(Boc₂AA)

N,O-Bis(trimethylsilyl)-
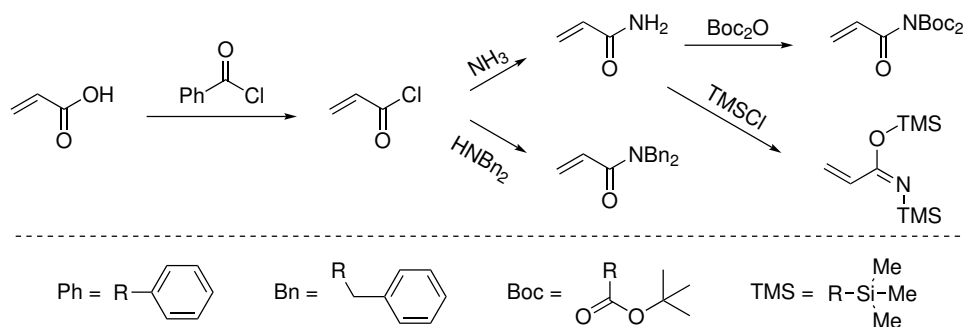acrylamide
(TMSAA)
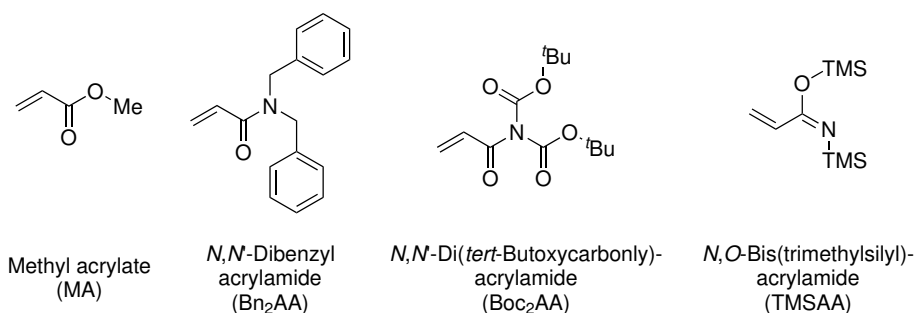
(b)

Figure 2.4: a) Monomers in scope of the thesis, b) synthesis routes of all monomers from acrylic acid.

In addition to the conventional methyl acrylate, Figure 2.4a shows three literature-known acrylamide derivatives. These monomers are, up to now, only polymerized by free-radical methods, but were not subjected to catalytic techniques. *N,N'*-Dibenzyl

acrylamide (Bn$_2$AA) was first mentioned by Wang *et al.* in 1975 in a study about intramolecular excimer formation of dibenzylamine and its derivatives.[75]

The monomer was synthesized by reacting acryloyl chloride with dibenzylamine in the presence of diisopropylethylamine.[76] Acryloyl chloride can be obtained from the reaction of acrylic acid with benzoyl chloride or thionyl chloride, which links all monomers to the previously described starting material glycerol (Figure 2.4b).[77,78] The polymerization with azobisisobutyronitrile (AIBN) was described by Yamate *et al.* in 2008 for the application as an adhesive material to polyolefin surfaces.[79,80]

N,N'-Di(*tert*-butoxycarbonyl)-acrylamide (Boc$_2$AA, Boc = *tert*-butoxycarbonyl protecting group) was synthesized from acrylamide and di-*tert*-butoxycarbonate in the presence of dimethylaminopyridine and polymerized radically by Larsen *et al.* The group also saw the potential of poly(*N,N'*-di(*tert*-butoxycarbonyl)-acrylamide) (PBoc$_2$AA) as a versatile platform for PAM-reactions and used the activated ester position of the amide carbonyl for nucleophilic attacks of amines and alcohols.[81]

The bis-silylated acrylamide derivative *N,O*-Bis(trimethylsilyl)-acrylamide (TMSAA) was synthesized first by Birkofer *et al.* in 1963 by protecting acrylamide with trimethylsilylchloride in an inert atmosphere.[82] Polymerization was then carried out in 1994 by Dasgupta *et al.* again using AIBN. They also investigated the deprotection under acidic conditions to result in PAA.[83]

2.2.1 Silyl ketene acetal - group transfer polymerization

Webster *et al.* discovered the group-transfer polymerization (GTP) at DuPont around 1980.[84,85] Research was driven by the need to find a living type polymerization method for MMA above room temperature, as until then, this was only possible anionically at –80 °C. The method should develop into a popular method to polymerize acrylates with defined molar masses and low polydispersity.

The polymerization was initiated by 1-methoxy-2-methyl-1-trimethylsiloxy-propen (silyl ketene acetal, SKA) with a nucleophilic anion such as bifluoride or Lewis acids as co-catalyst. Because of the living character of the reaction, each chain starts growing simultaneously with the amount of active chains correlating with the number of added initiator molecules. Polymerization stops when no more monomer is available but can be restarted even by the addition of other functional 1,4-unsaturated Michael acceptor vinyl monomers. This results in the formation of block copolymers.[86,87]
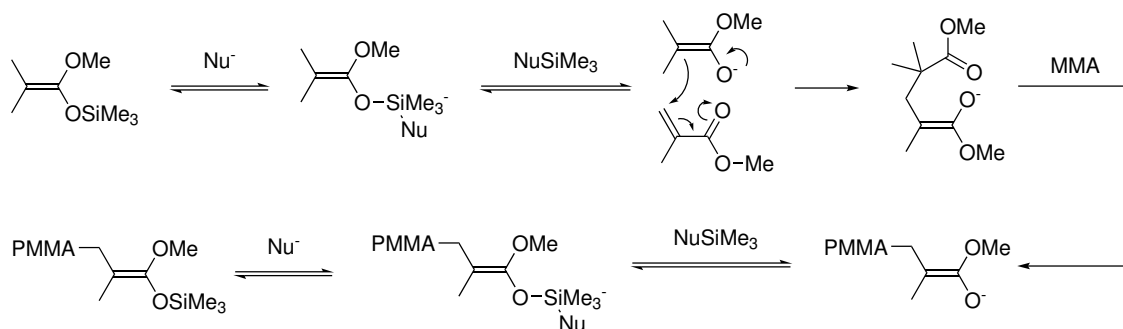
(a)
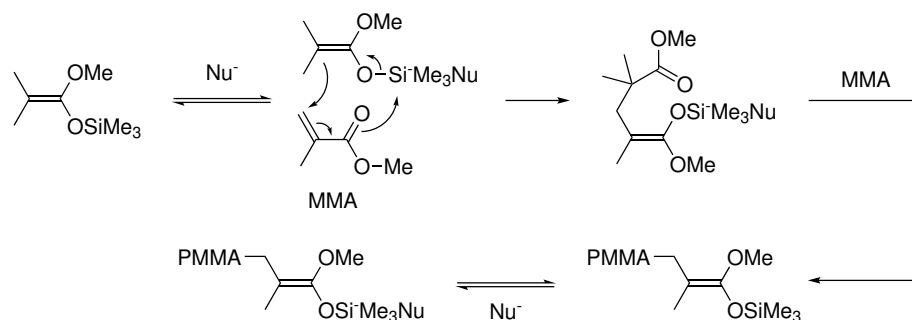
(b)

Scheme 7: Two mechanisms proposed for SKA-GTP. a) Associative group-transfer-mechanism, b) dissociative anionic mechanism.

Webster *et al.* proposed an associative mechanism starting with an intermolecular Michael addition of the SKA-enolate ester to a MMA-monomer catalyzed by a nucleophile. Throughout the polymerization process, the trimethylsilyl-group (TMS) is always attached to the growing chain end, which implies a transfer as shown in Scheme 7a. Later, this mechanism was questioned by Quirk *et al.* and Müller, who could observe the transfer of TMS-groups to other chains.[88,89] This lead to the development of a dissociative anionic mechanism in which the active chain ends are ester enolate anions which attack the vinyl monomer (Scheme 7b). This is equivalent to the chain propagation of an anionic polymerization with the difference that the anionic
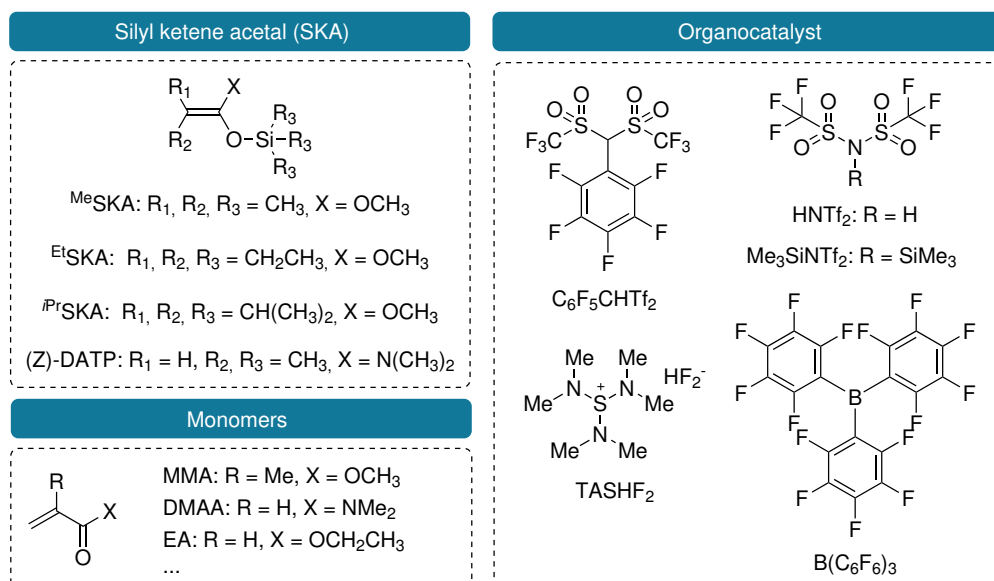
Figure 2.5: A selection of silyl ketene acetals, organocatalysts and monomers for SKA-GTP.

end groups can be reversibly trapped by TMS-groups allowing only a proportion of the chains to be active and mediate the polymerization.[87] The associative mechanism was thus refuted but nevertheless coined the term GTP and is still commonly used for (metal-catalyzed) poly-1,4-addition of 1,4-unsaturated Michael acceptor monomers.

Despite SKA-GTP being developed for MMA, other Michael monomers such as alkyl acrylates or acrylamides like *N,N'*-dimethylacrylamide (DMAA) were polymerized by this method. As can be seen in Figure 2.5, there is a variety of different SKA-compounds and organocatalysts to choose from the right combination for each monomer. For example, MMA can be polymerized with ^{Me}SKA and HNTf$_2$ (Tf = trifluoromethanesulfonate) while DMAA works best with (Z)-1-(dimethylamino)-1-trimethylsiloxy-1-propene ((Z)-DATP) and HNTf$_2$. The optimal system for ethyl acrylate can be found in ^{iPr}SKA and Me$_3$SiNTf$_2$, while for MA it is ^{iPr}SKA and (pentafluorophenyl)bis(triflyl)methane (C$_6$F$_5$CHTf$_2$).[90–93] Even acrylonitrile can be polymerized, although in the case of ACN there is heat generated which broadens the molecular weight distribution heavily.[86,94]
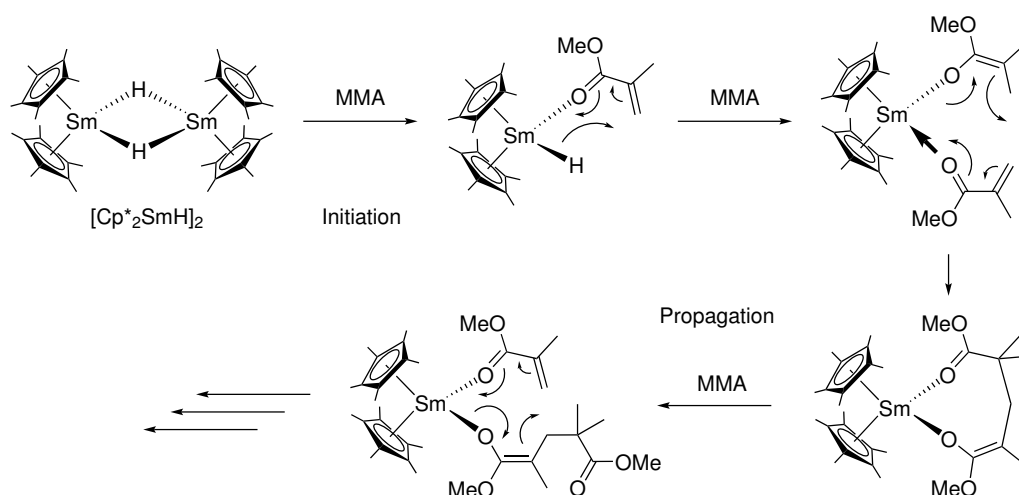
Scheme 8: Initiation and propagation steps of a Yasuda-type polymerization mechanism of MMA with [Cp*$_2$SmH]$_2$.[95]

2.2.2 Metal-catalyzed group transfer polymerization

Over the last years, rare earth metal (REM) mediated GTP has been a major subject of research. In 1992, two groups introduced novel metal-based catalysts for polymerizing MMA with high conversions, high molecular weight (M_n >100.000 g mol^{-1}) and low polydispersity ($Đ$ = 1.02 to 1.04). Additionally, the catalyst was active in a broad range of temperatures (–95 to 40 °C) and led to a syndiotacticity of 95 % at low temperatures. The complex used by Yasuda *et al.* for this was a samarocen hydrido complex [Cp*$_2$SmH]$_2$ (Cp* = 1,2,3,4,5-pentamethylcyclopentadienyl), which can be seen in Scheme 8. With this milestone set, the development of different lanthanocenes for polymerizing MMA started.[95,96]

Mechanistic investigations revealed that the bimetallic [Cp*$_2$SmH]$_2$] is initiated by the coordination of a MMA monomer to the metal center cleaving the η^2-hydrido-bridge. This MMA is then is isomerized to its enol-form by an attack of the hydride, which creates a free coordination center. Afterward, a MMA monomer can coordinate over the carbonyl in its keto form to the metal center. The nucleophilic attack then proceeds from the enol double bond to the vinyl end of the keto-MMA. During the propagation, an 8-membered metallacycle transition species is formed. This leads to a repeated 1,4-addition of the next MMA monomer.[95–97]
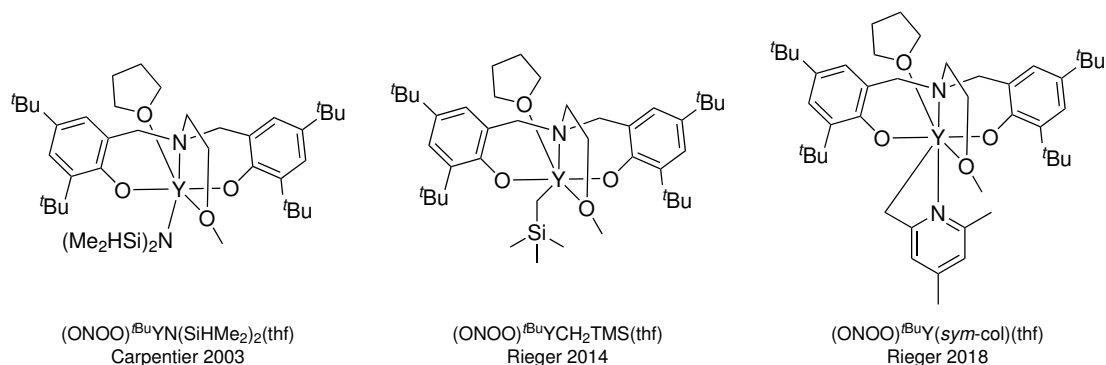
Figure 2.6: 2-Aminoalkoxy-bis(phenolate) yttrium catalysts suitable for the polymerization of DMAA.[100–102]

In addition to the well-studied metallocene catalysts, the group of Carpentier developed the first 2-aminoalkoxy-bis(phenolate) yttrium catalyst (Figure 2.6) for the polymerization of MMA in 2003 but observed no activity for the CH_2TMS derivative. Later, the group of Rieger added expanded scope of monomers and polymerized, for example, alkylated acrylamides (Figure 2.6).[98–101] Also, the same group found that the same catalyst CH-activated with *sym*-collidine (sym-col) is capable of polymerizing DMAA with high isotacticity at low temperatures. Transition metal complexes and d^0 lanthanides are known to undergo σ-bond metathesis *via* a [$2\sigma+2\sigma$]-cycloaddition leading to CH-activated complexes.[99,102] The initiating group CH_2TMS is strongly basic and starts the polymerization by means of a nucleophilic transfer. In contrast, the *sym*-col derivatives show less nucleophilicity.[99,102]

Ihara *et al.* described the polymerization of methyl acrylates with $Cp*_2SmMe(thf)$ and $Cp*_2YMe(thf)$ and reported narrow molecular weight distributions and high molecular weights combine with high initiator efficiencies.[103,104]

2.2.3 Deprotection strategies of acrylamide derivatives

There are numerous strategies to protect functional groups in organic or bioorganic synthesis from undesired reactions by attaching so-called protecting groups. The in Section 2.2 introduced monomers can be understood as a part of the protection strategy. However, there is a difference to the classical protecting group strategy

just described. In the case of monomers, the aim is not to protect the amide functionality but rather the organometallic catalysts. The GTP is generally sensitive to protic compounds such as alcohols, amines, or water, which explains why monomers such as acrylic acid or acrylamide cannot be polymerized catalytically. The following describes some common deprotection reactions of benzyl, *tert*-butoxycarbonyl-, and trimethylsilyl-groups in organic chemistry.

2.2.3.1 Cleavage of benzyl-groups

Benzyl groups (Bn) can be split off in various ways. In addition to catalytic hydrogenations, acidic, and radical deprotections are also described in the literature. Hydrogenolysis is performed as a palladium-catalyzed reaction, usually supported on activated carbon.

Plenty of references describe pressurized reactions with hydrogen under variations of different supplements and solvents. Quantitative conversions are reported for the debenzylation with 10 % Pd/C under H_2-atmosphere at room temperature in ethanol as a solvent over three days.[105,106] Other methods add chlorine-containing compounds which release HCl during the reaction or add HCl directly to result in the amine hydrochlorides in high yields up to 97 %.[107,108] Yakukhnov *et al.* developed a method with Pd on graphitized carbon, adding formic acid and potassium hydroxide under hydrogen atmosphere forming the deprotected species at almost quantitative yields.[109] Yamamoto *et al.* investigated the effect of adding $Nb_2O_{5/}C$ to Pd/C and experienced shorter reaction times.[110] Some studies also deal with the influence of pH on the cleavage of the benzyl group. Accordingly, the reaction rate decreases strongly when the pH of the medium falls below the pK_a of the protected amine.[111–114]

Deprotection can also be performed in the presence of Lewis or Brønsted acids. Watanabe *et al.* reported yields up to 75 % using $AlCl_3$ in benzene or anisole as a solvent. There were also reactions conducted with BBr_3 or BCl_3, but as these methods are designed for special applications on specific molecules, this is not further elaborated here.[115–117] In terms of Brønsted acids, there are examples using

concentrated sulfuric acid and also more mild conditions with *para*-toluene sulfonic acid in toluene with yields up to 88 %.[118,119]

Another approach of debenzylation of amides can be found in radical methods using sodium in ammonia, *N*-bromosuccinimide and AIBN, or similar.[120–122]

2.2.3.2 Cleavage of *tert*-butoxycarbonyl-groups

Boc is typically used as a protecting group for amines in, for example, solid-phase peptide synthesis.[123] Due to the incredible popularity, a variety of deprotection methods exist, which will be briefly discussed in the following.

Removal of the Boc group is usually achieved by the use of strong acids such as trifluoroacetic acid (TFA), HCl/acetic acid, etc.[124,125]

Related to acid cleavage is Lewis acid-catalyzed ammonolysis. Calimsiz *et al.* reported a method using ytterbium salts such as $Yb(OTf)_3$ in combination with $AlMe_3$ or Me_2AlCl which produces up to 91 % yield in 60 min.[126]

A milder method was reported by Stafford *et al.* with a highly selective protocol for the deprotection of Boc-protected amides and carbamates in 1993. They found that $Mg(ClO_4)_2$ cleaves Boc in acetonitrile and produces high yields up to 99 % at room temperature or 50 °C.[127,128]. A similar method using a magnesium salt was published by Wei *et al.* They described a method using $Mg(OMe)_2$ in methanol for the deprotection in yields up to 90 % at room temperature.[129]

Boc cleavage can also be achieved using trimethylsilyl trifluoromethanesulfonate in dichloromethane or under reflux with NaN_3 and NH_4Cl in a methanol/water mixture.[130,131]

Although the use of microwave-assisted deprotection has been investigated for a long time and was published by Siro *et al.* in combination with silica gel in 1998, this method is still being developed today.[132] More recent publications use bases such as $K_3PO_4 \cdot H_2O$ in methanol under microwave irradiation. However, the reaction also

proceeds without the influence of a microwave heating the reaction mixture to reflux. Both ways deliver high yields up to 96 % in 15 min.[133] Microwave irradiation also was found to speed up the reaction in the case of the method using ytterbium salts described earlier.[126]

2.2.3.3 Cleavage of trimethylsilyl-groups

Similar to the deprotection of Boc, TMS-groups can be cleaved under acidic conditions. In contrast to the previously described protection groups, which have so far been applied exclusively to small organic molecules or polypeptides, TMS is known to be used on polyacrylamide. Thus, the polymer-analogous cleavage by 0.5 M HCl in thf is described by Dasgupta *et al.* in 1994.[83]

Of course, in literature, other methods are described. The cleavage product TMS is often captured by fluorides such as Bu_4NF in thf or by H_2SiF_6.[134,135]

The method of methanolysis is described by Sarpe *et al.* using potassium carbonate in dry methanol at 0 °C in quantitative yields.[136] Also, the use of other acids readily cleaves TMS. Bundy *et al.* reported successful acidic hydrolysis with citric acid in methanol at 0 °C.[137]
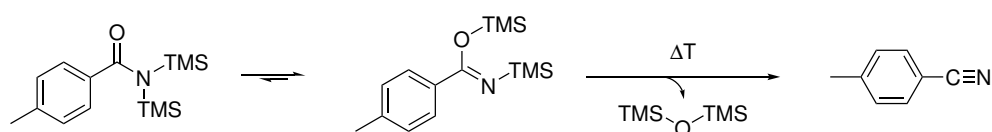
Scheme 9: Thermal decomposition of bis(trimethylsilyl)amide derivatives. Adapted from Hanada *et al.*[138]

All in all, the silyl group is comparatively easy to split off. Also interesting - especially in the context of this work with regard to the polymer analog conversion to PAN - is the thermal cleavage reported by Hanada *et al.* As can be seen in Scheme 9, bis(trimethylsilyl) amide derivatives can be converted directly from the nitrile by thermal elimination of $O(TMS)_2$. However, this reaction was found to produce only 27 % of the nitrile, which can be increased up to 57 % in the presence of a ruthenium catalyst.[138]

2.3 Epoxy polymer matrices

The development of epoxy resins was initiated by the discovery of the oxidation of unsaturated compounds by Prilezhaev in 1909.[139] Generally, epoxides (oxiranes) are three-membered cyclic ethers with a high ring strain of $114\,kJ\,mol^{-1}$.[140] This ring strain is because of the reduced bond angle of $60°$ as can be seen in Figure 2.7 in contrast to the tetrahedral carbon angle of $109.5°$.[141] Also, the C–O bond is weaker compared to a normal carbon-oxygen bond because the atom-orbitals do not overlap as good.[142] As a consequence, epoxides are prone to nucleophilic attacks and base- or acid-catalyzed reactions.[143] An electron-withdrawing group attached to the oxirane (Figure 2.7, right) increases the positive partial charge on the carbon and facilitates a nucleophilic attack.[142] Vice versa are electron-donating groups stabilizing the oxirane group.[144]


Figure 2.7: left: atomic orbital overlap and ring angle strain,[145] right: effect of a electron-withdrawing group.[142]

2.3.1 Epoxidation methods

The oxidation of alkenes is industrial of high interest since epoxides are valuable chemical intermediates. Propylene oxide (PO), for example, is produced on a scale of 11 million tonnes per year in 2020.[146] Traditionally, PO is synthesized by the chlorohydrin process converting propylene with chlorine and water into propene chlorohydrin. By the application of a base, dehydrochlorination occurs, resulting in PO.[147]

A similar approach is pursued with the synthesis of epichlorohydrin (ECH) shown in Scheme 10. Here, propylene is first converted into allylchloride, which reacts then with hypochlorous acid to dichloropropanol. By treatment with a base, the oxygen
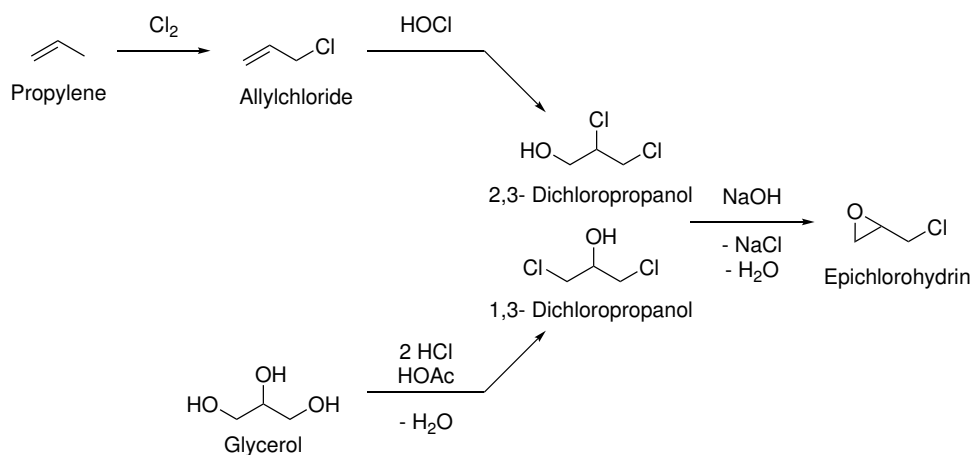
**Scheme 10:** Routes to epichlorohydin starting from propylene or from glycerol.

attacks internally to form the oxirane.[148] Glycerol moved into focus for conversion to ECH as an alternative to oil-based feedstock because of its availability from biofuel processing.[149] Synthesis, in this case, is a two-step procedure starting with the hydrochlorination of glycerin with hydrogen chloride to give dichloropropanol analog to the route starting from propylene.[150]

Besides the epoxidation of small molecules *via* chlorination, there are various approaches to oxidizing double bonds of unsaturated compounds. The Prilezhaev method is widely used and uses peroxycarboxylic acids such as peracetic or performic acid.[139] As can be seen in Scheme 11 on the example of oleic acid, Prilezhaev reactions are two-phase systems: peracids are formed *in situ* in the aqueous phase by the oxidation of a carboxylic acid with hydrogen peroxide. This then forms the oxirane ring in which the electrophilic oxygen is added to the double bond *via* the transition state shown in Scheme 11.[151] Because of its relative easily handling, *meta*-chloroperoxybenzoic acid (*m*CPBA) is often preferred over other peracids. Other peracids, such as performic acids, are unstable and require preparation immediately before use. In contrast to that, *m*CPBA is commercially available and ready for synthesis. In terms of reaction rate, more nucleophilic and higher substituted C=C react faster.[152]

Another interesting epoxidation reaction is the use of potassium peroxymonosulfate, also known as Oxone®, in combination with acetone. Oxone® refers to the triple salt
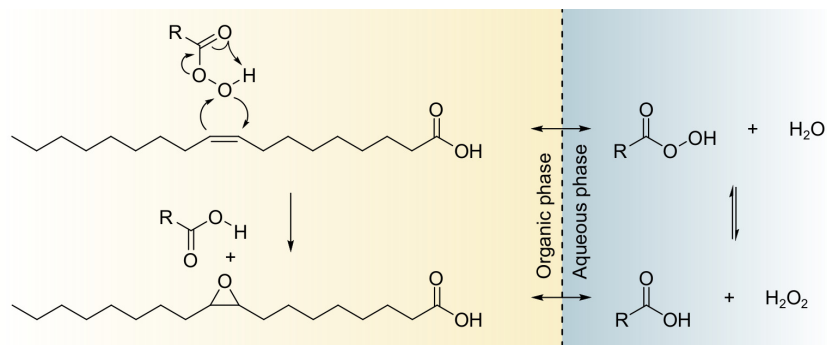
Scheme 11: Epoxidation of oleic acid with acetic acid and hydrogen peroxide. Adapted from Meng *et al.*[151]
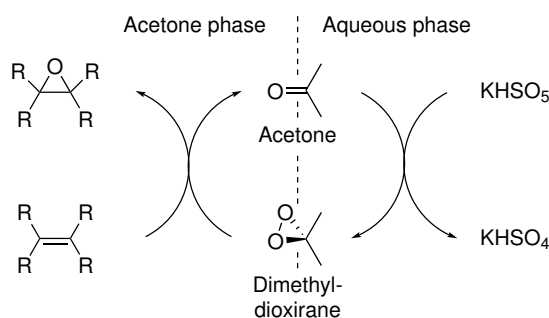
Scheme 12: Epoxidation with potassium peroxymonosulfate oxidizing acetone to dimethyldioxirane forming the active epoxidation spezies.

$2\,KHSO_5 \cdot KHSO_4 \cdot K_2SO_4$. This epoxidation method can be considered fast, catalyst-free, comparable green, and it can be performed at room temperature. As displayed in Scheme 12, during the reaction, dimethyldioxirane (DMDO) is formed from acetone which epoxidizes mainly alkenes. Again, a two-phase system consisting of an aqueous and an acetone phase is formed, which can be limiting in terms of the solubility of the substrate. Also, since the formation and stability of DMDO is dependent on a pH of < 6.5 which makes the addition of a base or some kind of buffer medium necessary to obtain high yields.[153–156]

Enzymatic methods are getting more attention, especially in the synthesis of epoxidized vegetable oils (EVOs), since enzyme-catalyzed reactions are considered green. Chemo-enzymatic processes are performed by adding the enzyme, hydrogen peroxide, and the oil substrate to the reaction mixture. Usually, the enzyme belongs to the family of lipases and is immobilized to enhance stability and reusability.[151,157,158] However, drawbacks are still the low stability of the enzyme since they tend to deactivate if exposed to too high temperatures or hydrogen peroxide concentrations.[159]

There are also metal-catalyzed epoxidation methods that play a major role in organic synthesis. Although, these are only applied little in industry and are therefore described here only for the purpose of completeness. In 1980, Sharpless *et al.* published the first metal-catalyzed epoxidation reaction. The method uses catalytic amounts of titanium (IV) isopropoxide and a chiral ligand, such as diethyl tartrate, to convert allylic alcohol into an enantiomerically pure epoxide. The oxidizing agent is *tert*-butyl hydroperoxide.[160] Another metal-catalyzed method can be found in the Jacobsen-Katsuki epoxidation. In contrast to the Sharpless reaction, a wider range of substrates like *cis*-olefins are accessible. The catalyst is formed by manganese(III) salen-ligands which must be oxidized into the active manganese(V)-species. Depending on the structure of the salen-ligand, the enantioselectivity of the product can be controlled.[161–163]

2.3.2 Epoxy resins

Multifunctional epoxy compounds can be used as thermosetting resins when curing using a suitable curing agent.[164] Because of their versatile applications, epoxy resins have become more and more important over the years. They are used industrially not only for the production of carbon fiber composites but also find their use in electronics coatings, flooring, or as multi-component adhesives.[164–167] In the following, some commercially important resins illustrated in Figure 2.8 will be described in more detail.

Approximately 75 to 90 % of epoxy thermoset used worldwide derive from oil-based diglycidyl ether of bisphenol A (DGEBA), typically cured with amine hardeners.[168,169] This high market share is explained by the excellent mechanical properties and resistance against thermal or chemical effects deriving from the aromatic structure and the interactions it induces.[164,170,171] One downside of pure DGEBA is that it is a solid melting at 43 °C.[169] The Bisphenol F-derivative DGEBF (diglycidyl ether of bisphenol F, Figure 2.8) overcomes this problem with a lower melting point (T_m) and lower viscosity, which is why DGEBA and DGEBF often are used as blends.[172]
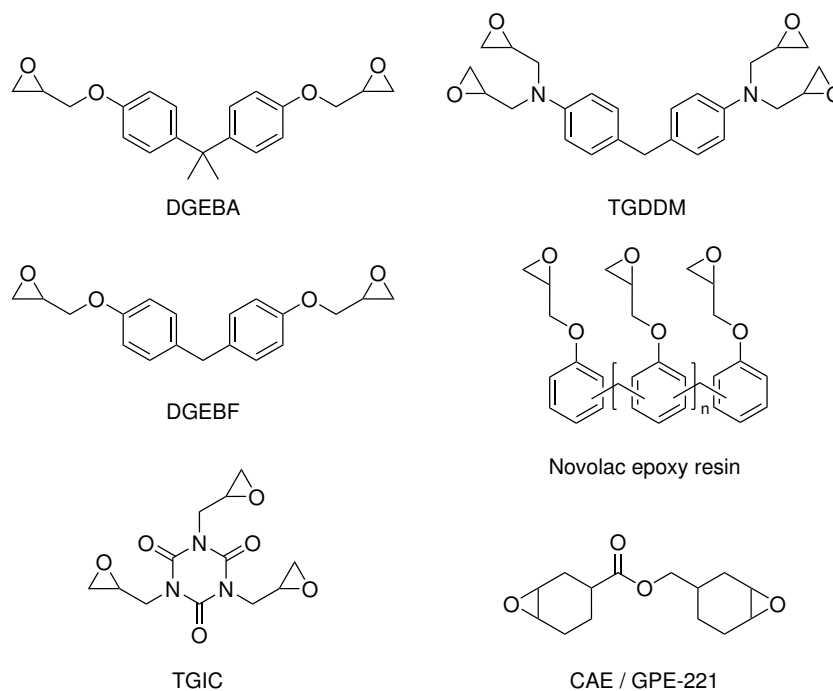
Figure 2.8: Structure of commercially important epoxy resins.

Triglycidyl isocyanurate (TGIC) is a crystalline compound that is used as a powder coating with polyesters for outdoor applications due to its outstanding weatherability.[169,173] *N,N,N',N'*-Tetragylcidyl-4,4'-diaminodiphenylmethane (TGDDM) in combination with the curing agent diaminodiphenyl sulfone (DDS, Section 2.3.3) forms a high-density-cross-linked network with a high glass transition temperature (T_g), excellent mechanical strength, and heat resistance which makes it ideal for high-performance applications in the aerospace industry or military.[169,174]

In contrast to the previously described resins, 3',4'-epoxycyclohexylmethyl-3,4-epoxy-cyclohexanecarboxylate (CAE, cycloaliphatic epoxy) is a fully saturated structure. CAE is usually cured with anhydridic curing agents such as methyltetrahydrophtalic anhydride (MTHPA, Figure 2.9).[175] The aliphatic backbone gives the resin high ultraviolet radiation stability and good thermal resistance, which are crucial properties for structural components in high-temperature applications.[164,175] Novolac epoxy resins are prepared by the condensation of phenolic resins with ECH. Novolac epoxy resins have excellent chemical and thermal resistance due to their high functionality and are used for composite adhesives and matrices.[141,172]
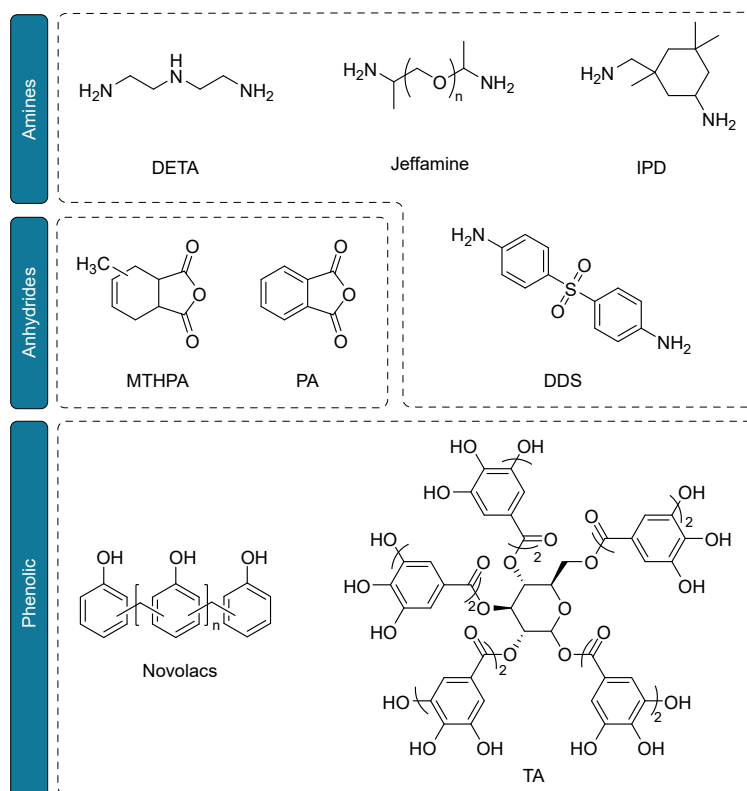
Figure 2.9: Structure of commercially important and/or in this work used hardeners.

2.3.3 Hardeners and curing reactions

Generally, hardeners for curing epoxy resins are aliphatic or phenolic molecules with two or more functional (nucleophilic) groups. The most commonly used are amines, where the number of protons on the nitrogen atoms represents the number of bonds that can be formed.[169] This means $-NH_2$ can react with two epoxy groups while $-NH-$ can only form one bond. Primary amines react twice as fast as secondary amines[176,177] Aliphatic compounds such as diethylene triamine (DETA) or Jeffamine®, cycloaliphatic molecules like isophorone diamine (IPD), or aromatic amines, for example, DDS are used (see Figure 2.9).

Aliphatic amines offer low viscosity and cure already at room temperature but are not suitable for high-temperature applications above 100 °C. They are therefore used in flooring and other coverings and as adhesives. Cycloaliphatic amines offer higher temperature resistance and better mechanical properties but react more slowly. They are used for similar purposes as aliphatic curing agents but are also frequently found in

composite materials. Even better (thermo)mechanical properties with glass transition temperatures above 150 °C can be achieved with aromatic hardeners.[169]

Anhydride hardeners (Figure 2.9) such as MTHPA or phtalic anhydride (PA). Anhydride curing agents react much more slowly and less exothermically than amines, which is why they require longer curing cycles at higher temperatures (200 °C). This makes them easier to process, and they also offer good thermal and mechanical properties and high T_gs. Anhydrides are used for composites, encapsulations, and castings.[169]

Phenolic hardeners such as novolac (Figure 2.9) play a minor role commercially. Since they are mostly solids, they are more difficult to process and require high temperatures for curing. The advantages include durability and high-temperature resistance.[169]

Tannic acid (TA, see Figure 2.9) is currently attracting increased attention in research because it is a polyphenolic, highly functionalized, and nontoxic biomolecule.[178] TA can be extracted *e.g.* from tree bark, nuts, or seeds and is industrially available. The potential of TA as a bio-based hardener has been investigated, and it is possible to reach T_gs as high as 200 °C when used with DGEBA.[178] TA has also been used in combination with EVOs. Qi *et al.* used epoxidized soybean oil as a resin to create a fully bio-based thermoset but only could reach moderate thermal (T_g = 77 °C) and mechanical properties such as a storage modulus of 1103 MPa.[179] Most of the studies try to overcome the limitations coming from low compatibility of the solid TA when curing. There are approaches using solvents such as ethanol to dissolve TA homogeneously in the resin. However, this leads to major drawbacks since solvents being present in the mixture have a negative impact on the final material properties of the epoxy. This is why the solvent needs to be removed, which is a challenging task due to the high viscosity of the resins.[178–182]

Scheme 13 gives an overview of the curing mechanisms observed with different types of hardeners. Primary amines attack at the less substituted oxirane carbon (Scheme 13a) to form a secondary amine and a secondary alcohol following a S_N2 mechanism. A transition state is formed in which the C–O bond is weakened because

(a)

(b)

(c)
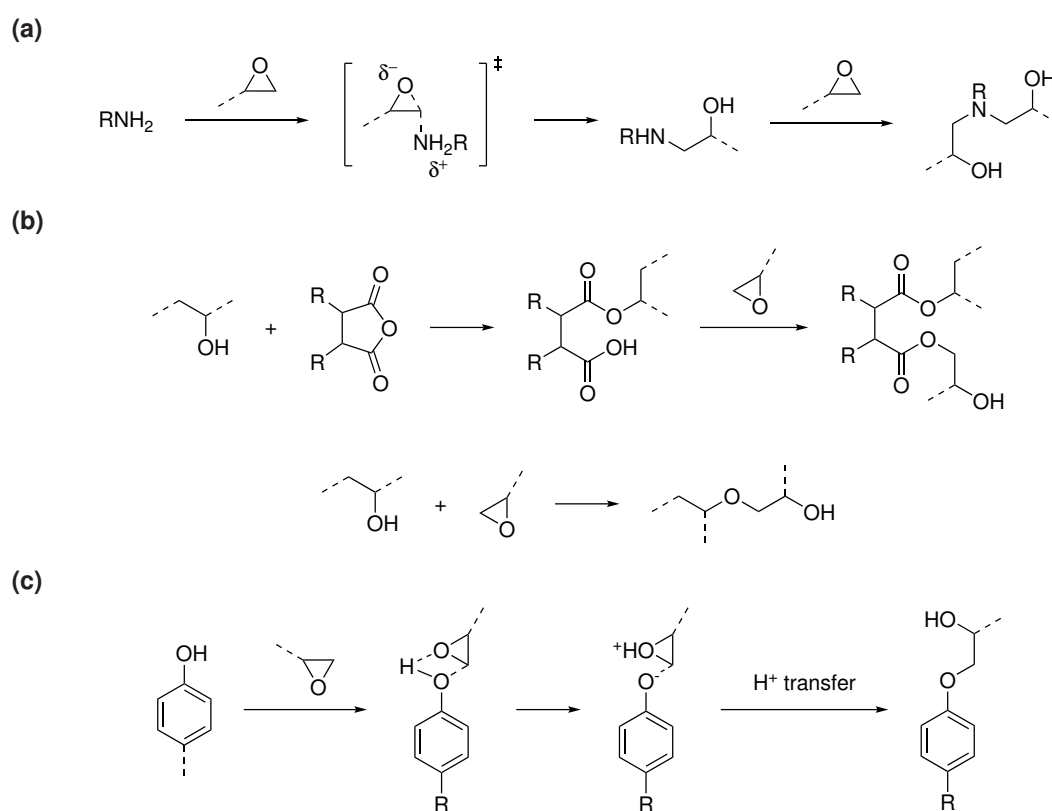
Scheme 13: Curing mechanisms of a) amines,[169] b) anhydrides,[169] and c) phenols with epoxy groups.[179]

the atomic orbitals do not overlap completely. The secondary amine can then react with a further epoxy group to give a tertiary amine. The attack of a hydroxy-group which would result in a ether-bond-formation is very unfavored and only observed when all amino groups have reacted into tertiary amines.[142,183]

However, coming back to the epoxy compounds, there are concerns related to DGEBA and its impact on organisms and ecosystems. Both starting materials - bisphenol A (BPA) and ECH - have been classified as hazardous to health or endocrine disruptors.[184–189] As a result, there is a great interest in finding alternative compounds for use in epoxy resins.

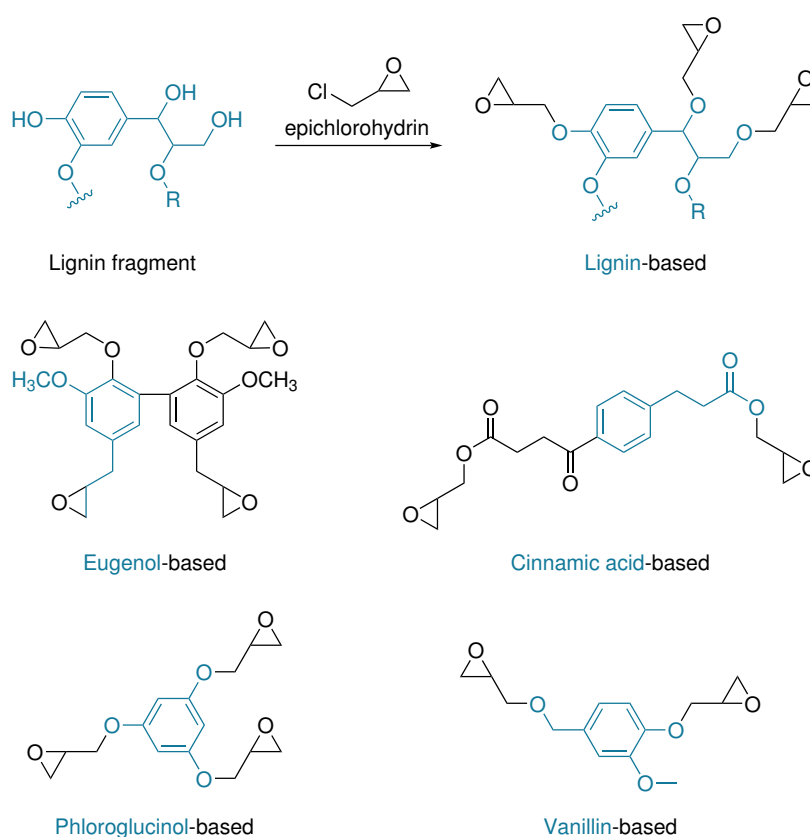## 2.3.4 Alternative feedstocks for epoxy polymer matrices

Figure 2.10: Exemplary reaction for the introduction of epoxide groups with ECH as reagent. Structures of some phenolic bio-based developments. In blue: fundamental biomolecule.
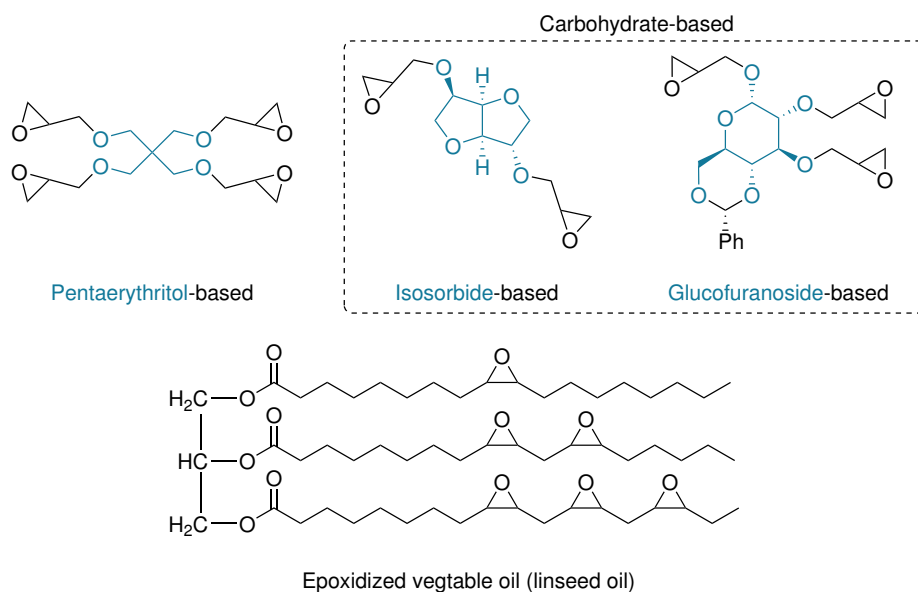
Epoxidized vegtable oil (linseed oil)

Figure 2.11: Structures of epoxy resins starting from biobased aliphatic raw materials pentaerythritol or carbohydrates (sugars). Ph = phenyl. Bottom: Exemplary reaction for the introduction of epoxide groups with epichlorohydrin as reagent.

A large part of the research is focused on the identification of suitable natural products as building blocks for epoxy resins. Among the most promising are phenolic structures such as eugenol, phloroglucinol, cinnamic acid, or fragments derived from lignin such as vanillin because of their aromaticity and structural similarity to DGEBA (Figure 2.10).[190] Phloroglucinol occurs naturally in plants as a secondary metabolite.[191] Compounds of this type are reacted with ECH to introduce the required epoxy groups.[192–196] In other approaches, aliphatic polyols such as sugar, pentaerythritol, or glycerol are used, which again are used in combination with ECH to form epoxy resins (Figure 2.11).[197–200] The main disadvantage of these alternatives is the use of ECH and the associated risks already mentioned.

For some time, attempts have been made to produce ECH, which is normally synthesized from fossil raw materials from biobased glycerol. This optimizes the CO_2 balance but not the environmental impact.[150,201] In addition, due to the aforementioned structural disadvantages, resins made from the saturated hydrocarbons just described cannot offer the same thermal and mechanical properties as those based on aromatics. This is clearly shown by the T_gs described in the literature: While DGEBA in combination with IPD reaches a T_g of 114 °C[200], the sugar-based
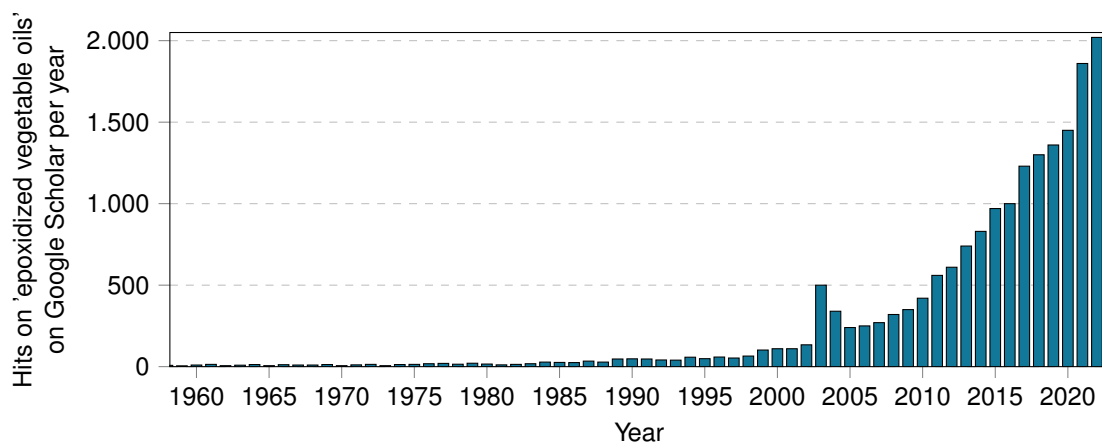
Figure 2.12: Number of hits for the keywords "Epoxidized Vegetable Oils" on Google Scholar broken down by year.

isosorbide epoxy (see Figure 2.11) reaches a T_g of 73 °C.[199] A chemically different approach is taken in the use of unsaturated vegetable oils (Figure 2.11, bottom). Here, the double bonds embedded in the long hydrocarbon chains are epoxidized by using peracids. However, the disadvantage of these resins is reduced reactivity during the curing process and the low glass transition temperatures that can be observed in such systems.[202–204]

As can be seen from the development of search results on Google Scholar concerning 'epoxidized vegetable oils' over the last decades (Figure 2.12), epoxidation of unsaturated plant-based oils more and more came into the focus of research. Vegetable oils and their derivatives are abundant, renewable and find various applications as lubricants in cosmetics or pharmaceuticals.[205] Due to structural drawbacks of triglycerides, such as the high flexibility of the aliphatic chains and the lack of rigid substructures, especially polyunsaturated triglycerides, and fatty acids have been identified as feedstock for bio-based epoxy thermoset alternatives. A high double-bond content can be found in soybean oil, canola oil, or linseed oil.[202–204,206,207] Epoxidation reactions of vegetable oils are usually performed by the use of peracids. A high number of double bonds allows the synthesis of epoxy resins with high epoxy content, which is why epoxidized linseed oil (ELO, see figure Figure 2.11) is one of the best candidates to obtain densely cross-linked networks.[208,209] Additional, hardeners with a rigid structure such as anhydrides shown in Figure 2.9 are beneficial to obtain stiff thermoset.[210–212] The combination of EVOs and TA was studied.[179,180]

36

Qi *et al.* cured epoxidized soybean oil with tannic acid and found a T_g of 77 °C and a storage modulus of 1103 MPa at 25 °C.[179] The greatest difficulty when using TA as a hardener is to obtain a homogeneous distribution of the solid TA in the resin. There are attempts with ethanol to dissolve TA in the resin, but solvents are then difficult to remove, which is necessary to obtain defect-free cured resins.[188,213–215] Also, high curing temperatures are needed to cure the thermoset.[178–180,216]

Apart from the approaches starting from biomolecules, there are some publications on ester-containing resins. Endo *et al.* describe a whole series of epoxy resins for application in electronic components or optical materials.[217] The epoxy function is introduced *via* an acid-catalyzed esterification reaction to anhydrides in the form of allyl groups which are then epoxidized.
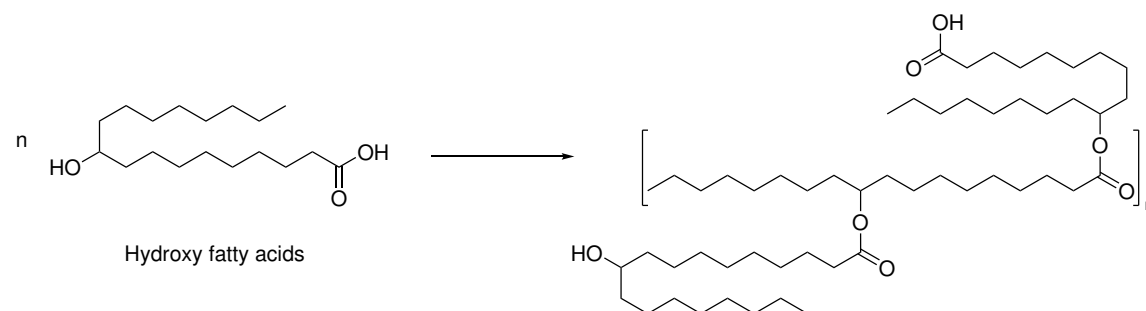
2.4 Estolides

Estolides belong to a class of biobased substances that are synthesized from fatty acids and have unique chemical and physical properties. They are short-chain oligo-fatty acids and are synthesized by condensation of one or more fatty acids. Compared to conventional lubricants, their properties include high molecular weight with high viscosity and excellent lubricity. Since estolides are derived from fatty acids, they are renewable and also biodegradable due to the ester bonds, which makes them alternatives to conventional petroleum-based lubricants. Another field of application is as a base oil in the cosmetics industry. As can be seen in Scheme 14, estolides can be synthesized from hydroxy fatty acid containing triglycerides (or tri-acylglyceride, TAG) (Scheme 14a) or from free fatty acids bearing hydroxy groups (Scheme 14b).[218,219]

TAGs with hydroxy groups can be found in castor oil (from the seeds of *Ricinus communis*). Castor oil contains about 90 % ricinoleic acid (12-hydroxy-9-*cis*-octadecanoic acid), which makes it ideal for the use in the synthesis of fully-capped triglyceride estolides with saturated fatty acids such as dodecanoic acid.[221] Another source of

(a)

Triglyceride

+

Capping fatty acid

Mono-capped triglyceride estolides

Fully-capped triglyceride estolides

(b)
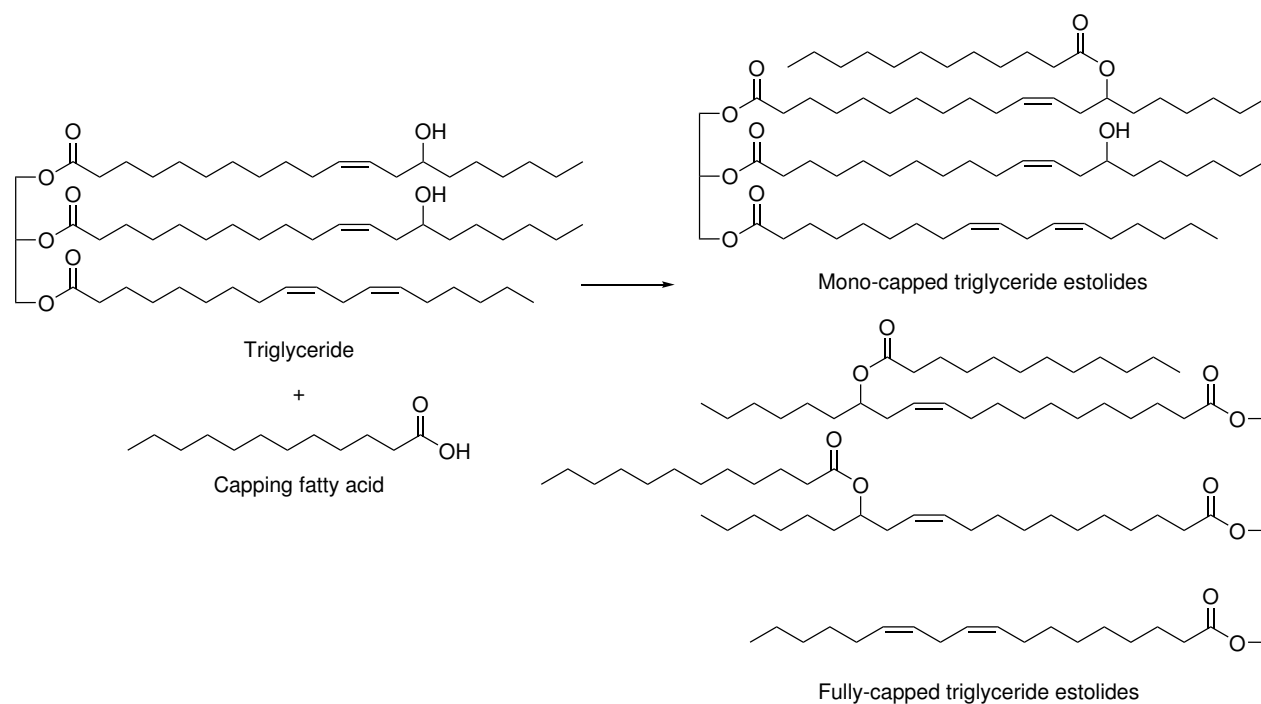
Hydroxy fatty acids

Scheme 14: a) Estolides from triglycerides, and b) from fatty acids. Figure adapted from Chen *et al.*[220]

hydroxy-containing TAGs could be identified in Lesquerella oil, which can be obtained from *Lesquerella fendleri* seed which is an oil crop native to the desert southwestern United States.[218] In the present work, estolide synthesis was performed following the scheme in Scheme 14b from 12-hydroxystearic acid. This saturated and hydroxylated fatty acid can be gained by a catalytic hydration of the already-mentioned ricinoleic acid.[222] Current research by the group of Brück allows the synthesis of the structurally related 10-hydroxystearic acid by enzymatic catalysis from monounsaturated oleic acid, which could open up another source of fatty acids for estolide synthesis in the future.[223]

During the oligomerization reaction of estolide synthesis, the hydroxyl groups of the fatty acids are esterified with a carboxyl group of another fatty acid with the elimination of water. In contrast to classical polycondensation reactions, which are often catalyzed by titanium alkoxides, a typical synthesis route for the condensation reaction of estolides is by esterification at temperatures around 200 °C, sometimes in the presence of a catalyst such as sulfuric acid.[218,224]

In the case of the oligomerization of bifunctional free fatty acids as shown in Scheme 14b, the reaction follows the principles of a step-growth polymerization in which the degree of polymerization $\bar{X}_n$ can be described by the *Carothers* equation. In the simplest scenario, which is the case of bifunctional fatty acids as monomers (AB-monomer), the equation is as follows:[225]

$$\bar{X}_n = \frac{1}{1-p}$$

with p = conversion.

Figure 2.13 shows the relationship between X_n and p graphically. Only at very high conversion rates are appreciably high degrees of polymerization achieved. At a monomer conversion of $p = 0.5$, X_n is just 2, and a chain length of 20 repeating units is reached at 95 %.
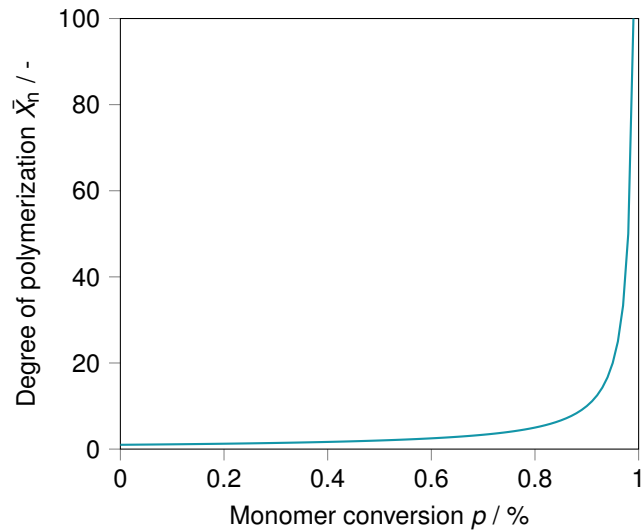
Figure 2.13: Correlation between monomer conversion p and degree of polymerization X_n according to Carothers for AB-monomers.

With regard to estolides, the term degree of polymerization is used less frequently than the estolide number EN, which is defined by the average number of fatty acids attached to the base molecule (fatty acid or TAG).[226] In the case of estolides built of one kind of fatty acid, X_n and EN can be used equivalently.

For application as a bio-lubricant, the viscosity of course is of special interest. Interestingly, kinematic viscosities in the context of estolides still are given in the unit Stokes, which is not SI-compliant (1 St = 10^{-4} m^2/s). In addition to viscosity, thermal properties are of interest for the use as a lubricant, such as low-temperature flow properties. The phase transitions of lubricants are not usually indicated by conventional thermal parameters such as the melting point. For the application, the cloud point and pour point are of interest. The cloud point refers to the temperature at which the lower molecular weight fractions (e.g., monomer residues) begin to crystallize and could impair the effectiveness of oil filters, for example. Below the pour point, the viscosity increases, which affects the flow properties and immobilizes the oil.[220]

3 Aim

This thesis studies the preparation of polymeric compounds starting from biomolecules. Thematically, the two significant areas address the greener synthesis of carbon fiber composites (Figure 3.1). The thesis is subject to the preparation of both components of these composite materials, carbon fiber or its precursor polyacrylonitrile and epoxy resin matrices. Therefore, both of these materials are to be optimized with respect to the biobased carbon content by using biogenic starting materials. The last part investigates the synthesis of fatty acid-based lubricants (estolides). The starting materials in all the studied areas are of natural origin and in many cases can be obtained from vegetable oils. Accordingly, the work is divided into three subchapters:

- Monomer synthesis and controlled polymerization of Michael monomers for the polymer analogous conversion to polyacrylonitrile
- Investigations on biobased epoxy thermoset based on epoxidized linseed oil, tannic acid, or sorbic acid
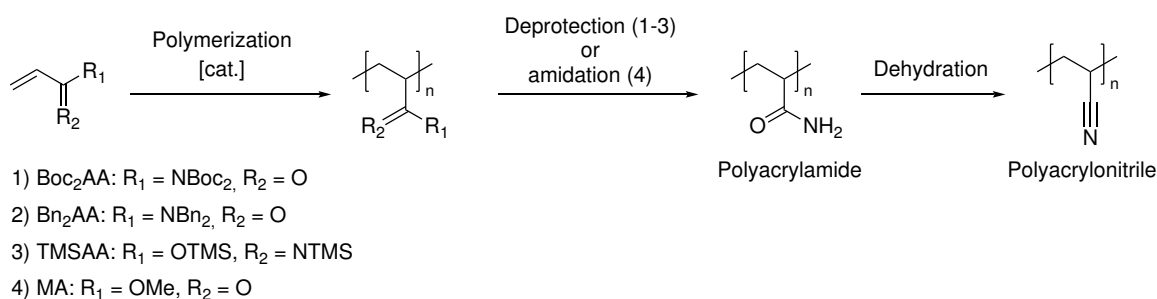- Investigations on fatty acid-based estolides
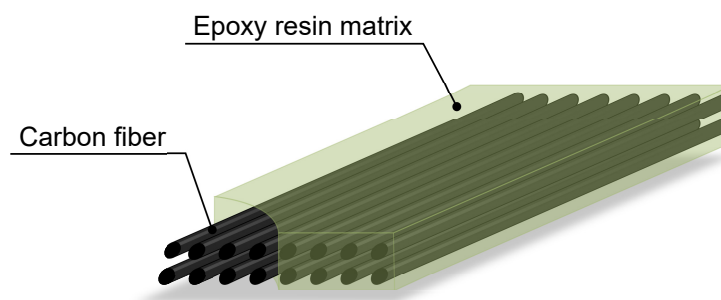
Figure 3.1: Schematic representation of a carbon fiber composite.

3.1 Innovative precursors for carbon fiber production

There are approaches towards carbon fibers with biobased carbon content using acrylonitrile from biomolecules or crayon as precursor material. In the case of ACN as a monomer, however, there are significant drawbacks concerning the toxicity of the monomer and also in the polymerization which is up to now performed industrially by free radical methods.[16,20,227] Polymerization of Michael monomers by rare earth metal complexes is widely studied and can be controlled to a high degree resulting in tuneable molecular weights and weight distribution. This advantage shall be transferred to a selection of monomers that are derivatives of acrylamide (Boc_2AA, Bn_2AA, TMSAA, Scheme 15) and methyl acrylate.

1) Boc_2AA: R_1 = $NBoc_2$, R_2 = O
2) Bn_2AA: R_1 = NBn_2, R_2 = O
3) TMSAA: R_1 = OTMS, R_2 = NTMS
4) MA: R_1 = OMe, R_2 = O

Scheme 15: Polymer analogous synthesis pathway to polyacrylonitrile starting from the polymerization of Michael monomers.

All acrylamide derivatives are known to be radically polymerized; catalytic methods are not reported up to now. To obtain polyacrylonitrile, polymer analogous deprotection of the acrylamides should lead to polyacrylamide. For this purpose, a variety of methods for cleavage exist for each of the protective groups known from organic chemistry, but these have never been tested on polymers. As illustrated in Scheme 15, polyacrylamide is also accessible from polymethyl acrylate in addition to the protected acrylamide derivatives. Here, the proof-of-principle was already demonstrated in a previous study. PMA can be converted into polyacrylamide in a pressurized reaction with ammonia. Similarly, it has already been shown that polyacrylonitrile is accessible from PAA *via* a dehydration reaction.[59,60] Also, the existing synthetic route to polyacrylonitrile for polymethyl acrylate will be scaled up to a multigram scale.

3.2 Biobased based epoxy thermoset

Epoxy resins are widely used and find applications in various industries. For sustainability reasons, greener alternatives from renewable resources are in high demand. Unsaturated vegetable oils have been in the focus of research for some time, but conventional, fossil-based hardeners are still often used here.

To address this issue, this work will deal with advancing epoxy resins based on unsaturated fatty acids or triglycerides. Part of the research will be to develop a fully biobased epoxy resin system from epoxidized linseed oil and tannic acid (Scheme 16). For this purpose, samples of different mixing ratios will be investigated with regard to their (thermo)mechanical properties of the cured thermoset and compared with standard systems. The aim here is to achieve the highest possible characteristic values in terms of temperature resistance and mechanical properties.
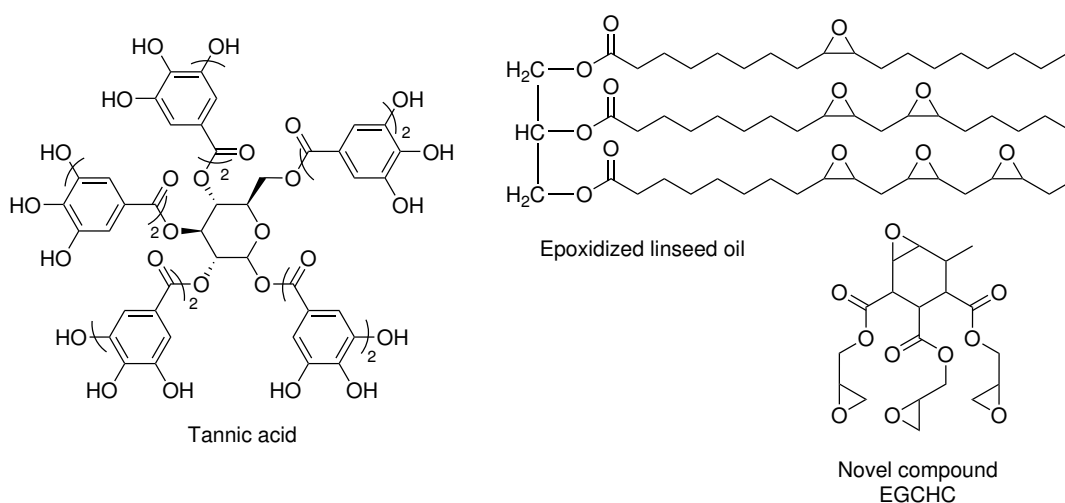
Scheme 16: Molecules used for the investigations on greener, high-performing epoxy resins.

Using sorbic acid as a model substrate for conjugated unsaturated fatty acids, a novel epoxy resin will be synthesized and characterized in the further course (Scheme 16). In a four-step synthesis in which a six-membered ring is introduced by a Diels-Alder reaction and further double bonds are introduced by esterification with allyl alcohol, a previously unknown molecule is developed by epoxidation of these. The reactivity of this epoxy compound is characterized in combination with conventional amine

hardeners, which allows comparison of the thermal and mechanical properties to standard, high-performance resins.

3.3 Estolides from fatty acids

To investigate the use of unsaturated fatty acids for the synthesis of biobased lubricants (estolides), 9- and 10-hydroxystearic acid is synthesized and oligomerized as model molecules for enzymatically accessible 12-hydroxystearic acid in the last part of the work (Scheme 17). For this purpose, the monounsaturated oleic acid is first converted into its methyl ester, hydroxylated, and then thermally esterified under the influence of a catalyst to short-chain oligomers. The influence of the degree of polymerization on the viscosity and thermal properties is a central part of the investigations, along with the possibilities for purifying the estolides.
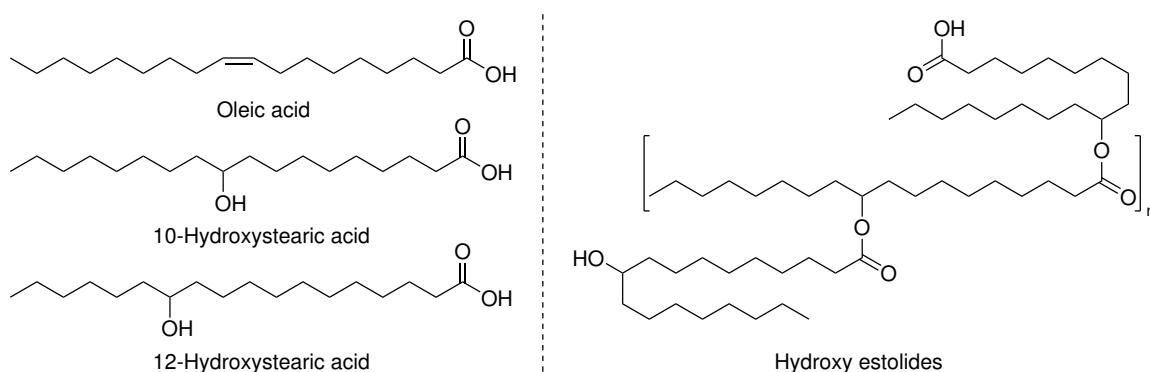
Scheme 17: Fatty acids for the synthesis of hydroxy estolides.

4 Results

4.1 Synthesis and polymerization of protected acrylamide derivatives

4.1.1 *N,N'*-Dibenzyl acrylamide

Bn$_2$AA was synthesized according to literature from acryloyl chloride and dibenzyl-amine.[76] In the ^{1}H-NMR-spectrum of the product (Figure 4.1) all relevant signals can be found. The multiplet from 7.43 to 7.24 ppm represents, in combination with the multiplet at 7.18 ppm, the aromatic protons of the phenyl rings. The vinyl-protons can be found as doublets of doublets at 6.62, 6.50, and 5.74 ppm. In addition, two singlets, each with an integral of 2 in the upfield, can be seen, which do not couple with other signals. These represent the CH$_2$-protons of the benzyl-groups, which form their own spin system and thus do not couple with other protons. The ^{1}H-NMR data were in agreement with the literature.[76]

In order to optimize the polymerization of Bn$_2$AA regarding molar weight distribution and initiator efficiency (IE), different REM-catalysts (Figure 4.2) were tested. To begin with, tris-cyclopentadienyl (Cp) REM complexes (Cp$_3$Ln, Ia, Ib) were used for the polymerization of Bn$_2$AA since they are synthesized comparable easily from sodium cyclopentadienyl (NaCp) and the REM chlorides.[228]
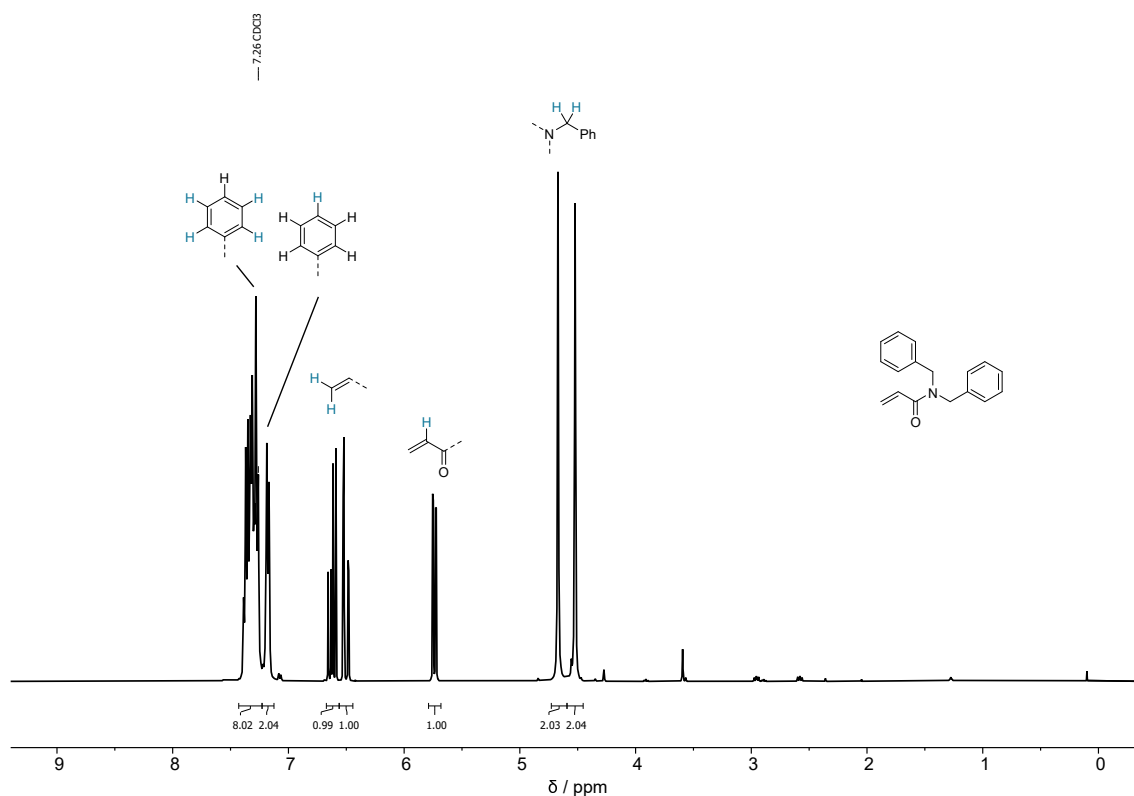
Figure 4.1: ^{1}H-NMR in chloroform-d of Bn$_2$AA.

Table 4.1: Polymerization of Bn$_2$AA with different catalysts (see Figure 4.2).

#	Catalyst	$M_{n,theo}$[a] / kg mol^{-1}	$M_{n,abs}$[b]/ kg mol^{-1}	$Đ$[c]	IE[d] / %
1	Ia	50.5	866	2.3	6
2	II	53.5	72.4	1.57	74
3	IIIa	51.3	58.6	1.22	87
4	IV	50.7	77.5	1.12	65
5	IIIb	49.4	112.4	1.02	44
6	Ib	66.2	155	1.19	43

[Bn$_2$AA]:[Cat] = 200:1 in toluene at room temperature.
[a] $M_{n,theo}$ = M × (([M]/[Cat]) × conversion),
[b] determined by SEC-GPC in thf, dn/dc = 0.195 mL g^{-1},
[c] $M_{w,abs}/M_{n,abs}$,
[d] determined by ^{1}H-NMR, IE = $M_{n,theo}/M_{n,abs}$ at the end of the reaction.
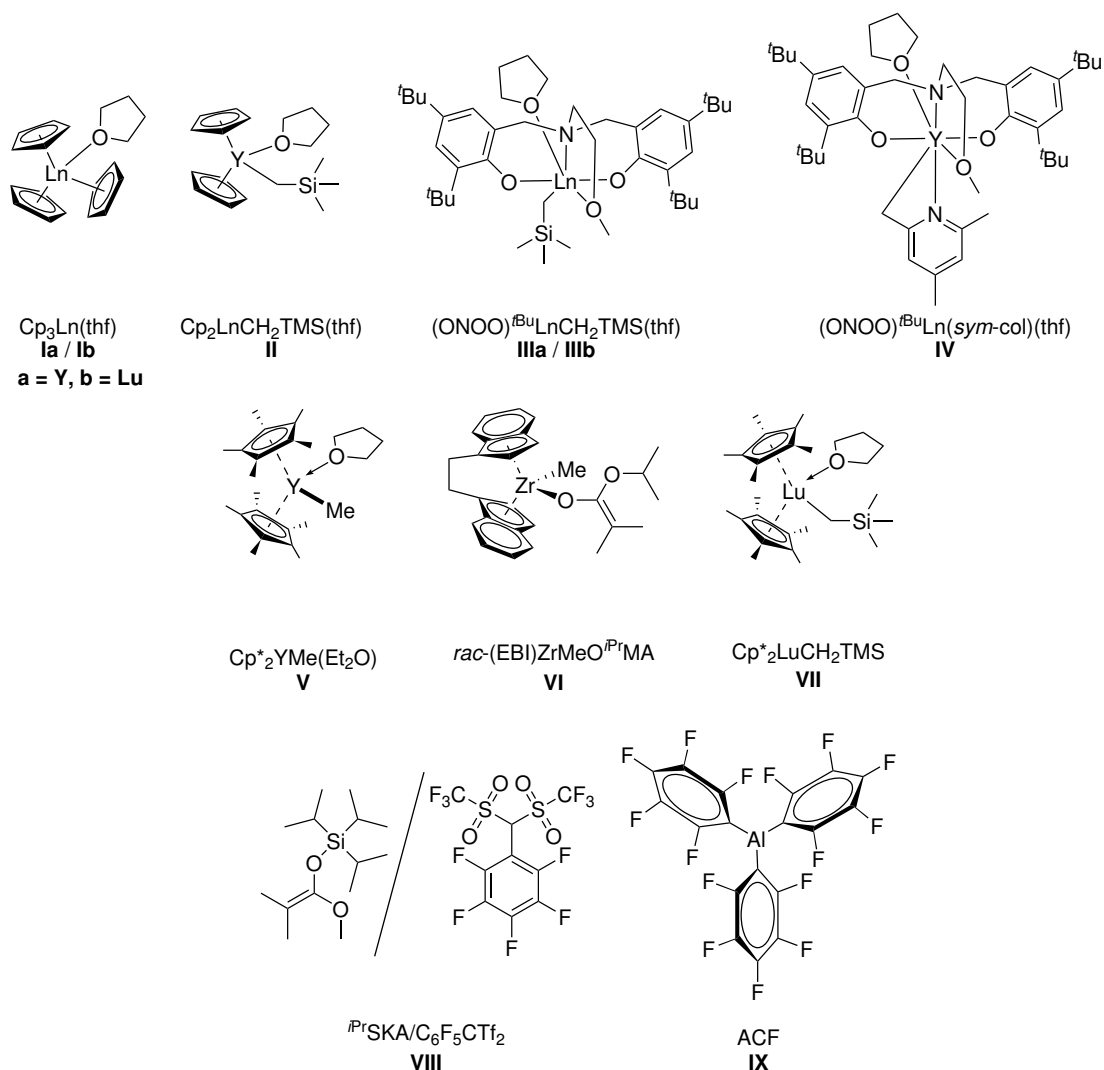
Figure 4.2: Catalysts used for the Polymerization of Bn_2AA. a: Ln = Y, b: Ln = Lu.

As can be seen in Figure 4.3, the acrylic signals of the monomer vanish throughout the polymerization reaction, and the for polymers typical broad signals of the backbone CH and CH_2 evolve in the aliphatic region. Also, the signal of the CH_2 linking group between the nitrogen and the phenyl groups broadens. The disappearing acrylic signals were used for conversion determination.

Tris-(cyclopentadienyl)-yttrium ($Cp_3Y(thf)$, Ia) is capable of forming poly(*N*,*N*'-dibenzyl acrylamide) (PBn_2AA) but leads to a comparable high *Đ* of 2.3 and a low IE of 6 %. This rather uncontrolled polymerization behavior can be attributed to the initiation process. Cp_3Ln complexes initiate polymerization reactions by a nucleophilic transfer of one Cp-group to the monomer. This becomes possible due to the small
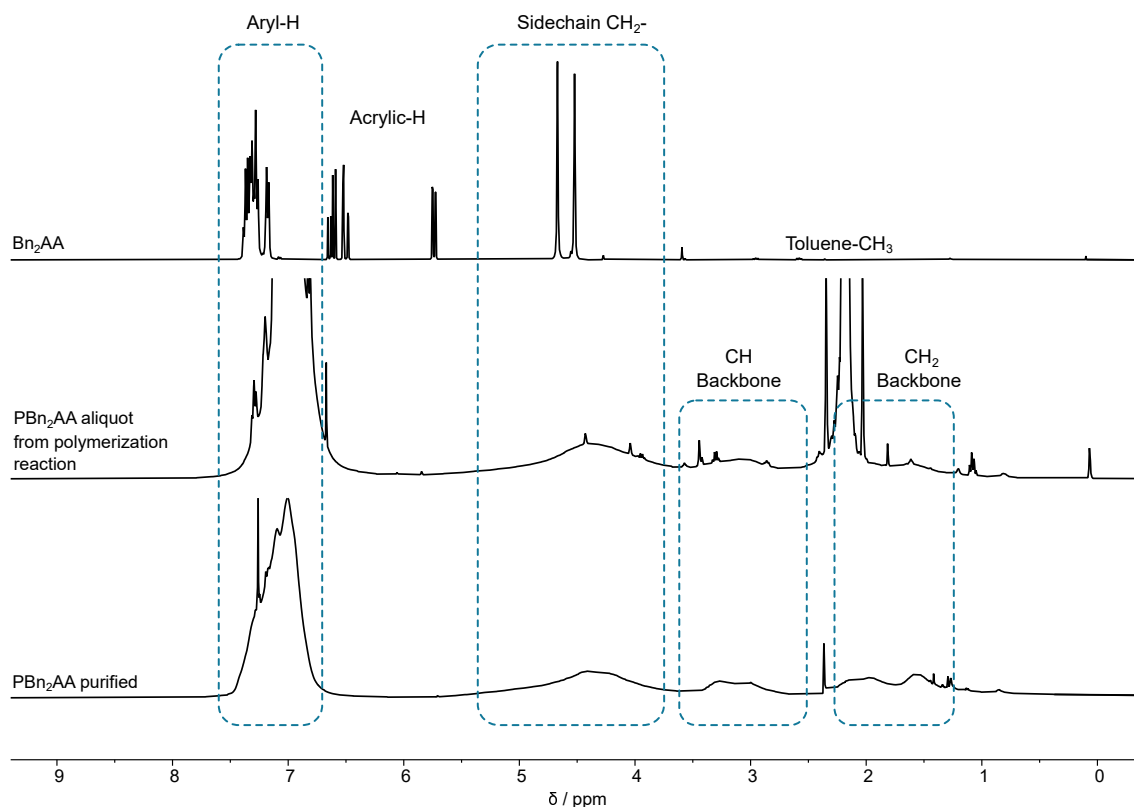
Figure 4.3: ^{1}H-NMR spectra of pure Bn$_2$AA (top), an aliquot taken from the reaction mixture (mid), and purified PBn$_2$AA (bottom) in chloroform-d.

ionic radii of late trivalent rare earth metal complexes in combination with sterically demanding Cp ligands. Rieger *et al.* assumed that due to the crowded ligand sphere, not all Cp ligands could coordinate, forming a η^5 bond and weakening the coordination of one Cp ligand, switching its binding motif to η^3 or η^1. This then allows a strongly coordinating monomer to enter the coordination sphere and allows the initiating nucleophilic transfer by the nucleophilic η^1-bonded Cp ligand.[229] In order to improve the IE, the initiating group was changed to the weaker bonded and thus more nucleophilic CH$_2$TMS (TMS = trimethylsilyl) while leaving the metal center and ligand sphere unchanged. This initiator increases the IE to 74 % while narrowing the Đ to 1.57 through the change from Ia to (Cp$_2$YCH$_2$TMS(thf)) (II). Since the change of the initiating group led to a more controlled reaction, the effect of the ligand needs to be investigated. 2-Methoxyethylamino-bis(phenolate)-yttrium CH$_2$TMS(thf) complexes [(ONOO)^{tBu}YCH$_2$TMS(thf)] (IIIa) are known to polymerize derivatives of acrylamide such as *N,N'*-dimethyl acrylamide.[102] The (ONOO)^{tBu}-ligand covers only

about a quarter of the ligand sphere whereas Cp_3-ligands demand approximately two-thirds leaving more space for the monomer to coordinate.[102] This allows catalyst IIIa to control the reaction better and enhances both $Đ$ (1.22) and IE (87 %). Also reported by Rieger *et al.* is the C–H bond activation of IIIa with *sym*-col to result in [(ONOO)^{tBu}Y(*sym*–col)(thf)] (IV) *via* a σ-bond metathesis.[102] Polymerization with IV led to a decreased IE of 65 % while $Đ$ was further narrowed to 1.12. The lower IE of IV compared to IIIa arises from the η^3-(*C,C,N*)-aza-allylic binding of *sym*-col to the metal center which makes the initiator more difficult to split off and thus less nucleophilic compared to CH_2TMS, however still more active than Cp.[102] Further improvements in polymerization control can be achieved by changing the central metal to lutetium. Lu-catalysts generally show a considerably lower IE than their yttrium pendant. The 4f-electrons of lutetium do not contribute to the binding valence orbitals. For this reason, lutetium and yttrium can be assumed to be isoelectronic to each other. By means of higher Lewis acidity and electrophilicity, lutetium has a stronger bond to the nucleophilic initiator CH_2TMS, lowering the IE and polarizing the coordinating monomer more than yttrium. The stronger polarization of the coordinating monomer leads to faster chain propagation.[102] [(ONOO)^{tBu}LuCH$_2$TMS(thf)] (IIIb) leads to a very narrow $Đ$ of 1.02.

4.1.2 Deprotection of PBn$_2$AA

After successful polymerization, polymer analog deprotection of the amide group was investigated. The first experiment was the classical reductive hydrogenation catalyzed by palladium on activated carbon with gaseous hydrogen under pressure. For this purpose, a solution of pBn$_2$AA (100 kg mol^{-1}) in THF was prepared, and the reaction was stirred for six days at 60 °C and an overpressure of 50 bar hydrogen. After evaluation of the ^{1}H-NMR, no conversion could be detected. To exclude the possibility that the high molar masses impede the reaction, short-chain PBn$_2$AA was prepared by free radical polymerization using AIBN as an initiator (Table 4.2). The catalytic hydrogenation was repeated with these low molecular weight polymers, but again without success.

Table 4.2: Free radical polymerization of Bn$_2$AA for PAM conversion to PAA.

#	V(solv.) / mL	Time d	$M_{n,abs}$[b] / kg mol^{-1}	Đ[c]
1[c]	0.77	1	2.8	2.4
2[d]	1.0	2	8.0	1.6

Reaction in toluene at 65 °C[Bn$_2$AA]:[AIBN] = 5:1.
[a] Determined by SEC-GPC in thf, $dn/dc = 0.195$ mL g^{-1}
[b] $M_{w,abs}/M_{n,abs}$,
[c] 0.34 g Bn$_2$AA,
[d] 0.68 g Bn$_2$AA.

A significant problem in the reaction process could also be the dramatic change in the polarity or solubility of PBn$_2$AA and the product PAA. While PBn$_2$AA dissolves in toluene or similar nonpolar solvents, PAA is soluble only in strongly polar media such as water or DMSO. To investigate this, PBn$_2$AA was dissolved in toluene and water as a two-phase mixture, and the Adams catalyst (Pt$_2$O·H$_2$O) and pressurized with H$_2$ (50 bar). After 3 d reaction time at 60 °C, the phases are separated, and unreacted PBn2AA could be precipitated from the toluene phase with pentane. However, the aqueous phase did not contain any polymer.

Another tested modification of the hydrogenation is with Pd/C and acetic acid instead of gaseous H$_2$ as a hydride source. For this, PBn$_2$AA was dissolved in as little THF as possible, mixed with acetic acid, and suspended with the catalyst. Again, stirring was carried out at 60 °C for 3 d, and then the reaction solution was precipitated from pentane, but again only unreacted PBn$_2$AA could be isolated.

Also, in the acidic but without metal catalysts are the methods using TFA or trifluoromethanesulfonic acid (TfOH). In the case of TFA, the polymer is dissolved in chloroform, and TFA and acetic acid are added. The reaction solution is stirred under reflux for 7 d. After neutralization and addition of cyclohexane, a precipitate is formed, which could be identified as PBn$_2$AA. For the deprotection experiment with TfOH, the polymer is dissolved in toluene, and the acid is added. The mixture is stirred at 65 °C for 3 d. Upon extraction with water, the PBn$_2$AA reactant precipitates without evidence of the deprotection product.

As further attempts to cleave the benzyl groups, a radical approach with *N*-bromo-succinimide (NBS) and AIBN was performed. Here, the CH_2 groups between the amide and phenyl rings should first be brominated and then hydrolyzed and cleaved by the addition of water. In the ^{1}H-NMR, no signals of PAA or the brominated species could be assigned, which leads to the assumption that the reaction already failed during bromination by NBS.

In summary, the polymer analogous cleavage of benzyl groups was unsuccessful. Despite the many methods described for smaller organic molecules, none could be transferred to the polymer. Several possible reasons can be listed for this. Firstly, the benzyl groups are sterically demanding, meaning the surface reaction cannot occur with heterogeneously catalyzed methods using Pd/C, for example. In addition, the polarity change from reactant to the hypothetical product described above could be more optimal since this would require two-phase solvent systems, and the polymer would have to switch between phases during the reaction.

4.1.3 *N,N'*-Di(*tert*-butoxycarbonyl) acrylamide

Synthesis of Boc_2AA was conducted according to literature from acrylamide and di-*tert*-butoxycarbonate. The ^{1}H-NMR spectrum of the Boc-protected acrylamide (Figure 4.4) shows, in addition to the signals of the vinylic protons at 6.98, 6.48, and 5.85 ppm, the aliphatic signal of the *tert*-butyl protons (1.52 ppm). The two *tert*-butyl groups contain a total of 18 protons in six non-coupling methyl groups. Spectroscopic data are consistent with the literature.[81]

The free radical polymerization of Boc_2AA has been previously studied in the literature.[81] Here, the catalytic (REM-)GTP polymerization will now be investigated. For this purpose, some of the catalysts applied to the other monomers were tested to Boc_2AA, and the conversion, as well as the molecular weight and molar mass distribution, were observed. All subsequent polymerizations were carried out with a monomer-to-catalyst ratio of 200:1 in toluene and at room temperature unless otherwise noted.
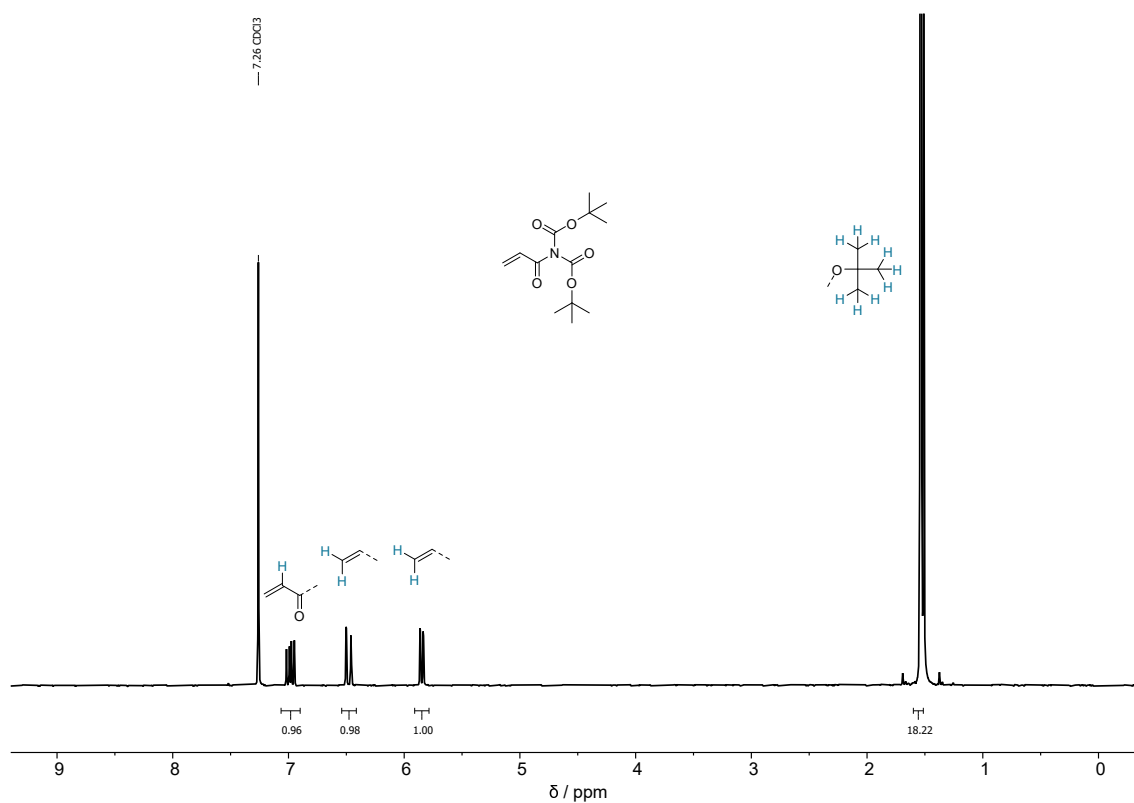
Figure 4.4: ^{1}H-NMR in chloroform-d of Boc$_2$AA.

Table 4.3: Polymerization of Boc$_2$AA with different catalysts (see Figure 4.2).

#	Catalyst	Time / d	Conversion / %[a]	$M_{n,rel}$[b]/kg mol^{-1}	$Đ$[c]
1	Ib	7	56	32.0	1.1
2	V	6	78	71.3	1.6
3	VI	4	14	8.7	2.0
4	IX	9	74	52.4	1.7
5	IV	14	100	24.1	1.5
6	IV[d]	2	65	16.3	1.6
7	IIIa	2	73	62.8	1.5
8	IIIa[d]	1	73	52.1	1.2
9	II	10	64	34.1	1.2
10	VII	7	58	—[e]	—[e]

Reaction in toluene at room temperature, [Boc$_2$AA]:[Cat] = 200:1.
[a] Determined by ^{1}H-NMR,
[b] determined by SEC-GPC in thf relative to a polystyrene standard,
[c] $M_{w,rel}/M_{n,rel}$,
[d] reaction temperature 60 °C,
[e] insoluble in GPC solvent.
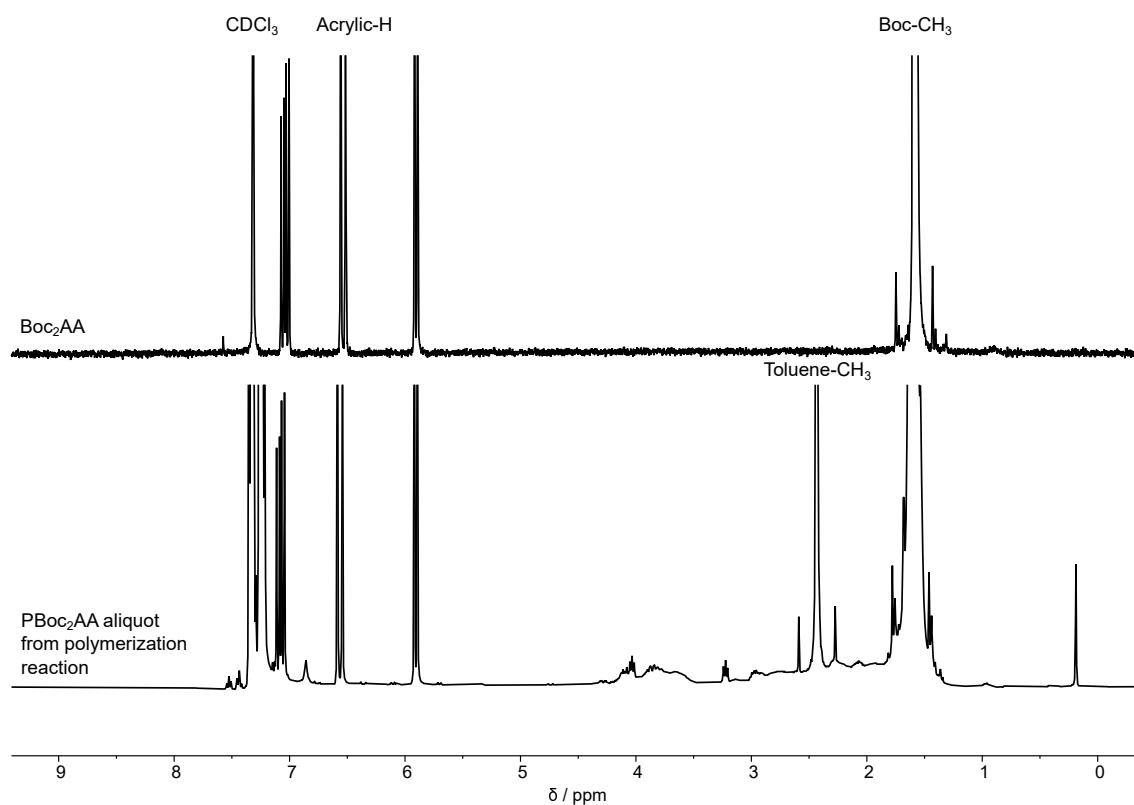
Figure 4.5: ^{1}H-NMR spectra of pure Boc$_2$AA (top) and an aliquot taken from the reaction mixture (bottom) in chloroform-d.

To begin with, Boc$_2$AA was tested in combination with Cp$_3$Lu(thf) (Figure 4.2, Ib). Already in this first experiment, it became clear that the polymerization proceeds very slowly in time intervals of days. Thus, 40 % conversion was observed for Ib after 24 h and 56 % after 7 d. An aliquot-^{1}H-NMR (Figure 4.5) showed the expected broadening of the signal of the Boc-CH$_3$ protons. Also, between 2.0 to 4.5 ppm, some new signals appeared which could represent the protons of the forming polymer backbone. GPC-analysis (Figure 4.6) revealed that although some polymer with an M_n of 32.0 kg mol^{-1} was formed, a non-negligible amount of low molecular weight compounds (dark blue) was also produced. One explanation for this could be the presence of several different carbonyl groups in Boc$_2$AA. During chain growth, the next monomer in the catalytic cycle must pre-coordinate to the metal center via the carbonyl that is in conjugation with the double bond. Since the Boc groups also have carbonyl oxygens, these can also coordinate the catalytic center and hinder polymerization (Scheme 18).

Cp$^*_2$YMe(thf) (V) produces 78 % conversion in 6 d and in GPC (Figure A6) the amount of low-molecular compounds is less compared to Ib. Here, the greater steric demand
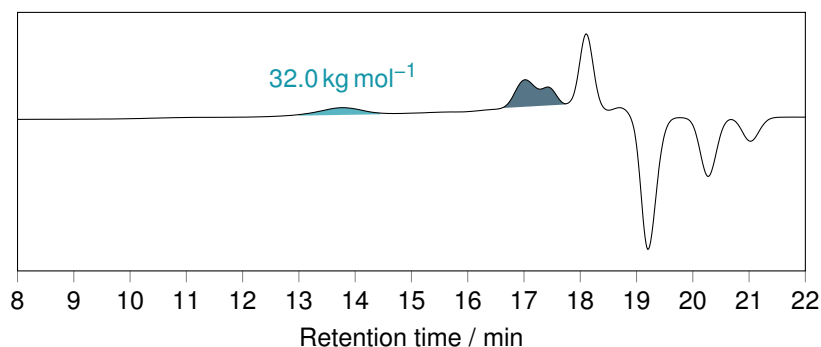
Figure 4.6: SEC-GPC trace of Boc$_2$AA polymerized with catalyst Ib (Table 4.3).
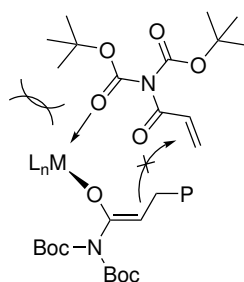
Scheme 18: Miscoordination which prevents chain propagation and influence of the steric demand of the ligands.

of the Cp* ligands compared to the Cp ligands could influence the reaction. The miscoordination showed in Scheme 18 could be reduced by the steric repulsion between the ligand and the *tert*-butyl group, which allowed higher molar masses of 71.3 kg mol^{-1} to form.

The zirconocene (VI, entry 3) only shows a low conversion of 14 % in ^{1}H-NMR and a M_n of 8.7 kg mol^{-1} with a very broad Đ (Figure A7). ACF (IX) is known to polymerize Michael monomers in a so far unknown mechanism.[230] Polymerization with Boc$_2$AA was also successful and produced 74 % conversion with molar masses of 52.4 kg mol^{-1} and a Đ of 1.7.

The ONOO-type yttrium catalyst with *sym*-col as initiating group (IV, entry 5) left no monomer after 14 d of reaction and resulted in monomodal and comparable narrow weight distribution (Đ = 1.5, M_n = 24.1 kg mol^{-1}, Figure 4.7). Rising the temperature from r.t. to 60 °C speeds up the polymerization and in 2 d 74 % conversion is reached (entry 6). The molar mass is 16.3 kg mol^{-1} and the Đ is broadened to 1.6 (Figure A9). The same catalyst system with CH$_2$TMS as initiating group can also polymerize
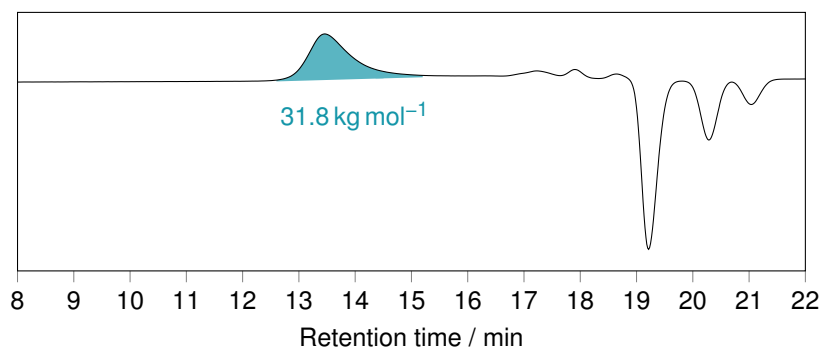
Figure 4.7: SEC-GPC trace of Boc$_2$AA polymerized with catalyst IV (Table 4.3).

Boc$_2$AA. [(ONOO)^{tBu}YCH$_2$TMS(thf)] (IIIa) reaches 65 % conversion after 2 d at room temperature. The M_n is comparable high with 62.8 kg mol^{-1} which could indicate a lower initiator efficiency (Figure A10). Due to the higher nucleophilicity of CH$_2$TMS, side reactions such as nucleophilic attacks to the Boc-carbonyl groups are possible. Again, rising the temperature to 60 °C (Table 4.3, entry 9) increases the reaction speed as after 24 h already 73 % conversion is reached. GPC shows that besides the peak representing an M_n of 52.1 kg mol^{-1} ($Đ$ = 1.2), there is also the formation of some lower molecular weight compounds visible (Figure A11). This could again be due to side reactions brought about by the initiator that are more pronounced at 60 °C.

Last, two Lutetium metallocenes were tested. While the conversion was for both Cp$_2$LuCH$_2$TMS(thf) (II) and Cp*LuCH$_2$TMS(thf) (VII) was slow and reached approximately 60 % conversion after 7 to 10 d, molar masses were either very low (Figure A12, catalyst II) or the resulting polymer was insoluble in the GPC solvent.

4.1.4 Deprotection of Boc$_2$AA

Polymer analog cleavage of the Boc-groups was examined by acidic methods following the instructions of Boc-deprotection strategies for small organic molecules. Two acids, TFA and TfOH, were used to investigate the deprotection and were performed analogously. PBoc$_2$AA was dissolved in chloroform, and TFA was added. The mixtures were stirred for one week under reflux. Then, the reaction was worked up

aqueous, with the potentially formed PAA dissolving in the aqueous phase. After separating the phases, methanol was added to the aqueous one to precipitate PAA, but this was not observed in both cases.

As with PBn$_2$AA, the problem with the cleavage of Boc is probably the significant change in polarity from the protected polymer to PAA. The PAMs presented by Larsen *et al.* are carried out in THF as a solvent with the nucleophilically introduced groups, not changing the polarity of the polymer.[81]

4.1.5 *N,O*-Bis(trimethylsilyl) acrylamide

TMSAA was synthesized following literature from acrylamide and trimethylsilyl chloride. The ^{1}H-NMR spectrum (Figure 4.8) shows the acrylic signals at 6.0 ppm representing two protons and the methin-proton at 5.52 ppm. The 18 protons of the TMS groups can be found at 0.24 and 0.15 ppm. This splitting already indicates, because of the chemically different environments, that the protected acrylamide is not *N,N*-but *N,O*- substituted. Besides the product signals, only minor residues of triethyl amine can be seen at 2.54 and 1.03 ppm. Spectroscopic data are consistent with the literature.[83]

The polymerization experiments with the catalysts previously used for the other monomers did not lead to a successful conversion. No evidence of polymer formation could be detected in the aliquots measured by ^{1}H-NMR. Since TMSAA had been polymerized exclusively by free radical polymerization, doubts arose about its suitability for catalytic methods. At the beginning of the study, an *N,N*-bis-silylated species was assumed, which would have had an analogous structure to other known disubstituted acrylamides as displayed in Figure 4.9a on the left. As just mentioned, ^{1}H-NMR analysis revealed that the *N,O*-substituted species was present instead. As can be seen in the structure in Figure 4.9a, a Michael system is also present here *via* the imine, which should theoretically be able to undergo a 1,4 polyaddition reaction.
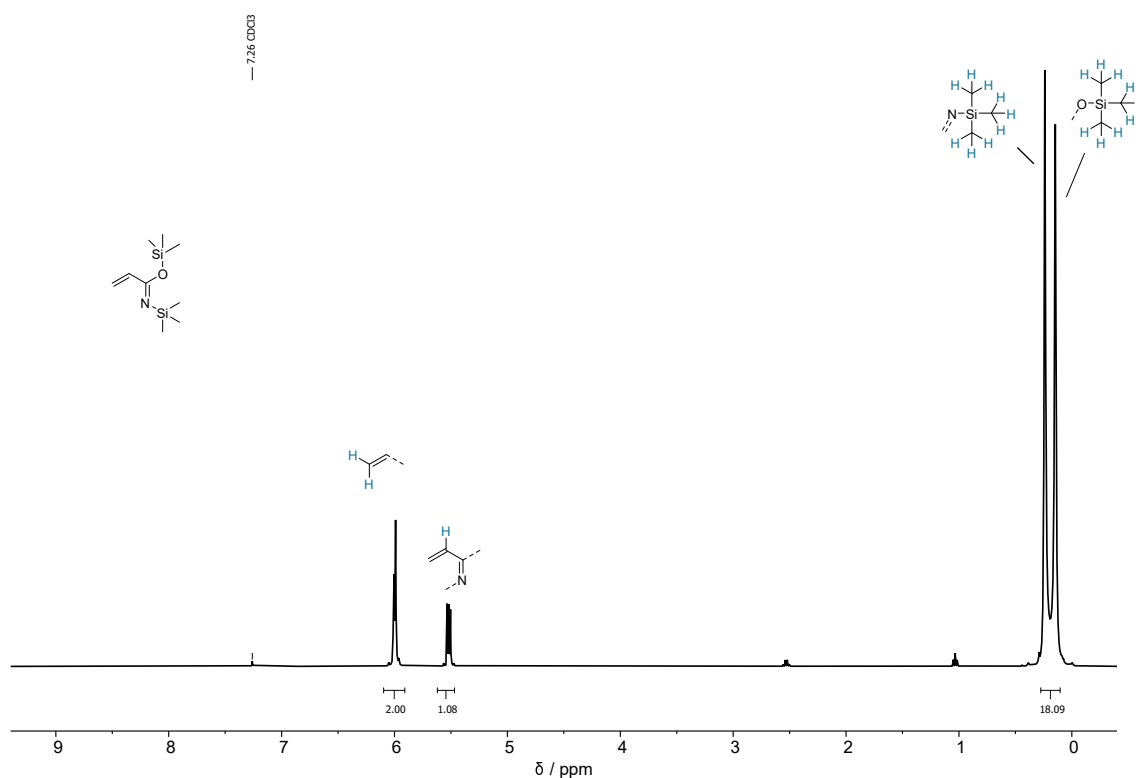
Figure 4.8: ^{1}H-NMR in chloroform-d of TMSAA.

Also, in theory, the 8-membered transition state, which is necessary for propagation in Yasuda-like polymerizations, should be theoretically possible (Figure 4.9b).

However, the presence of this basic structure is not sufficient for a monomer that can be polymerized in practice. A sufficient overlap of the p-orbital is mandatory to establish the conjugation of the 1,4-system. The overlap is optimal at an s-*cis* position, where the torsion angle θ should deviate as little as possible from 0° (Figure 4.9c). The torsion can also be described as the dihedral angle of the planes opened by the C=C and C=A bonds as displayed in Figure 4.9d.

In Table 4.4, the influence of torsion is considered using some exemplary molecules. Kodaira *et al.* compared the NMR-spectra of some different acrylamide derivatives and found that the quality of the orbital overlap can be estimated by ^{1}H-NMR and ^{13}C-NMR. They found that unconjugated monomers appear shifted upfield caused by shielding effects.[232] This can be seen in the values of the chemical shift of dimethyl methacrylamide (DMMA) and methacryloyl carbazole (MCBz), which are known to be not be subjected to polymerization compared to DMAA which is polymerizable.
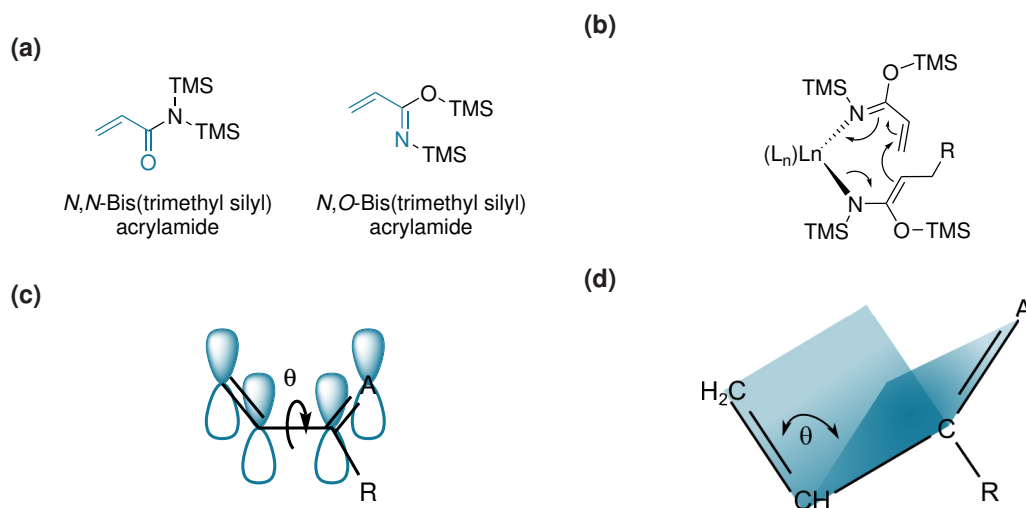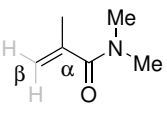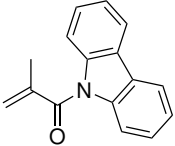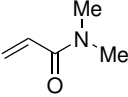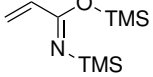
Figure 4.9: a) Hypothetical, *N,N*-bis(trimethyl silyl) acrylamide and observed *N,O*-bis(trimethyl silyl) acrylamide structure found. Michael-system highlighted in blue, b) theoretical 8-membered transition stated in Yasuda-type propagation c) torsion angle θ visualized with the relevant p-orbitals, and c) dihedral angle between the planes of the double bond and Michael acceptor.

Table 4.4: Influence of the torsion angle θ to ^{1}H-NMR and ^{13}C-NMR shifts of dimethyl methacrylamide (DMMA), methacryloyl carbazole (MCBz), TMSAA and DMAA.

Structure				
Name	DMMA[231]	MCBz[231]	DMAA[232]	TMSAA
Torsion angle θ (s-*cis*) / °	131.0	137.7	6.3	0
^{1}H-NMR-shift CH$_2$ / ppm	5.19, 5.04	5.69, 5.63	6.52, 5.61	6.01, 5.99
^{13}C-NMR $\Delta\delta$ α/β-C / ppm	25.4	19.1	1.5	7
GTP polymerizable	no	no	yes	?
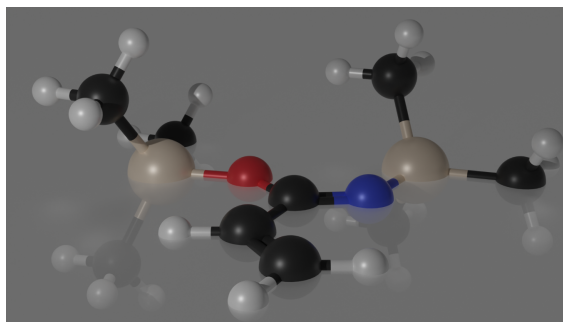
Figure 4.10: Render image of the DFT-calculated structure of BTSAA in s-*cis* configuration.

While CH_2 proton shifts of DMMA and MCBz range in the area of 5.0 to 5.7 ppm, the respective protons of DMAA are located at 5.6 to 6.0 ppm. This hypothesis could be supported by ^{13}C-NMR. Here, the difference of the chemical shifts of the α and β carbon atoms ($\Delta\delta$) is smaller, the better the orbital overlap. This again can be seen comparing DMMA/MCBz ($\Delta\delta$ = 19.1 to 25.4 ppm) to DMAA (1.5 ppm). In summary, it can be stated that downfield shifted vinylic protons in ^{1}H-NMR represent the more reactive C=C bond and small $\Delta\delta$-values between α and β carbon chemical shifts represent effective conjugation in ^{13}C-NMR.[231,232] Miyake *et al.* determined in addition the torsion angles by density functional theory (DFT) calculations. This showed that the α-methyl substituted unpolymerizable derivatives are highly twisted. At the same time, DMAA has a torsion angle of only 6.3°.

All these characteristics were also determined for TMSAA in this work. ^{1}H-NMR shifts of the CH_2 protons are comparably high field shifted with values of 5.99 and 6.0 ppm, but do not reach as high values as DMAA. $\Delta\delta$ of the α and β carbons is 7 ppm, which again is low compared to DMMA and MCBz, but not as low as DMAA. The torsion angle was calculated to be exactly 0° (Figure 4.10). These values lead to the conclusion that TMSAA should be catalytically polymerizable.

Structurally related bis-silylated amides are known in the literature and are used as TMS donors for the silylation of other organic molecules.[233] This methodology is mainly used in GC-MS analysis to mask highly polar functionalities such as
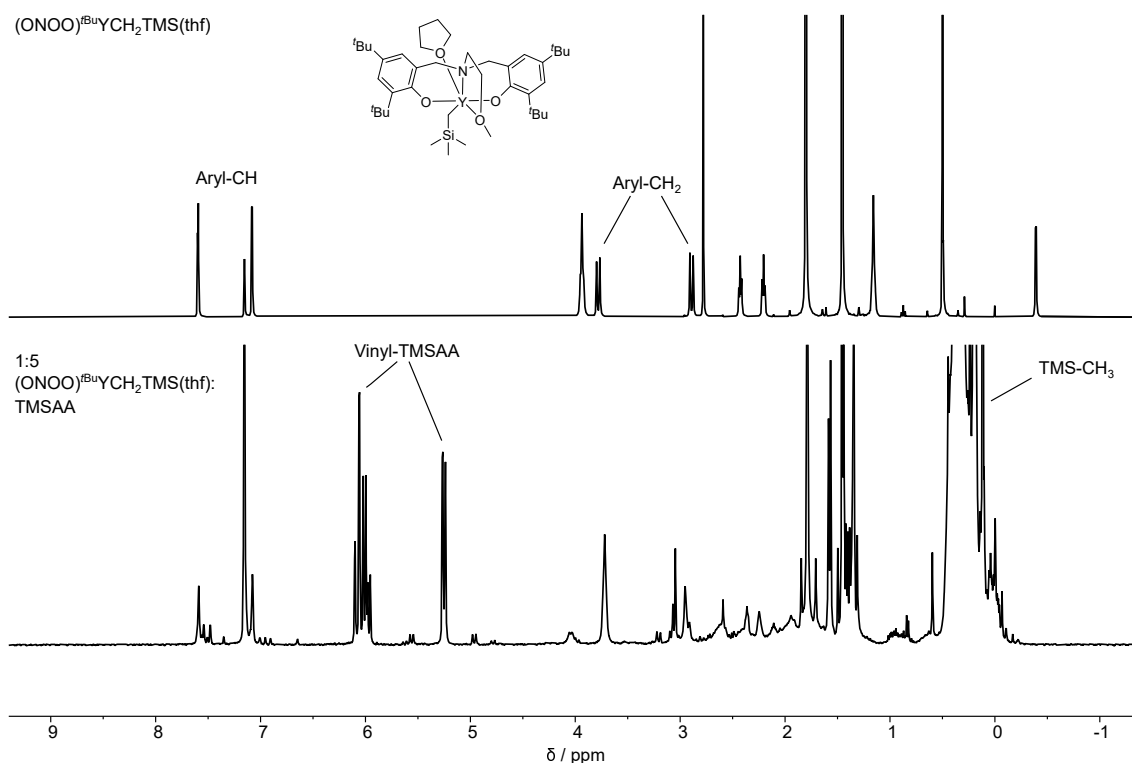
Figure 4.11: Top: ^{1}H-NMR of ((ONOO)tBuYCH$_2$TMS(thf), IIIa) in benzene-d$_6$,[235] bottom: reaction mixture of the catalyst with 5 eq. TMSAA.

R–OH, R–SH, R–NH$_2$ or R–COOH. Common molecules for this purpose are acetamides such as bis(trimethylsilyl) acetamide or *N*-methyl-*N'*-trimethylsilyl trifluoroacetamide.[233,234] The ability to transfer silyl groups could be one reason for the failed catalytic polymerizations. Catalysts bearing the ONOO ligand could have been silylated by the TMSAA, which alters the ligand sphere and compromises the catalytic capabilities. Evidence for this reactivity was found in the ^{1}H-NMR spectrum of an experiment with (ONOO)^{tBu}YCH$_2$TMS(thf) (IIIa) and five equivalents TMSAA.

As can be seen in Figure 4.11, signals near heteroatoms experience signal broadening or multiplication. For example, in the region of aryl-CH signals in close proximity to the coordinating oxygen atoms above 7 ppm, a few more signals are seen after the addition of TMSAA. Something similar happens with the aryl-CH$_2$ signals of the N–CH$_2$CH$_2$–O bridge. Also, the singlets of the TMS protons, which were previously very defined in the monomer spectrum, are very undefined in the reaction mixture. This indicates the presence of different silylated species.
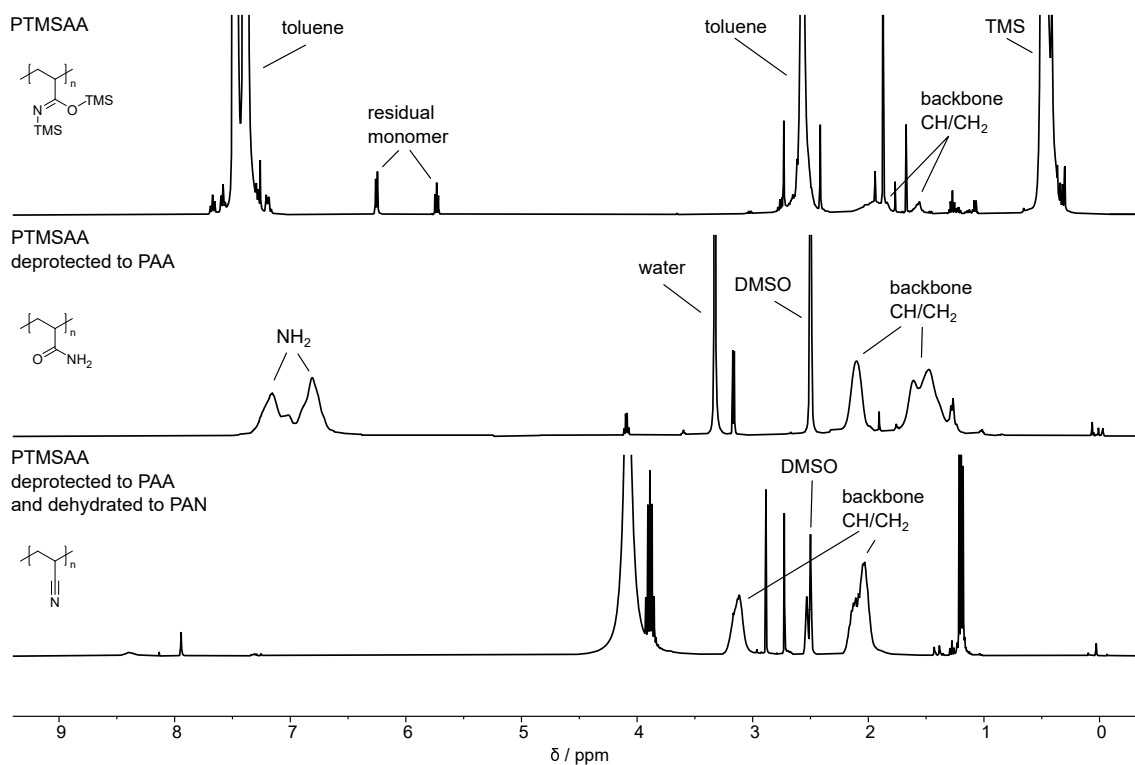
Figure 4.12: Aliquot-^{1}H-NMR of PTMSAA in toluene (top), deprotected PTMSAA to PAA (mid), and converted to PAN (bottom).

BTSAA was radically polymerized using AIBN as an initiator for replication purposes and proof-of-principle. The monomer was almost completely consumed, and the polymer was precipitated in pentane after 5 h of reaction. ^{1}H-NMR signals were in accordance with the literature.[83]

4.1.6 Deprotection of TMSAA and conversion to PAA and PAN

Also, following instructions from the literature, PTMSAA was deprotected to PAA. For this purpose, PTMSAA was stirred in a HCl-acidic tetrahydrofuran solution and then precipitated in methanol. PAA was thus obtained in quantitative yield. The signals of PTMSAA can be seen in the aliquot-^{1}H-NMR in Figure 4.12. The TMS groups remain unchanged at 0.47 ppm while the acrylic signals vanish and some broad peaks representing the CH–CH$_2$-backbone are forming. After the deprotection procedure, the TMS-peaks are gone completely, and the amine protons appear between 6.64 to 7.39 ppm, proofing the complete cleavage of the silyl groups.

(a)

(b)
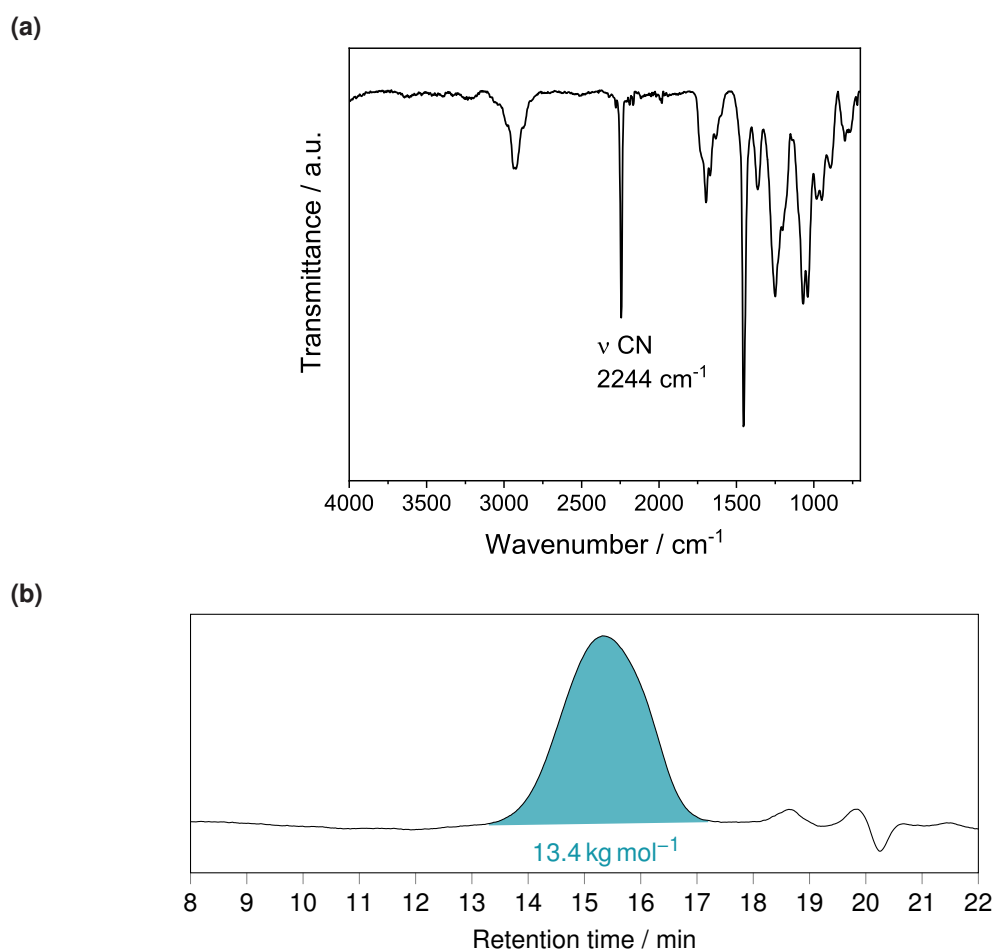
Figure 4.13: ATR-IR (a) and GPC-measurements (b) of PAN produced polymeranalogous by dehydration of PAA gained from the polymerization of TMSAA.

Dehydration was performed using diethyl chlorophosphate (DECP) as a dehydrating agent.[59] For the reaction, PAA was suspended in dmf and heated to 50 °C. In combination with DECP, the resulting PAN dissolves in dmf, and the reaction is complete when the solution becomes clear. After precipitation of the polymer in water, the ^{1}H-NMR shows the typical signals of the PAN-backbone at 3.1 and 2.0 ppm. In an IR-measurement, the distinctive C≡N oscillation at 2244 cm^{-1} is clearly visible (Figure 4.13a). GPC-analysis showed an $M_{n,rel}$ of 13.4 kg mol^{-1} with a Đ of 1.5 (Figure 4.13b) which is comparable broad because of the free radical polymerization of TMSAA.

4.2 Polymerization of methyl acrylate

Initially, the catalyst Cp*$_2$YMe(thf) (see Figure 4.2, V) known from literature was used for the polymerization of MA. The catalyst was reported to polymerize MA at 0 °C in toluene and 10 min reaction time resulting in 99 % conversion. As can be seen from Table 4.5, entry 1, the experiment was not reproducible. Contrary to the literature, the yttrium metallocene yields only 15 % conversion under the described conditions. Rising the reaction temperature to 25 °C (Table 4.5, entry 2) and a significantly elongated reaction time of 8 days lead to 60 % while a reaction at 60 °C (entry 3) also resulted in 59 % conversion after 3 days. Depending on the conversion, the experiments yielded molar masses of about 10 kg mol^{-1} and narrow Đs of 1.3, with only sample 3 conducted at 60 °C showing a slight broadening to 1.4. The same catalyst was also reported to polymerize *tert*-butyl acrylate (*t*BuA) in the same controlled manner. To draw conclusions about the suboptimal MA polymerization, reproduction with *t*BuA was also attempted. The polymerization with a monomer-to-catalyst ratio of 200:1 was successfully carried out, and a conversion of 99 % at room temperature in 24 h was achieved according to the literature results. A molecular weight of 34 kg mol^{-1} with a narrow molar mass distribution of 1.1 excludes the catalyst as a source of error in the polymerization of MA.

Due to the difficulties in reproducing, the catalysts used for the polymerization of Bn$_2$AA (Figure 4.2) were also investigated for their reactivity with MA. Cp$_3$Y(thf) (Figure 4.2 Ia) also only could polymerize MA to a conversion of 34 % (entry 4), Cp$_3$Lu(thf) (Figure 4.2 Ib) showed similar activity and produced 33 % pMA wit M_n = 16.0 kg mol^{-1} and a Đ of 1.5 (entry 5). Cp$_2$LuCH$_2$TMS(thf) (Figure 4.2 II) also lead to a slightly higher conversion of 38 % (entry 6) which could be a hint that CH$_2$TMS is the better initiator compared to Cp, however the conversion is still low. Both bisphenolate-type yttrium catalysts with CH$_2$TMS (Figure 4.2 IIIa) or *sym*–col (Figure 4.2 IV) as initiating group did polymerize MA (13 and 40 % conversion, entry 7 and 8) but the resulting polymer was insoluble in GPC solvents indicating high molecular masses resulting from low initiator efficiencies. The zirconocene *rac*-(EBI)ZrMeO^{iPr}MA (Figure 4.2 VI) was tested (entry 9) because it is known to polymerize methyl methacrylate.[236,237]

With this catalyst, again only low conversions of 25 % could be observed, GPC-analysis revealed a broad distribution of molecular weights ($Đ$ = 5.5). A narrower $Đ$ of 2.5 was produced by the Lewis acid tris tetrafluorophenyl aluminum (Figure 4.2 IX) (entry 10). Here, 84 % conversion after 13 days could be obtained with a M_n of 76.4 kg mol^{-1}.

The most successful polymerization attempt was the use of ^{iPr}SKA and $C_6F_5CTf_2$ as a nucleophile (Figure 4.2 VIII). In a monomer-to-initiator ratio of 100:1 and 0.02 eq. of the nucleophile >99 % of the monomer were consumed at room temperature within 1 h. This result is consistent with the literature, as well as the determined molecular weight of 10.9 kg mol^{-1} and the $Đ$ of 1.0.

Table 4.5: Polymerization of MA with different catalysts (see Figure 4.2).

#	catalyst	time / h	Conversion[a] / %	$M_{n,rel}$[b] / kg mol^{-1}	$Đ$[c]
1	V[d]	0.17	15	6.3	1.3
2	V	168	60	10.7	1.3
3	V[e]	71	59	10.2	1.4
4	Ia	192	34	—	—
5	Ib	240	33	16.0	1.5
6	II	192	38	—	—
7	IIIa	96	13	—	—
8	IV	312	40	—	—
9	VI	168	25	—	5.5
10	IX	312	84	76.4	2.5
11	VIII[f]	1	99	10.9	1.0

[MA]:[Cat] = 200:1 in toluene at room temperature.
[a] determined by ^{1}H-NMR,
[b] determined by SEC-GPC in thf relative to polystyrene,
[c] $M_{w,rel}/M_{n,rel}$,
[d] [MA]:[Cat] = 500:1, 0 °C,
[e] T = 60 °C,
[f] [MA]:[^{iPr}SKA]:[Nu] = 100:1:0.02.

As a next step, various molecular weight polymers were synthesized with different ratios of [MA]:[^{iPr}SKA] = 20, 100, 300, 500 and 1000 (Table 4.6). As can be seen from the SEC-GPC-traces (Figure 4.15a) and the plot of the molecular weight against the used monomer to initiator-ratio (Figure 4.15b), the polymerization can be precisely tuned regarding chain-length in a wide range (2.66 to 113.4 kg mol^{-1}) with a constant
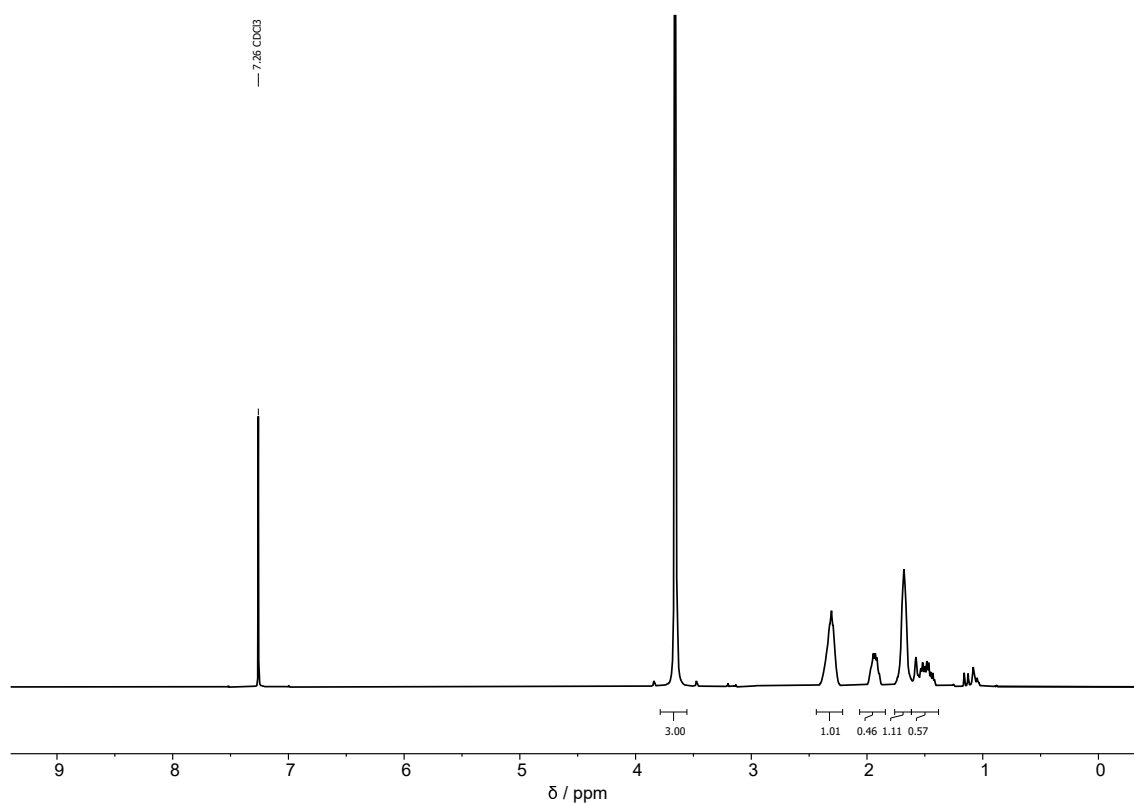
Figure 4.14: ^{1}H-NMR of polymethyl acrylate in cloroform-d.

perfectly narrow weight distribution. For the subsequent polymer analog conversion to pAA, the polymerization of MA was scaled up to a batch size of 100 g. This was carried out with the ratios 1:300 and 1:1000 to achieve similar molar masses as in the small-scale experiments. Additionally, to be able to compare the M_n before and after the PAMs, the refractive index increment (dn/dc) was determined for pMA in dmf at 30 °C (Figure A14). This allows the calculation of absolute molar masses ($M_{n,abs}$) from SEC-GPC measurements with a triple detector setup. Entries 7 and 8 of Table 4.6 display the outcome of the up-scaling: The molar masses are slightly lower than in the small reactions, the molar mass distribution remains constant at 1.0. The lower molar masses are due to the weighing error, which is considered relatively large since the polymerization was carried out in a glovebox, and the monomer was added and distributed over 25 mL syringes. Due to the heat of the reaction, the mixtures warm up to about 50 °C on a large scale, which, however, does not have a negative effect on the Đ.

Table 4.6: Polymerization of MA with ^{iPr}SKA and $C_6F_5CTf_2$ as nucleophile (see Figure 4.2, VIII).

#	ratio[a]	$M_{n,rel}$[b]/ kg mol^{-1}	$M_{n,abs}$[c]/ kg mol^{-1}	$Đ$[d]
1	20 : 1 : 0.02	2.66	2.96	1.0
2	100 : 1 : 0.02	10.9	9.62	1.0
4	300 : 1 : 0.02	24.7	27.9	1.0
5	500 : 1 : 0.02	49.8	32.7	1.0
6	1000 : 1 : 0.02	113.4	80.0	1.0
7[e]	300 : 1 : 0.02	—	22.5	1.0
8[e]	300 : 1 : 0.02	—	22.1	1.0
9[e]	1000 : 1 : 0.20	—	71.0	1.0

[a] [MA]:[^{iPr}SKA]:[Nu] in toluene at room temperature, conversion in each polymerization >99 % (determined by ^{1}H-NMR),
[b] determined by SEC-GPC in thf relative to polystyrene,
[c] determined by SEC-GPC in dmf, dn/dc = 0.0528 mL g^{-1},
[d] $M_{w,abs}/M_{n,abs}$,
[e] big-scale 100 g experiments.
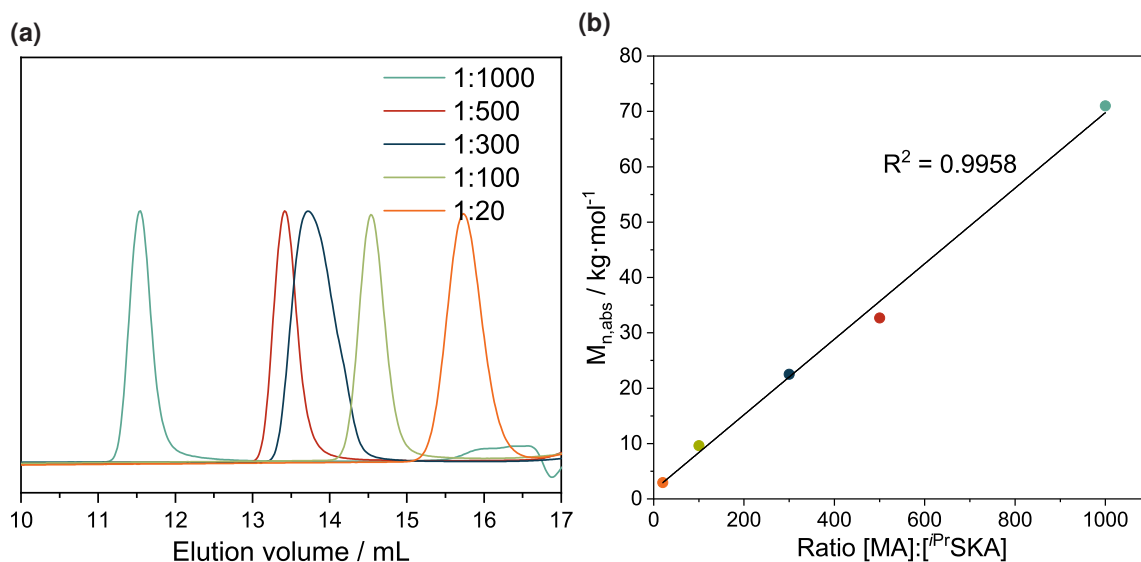
Figure 4.15: a) GPC-elugrams of PMA produced by different ^{iPr}SKA to MA ratios, b) linear correlation between the molar mass and the ratio.

4.3 Polymer-analogous amidation of PMA

With the extremely precise and controllable polymerization method in hand, the poly-mer analog amidation should be investigated and scaled up. As mentioned in Sec-tion 2.1.4, amidation reactions of PMA can be performed by pressurizing a solution of the polymer in a mixture of thf and methanol (2/1 vol.%) with ammonia and heating the reaction to 60 °C. In the preceding work, 500 mg of PMA was reacted in 50 mL steel autoclaves; in the present work, this reaction will be implemented at a 100 g scale.[59] For this purpose, a 5 L pressure reactor with a heatable mantle and stirrer was used (see Figure A15). The first big-scale amidation was performed using 71.0 kg mol^{-1} PMA from entry 9 of Table 4.6. As for the small-scale experiments, the polymer was dissolved in 2 L of a thf/methanol mixture (2:1 v/v), which was then loaded into the reactor, heated to 60 °C.
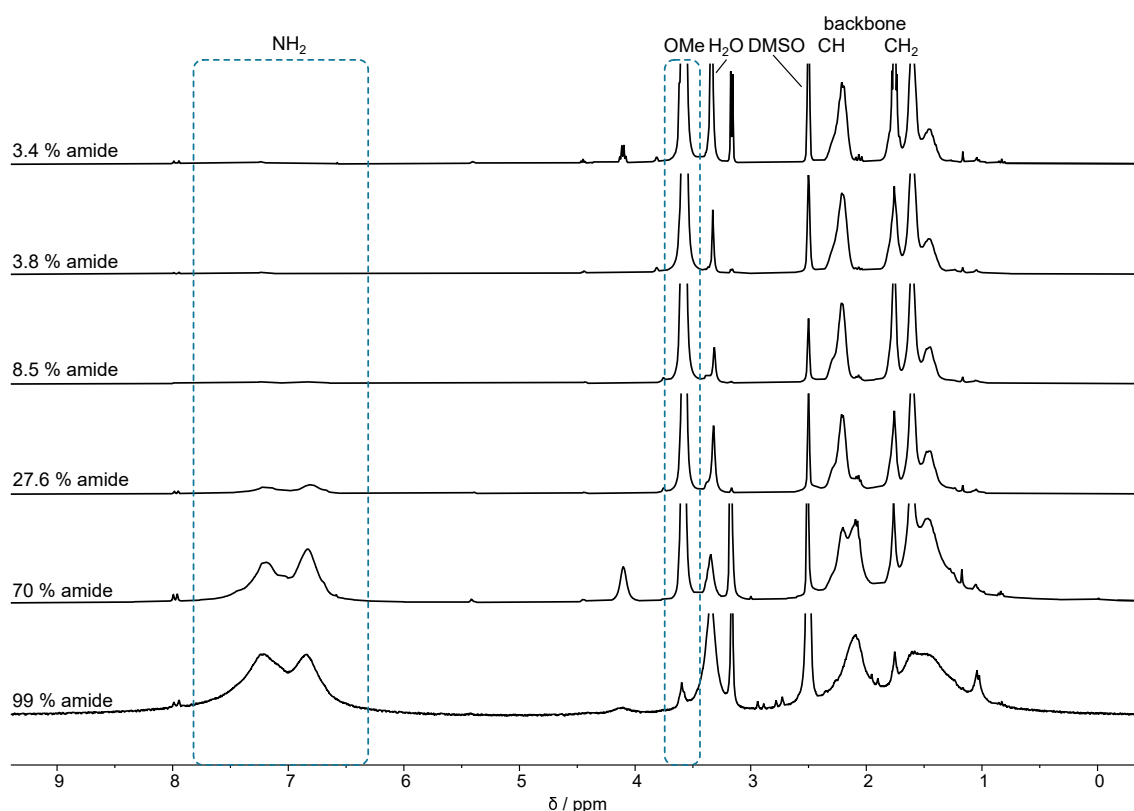
Figure 4.16: Progress of the amidation reaction of PMA (71.0 kg mol^{-1}) in ^{1}H-NMR in DMSO-d$_6$.

The progress of the amidation reaction can be monitored by ^{1}H-NMR. As can be seen in Figure 4.16, a broad signal group develops in the region from 6.57 to 7.60 ppm,
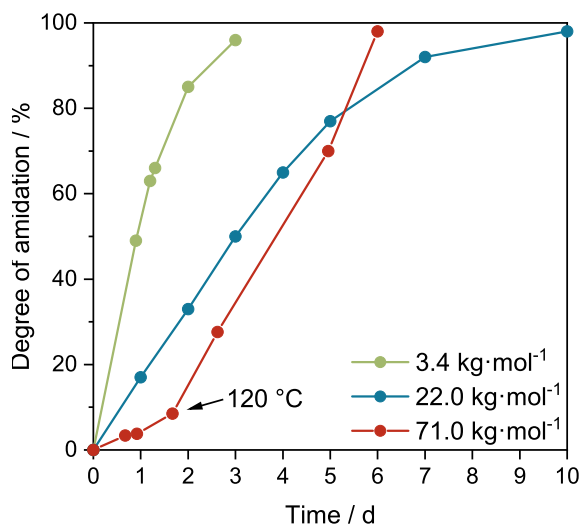
Figure 4.17: Progress of different molecular weight PMA amidation reactions dependent from time. Polymers with 3.4 and 22.0 kg mol^{-1} are prepared in a 500 mg scale, PMA of 71.0 kg mol^{-1} scale is 100 g.

which can be assigned to the protons of the introduced amine. At the same time, the methoxy signal at 3.57 ppm becomes smaller. In the aliphatic region, the methine and methylene resonances experience a slight high-field shift.

The trend that the amidation becomes slower with increasing molecular weight of the polymer was already observed in the previous work. As displayed in Figure 4.17, the low molecular weight sample (M_n = 3.4 kg mol^{-1}) requires just under three days for full conversion, while the polymer with 22.0 kg mol^{-1} takes ten days. As expected, the high molecular weight PMA (71 kg mol^{-1}) used now reacts even more slowly. After 2.6 days, only 27 % conversion is measured. This was the reason why the temperature in the reactor was increased to 120 °C from this measuring point, which greatly accelerates the reaction, and 98 % conversion is achieved after six days. Instead of flattening out more and more as the conversion is observed for the green and blue curves, the read curve bends upwards. This can be explained by the fact that the higher molecular weight copolymer with high amide contents starts to become insoluble in the thf/methanol mixture and finally precipitates (see Figure A15). This could be a driving force for the reaction, accelerating it from a conversion of about 70 %. The rate increase is positive regarding a shorter reaction time but makes it more difficult to stop the reaction at about 90 % conversion to achieve the desired amount of MA in the later PAN copolymer.

With these findings, 100 g each of P(MA-*co*-AA) of 71.0 kg mol^{-1} with a degree of amidation of 98 % and 22.5 kg mol^{-1} with 99 and 90 % PAA content was produced for use in the polymer-analogous dehydration reaction. Although the dry PAA is present as a white solid, it appears brownish in solution, which is why the resulting PAA was purified by dissolving/swelling in water and precipitation in methanol. An average yield of 85 % was achieved. Losses are due to purification by precipitation in methanol. The size of the precipitated polymer flakes depends on the polymer concentration in the water. In high concentrations, it tends to form fibers or strands, which has a negative effect on the purification efficiency. In low concentrations, the polymer precipitates in finer flakes, making a recovery more complex. The use of paper filters is not possible because the polymer clogs the pores, so the method of choice was to skim the polymer through a tea strainer (Figure A15). However, the finer particles are lost in the process and reduce the yield.

4.4 Polymer-analogous reaction to PAN

Dehydration of PAA to PAN was performed in the previous work with an amount of 50 mg PAA and 2 mL each of diethyl chlorophosphonate and dmf, representing almost 20 equivalents of DECP. This high excess is due to the assumption that the polar reagent plays a role in the solvation of the polymer and facilitates the reaction.[59] In order to determine the actual amount needed, a series of experiments (Table 4.7) was performed. For optimization, a constant amount of 50 mg PAA-*co*-PMA (approximately 90 % PAA, rest PMA from entry 7, Table 4.6) was suspended in 2 mL dmf and the volume of DECP was varied from 1.75 mL down to 0.25 mL (Table 4.7). After 24 h reaction time at 60 °C, samples were precipitated in water, washed with methanol, dried, and analyzed by ^{1}H-NMR. As can be seen in Figure 4.18, at sample 6, there are minor amounts of the amine-signal left. It was concluded that 7.4 eq. of DECP are necessary to dehydrate PAA completely. In the next step, using these conditions, the reaction was scaled up stepwise to 100, 500 and 1000 mg of PAA (Table 4.8, entries 8-10).

Table 4.7: Condition screening to optimize the dehydration reaction of 50 mg PAA with DECP in dmf (2 mL, 0.025 g L^{-1} PAA).

#	V(DECP) / mL	equivalents DECP
1	1.75	17.2
2	1.5	14.7
3	1.25	12.3
4	1.0	9.8
5	0.75	7.4
6	0.5	4.9
7	0.25	2.5
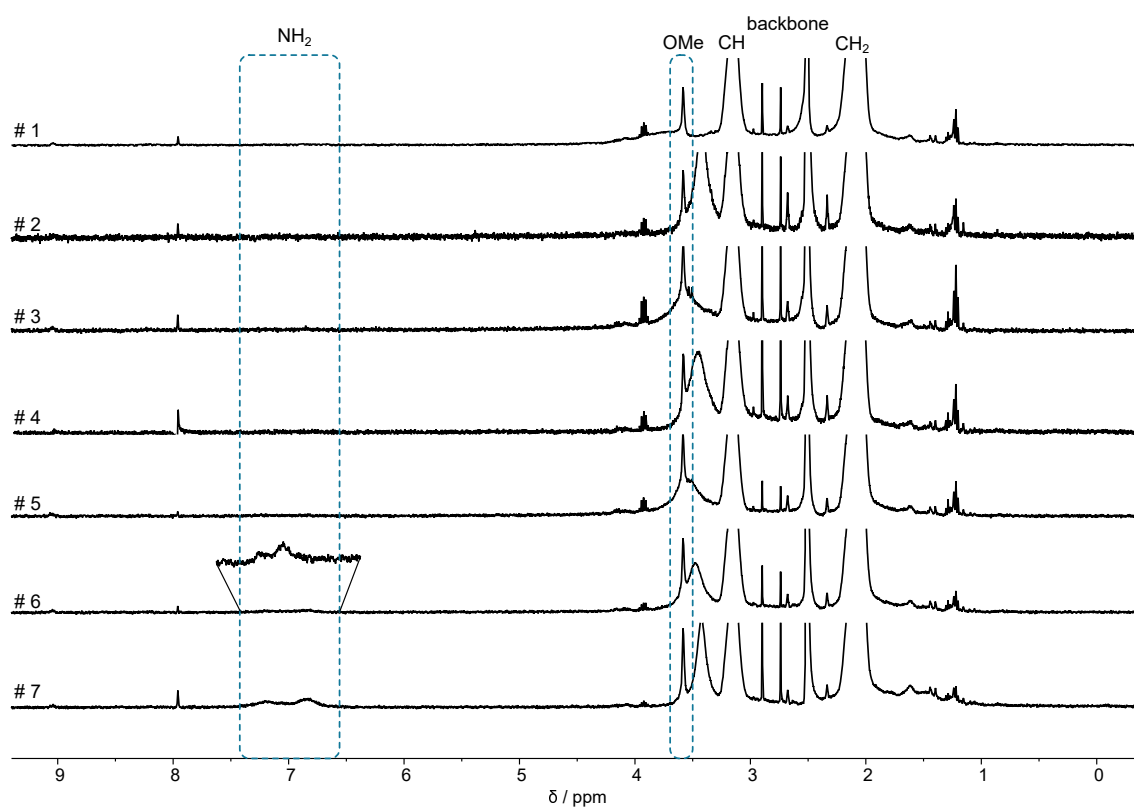
Figure 4.18: ^{1}H-NMR spectra of the reaction condition screening of the dehydration of PAA described in Table 4.7 in DMSO-d$_6$ as solvent.

Table 4.8: Scaling experiments ot the dehydration reaction of PAA with DECP at a concentration of PAA in dmf of $0.025\,\mathrm{g\,mL^{-1}}$.

#	m(PAA) / g	V(DECP) / mL	V(dmf) / mL	equivalents DECP
8	0.1	1.6	4	7.9
9	0.5	8	20	7.9
10	1.0	16	40	7.9
11	8.0	132	320	8.1
12	9.2	152	370	8.1
13	9.9	163	400	8.1
14	10.6	175	420	8.1
15	12.8	211	510	8.1
16	15.0	248	600	8.1

While the experiment number 9 with 100 mg PAA showed full conversion (Figure A16), minor residues of the NH_2-group could again be detected in the ^{1}H-NMR of experiments 9 and 10 (Figure A17). This is why the the excess DECP was increased to 8.1 eq. for the following experiments 11 to 16. In addition, the reaction time was extended to 2 days at 60 °C. Thus, the polymer analog synthesis of PAN could be scaled up to a batch size of 15 g PAA (Table 4.8, entry 16) and a total of 43 g of the copolymer could be produced. The total yield of all these experiments was 70 %, but varied widely among the individual reactions, peaking at 86 % for experiment 16. The largest losses are again likely to be found in the purification of the polymer. The crude product after the first precipitation is dark brown to black and was therefore dissolved again in dmf and precipitated in water once more. PAN has an even greater tendency than PAA to form fibers at high concentrations, and the fine particles form relatively stable dispersions, which are difficult to separate. The variation in the yield can thus be attributed to the recovery of the polymer after precipitation. If the polymer precipitates too finely, the yield is reduced. Therefore, optimizing the purification process with regard to yield is advisable and should be the subject of further research. PAA produced from the $M_{n,abs}$ = $71.0\,\mathrm{kg\,mol^{-1}}$ showed no reaction towards PAN, which could be due to solubility problems with the high-molecular-weight polymer.

As mentioned earlier in the dehydration of the PAA obtained from PTMSAA, IR can be used to characterize the polymers in addition to ^{1}H-NMR. Figure 4.19 shows the IR
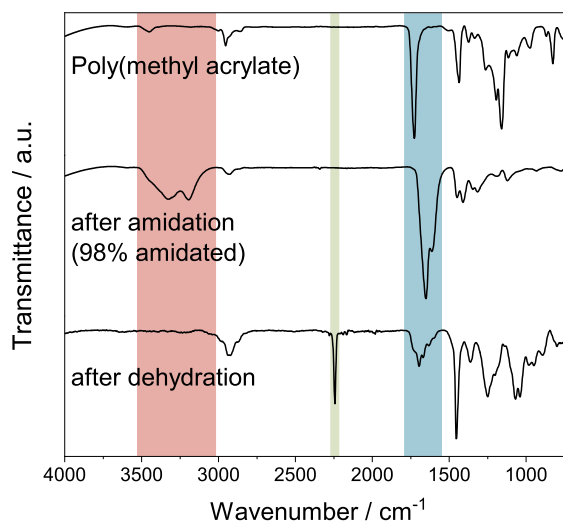
Figure 4.19: IR-spectra of PMA after polymerization, PAA and PAN produced polymer analogous.

spectra of all steps. As can be seen, from PMA to PAA, the signal of the carbonyl vibration shifts slightly from 1728 to $1654\,\text{cm}^{-1}$ and at 3331 and $3192\,\text{cm}^{-1}$, the antisymmetric stretching vibration of the N–H-bonds occurs. Both the signals of the amide and the carbonyl signal disappear after dehydration to PAN, and the distinct C≡N-band at $2244\,\text{cm}^{-1}$ becomes visible.

Comparing the GPC-traces of the PMA from which the PAM (Figure 4.20a) was started with the PAN produced (Figure 4.20b), one sees a slight widening of the relatively determined molar mass distribution from 1.1 to 1.4. The broadening is due to the shoulder shifting towards higher molar masses in the PAN sample. Since the shape of the principal peak is very similar to that of PMA, it can be assumed that the polymer chains remain largely intact during PAM. The shift in retention time is explained by the fact that GPC separates by hydrodynamic molecular radius. Due to the chemically different properties of the polymers, the retention time thus changes slightly.

The comparison with commercially available PAN prepared from ACN by free radical polymerization (Figure 4.20c) illustrates a significant advantage of the PAM route: The controlled polymerization of PMA at the beginning of the synthesis makes it possible to produce relatively narrowly distributed PAN that is not accessible by radical methods.

(a)

(b)

(c)
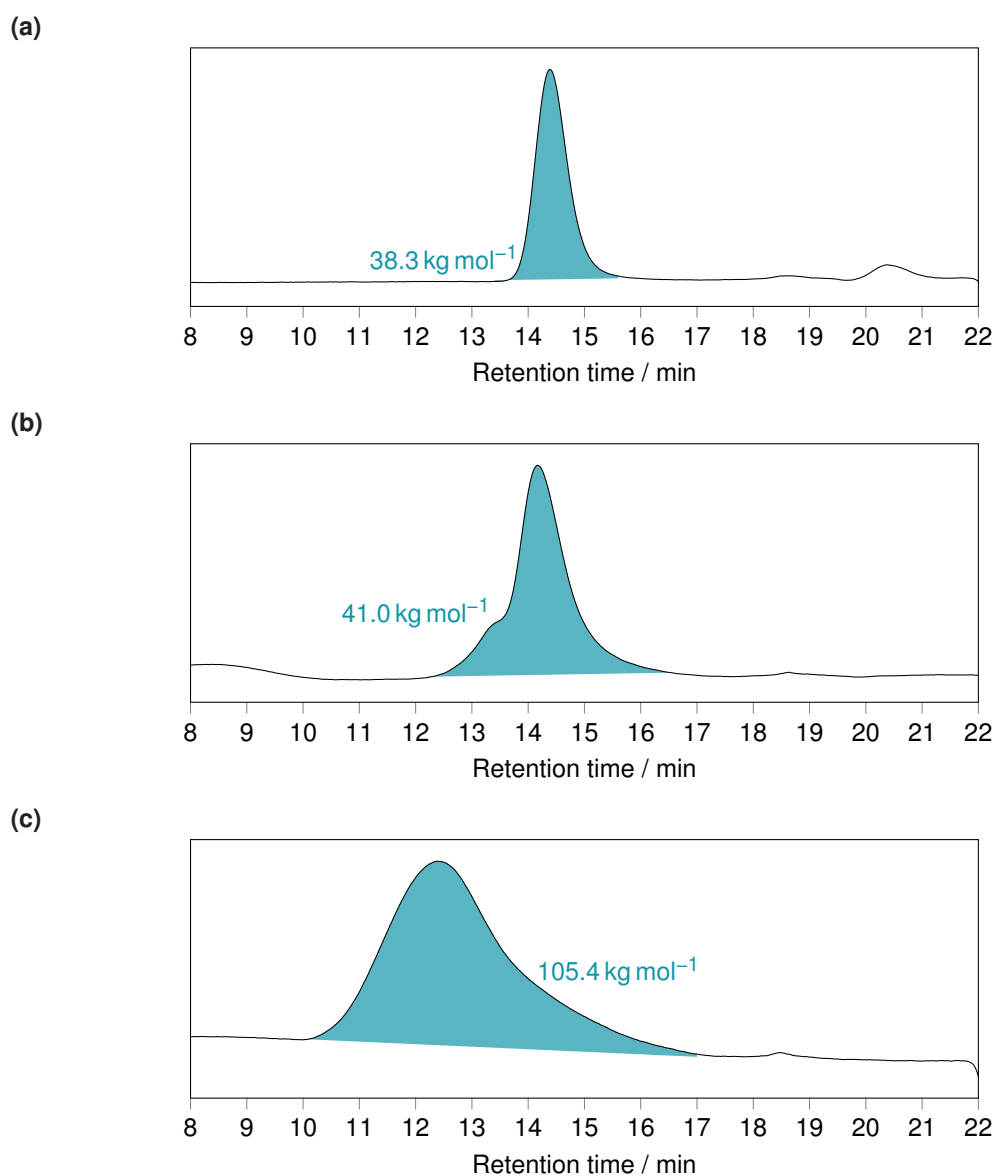
Figure 4.20: a) GPC-elugrams of PMA ($M_{n,rel}$ = 38.3 kg mol^{-1}, Đ = 1.1), b) PAN produced polymeranalog from PMA ($M_{n,rel}$ = 41.0 kg mol^{-1}, Đ = 1.4), c) commercially available PAN with $M_{n,rel}$ = 105.4 kg mol^{-1}, Đ = 3.1.

4.4.1 Thermal properties of poly(methyl acrylate-*co*-acrylamide-*co*-acrylonitrile)

DSC scans can visualize the thermal processes during the heating of PAN samples. Figure 4.21a shows exothermic events during the first heating cycle. A sample consisting mainly of PMA and containing only 25 % PAN shows only low thermal activities.
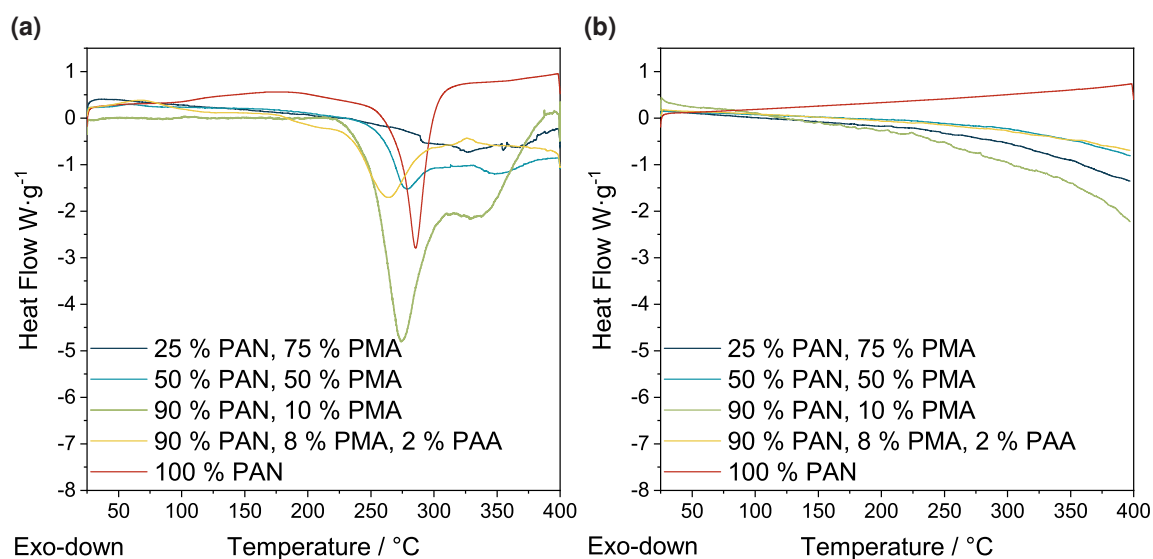
Figure 4.21: DSC-scans of samples with different PAN-content. a) 1st heating cycle, b) 2nd heating cycle.

The cyclization reaction responsible for the exothermic processes cannot occur because of the low nitrile content since neighboring C≡N repeating units are needed in the chain.

The sample, which consists of 50 % PAN, already clearly shows an exothermic bulge originating from the stabilization. The higher the PAN content in the other samples, the more pronounced the exothermic process. Compared with the 100 % PAN sample, the influence of the methyl acrylate is also evident. While the peak maximum in the homopolymeric PAN is located at 286 °C, it is shifted to lower temperatures in the samples containing PMA (275 °C at 10 % PMA, 278 °C at 50 % PMA). In addition, the range of the exothermic process widens and starts already at lower temperatures.

No such clearly pronounced thermal processes are visible in the second heating cycle (Figure 4.21b). This indicates that the stabilization reaction after the initial cycle has already progressed to a high level. However, the slight bending of the curves from the copolymer samples could indicate that structural defects are repaired upon reheating. Since these defects should be statistically distributed throughout the chain, this exothermic process no longer appears as a sharp signal but extends over a wide temperature range.

In particular, the sample containing a residual percentage of PAA in addition to PMA shows a clearly accelerated start of the reaction at a temperature of about 195 °C and reaches the maximum at 264 °C. Overall, these observations are in agreement with the literature, as is the accelerating influence of PAA.[34,238] This suggests that the polymer analogously prepared PAN-PMA copolymer is suitable to be used as a precursor material for carbon fibers analogously to the industrial standard, the copolymer prepared radically from the monomers.

4.5 Conversion of the polymer-analogous prepared PAN into carbon fibers

To verify this assumption, a sample of 50 g was spun by the Fraunhofer Institute for Applied Polymer Research IAP (Dr. André Lehmann) and subsequently stabilized and carbonized (Dr.-Ing Jens Erdmann). To prepare the spinning solution, a 17.5 % solution was prepared from the sample using a Getzmann dissolver in N,N'-dimethylacetamide (DMAc) and a stirring speed of 1500 rpm at 60 °C for a period of 120 min. Since the solution showed a significant amount of undissolved particles under the light microscope, purification was performed by centrifugation followed by depth filtration (13 microns). Rheological measurements of the sample in solution showed a significantly lower viscosity in the flow curve compared to a commercial CF-PAN sample (1.5 Pa s vs. 34.3 Pa s at 25 °C). This is due to the already mentioned, significantly lower molar masses (Figure 4.20a, Figure 4.20c) as well as the real polymer content, which is lower than the addressed due to the undissolved components. However, a precipitation test of the dissolved sample in DMAc/H_2O (70:30 v/v) was positive, which allowed a spinning experiment on the wet-spinning line.

(b)

(a)

(c)

(d)
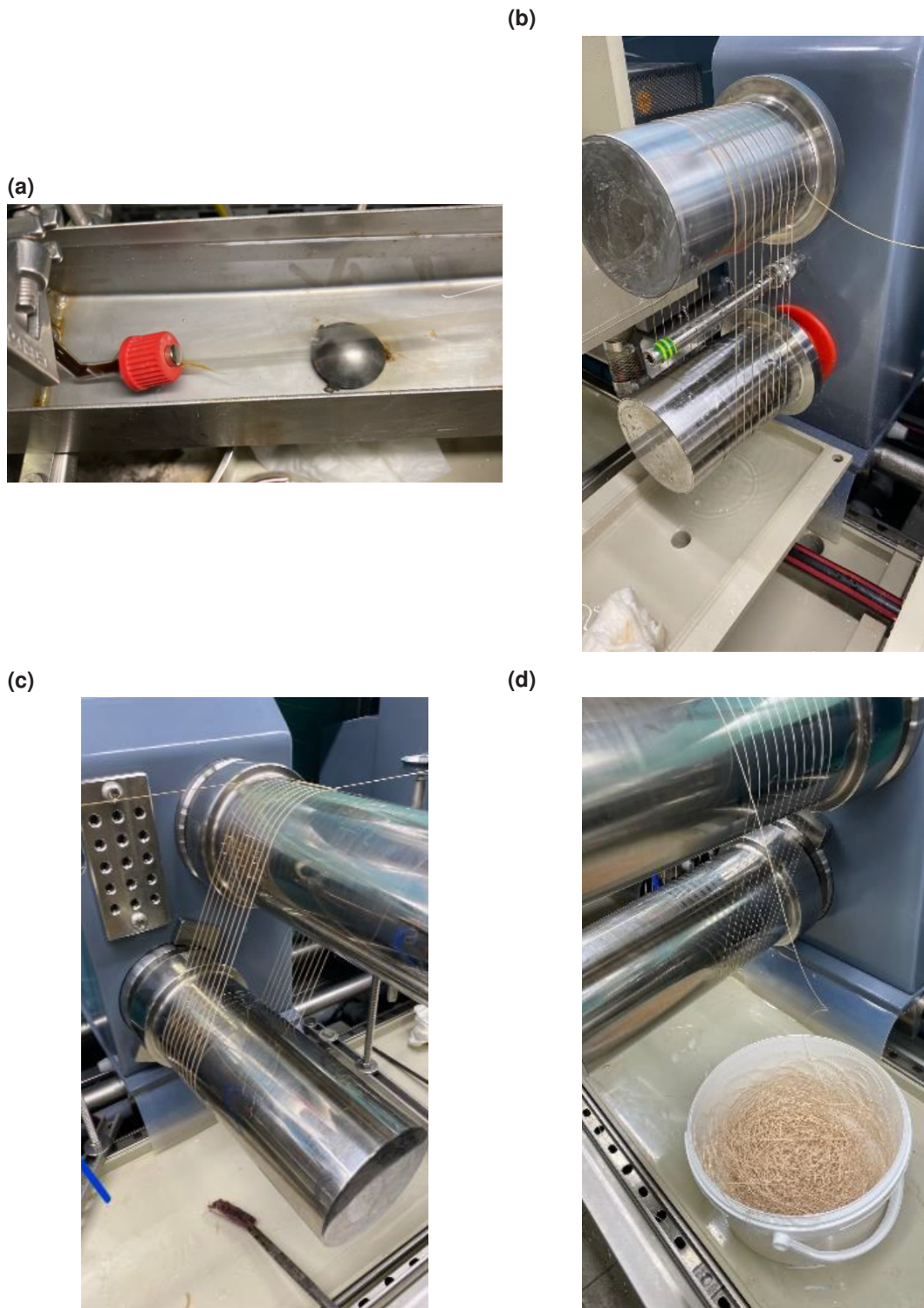
Figure 4.22: a) Spinneret with initial moist filament sheet forming in the regeneration bath, b) filament yarn running onto a godet rollers, c) filament yarn running onto dryer rolls (heatable godet duo), d) collection of filament yarn as free deposit (whirl deposit). Photos taken by Fraunhofer IAP.

4.5.1 Fiber spinning

As can be seen in Figure 4.22, the dissolved PAN-sample is guided through a spinning nozzle (120 holes with 0.06 mm in diameter) into a precipitation bath (DMAc/H_2O 70:30 v/v). Here, constant pressure conditions could be observed due to the filtration carried out beforehand; moreover, the spinning behavior at the nozzle was almost stable. The spun filament yarn was then guided over godet rolls and dried on heated dryer rolls. Since the fibers had very low strength, the yarn could not be wound onto a spool but was deposited in a random orientation. Due to the low tensile strength, the filament yarn could not be stretched during the spinning process as it is normally done. Tensile tests on the strand show a Young's modulus of 0.3 GPa, a strength of 4.5 MPa, and an elongation at break of approximately 1.0 %. Raster electron microscopy (REM) images (Figure 4.23) illustrate the described problems with the brittleness of the fiber and the low values for tensile stresses. Although the top view of the fibers appears very smooth and uniform, and the cross-sectional areas have a round appearance, the fibers are interspersed with voids and have an extremely porous morphology (Figure 4.23d).

The explanation for this can again be traced back to the low molar masses of the polymer, which do not permit any stretching of the fibers during the spinning process. This leads to fibers that are six times thicker (41.5 µm) than fibers made from higher molecular weight commercial PAN and show a density of 0.45 g cm^{-3}.[239] The lack of stretching results in a lower orientation along the fiber axis, which affects the mechanical properties of the precursor fiber and also the later CF.

DSC and TGA investigated the precursor filament with respect to thermal properties. As can be seen from Figure 4.24a, an exothermic process representing the stabilization reaction can be observed when heating the polymer-analogous starting material (magenta curve). As a comparison, fibers made of commercially available CF-PAN (orange curve) were measured in which thermal processes occur in the same temperature range (220 to 320 °C). The enthalpy of the cyclization reaction of 440 J g^{-1} is also in a similar range compared to the commercial sample (540 J g^{-1}). The sample
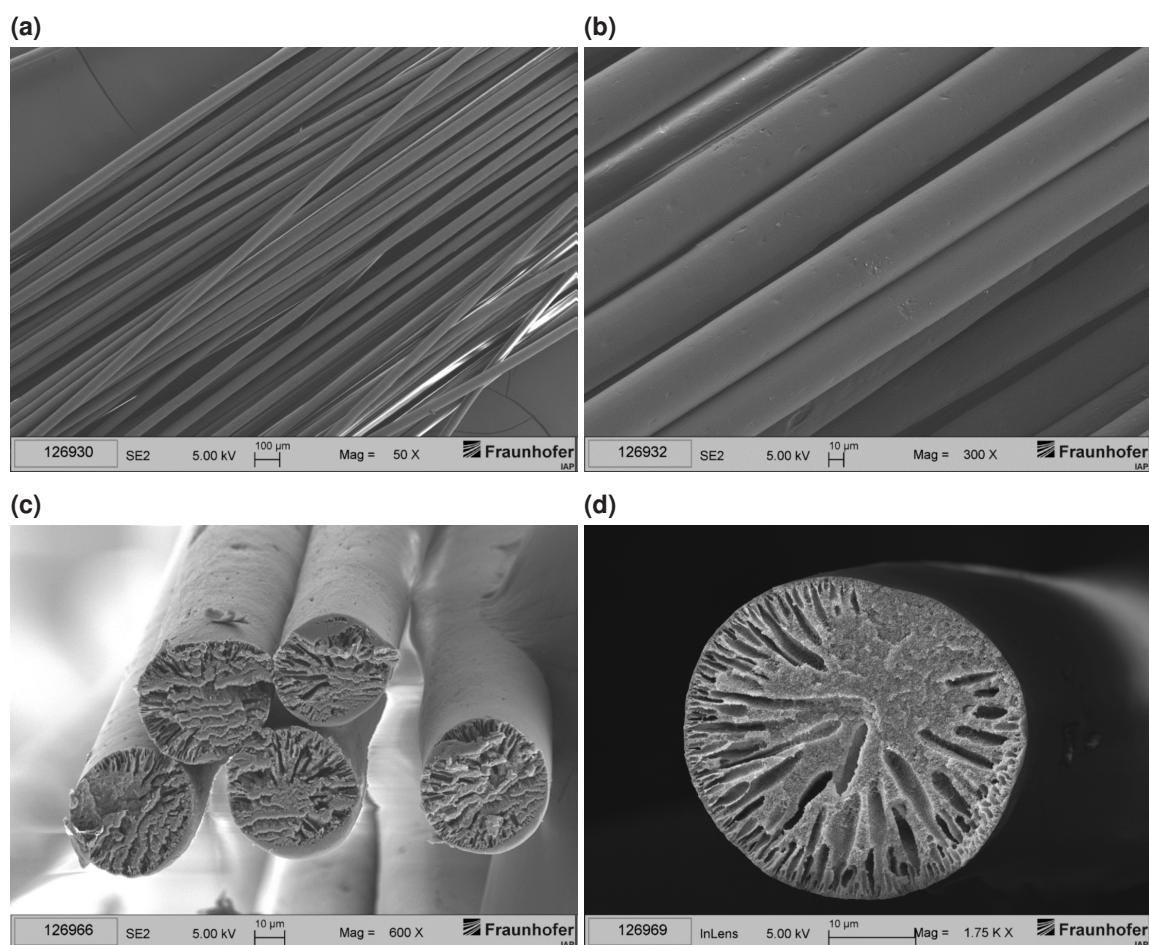
Figure 4.23: REM-pictures of the PAM-PAN filament. a) Top view of the strands and zoom in b), cross-sectional area (c and d). Images taken by Fraunhofer IAP.

also shows very similar thermal behavior in a TGA measurement. The fiber resulting from this work (Figure 4.24b, green curve) shows almost the same inflection points at 300 and 425 °C as the commercial fiber (blue curve), also the residual mass after 1100 °C of 34 % is identical.

4.5.2 Stabilization and carbonization

For continuous conversion of the spun PAN, the fibers are first passed through a three-zone stabilizing furnace in which temperatures of up to 300 °C are reached. As can be seen in Figure 4.25a, the fiber is picked up from the random laydown and enters the stabilizing furnace. At the exit (Figure 4.25b), it can already be seen that the fiber is darker than before. The discoloration of the stabilized yarn as a function

(a)

(b)
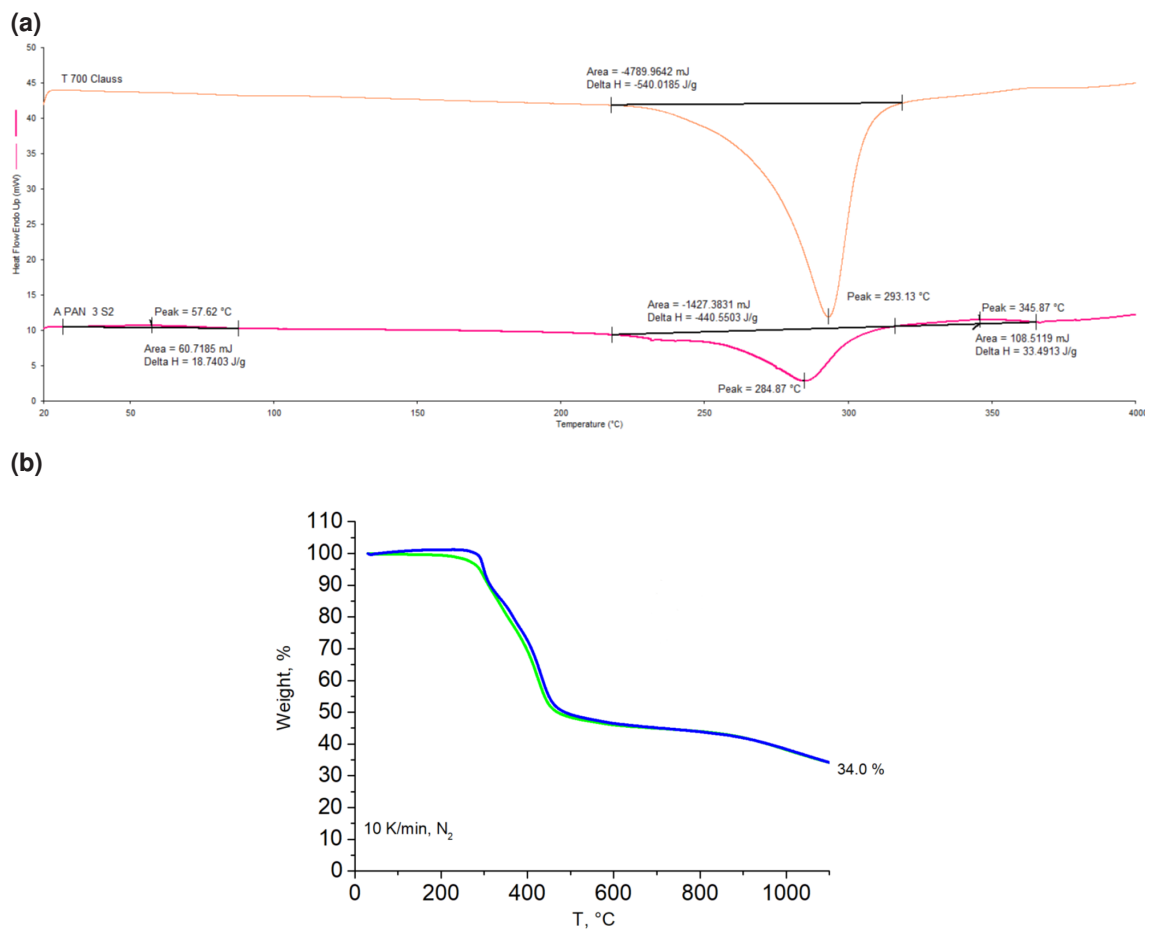
Figure 4.24: a) DSC-scans of a commercial CF-PAN filament (orange) and the PAM-PAN filament (magenta), b) TGA measurements of a commercial CF-PAN filament (blue) and the PAM-PAN filament (green). Measurements and analysis by Fraunhofer IAP.

of the applied temperature is visible in Figure 4.25c. Here, the color slowly changes from the original beige/white to brownish and finally to black. After completion of the process, about 25 m of the stabilized filament was obtained (Figure 4.25d).

(a)

(b)

(c)

(d)
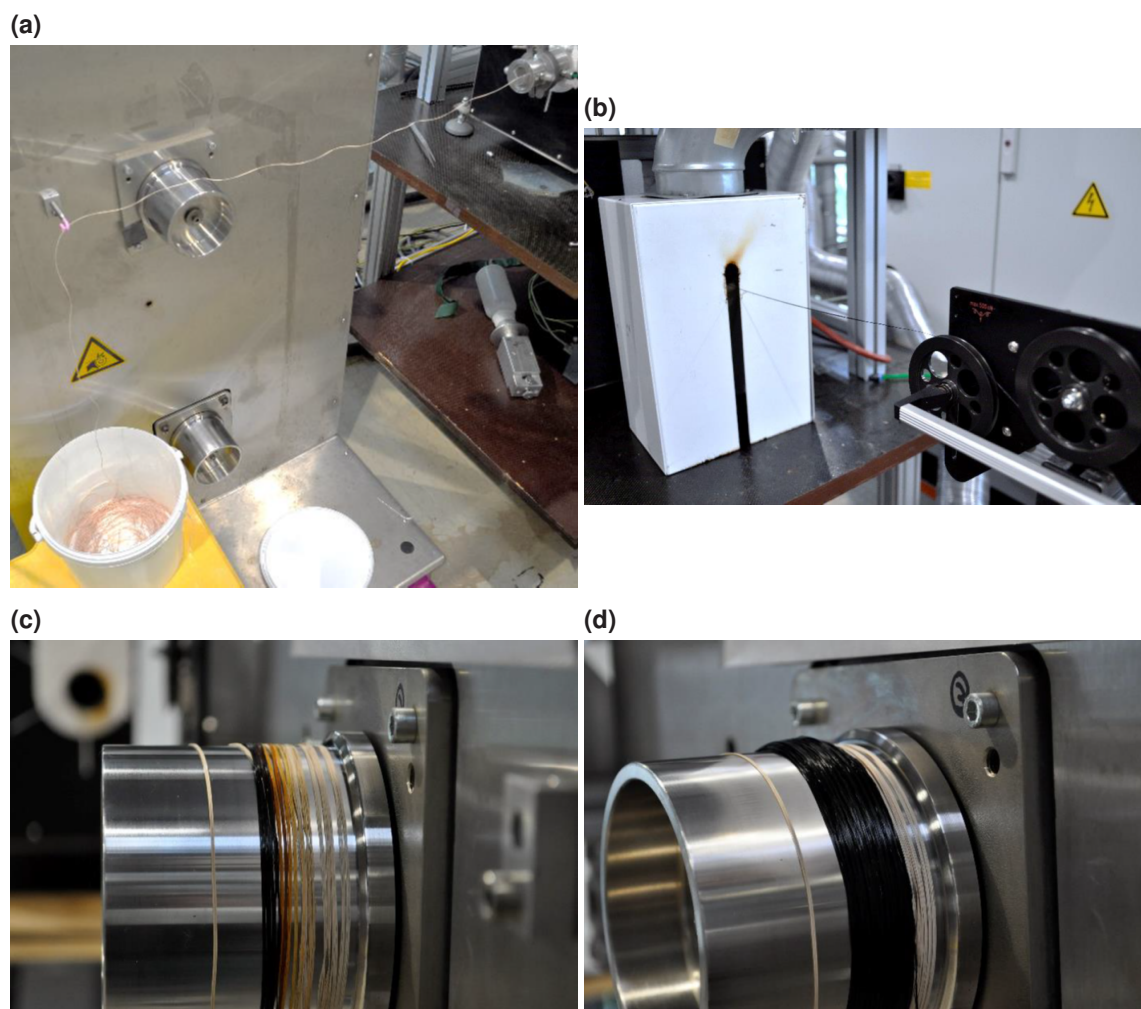
Figure 4.25: a) Pick-up of the filament from random laydown and entry into stabilizing furnance, b) Exit of the stabilized yarn from the stabilizing furnace, c) discoloration of the stabilized yarn as a function of the applied temperature, d) After completion of the process. Photos taken by Fraunhofer IAP.

The stabilized fiber was again analyzed by REM and tensile tests. As expected, the diameter of the fibers decrease to 30.3 µm while the density increases to 1.05 g cm^{-3}. In addition, the Young's modulus increases to 1.7 GPa, the strength to 59 MPa, and the elongation at break to 4.0 %. These values are approximately five times lower than in commercially stabilized CF-PAN precursors.[239] REM images of a bundle of the filaments again show homogeneous, round fibers at the surface (Figure 4.26a).

As with the precursor, the cross sections are riddled with voids (Figure 4.26b). These cavities, as well as the poor orientation in the fiber due to the lack of stretching during the spinning process, are again responsible for the low strength values.

(a)

(b)

(c)
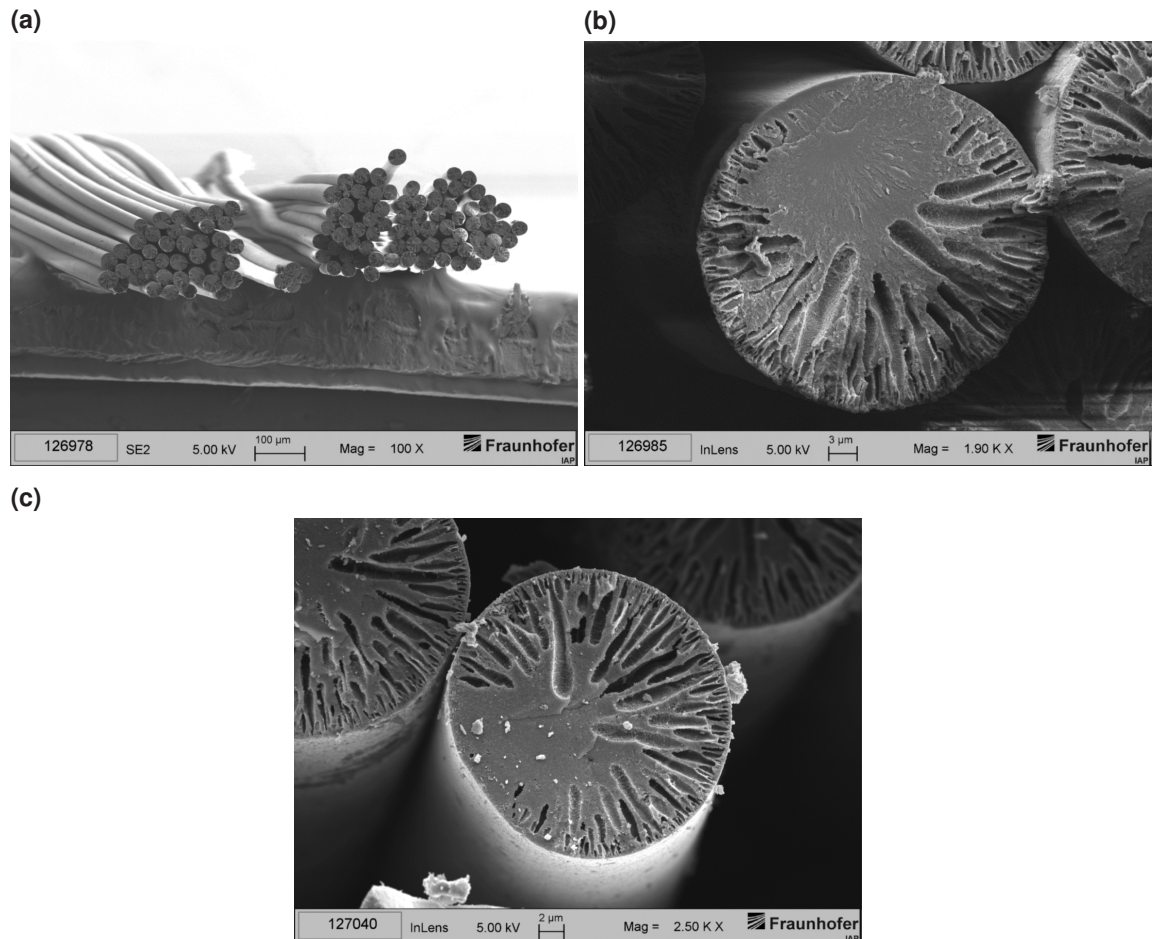
Figure 4.26: REM-pictures of a) the fiber cross-section of a stabilized fiber bundle, b) close-up view of a stabilized fiber, and c) of the low-temperature carbonized fiber. Images taken by Fraunhofer IAP.

After stabilization, the yarn was fed by hand into a three-zone low-temperature carbonization furnace. In the continuous process, temperatures up to 1000 °C are reached. Due to the brittleness of the fibers, only tension-free yarn transport was possible here as well. The product was wound onto a godet head. After this process step, the E-modulus increases to 1.8 GPa, the strength reaches 6.6 MPa and the elongation at break drops to 0.3 %. The diameter of a single filament is 24.2 µm, the density increases to 1.28 g cm^{-1}. At this process step, commercial samples reach values of around 6000 MPa for the Young's modulus, which is around 600 times higher.[239]

Because of the increasing brittleness, the product of the low-temperature carbonization could not be continuously fed into the high-temperature carbonization process. Therefore, about 3 m of low-temperature carbonized filament was high-temperature carbonized in an ultra-high temperature batch furnace (Figure 4.27a) in a retort (Figure 4.27b). The resulting fibers showed an E-modulus of 1.9 GPa at a strength of 9.7 MPa. The elongation at break is still comparably low with a value of 0.5 %. During the high-temperature process, the diameter of a fiber decreases to 23.7 µm and the density reaches 1.13 g cm^{-3}. As can be seen in the REM image, cavities are still present. All values for the individual steps are summarized in Table 4.9. The total mass-loss of 50.5 % is comparable to the conversion of conventional PAN fibers. In the elemental analysis, too, only traces of nitrogen were detectable in addition to carbon, which confirms the successful implementation.
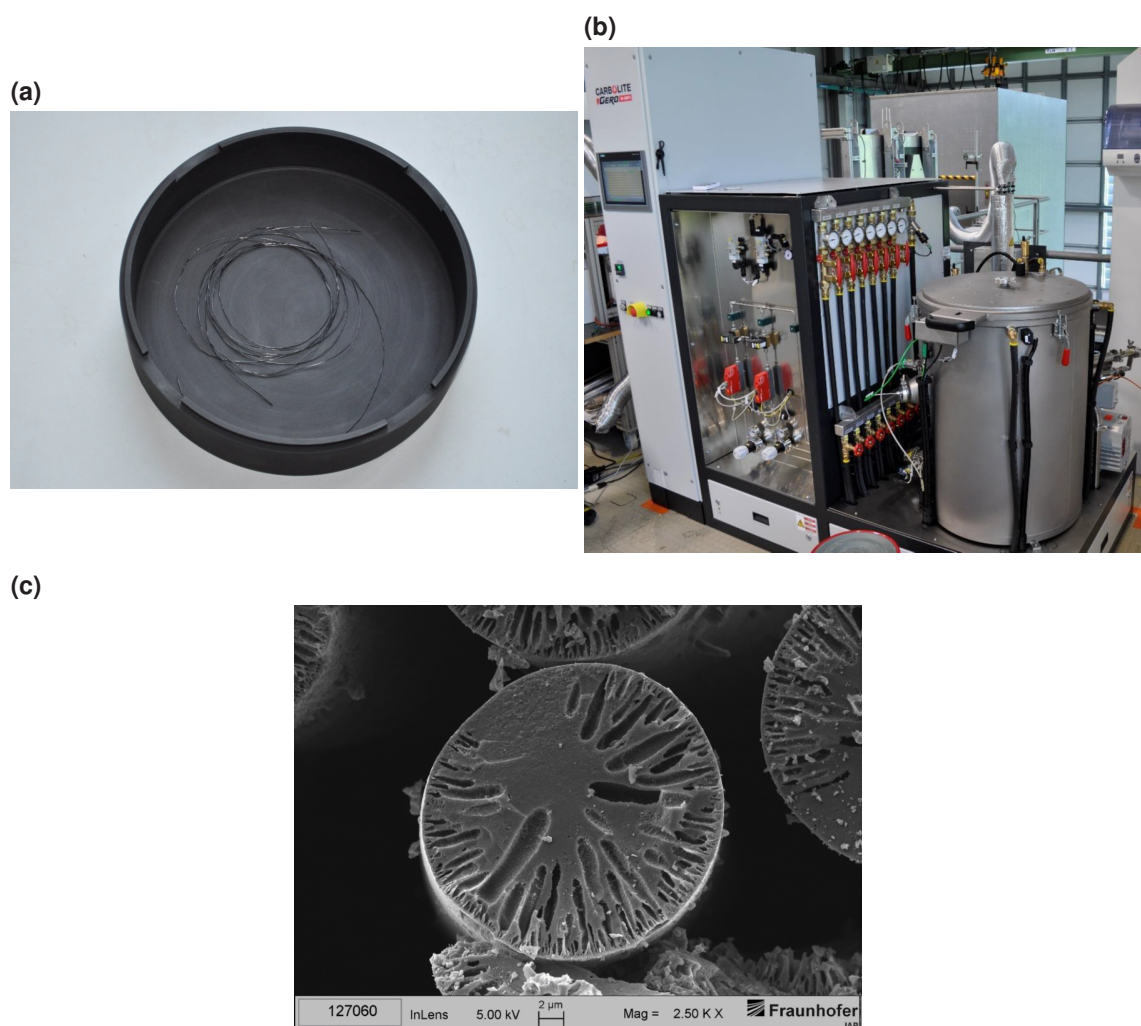
Figure 4.27: a) High-temperature carbonized yarn in retort, b) Ultra-high-temperature batch furnace, and c) REM-picture of the high-temperature carbonized fiber. Photos taken by Fraunhofer IAP.

The following can be summarized about the conversion of the polymer analog produced PAN: The cyclization reaction in the DSC behaves very similarly to the benchmark system (commercially available CF-PAN), and the curve progression in the TGA is almost identical. After spinning the PAN, the fibers are interspersed with voids, which in combination with the comparatively low molecular weight of the polymer, leads to low mechanical properties and brittleness. This severely limited the process capability, which meant that the actually continuous process had to be solved by hand through various furnaces. The final step in the high-temperature oven was also carried out in batches.

Table 4.9: Summary of process parameters and results of individual conversion steps from PAN to CF. Process and value determination by Fraunhofer IAP.

Fiber	Length change[d] %	Mass loss[e] %	E-Modulus[f] GPa	Strength[f] MPa	Density[g] $g\,cm^{-3}$	Diameter[h] µm
PAN			0.3	4.5	0.45	41.5
Stabilized[a]	–21.5	2.0	1.7	59	1.05	30.3
LT carbonized[b]	–10	40.3	1.8	6.6	1.28	24.2
HT carbonized[C]	0	15.5	1.9	9.7	1.13	23.7
Over all	–31.5	50.5				

[a] Stabilization process at a temperature of 260 °C,

[b] low-temperature carbonization process at a temperature of maximum 1000 °C,

[c] high-temperature carbonization process at a temperature of maximum 1600 °C,

[d] determined by measuring position changes of markers on the strand,

[e] Calculation from titer ($g\,m^{-1}$) before and after the process, taking into account the change in length,

[f] Conversion of cN/tex into MPa or GPa by application of the determined density

[g] Calculation from titer ($g\,m^{-1}$) by weighing and cross-sectional are (m^2) by REM,

[h] Calculated from cross-sectional area assuming an ideal round cross-section.

4.6 Conversion of vegetable oils to epoxy thermoset

4.6.1 Epoxidation of free unsaturated fatty acids

For the conversion into epoxy thermoset, unsaturated fatty acids oleic acid and linoleic acid were epoxidized by the Prilezhaev method using *m*CPBA as peroxycarboxylic acid or by the use of Oxone®. Both methods successfully converted the fatty acids into the (di)epoxy compounds at room temperature. As can be seen from the comparison of the ^{1}H-NMR spectra of oleic acid and the epoxidation product (Figure 4.28), the progress of the reaction can be easily monitored by the vanishing signals of the double bonds at 5.3 ppm and the signals of the protons in the vicinity of the epoxide groups appear (3.08 ppm and 2.96 ppm). Because of the byproduct *m*-chlorobenzoic acid remaining in the epoxidized compound, purification in the case of using *m*CPBA is complex. The best method of removing the impurity is cooling down the reaction mixture to 0 °C to precipitate residues of *m*CPBA and benzoic acid. Then adding an aqueous solution of Na_2SO_4 allows excess *m*CPBA to react off to form the acid and, simultaneously, washes it out. In order to remove most of the peroxycarboxylic acid, this washing step has to be repeated several times, followed by washing steps with saturated solutions of $NaHCO_3$ and NaCl. As can be seen in the ^{1}H-NMR of epoxidized oleic acid (Figure A19), depending on the success of this procedure residues of *m*CPBA still can be present (residual peaks between 7.3 to 8.0 ppm) and flash chromatography can be necessary.

The workup is less tedious for the epoxidation with Oxone®. Extraction can remove the salts, resulting in a pure epoxidized product. The purity of 9,10-12,13-diepoxystearic acid (DESA) can be seen in the ^{1}H-NMR in Figure 4.29. Nevertheless, the reaction procedure also poses some problems here. Since the free fatty acid acts like a surfactant in the presence of potassium salts in an aqueous solution, vigorous foaming occurs during the reaction, especially when working up with saturated $NaHCO_3$-solution. Besides ^{1}H-NMR, successful epoxidation of linoleic acid could be proved by GC-MS (Figure A21).
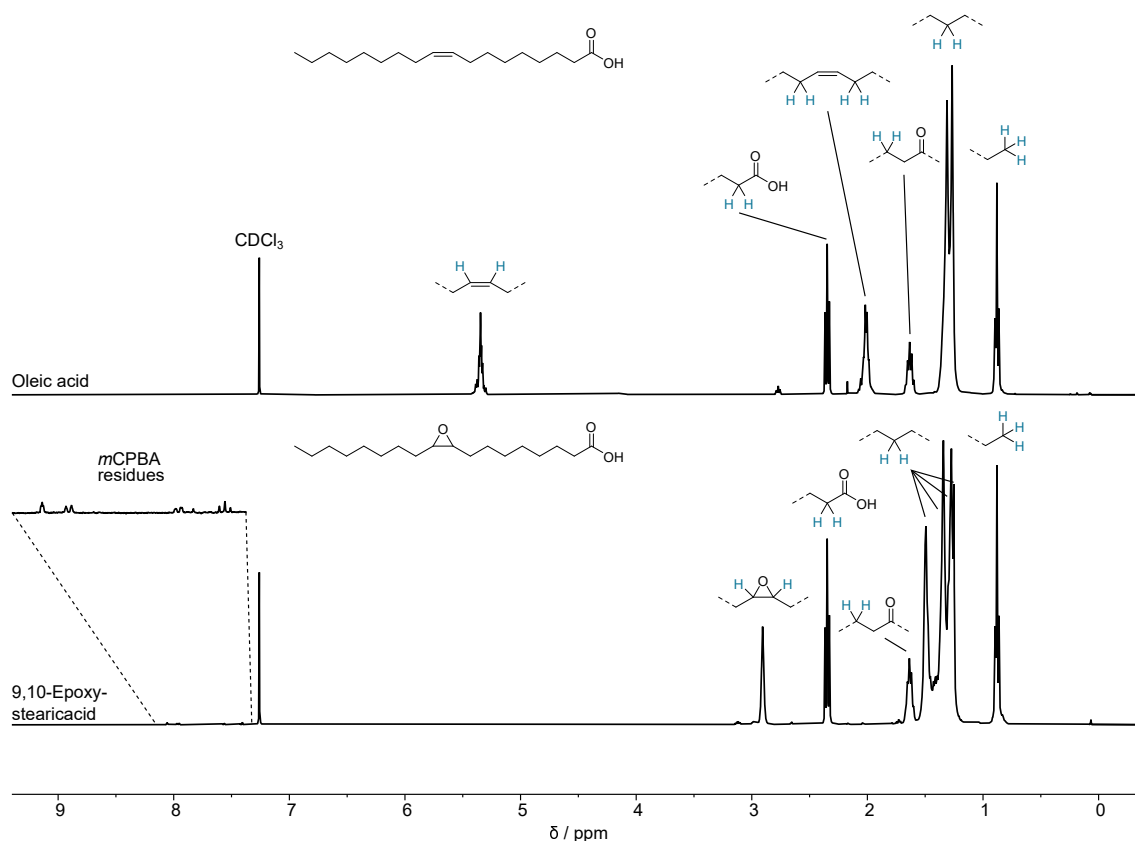
Figure 4.28: ^{1}H-NMR of oleic acid (top), and epoxidized oleic acid (9,10-epoxystearic acid, bottom) in chloroform-d as solvent.

The problem with foaming fatty acids can be overcome by first transferring the free fatty acids into their methyl ester. A *Fischer*-esterification can be performed by stirring the fatty acid in methanol at 70 °C containing concentrated sulfuric acid as a catalyst. The mesomerically stabilized cation of the unsaturated fatty acid formed after protonation by sulfuric acid is nucleophilically attacked by the free electron pair of methanol. The resulting oxonium ion splits off water to form a cation and, after deprotonation, forms the desired fatty acid ester. A certain amount of water is advantageously removed from the reaction equilibrium of ester formation by the hydration capacity of H_2SO_4. Following this method, the methyl esters of oleic acid and linoleic acid were prepared, which resulted after epoxidation in 9,10-epoxy methyl stearate and 9,10-12,13-diepoxy methyl stearate (DESMe). The success of the esterification can be verified by ^{1}H-NMR, the introduced methyl group appears at 3.66 ppm at both fatty acids (Figure A23, Figure A26). The purity of the product could be confirmed by GC-MS since only one species is visible in the elugrams (Figure A28, Figure A25).
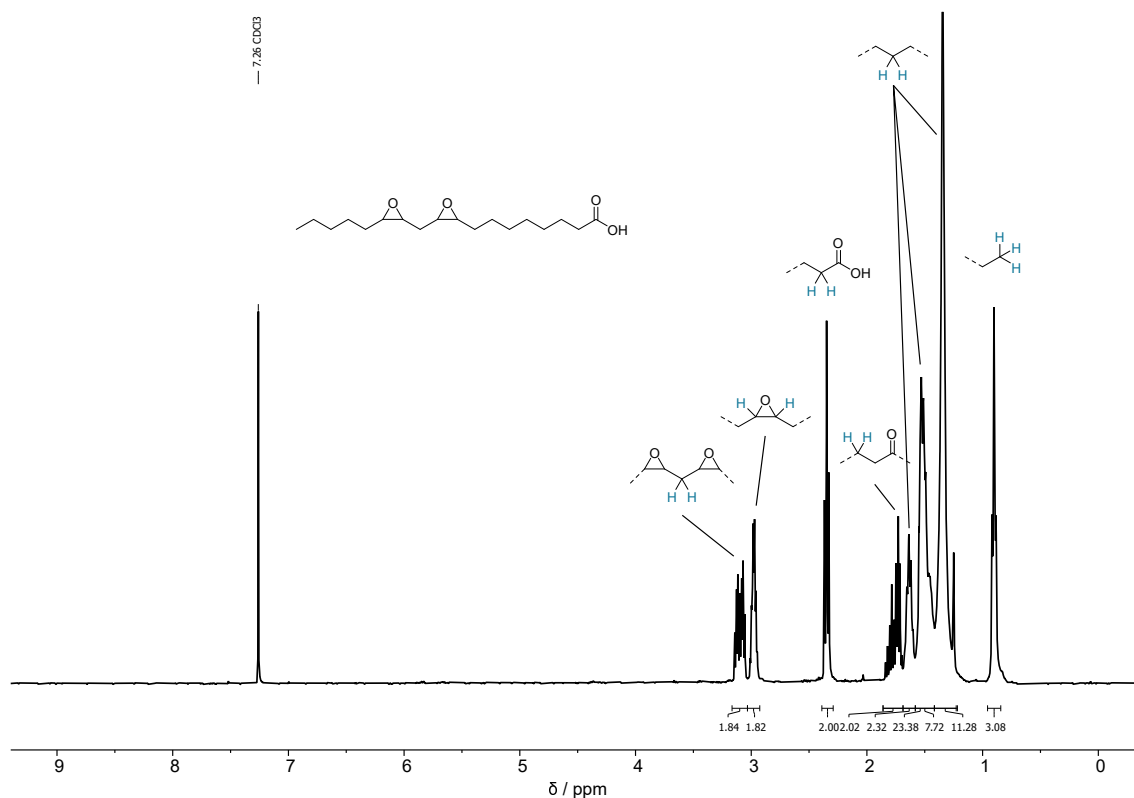
Figure 4.29: ^{1}H-NMR of epoxidized linoleic acid (9,10-12,13-diepoxystearic acid) in chloroform-d as solvent.

This esters were then also epoxidated with *m*CPBA and Oxone®. For this type of reactant, the method with Oxone® has a clear advantage due to the ease of work-up. Figure 4.30 shows the ^{1}H-NMR of epoxidized methyl linoleate. Compared with the spectrum of epoxidized linoleic acid, the methyl group at 3.66 ppm is clearly visible. Apart from that, the signals of the protons located at the epoxy-carbons and the neighboring protons can be seen at 3.08 ppm and 2.95 ppm.

4.6.2 Curing of epoxidized fatty acids

As described in Section 2.3.2, an epoxy thermoset normally consists of two components: an epoxy resin and a hardener. However, no second component is required in the case of epoxidized free fatty acids with their functionality given by the presence of epoxide and carboxylic acid in one molecule. The thermally induced curing reaction can be monitored with a DSC-scan of DESA (Figure 4.31a). In the first heating starting from −50 °C there are two melting transitions at 26 °C and 63 °C visible. The presence
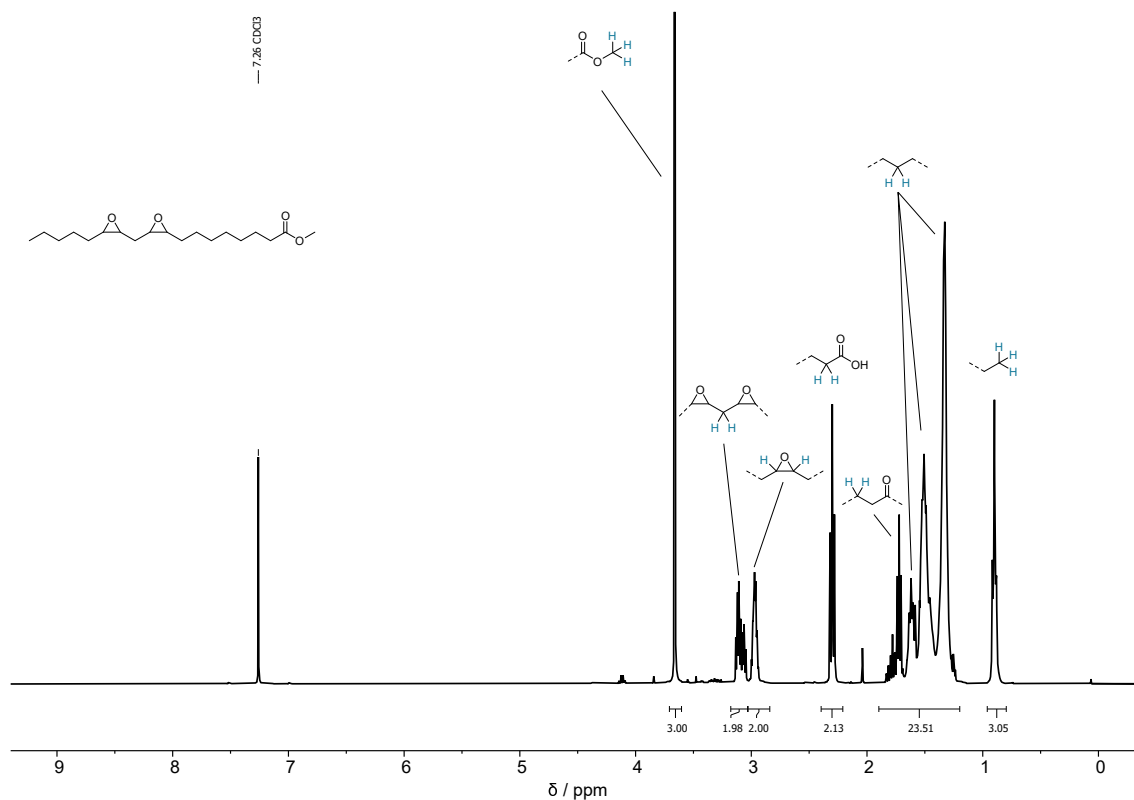
Figure 4.30: ^{1}H-NMR of epoxidized methyl linoleate (9,10-12,13-diepoxy methyl-stearate) in chloroform-d as solvent.

of two melting points initially raised doubts about the purity of epoxidized fatty acid. However, this phenomenon has been the subject of research and literature known and is due to stereoisomerism. While the two oxygens are opposite in the lower melting isomer, in the higher melting, they are on the same side of the molecular plane.[240] At a temperature of around 100 °C, an exothermic process is starting, which represents the curing reaction between the epoxy- and acid functionalities. After cooling down again (not displayed) and heating again, now a glass transition is observable at –21.5 °C. Since no second exothermic curing process is visible in higher temperature regions, it can be assumed that all potential reactants have already reacted completely. The cured product is very elastic and rubbery due to the T_g considerably below room temperature. A TGA measurement (Figure 4.31b) shows a temperature of 5 % weight-loss ($T_{5\%}$) at 265 °C.

In order to form a dense network and reach the highest possible thermal proper-ties, the ratio of epoxy resin and hardener should be stoichiometrically balanced. Of course, when hardening a diepoxy fatty acid with itself, the stoichiometry of oxiranes
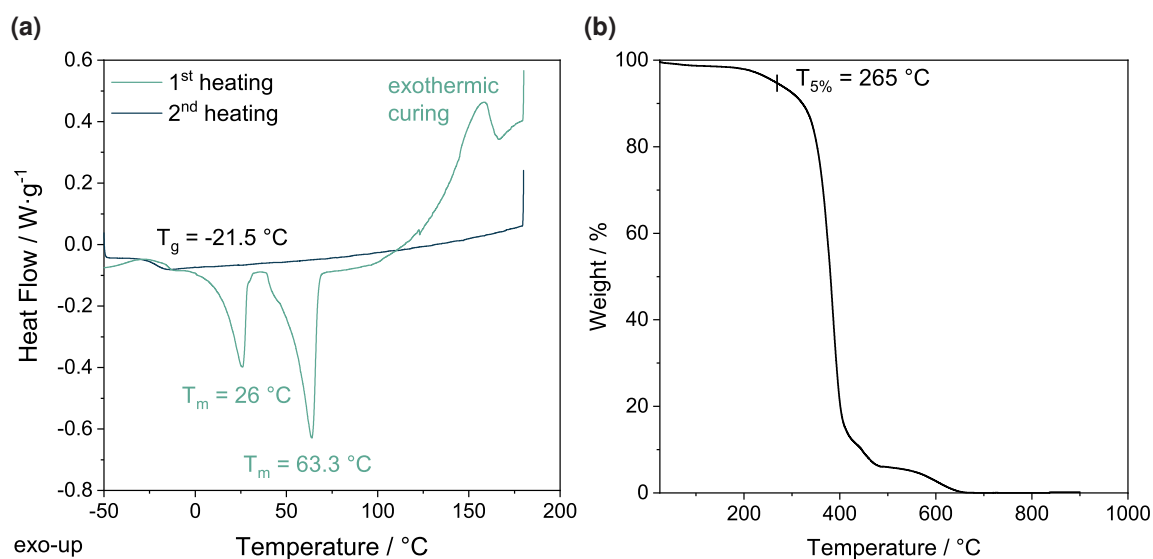
Figure 4.31: a) DSC-scan of 9,10-12,13-diepoxy stearic acid, b) TGA-scan of the cured resin of 9,10-12,13-diepoxy stearic acid.
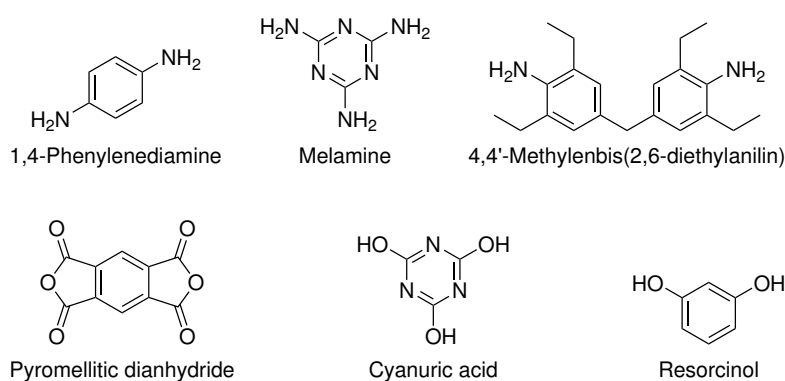
Figure 4.32: Amine, anhydride, and hydroxyl hardeners for curing screening with DESMe.

to acid groups is not ideal. This is why the carbonic acid functionalities were masked by esterification, and the methylated epoxidized fatty acids were used in combination with traditional hardeners. For this, several different multifunctional amines, alcohols, and anhydrides were identified as potential hardeners and tested in curing experiments with DESMe. Besides the hardeners IPD, DETA, and TA introduced in Section 2.3.3 (Figure 2.9), also 1,4-phenylenediamine, melamine, 4,4'-methylenbis(2,6-diethylanilin), pyromellitic dianhydride, cyanuric acid and resorcinol (Figure 4.32) were tested. For all mixtures, stoichiometric ratios were used to obtain the densest possible network. Only TA is an exception here, as it is not possible to calculate the optimum mixing ratio due to its numerous phenolic hydroxyl groups.

Table 4.10: Screening of different hardeners, stoichiometric reacted with DESMe. T_m = melting points of the pure hardener substances. Curing temperature 180 °C. MBDA = 4,4'-Methylenbis(2,6-diethylanilin).

Hardener	T_m / °C	Time / h	Nature of Product
1,4-Phenylenediamine	140	1	viscous liquid
MBDA	88	1.5	liquid
DETA	–39	1.5	liquid
IPD	10	1.5	rubbery
Melamine	—	12	brittle, powdery
Pyromellitic dianhydride	284	2	solid, brittle
Cyanuric acid	—	2	decomposition
Resorcinol	110.7	1.5	rubbery
TA	—	1.5	solid, stiff

Table 4.10 summarizes the screening of the different potential hardeners. Basically, the hardeners used can be divided into two categories. The majority is solid at room temperature; only IPD and DETA are liquid. Solid-solid or liquid-solid epoxy resin-hardener mixtures turned out to be hard to process. The difficulty lies in a homogeneous mixture of the solid part in the liquid to ensure uniform curing. Some of the hardeners listed in Table 4.10 melt below the curing temperature of 180 °C, which basically results in a liquid-liquid system again, but this is not the case for pyromellitic dianhydride with a very high melting point of 284 °C and the molecules which lack a T_m due to decomposition.

The outcome of the curing tests showed very different results. Beginning with the amine hardeners, 1,4-phenylenediamine, MBDA, and DETA stayed liquid after 1 to 2 h in the oven and did not cure to a solid thermoset. IPD seems to form a 3D network resulting in a rubbery product with an T_g of 38 °C (Figure A30). Melamine, on the other hand, becomes very brittle and powdery during curing, which could indicate insufficient mixing and, thus, only partial curing. In the literature, a processing procedure is described, which includes a pre-heating to 60 °C and the addition of catalytic amounts of NaOH to facilitate dissolution when working with Melamine. Additionally, high brittleness is also described, which makes the hardener less attractive.[241] The experiment with pyromellitic dianhydride resulted in a solid, but again brittle cured thermoset. As can be seen in the DSC-scan (Figure 4.33a), the exothermic process
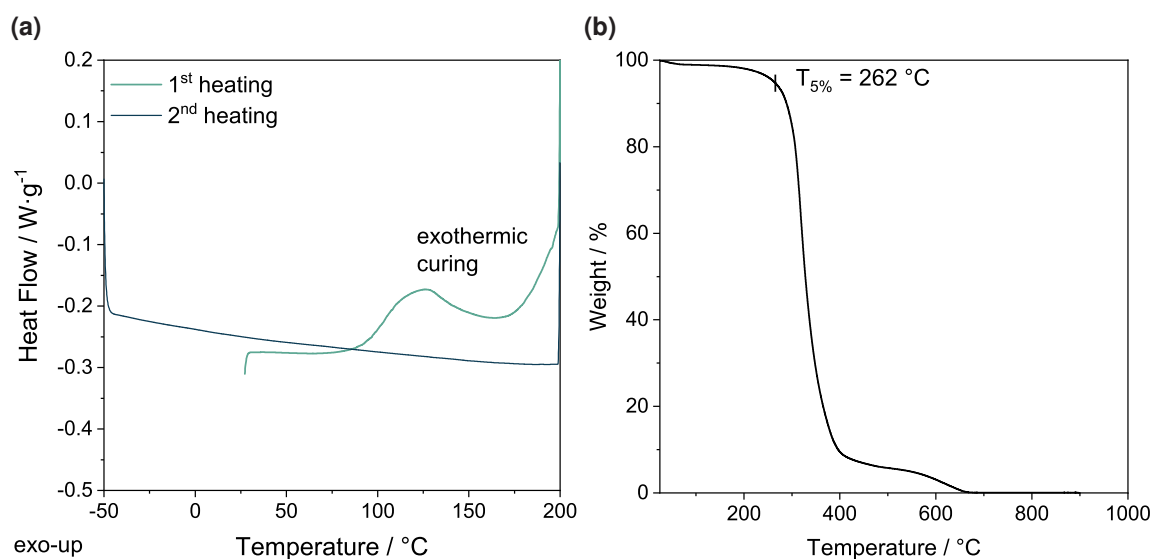
Figure 4.33: a) DSC-scan of DESMe curing with pyromellitic dianhydride, b) TGA-scan of the cured resin of the same sample.

starts again at a temperature of 100 °C. In the second heating cycle, there are no further thermal processes visible which indicate the curing to be complete, with no T_g observed either. In the TGA-scan (Figure 4.33b), decomposition starts at 262 °C.

The combination of DESMe and cyanuric acid lead to decomposition when heated to the curing temperature, which explains why no use of cyanuric acid as a curing agent for epoxy resins is documented in the literature. While resorcinol leads to a rubbery product analog to IPD, a hard and stiff thermoset could be obtained with the structurally related tannic acid. Again, curing starts at around 100 °C (Figure 4.34a), and it is noteworthy that the maximum of the curing enthalpy is located at high temperatures of approximately 240 °C. Here, too, the resin is completely cured after the first heating ramp. The T_g is located at 35.6 °C but is not very clearly visible. Decomposition is shifted towards higher temperatures (288 °C, Figure 4.34b), which makes TA in combination with the T_g a promising candidate for curing with epoxidized fatty acids or vegetable oils.

With regard to the thermal properties, the results of the screening allow some conclusions to be drawn. The highest T_g observed is around 36 °C, which leaves room for improvement. To achieve higher thermal stability, a denser, less flexible network is essential. This can be achieved either by more covalent bonding points (epoxy groups),
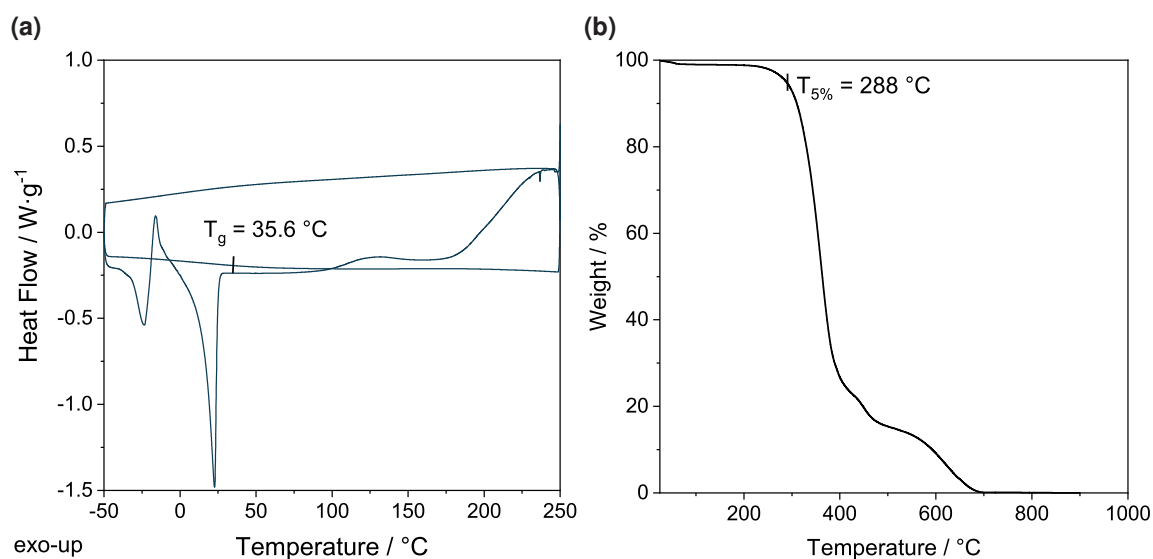
Figure 4.34: a) DSC-scan of DESMe curing with tannic acid, b) TGA-scan of the cured resin of the same sample.

more rigidity in the molecules, or by intermolecular interactions (polar or aromatic). Each of these approaches or combinations of these to improve the properties of the cured thermoset will be addressed in more detail in the following sections.

4.6.3 Epoxidation of vegetable oils

First, the influence of the number of crosslinking points in the form of epoxide groups will be examined in more detail. For this purpose, the free fatty acids are no longer used, but the whole triglycerides. Edible oils obtained from olives, canola, hemp, or linseed, as well as oil obtained from yeast cultures, were investigated by NMR for their double bond content (Figure 4.35). The yeast oil was produced and provided by the Chair of Synthetic Biotechnology (WSSB) of the Technical University of Munich.

From the NMR, some information about the molecular constitution of the respective oil can be obtained. On the one hand, the average double bond content of the whole triglyceride can be determined by integration of the respective signals at around 5.35 ppm, also the protons between two double bonds are visible at 2.79 ppm. The number of double bonds was found to be 1.5 for yeast oil, 2.5 for olive oil, 3.5 for canola oil, 5 for hempseed oil, and 6.3 for linseed oil. Additionally to that, the methine and
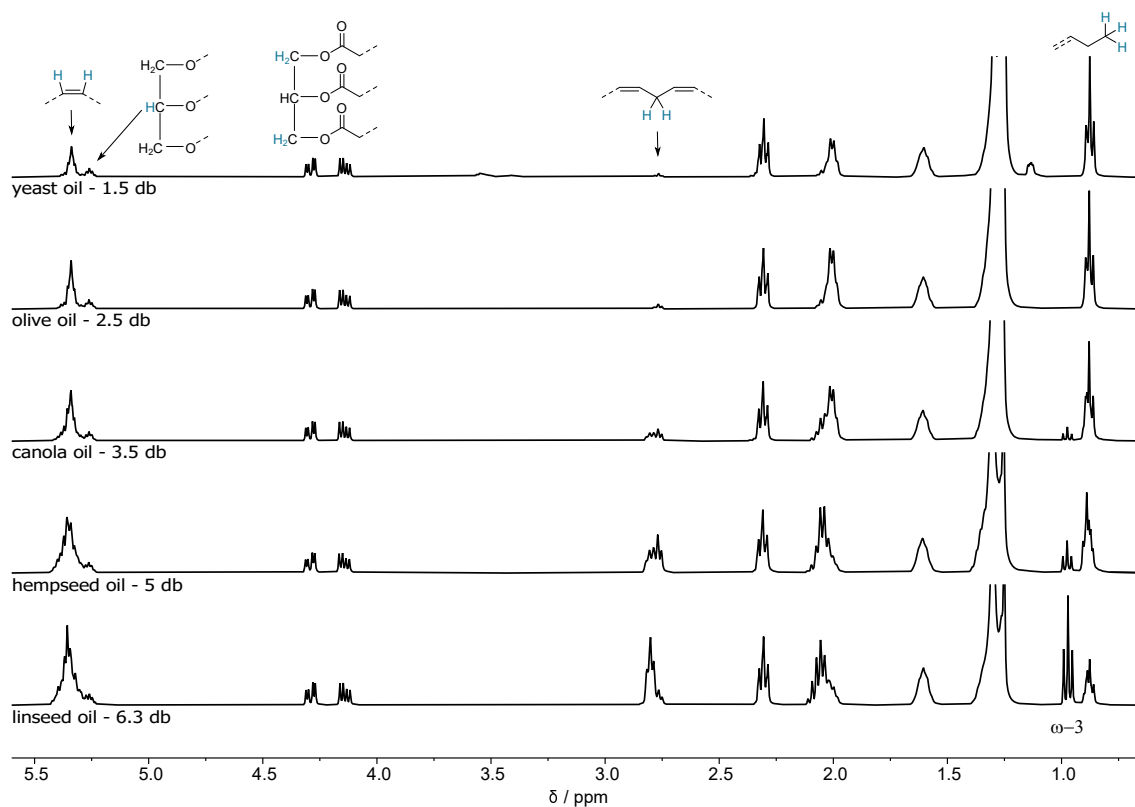
Figure 4.35: ^{1}H-NMR for double bond (db)-determination of yeast oil and different vegetable oils in chloroform-d as solvent.

methylene signals of glycerin can be observed at 5.26, 4.29 and 4.13 ppm. Interesting is also the triplet at 0.97 ppm appearing in the spectra of oils with higher double-bond content, which represents the terminal methyl-group of ω-3 fatty acids.

These vegetable oils can be epoxidized on a big scale using formic acid and H_2O_2 to form *in situ* the oxidizing peracid. Because performic acid is rather corrosive to steel, the reaction was performed in a 2 L glass reactor at 50 °C.[207] As can be seen in the ^{1}H-NMR-spectrum of the product (Figure 4.36), no residual signals of the former double bonds are visible. The protons around the introduced epoxy groups appear analog to the free fatty acids before around 3.0 ppm.

Curing these EVOs with IPD reveals the importance of the number of double bonds or epoxy groups. As can be seen from Figure 4.37, there is a linear correlation between the T_g and the number of epoxy groups per triglyceride between olive oil and linseed oil. Epoxidized yeast oil breaks out this trend as the 1.5 db are statistically not sufficient to form a true 3D network.
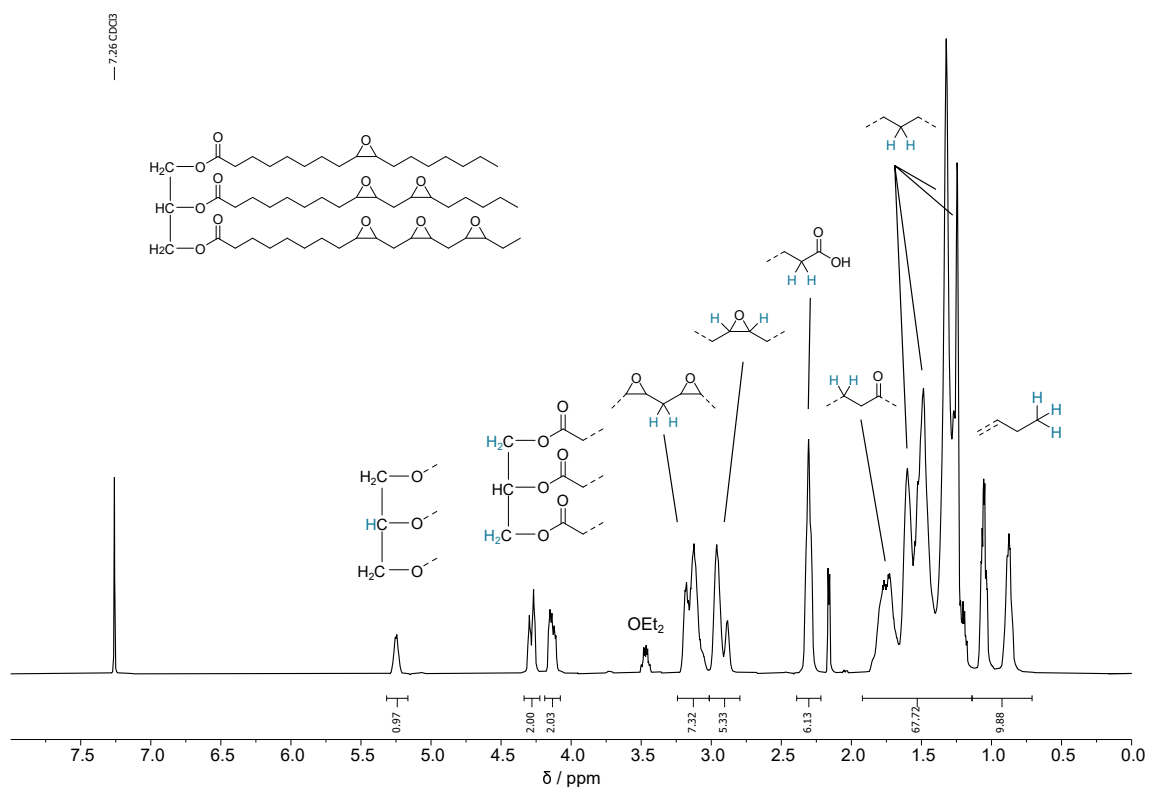
Figure 4.36: ^{1}H-NMR of epoxidized linseed oil in chloroform-d as solvent.
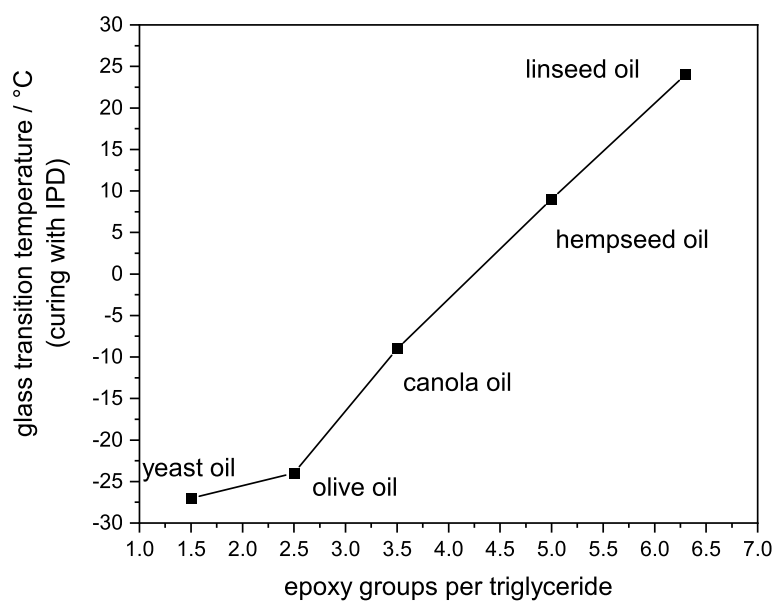
Figure 4.37: Correlation between T_g and the amount of epoxidized double bonds in different EVOs. All samples are cured with IPD.

The high epoxy-group content in ELO makes the oil an ideal product for further investigations in combination with TA to obtain high thermo-mechanical and mechanical properties of the cured thermoset.

4.7 A fully bio-based epoxy thermoset using epoxidized linseed oil and tannic acid

Parts of this chapter were published in the Journal *Macromolecular Materials and Engineering* with the article entitled "Fully Bio-Based Epoxy Thermoset Based on Epoxidized Linseed Oil and Tannic Acid".[182] The publication was developed in co-operation with the Chair of Carbon Composites (TU Munich) within the framework of the project "Green Carbon" funded by the German Federal Ministry of Education and Research (FKZ: 03SF0577A). Preparation and curing of the epoxy thermoset samples were performed by Nikita Reinhardt. Also, DMA, flexural testing, and stress-strain data were fully collected and analyzed by him, as well as parts of the DSC measurements. The contributors are listed in the reference:

Reinhardt, N.*, Breitsameter, J.M.*, Drechsler, K. and Rieger, B., Fully Bio-Based Epoxy Thermoset Based on Epoxidized Linseed Oil and Tannic Acid, *Macromolecular Materials and Engineering*, **2022**, 307, 12, 2200455. *These authors contributed equally.*
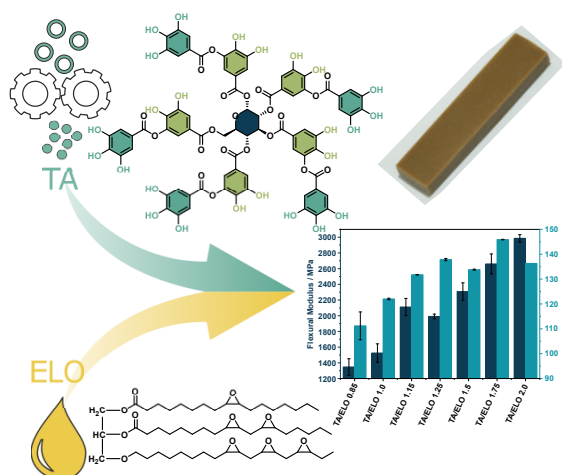
Figure 4.38: Graphical abstract of the publication "Fully Bio-Based Epoxy Thermoset Based on Epoxidized Linseed Oil and Tannic Acid". Reprinted from Reinhardt *et al.*[182]

4.7.1 Milling procedure of tannic acid

As already discussed earlier, in the case of solid hardeners, a homogeneous distribution in the liquid epoxy resin is crucial to obtain a uniformly cured epoxy thermoset with the highest possible thermo-mechanical properties. This is why TA was subjected to a milling procedure to properly disperse TA into ELO without using solvents. TA was first dried and then milled following a two-step ball-milling procedure. As can be seen from Figure 4.39, median particle size distribution was reduced significantly shifting the D_{50} from 50.2 μm to 6.6 μm.
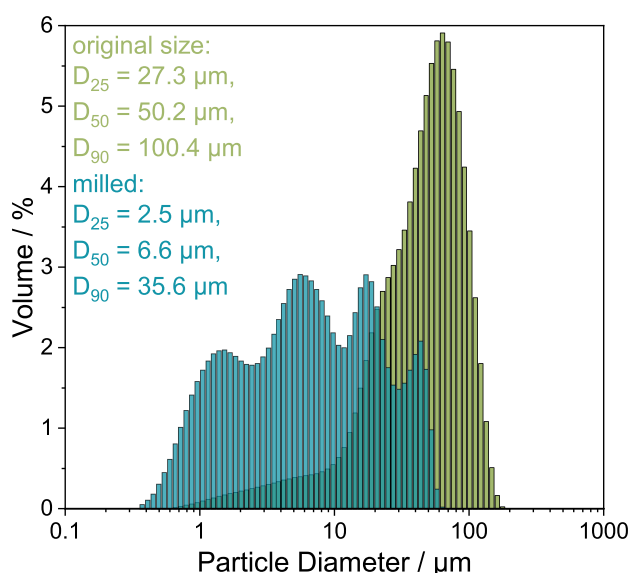
Figure 4.39: Particle size distribution of original size TA (as bought) and milled TA. Reprinted from Reinhard *et al.*.[182]

As can be seen from the microscopic images, the particles in the purchased TA are relatively large and appear bubble-shaped (Figure 4.40a). This shape could be from an industrial drying process. Bubble-like structures would hinder a homogeneous curing process, as air could be trapped in the center, and the inside is poorly accessible during the curing reaction. After milling, particle size is much smaller, as already seen in particle size determination (Figure 4.39). Dispersions from both the original size and milled TA in ELO (Figure 4.40c and Figure 4.40d) illustrate how much more homogeneously the milled product is distributed.
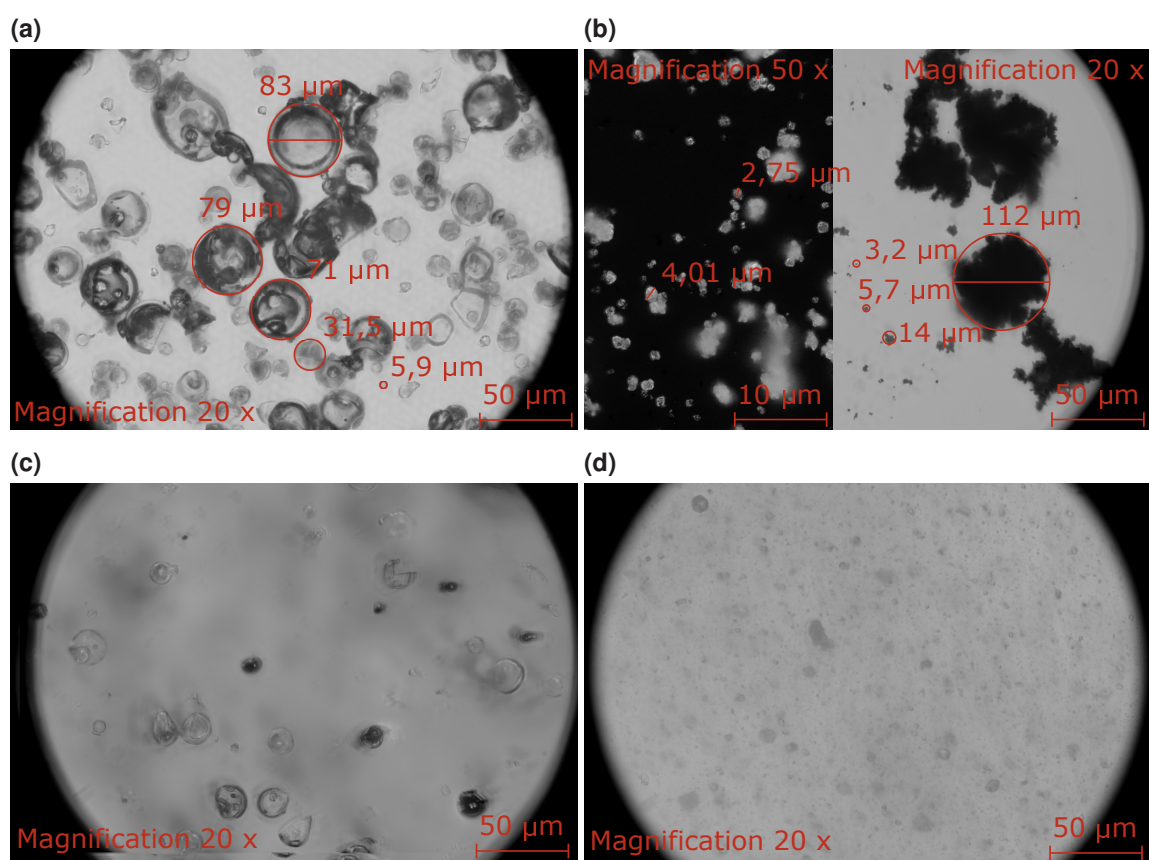
Figure 4.40: Microscope pictures of a) TA original size (as bought), b) TA after milling procedure, c) TA original size dispersed in ELO, d) TA milled and dispersed in ELO Figures adapted from Reinhardt *et al.*[182]

Table 4.11: Mixing ratios used for the different molar ratios of TA to ELO. Adapted from Reinhardt *et al.*[182]

Sample name	Molar ratio –OH : epoxide	m(TA) per 100 g ELO / g
TA/ELO 0.85	0.85	41.14
TA/ELO 1.0	1.0	48.40
TA/ELO 1.15	1.15	55.66
TA/ELO 1.25	1.25	60.50
TA/ELO 1.5	1.5	72.60
TA/ELO 1.75	1.75	84.70
TA/ELO 2.0	2.0	96.80

Table 4.12: Time and temperature used for the curing profiles of different TA to ELO mixtures. Adapted from Reinhardt *et al.*[182]

Curing profile	Curing	Post-curing
C1	16 h, 90 °C	3 h, 140 °C
C2	16 h, 120 °C	3 h, 140 °C

4.7.2 Epoxy sample preparation and curing

As described earlier, unlike conventionally used epoxy resin hardeners, curing with phenolic curing agents such as TA is more complex because of a poorly defined mixing ratio and the curing process. For this purpose, TA/ELO samples were prepared with different molar ratios of –OH/epoxide (Table 4.11). Ratios of 0.85, 1.0, 1.15, 1.25, 1.5, 1.75 and 2.0 were mixed to investigate the influence of the composition on the thermal and mechanical properties of the thermoset. An air release additive (Epinal EL 12.42) was added to remove air inclusions in the epoxy resin. Epinal EL 12.42 is a surface-active polyether siloxane that does not interfere with the curing reaction and whose carbon content is reported to be of certified bio-based origin. All specimens were cured at two different curing conditions C1 and C2 (Table 4.12), to investigate the influence of the curing conditions of the different mixing ratios on the thermal and mechanical properties.

4.7.3 Curing characteristics of tannic acid/epoxidized linseed oil

Because of the large amount of 25 hydroxyl groups in the hardener TA, all possible points to build a connection to an epoxy group of ELO, the curing characteristics need to be examined more deeply. The curing mechanism was already described in Section 2.3.3, Scheme 13c; however, hydroxyl functionalities are less reactive compared to amine groups, and due to steric hindrance, very unlikely that every –OH groups participates in the curing reaction.[180] To investigate the reaction between TA and ELO, DSC measurements were performed. Figure 4.41a shows an exemplary plot of heating the mixture TA/ELO 1.75. All mixtures show similar shapes, and the scans can be divided into three different areas.

First, from 25 °C to 100 °C, an endothermic peak can be observed, which corresponds to the evaporation of hydrated water (Figure 4.41a, I)). Comparing the DSC-scan of pure, dried TA (Figure 4.41c) shows the same endothermic process from approximately 25 °C to 120 °C. A TGA-scan could also confirm water being present despite the multiple drying steps (Figure 4.41d). Dry TA shows a weight-loss of 1.7 % at 120 °C. After one day of exposing dried TA to the laboratory atmosphere (55 % humidity, 25 °C), TGA showed a weight loss of almost 10 % at 120 °C. This shows the highly hygroscopic behavior of TA's polar hydroxyl- and ester functionalities.

Second, in the heating DSC-scan of TA/ELO 1.75 (Figure 4.41a, II)) the exothermic process of the curing reaction between –OH and epoxides starting at around 100 °C can be observed. The peak of the curing enthalpy reaches its maximum at 173 °C and ends at 250 °C. These curing characteristics are in accordance with the literature.[178,180,242]. Figure 4.41b summarizes the maximum curing enthalpies of the different TA/ELO mixtures. From this plot, it can be seen that the maximum of the hardening enthalpy shifts to lower temperatures with increasing TA content (TA/ELO 0.85: 194 °C, TA/ELO 2.0: 171 °C). Therefore, the highest reaction rate is achieved with excess TA at lower temperatures, reducing the energy demand and increasing the curing efficiency. This behavior can be explained by the high molecular mass of the hardener and the strongly sterically hindered hydroxyl groups. In the initial phase

of the curing reaction, the basic structure of the 3D epoxy network is already defined after forming only a few ether bonds. This makes the remaining hydroxyl groups less available for further onding, and a large part of the potential linkage points remain unreacted. A higher TA content leads to better availability of –OH groups, which increases the probability of a reaction and the overall degree of crosslinking due to the size of the curing agent.

The shoulder in the DSC-scan of TA/ELO 1.75 (Figure 4.41a, III)) at temperatures greater than 250 °C indicates starting of the degradation of TA and can also be observed in a TGA-scan (Figure 4.44a). The shoulder becomes more pronounced with increasing TA content since more TA is present unreacted and thus starts decomposing (Figure A31).

4.7.4 Thermo-mechanical properties

Thermo-mechanical properties were determined by means of DMA. In addition to the storage and loss modulus, the T_g can also be determined exceptionally precisely by DMA.[243] Figure 4.42a shows an exemplary DMA-measurement of TA/ELO 1.75 cured with condition C1. The curves for all other specimens were similar, but especially the broad tanδ is noteworthy. The relaxation of a heterogeneous network can explain this.[244,245] For the thermoset TA/ELO, the broad tanδ can also result from the complex crosslinked structure. Contrary to conventional epoxy thermosets like DGEBA, where the oxirane groups are always located at sites with chemically identical environments, the epoxides in ELO are statistically distributed in the aliphatic backbone of the triglyceride.[246] In addition, the influence of TA with its high molecular weight and the unequal reactivity of the hydroxyl groups, which changes during curing, comes into account.[178] The resulting unpredictable, complex network of TA and ELO broadens the T_g.

It is not uncommon for an epoxy thermoset to have the T_g affected by the ratio of epoxy resin to hardener. The crosslink density and structure vary with this ratio,
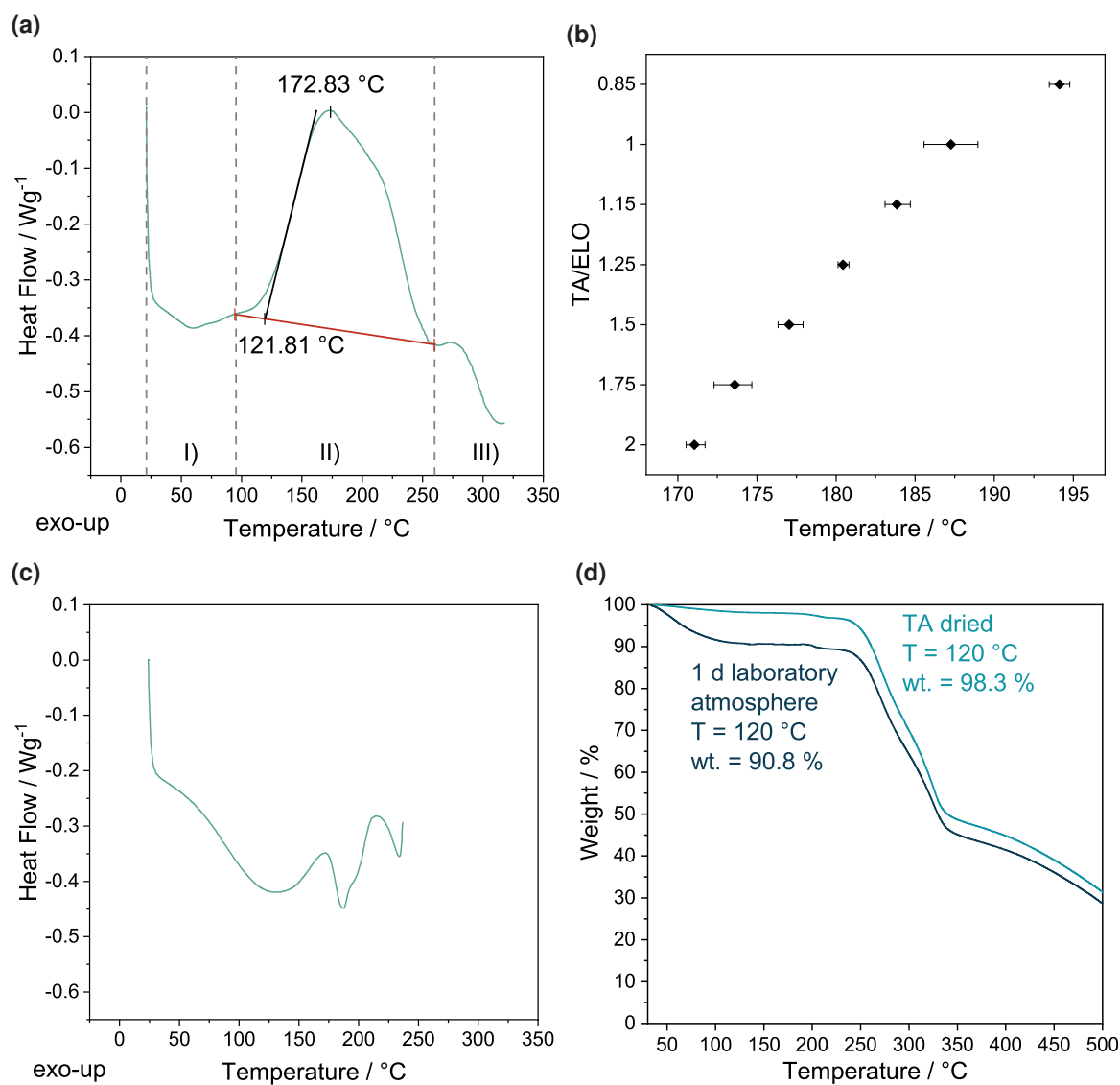
Figure 4.41: a) DSC-scan of the sample TA/ELO 1.75 with onset temperature of the curing enthalpy (121.81 °C) and temperature of the peak of the curing enthalpy of 172.83 °C, b) Average temperature of the peak of the curing ehtnalpy for the different TA/ELO mixtures, c) DSC-scan of pure milled and dried TA, d) TGA-measurements of dried TA and TA after being exposed one day to the laboratory atmosphere. Figures adapted from Reinhardt *et al.*[182]
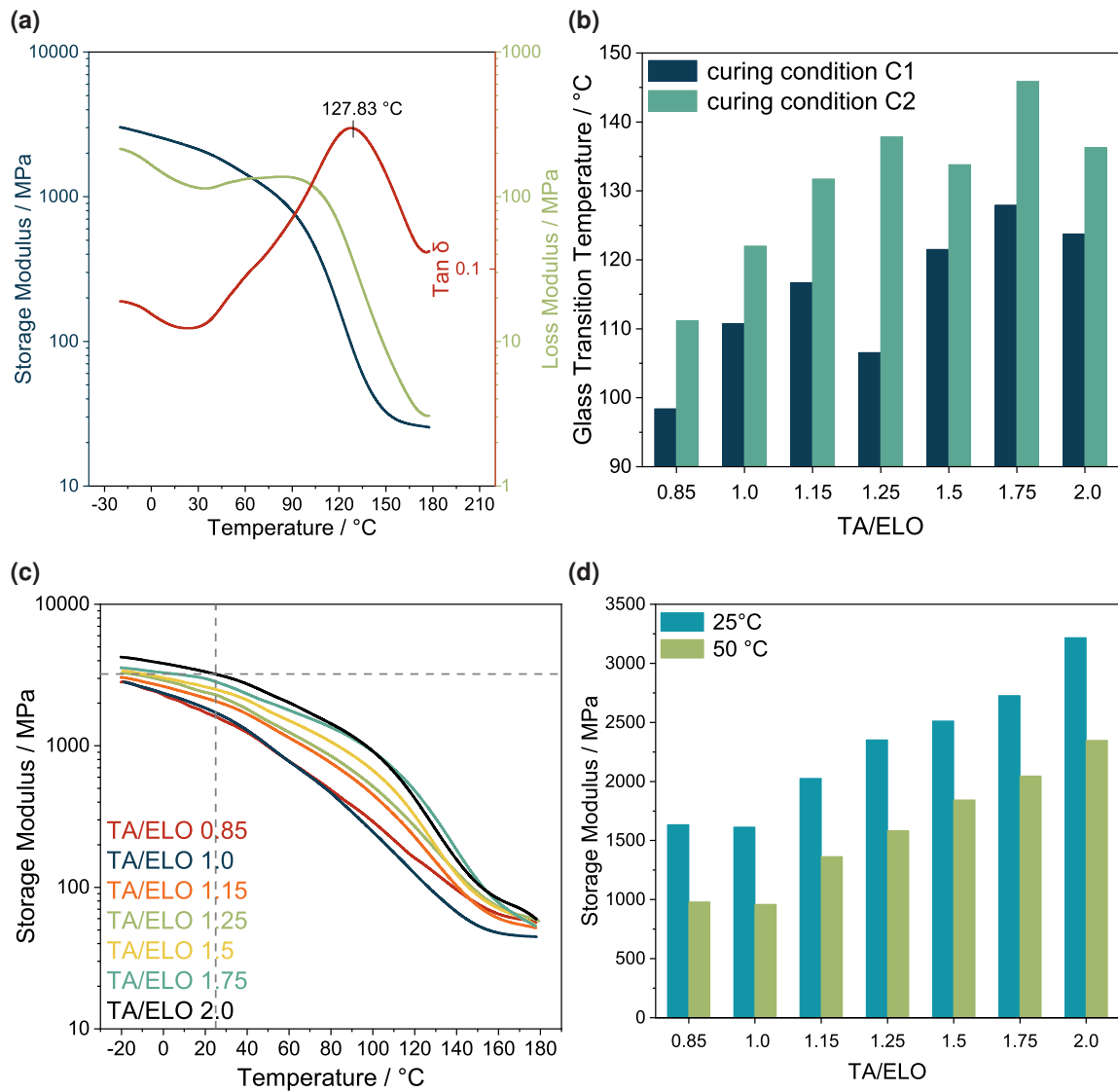
Figure 4.42: a) DMA-measurement of TA/ELO 1.75 cured with C1. T_g = 127.83 °C, b) Storage modulus curves (E') for the different TA/ELO specimens cured with C2, c) Comparison of T_gs obtained from DMA for the different TA/ELO samples cured with C1 and C2, d) Storage moduli at 25 °C and 50 °C cured with C2. Figures adapted from Reinhardt *et al.*[182]

affecting thermal properties.[247] Figure 4.42b clearly shows this correlation. Both curing conditions share the trend that the T_g rises with increasing TA content. In addition, with the higher applied temperatures of curing condition C2 as high T_gs as 145 °C for the sample TA/ELO 1.75 can be reached while the samples of C1 show lower T_gs. This indicates that the temperature profile of C1 is insufficient to reach the full crosslinking potential. The trend of rising T_g with rising TA content coincides with the literature.[178,216]

Measuring the gel content confirms that the samples cured with C1 have a lower degree of crosslinking. The gel content is determined by Soxhlet extraction of samples with the exact dimensions for 24 h with methanol as solvent. Also, curing above the T_g results in a higher crosslinking density. As the curing temperature with both C1 and C2 is below the T_g for almost every TA/ELO mixture, there occurs vitrification which makes the reaction-diffusion controlled.[248]

IR spectroscopy provides information about the conversion of the oxirane groups or the completeness of the curing reaction. For the pure ELO, the C–O epoxide vibration can be observed at $820\,\text{cm}^{-1}$. Accordingly, no residual signal should be visible in completely cured specimens. This is the case for the samples with a TA/ELO content above 1.0; only the sample TA/ELO 0.85 shows residuals of the vibration mode (Figure A33).

The elasticity of an epoxy thermoset sample is associated with stiffness and can be described by the storage modulus (E') obtained from DMA measurements.[249] The E'-curves for the samples cured with C2 can be seen in Figure 4.42c. As expected and correlating with the T_gs, stiffness is increasing with higher ratios of TA. The maximum average storage modulus of 3218 MPa could be observed at room temperature (marked with dotted lines in Figure 4.42c) for the sample TA/ELO 2.0 cured at condition C2.

Comparing these thermo-mechanical values to the literature, the obtained T_g and E' are high for an EVO cured with a biobased hardener. Directly comparable is a study by Qi *et al.*, who cured epoxidized soybean oil with TA and found a T_g of

77 °C and a storage modulus of 1103 MPa at 25 °C.[179] Also based on soybean oil, Altuna *et al.* obtained a T_g of 30 °C with citric acid as hardener.[250] With the same hardener, Todorovic *et al.* achieved a T_g of 82 °C with ELO and a storage modulus of 1380 MPa.[212] Comparably high properties could only be achieved by using the oil-based hardener MTHPA with ELO. Here, a T_g of 145 °C was achieved.[212]

4.7.5 Mechanical properties

Table 4.13 summarizes the results of flexural testing of the TA/ELO samples. In typical applications, epoxy thermoset experience flexural load, which makes the flexural modulus, flexural strength, and elongation at break interesting properties. Both flexural modulus and flexural strength are increased for the samples cured by C2. The material is stiffer and resists flexural loads better because of the improved polymer crosslinking.

As already observed for the storage modulus, the flexural modulus increases with a larger content of TA. The highest flexural modulus was observed for the sample TA/ELO 2.0 cured by the condition C2 of 2986 MPa. Thus, the fully bio-based TA/ELO thermoset can exhibit similar stiffness under load as commercial petroleum-based epoxy materials. For comparison, Sika's CR80 epoxy system has a flexural modulus of 2900 to 2950 MPa.[171] This thermoset finds application in high-performance fiber-reinforced composites in *e.g.* wind turbines.

As can be seen from the values of elongation at break (Table 4.13), brittleness comes with increasing stiffness and TA content. The high uncertainties in the specimens TA/ELO 0.85, 1.0, and 1.15 from C1 are probably due to the curing conditions and insufficient crosslinking, resulting in an inhomogeneous specimen that breaks unpredictably under load. In Figure 4.43, the stress-strain curves for the samples cured with C2 can be seen. The flexural strength peaks at 72 MPa for TA/ELO 1.5. Remarkable is the wide range of flexural properties that is tuneable by the amount of hardener, which makes the resulting material stiff and brittle or very flexible before failure.

Table 4.13: Average Flexural Modulus, Flexural strength and elongation at break obtained for the different TA/ELO mixtures cured with the curing conditions C1 and C2. Adapted from Reinhardt *et al.*[182]

| Sample ↓ | Flexural Modulus MPa | | Flexural Strength MPa | | Elongation at break % | |
Curing →	C1	C2	C1	C2	C1	C2
TA/ELO 0.85	924(102)	1347(105)	33(2)	46(2)	8.2(1.0)	7.8(0.9)
TA/ELO 1.0	1484(146)	1525(117)	48(3)	50(3)	8.4(2.0)	5.9(0.4)
TA/ELO 1.15	1711(48)	2111(110)	50(3)	67(1)	4.9(1.7)	4.7(0.4)
TA/ELO 1.25	1692(66)	1991(30)	50(1)	65(1)	4.9(0.7)	4.3(0.6)
TA/ELO 1.5	1943(175)	2308(111)	54(2)	72(1)	3.7(0.7)	3.7(0.1)
TA/ELO 1.75	2328(287)	2525(209)	63(9)	67(7)	2.8(0.7)	3.0(0.3)
TA/ELO 2.0	2686(176)	2986(47)	45(8)	66(3)	1.8(0.5)	2.5(0.1)
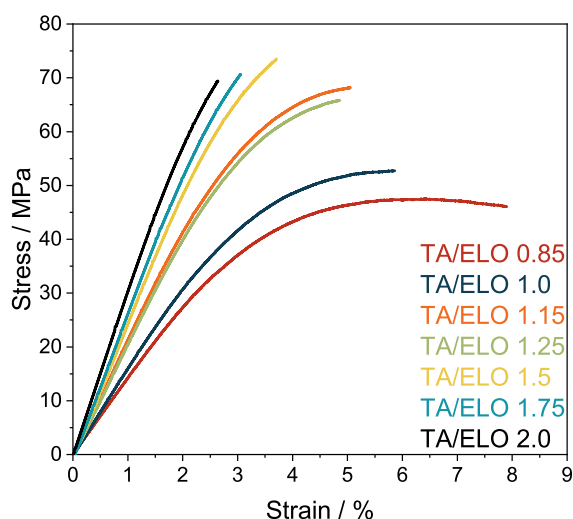
Figure 4.43: Stress-strain curves for the different TA/ELO samples cured with C2. Reprinted from Reinhardt *et al.*[182]

4.7.6 Thermal stability

Since the curing profile C2 leads to higher T_g and stiffness, thermal stability under an argon atmosphere was investigated for the samples of C2. Here, again a clear trend correlated with the amount of TA is visible. The more TA is present, the earlier decomposition starts since a large amount of TA remains unreacted and therefore is prone to thermal decomposition. As can be seen in Figure 4.44a, $T_{5\%}$ of pure TA is approximately at 235 °C which is also the temperature which is also the temperature the specimens approach which increasing TA-ratio.
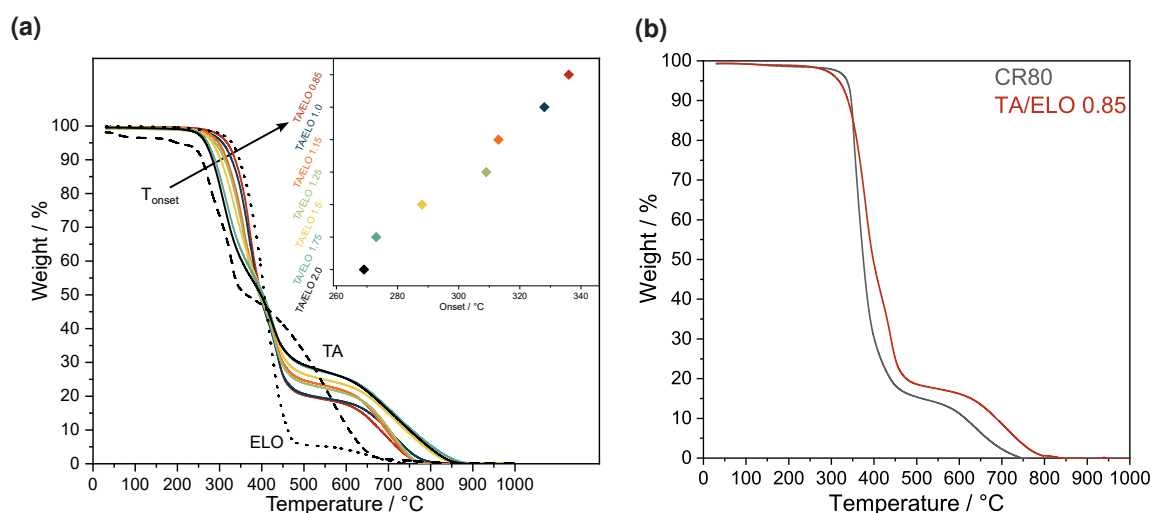
Figure 4.44: a) TGA curves of TA/ELO samples prepared with C2 and the pure components ELO (dotted) and TA (dashed) and respective temperature of 5 % weightloss. b) Comparison of TA/ELO 0.85 to the high-performance resin CR80 in TGA. Figures reprinted from Reinhardt *et al.*[182]

Samples with low TA content provide decomposition curves similar to those of conventional, commercially available high-performance epoxy resin systems. Figure 4.44b shows the comparison of the TA/ELO 0.85 sample with the high-performance CR80 by Sika. Although the onset of decomposition decreases with increasing TA content, the $T_{5\%}$ of sample TA/ELO 2.0 is high enough for applications under common conditions.

4.8 More rigidity by Diels-Alder-reactions

Since structures with fewer degrees of freedom should achieve better thermal properties, an attempt was made to create greater rigidity in the otherwise very mobile fatty acid chains. For this purpose, Diels-Alder reactions quickly became the focus of attention since six-membered rings can be easily created from conjugated dienes. In linoleic acid, the double bonds are separated by a CH_2 unit, which is why isomerization of the double bond is necessary first. Linoleic acid was isomerized by potassium hydroxide in a microwave reaction for this. The successful conjugation could be verified by ^{1}H-NMR since the double bonds which were present before the reaction as
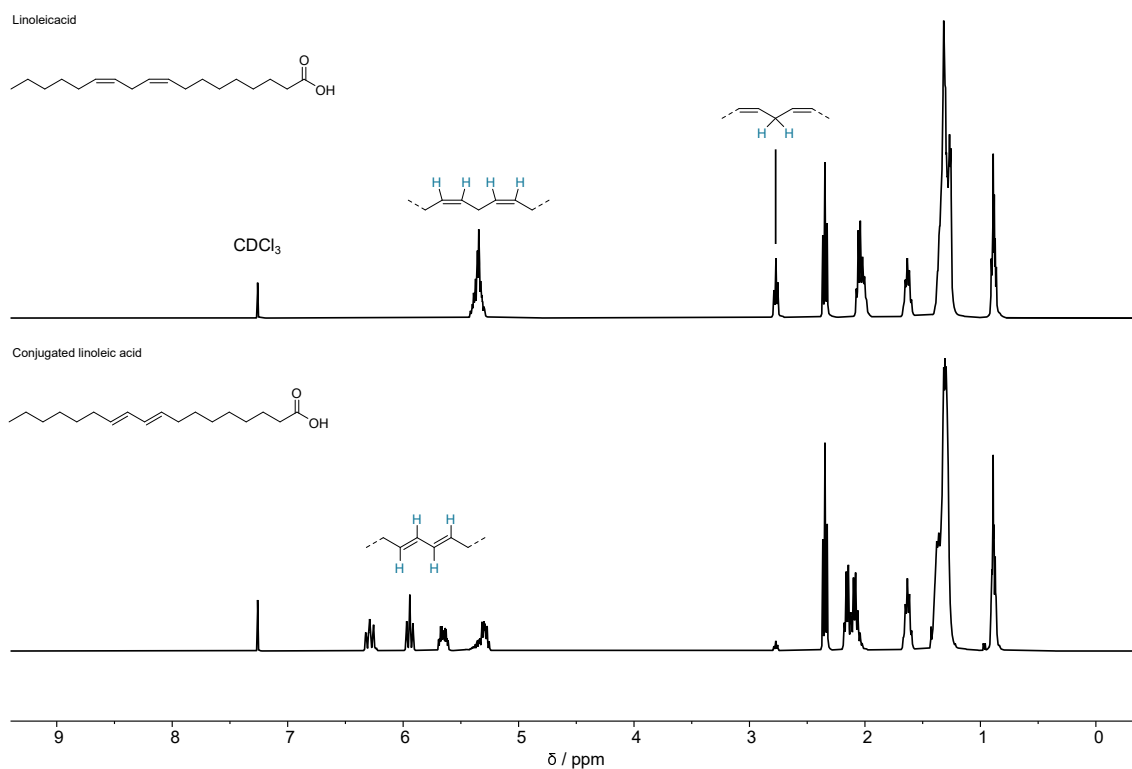
Figure 4.45: ^{1}H-NMR of linoleic acid before (top) and after conjugation (bottom).

one signal at 5.34 ppm show a characteristic splitting in four different signals at 6.29, 5.94, 5.67 and 5.29 ppm (see Figure 4.45). Also, the signal of the protons between the double bond in linoleic acid at 2.77 ppm vanishes during the conjugation reaction.

With the conjugated double bond now present in conjugated linoleic acid (CLA), cycloaddition with maleic anhydride as the dienophile should be possible. As shown in Figure 4.46a, after the Diels-Alder reaction, only one double bond is left in the molecule, which could be converted to the epoxide. In order to introduce further double bonds, the allylation of the carboxylic acid function as well as of the anhydride shown in Figure 4.46b was considered, which would provide a total of four epoxide groups in the fatty acid-base molecule.

The Diels-Alder reaction between CLA and MA did not produce a clear result. As can be seen in the NMR spectrum in Figure A2, the signals of the double bonds disappear, indicating a successful [4+4] cycloaddition, but in the remaining spectrum, the desired product could not be identified.

(a)

(b)

(c)

Isomerization   Diels-Alder-Reaction
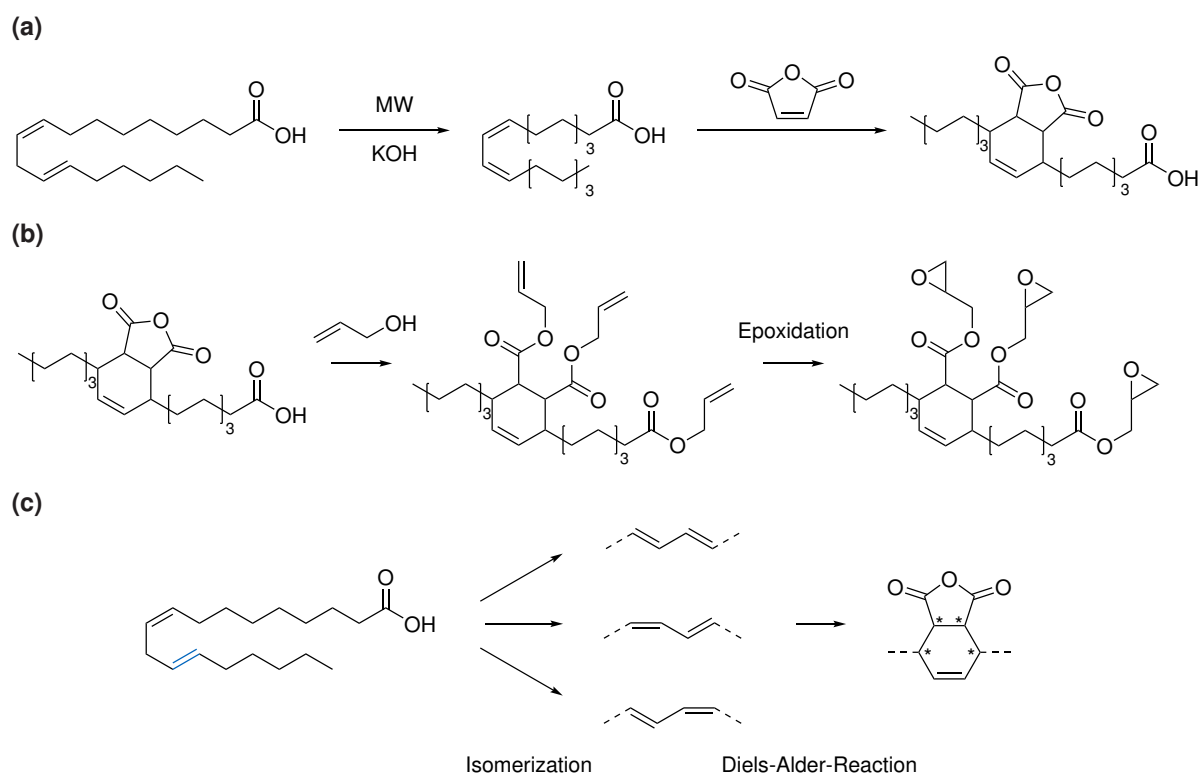
Figure 4.46: a) Isomerization of linoleic acid to the conjugated fatty acid and subsequent Diels-Alder reaction, b) theoretical reaction pathway towards a linoleic acid-based epoxy resin via a allylation reaction, c) possible structural isomers resulting from the isomerization reaction and stereocenters created during the Diels-Alder reaction.

109

The reason for this could be the large number of isomerization products resulting from the conjugation of the double bonds as shown in Figure 4.46c. This leads to various possible stereoisomers at the stereogenic centers in the Diels-Alder product, which leads to a plethora of signals in the ^{1}H-NMR. Additionally, the signals of the CH_2-groups of the fatty acids could overlay the emerging signals of the reaction. In order to simplify the spectrum, the following experiments were carried out using sorbic acid, or the allylated product allyl sorbate, as a model molecule for the fatty acid.

4.9 Synthesis of a new epoxy compound based on sorbic acid and characterization of the cured thermoset

Parts of this chapter were published in the Journal *Macromolecular Materials Engineering* with the article entitled "Synthesis of a sustainable and bisphenol A-free epoxy resin based on sorbic acid and characterization of the cured thermoset". The publication was developed in cooperation with the Chair of Carbon Composites (Technical University of Munich) and the Chair I of Technical Chemistry (Technical University of Munich) within the framework of the project "Green Carbon" funded by the German Federal Ministry of Education and Research (FKZ: 03SF0577A). Preparation and curing of the thermoset samples were performed by Nikita Reinhardt as well as the characterization by DMA and tensile testing. The contributors are listed in the reference:

Breitsameter, J. M.*, Reinhardt, N.*, Feigel, M., Hinrichsen, O., Drechsler, K. and Rieger, B., Synthesis of a sustainable and bisphenol A-free epoxy resin based on sorbic acid and characterization of the cured thermoset, *Macromolecular Materials and Engineering*, **2023**, 308, 9, 2300068. *These authors contributed equally.*
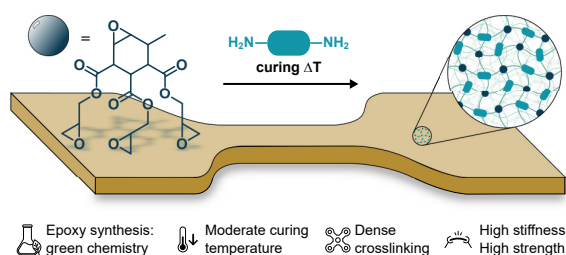
Figure 4.47: Graphical abstract of the publication "Synthesis of a sustainable and bisphenol A-free epoxy resin based on sorbic acid and characterization of the cured thermoset". Reprinted from Breitsameter *et al.*[251]

4.9.1 Synthesis of EGCHC epoxy monomer

Synthesis of the epoxy monomer 1,2-epoxy-6-methyl-triglycidyl-3,4,5-cyclohexanetri-carboxylate (EGCHC) follows a four-step procedure and is visualized in Scheme 19.

Starting from sorbic acid, the first reaction is an acid-catalyzed esterification with allyl alcohol, leading to allyl sorbate. This molecule is literature known but is usually synthesized by the reduction of allyl 2-hexynoate with triphenylphosphine,[252,253] esterification of allyl alcohol with a sorbic acid chloride,[254] or by reacting sorbic acid with allyl bromide or chloride.[255] All these synthesis routes are ecologically questionable due to the use of phosphines, chlorides, or bromides because of their toxicity. In contrast, the acid-catalyzed reaction used herein does not require such hazardous chemicals and only requires sulfuric acid in low concentrations to esterify the starting materials sorbic acid and allyl alcohol. The only by-product is water as a condensation product instead of corrosive gases such as hydrogen chloride, which must be scavenged. Another advantage is the high yield of up to 82 %, which outshines the other methods mentioned. The intramolecular Diels-Alder reaction be-tween the allyl and vinyl groups is a side reaction that reduces the yield. Martin *et al.* describe this reaction, which, however, normally takes place at much higher temperatures than the 97 °C used for esterification here.[254] The feedstocks sorbic acid and allyl alcohol can be obtained with high biobased carbon content. Sorbic acid, for example, is a biomolecule found in rowan berries and is approved in the EU as a food additive under the number E200.[256,257] As already described in Section 2.1.5, allyl alcohol can be obtained from biobased glycerol by treatment with formic acid or by catalytic methods.[61,258] The successful synthesis of allyl sorbate could be confirmed by ^{1}H/^{13}C-NMR spectroscopy (Figure 4.48, Figure A34) and analytical data are in agreement with literature.[254]

The next synthesis step towards EGCHC is a Diels-Alder reaction between allyl sor-bate and maleic anhydride. Here, the six-membered ring forming the basic framework of the final molecule is formed. Regarding efficiency, [4+2] cycloaddition reactions are interesting candidates to perform following the "green chemistry" rules. The high
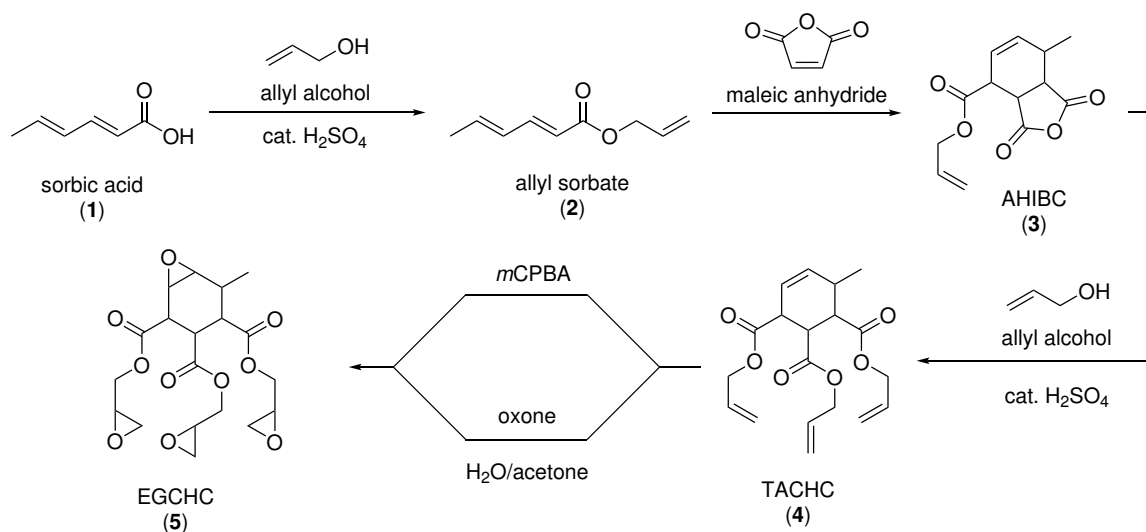
Scheme 19: Synthesis route towards the epoxy monomer EGCHC starting from the allylation of sorbic acid which then reacts in a with maleic anhydride in a Diels-Alder cycloaddition. After the allylation of the anhydride mojety the double bonds are epoxidized by *m*CPBA or Oxone®.[251]

atom efficiency and reaction speed creating complex molecular structures should be mentioned here. Maleic anhydride is a typical dienophile reactant for Diels-Alder reactions, which is readily available due to its great industrial importance and relatively low environmental hazard potential.[259–261] It is normally produced by catalytic oxidation of hydrocarbons such as benzene in the gas phase.[262] In recent publications, the use of renewable raw materials such as furfural and its derivatives, which can be obtained from carbohydrates, is discussed.[263–266] Cycloaddition can be performed at very high concentrations (10 M reffered to allyl sorbate) with minimal solvent demand. Solvent-free methods are also reported in the literature by Moreno *et al.* enabled by microwave irradiation.[260] The product can be easily purified by crystallization and successful synthesis of allyl-7-methyl-1,3-dioxo-1,3,3a,4,7,7a-hexahydroisobenzofuran-4-carboxylate (AHIBC) could be confirmed by ^{1}H-NMR (Figure 4.49) and ^{13}C-NMR (Figure A35). Purity of the product could be shown by GC-MS (Figure A36), HRMS and elemental analysis.

The product triallyl-6-methylcyclohex-4-ene-1,2,3-tricarboxylate (TACHC) is formed in a second allylation reaction. Analog to the first esterification, the allyl groups are introduced by sulfuric acid catalysis introducing two allyl ester bonds to the former
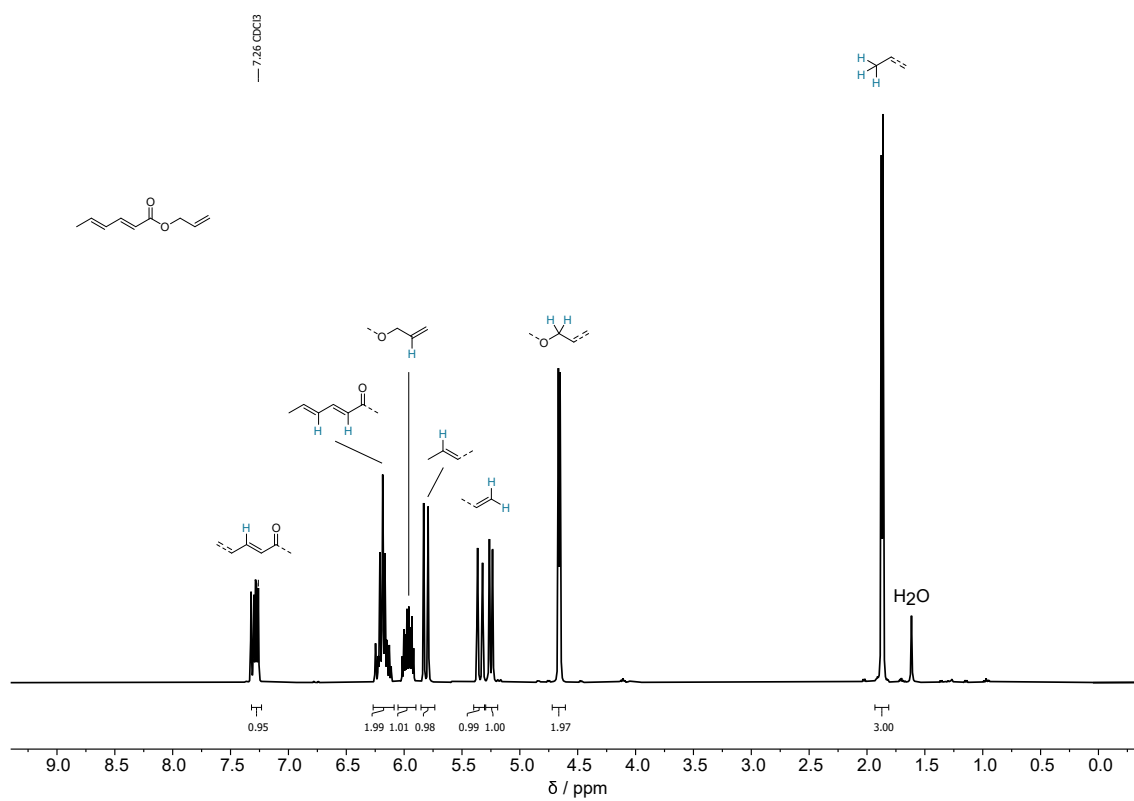
Figure 4.48: ^{1}H-NMR of allyl sorbate in chloroform-d as solvent.
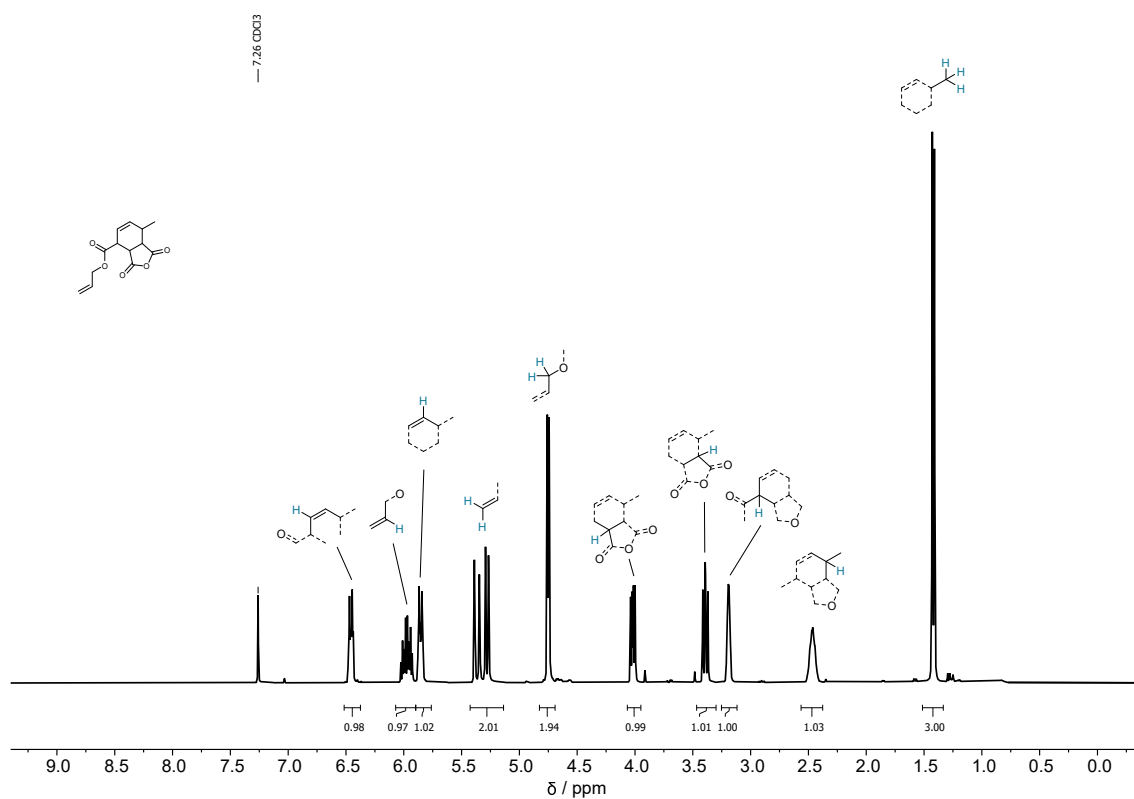
Figure 4.49: ^{1}H-NMR of AHIBC in chloroform-d as solvent.
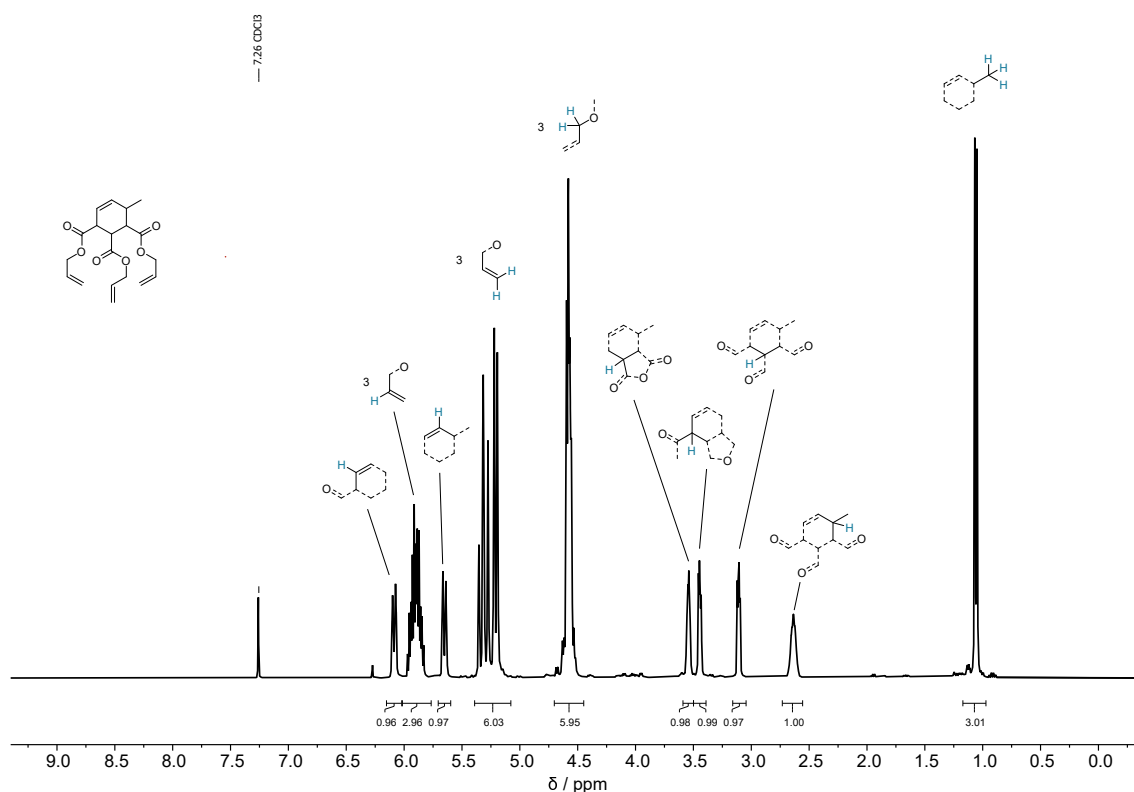
Figure 4.50: ^{1}H-NMR of TACHC in chloroform-d as solvent.

anhydride. Again, the success of the synthesis could be confirmed by ^{1}H-NMR (Figure 4.50), and ^{13}C-NMR spectroscopy (Figure A37) as well as GC-MS (Figure A38), HRMS and elemental analysis.

In the last step, TACHC is oxidized in a *Prilezhaev* reaction with *m*CPBAin dichloromethane at room temperature to yield 78 % of the epoxy compound EGCHC within 48 h. The reaction can be analog to the epoxidation of the fatty acids and oils monitored by ^{1}H-NMR watching the vanishing signals of the double bond. The use of 8 eq. *m*CPBAinitially seems high. However, the low purity of the peroxy acid, which is given to be 77 %, must be taken into account. The actual ratio is, therefore, 1.5 eq. per double bond. Adding hydrogen peroxide is conceivable to regenerate the active species during epoxidation to optimize this ratio.

An attractive alternative for mCPBA in terms of ecology is using Oxone®. As described in Section 2.3.1, the oxidation agent generates acetone *in situ* to dimethyloxirane. In the case of Oxone®, reaction speed is much slower and usually takes several days until completion, which is why using *m*CPBAwas the preferred method. Other green
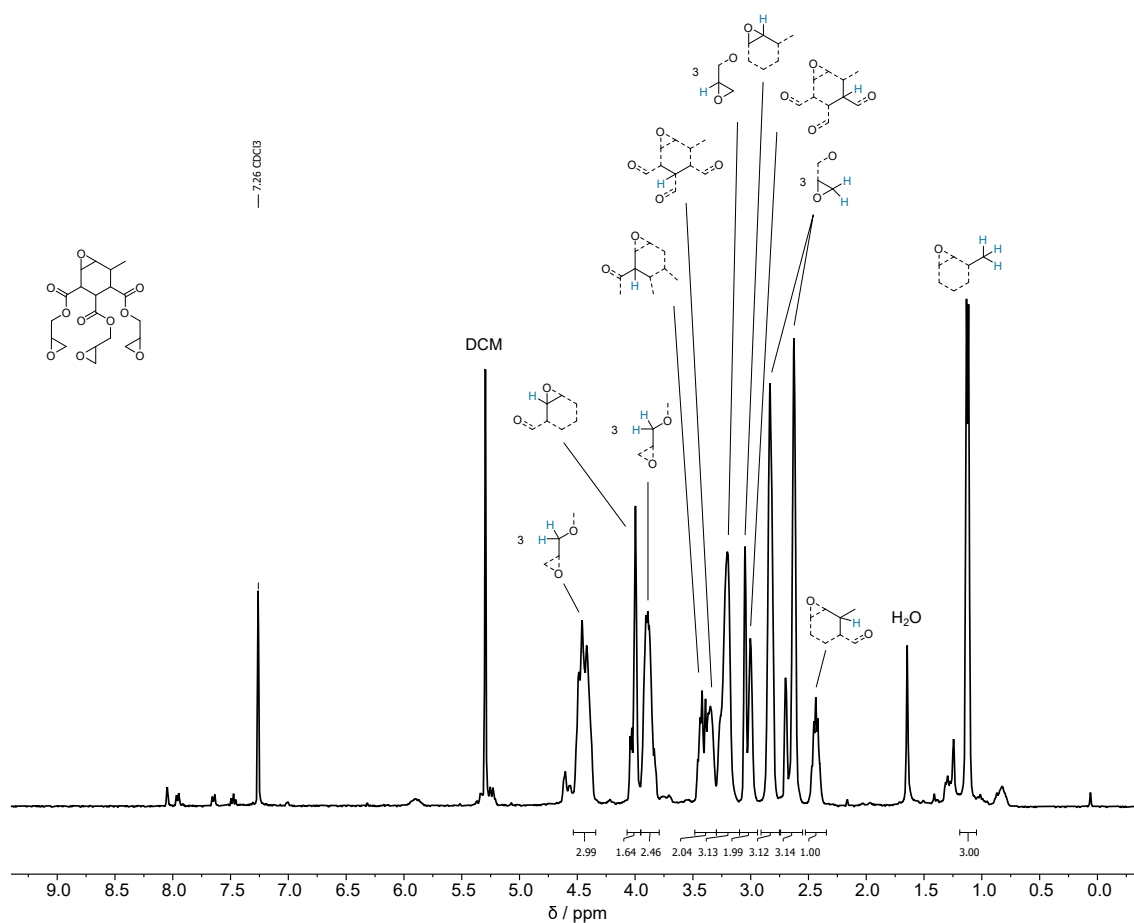
Figure 4.51: ^{1}H-NMR of EGCHC in chloroform-d as solvent.

alternatives to epoxidize TACHC could be using chemo-enzymatic methods reported by Aouf *et al.*[267] The successful synthesis of EGCHC could be confirmed by ^{1}H-NMR (Figure 4.51) and ^{13}C-NMR (Figure A39) as well as HRMS.

4.9.2 Epoxy sample preparation and curing

In order to investigate the curing behavior of EGCHC, two different hardeners, IPD and T403, were used. DGEBA samples were also prepared for comparison. Mixing ratios were as summarized in Table 4.14 and are calculated by the epoxy-equivalent values of $103.1\,g\,mol^{-1}$ (EGCHC), $170.2\,g\,mol^{-1}$ (DGEBA) and the amine equivalent values of $42.5\,g\,mol^{-1}$ (IPD) and $81.0\,g\,mol^{-1}$ (T403).

Table 4.14: Mixing ratios for the EGCHC and DGEBA samples with IPD and Jeffamine T403 as hardeners. Molar ratio of epoxy compound and hardener = 1.0. Table adapted from Breitsameter *et al.*[251]

Sample	curing agent per 2 g resin / g
EGCHC-IPD	0.842
EGCHC-T403	1.571
DGEBA-IPD	0.499
DGEBA-T403	0.950

Table 4.15: Curing and post-curing times and temperatures for the EGCHC and DGEBA samples with IPD and Jeffamine T403 as hardeners. Table adapted from Breitsameter *et al.*[251]

Sample	Curing	Post-curing
EGCHC-IPD	0.5 h, 45 °C	0.5 h, 120 °C
EGCHC-T403	2 h, 60 °C	2 h, 100 °C
DGEBA-IPD	2 h, 60 °C	2 h, 160 °C
DGEBA-T403	2 h, 80 °C	2 h, 120 °C

To find suitable curing conditions for the samples based on EGCHC, some DSC tests were performed. From the DSC-scans shown in Figure 4.52, the onset temperatures of the curing enthalpies were obtained (EGCHC-IPD: 44 °C, EGCHC-T403: 52 °C) which were chosen as a reference point for the curing temperature. For post-curing, temperatures higher than those of the maxima of the exothermic peaks were determined (EGCHC-IPD: 78 °C, EGCHC-T403: 94 °C). The DGEBA samples were cured using similar procedures as reported in the literature.[268,269] As can be seen in the isothermal DSC experiment of sample EGCHC-IPD (Figure 4.53a), the exothermic process flattens to the zero line after only about 10 min. In the subsequent isotherm at 120 °C, another exothermic process can be observed, which ends after about 5 min. After cooling and a heating ramp of 10 °C min^{-1} (Figure 4.53b), apart from a T_g at approximately 130 °C, no thermal process of an exothermic nature is visible, which shows that the sample is completely cured. The exact curing procedures used for both EGCHC and DGEBA samples can be obtained from Table 4.15. Analog to EGCHC-IPD, the completeness of the curing was verified for all other samples using non-isothermal DSC measurements.
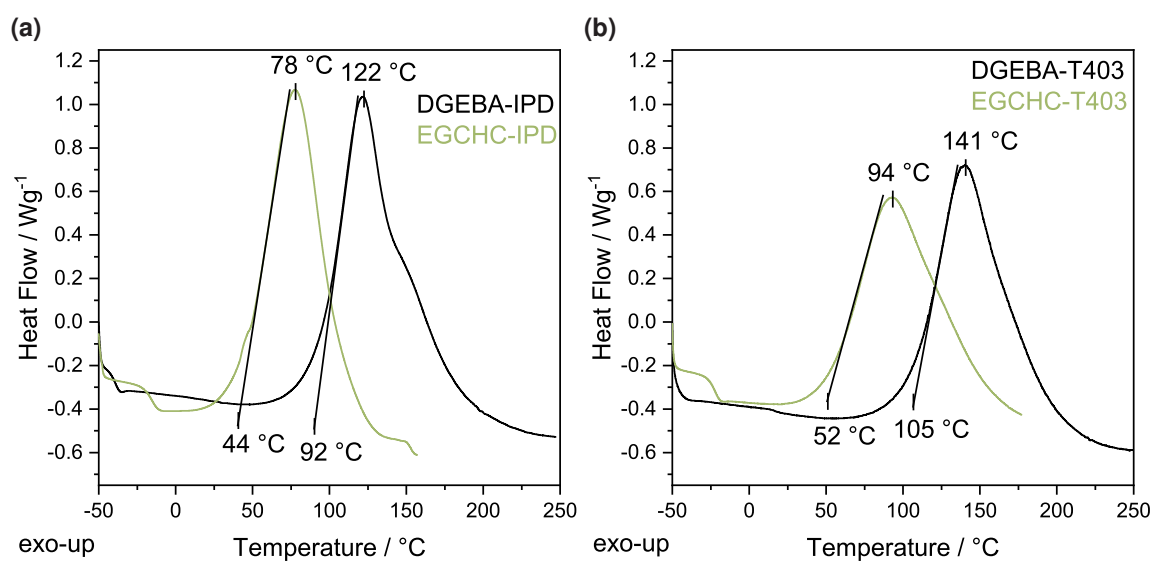
Figure 4.52: DSC scans of EGCHC/DGEBA-IPD (a) and EGCHC/DGEBA-T403 (b) with the onset temperature of the curing enthalpy and the temperature of the maximum of the exothermic peak. Figures reprinted from Breitsameter *et al.*[251]
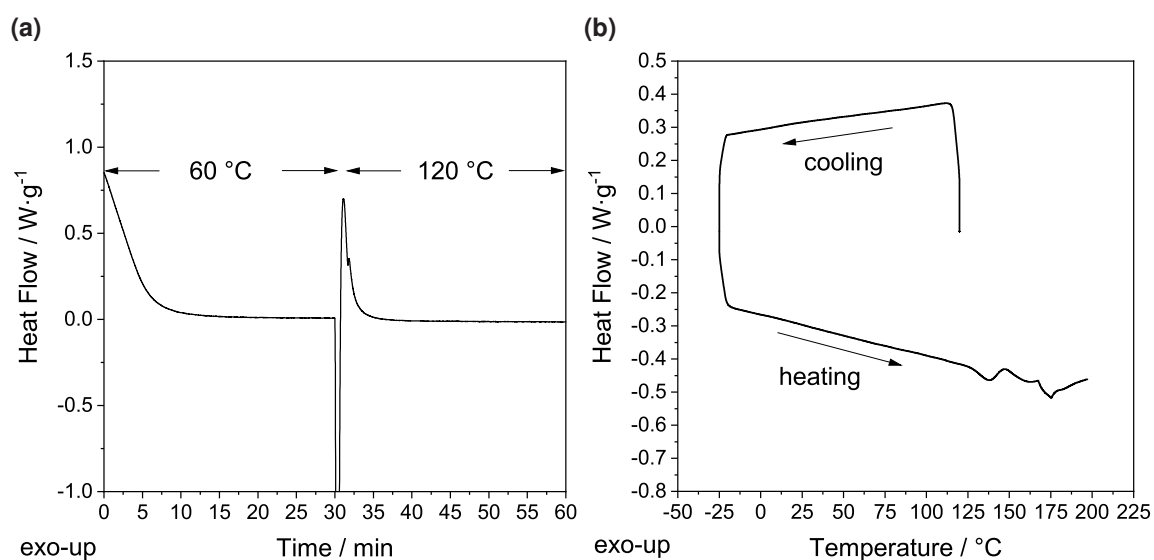
Figure 4.53: a) Isothermal DSC-scan of EGCHC-IPD. 30 min at 60 °C, 30 min at 120 °C. b) Subsequent cooling and heating cycle of the same sample.

Table 4.16: Gel-contents of cured EGCHC-samples determined by Soxleth-extraction with acetone as solvent. Extraction time: 24 h.

Sample	Gel−content / %
EGCHC-IPD	97.90(0.95)
EGCHC-T403	97.59(0.15)

In addition to DSC measurement, Soxleth-gel-contents also provide information on the completeness of the curing. The gel contents for the EGCHC samples (Table 4.16) are high and thus confirm the choice of curing conditions.

Overall, the EGCHC samples appear more reactive than DGEBA in the DSC scans since the onset temperatures of the curing enthalpy and the maximum of the curing peaks are found at lower temperatures (Figure 4.52). One explanation for this is the epoxy groups in close proximity to ester groups which facilitate the ring opening of the oxiranes by inductive effects and thus require less energy to start the curing reaction. Jeffamine T403 is less reactive than IPD due to the steric hindrance of the α-methyl groups to the amine.[270] The high reactivity of EGCHC thus allows energy-efficient, fast curing at low temperatures.

4.9.3 Thermo-mechanical properties

DMA was used to determine the T_gs of the specimens and also to determine the stiffness behavior for different specimens. Figure 4.54 compares the storage moduli, and tan δ curves of the EGCHC and DGEBA specimens hardened with IPD and T403, respectively. As expected, the specimens cured with IPD showed higher stiffness and T_gs than the specimens cured with T403 (Figure 4.54b and Figure 4.54d). Since the cycloaliphatic structure of IPD forms stiffer networks, the curing agent is more suitable for use at high temperatures than T403. It is noteworthy that EGCHC-T403 exhibits higher stiffness between −20 °C and about 38 °C than the DGEBA sample (Figure 4.54c). For the IPD samples, EGCHC shows higher stiffness than DGEBA between −20 °C and about 100 °C (Figure 4.54a). Due to the larger number of oxirane rings, EGCHC can form denser networks than DGEBA (two epoxy groups). However,
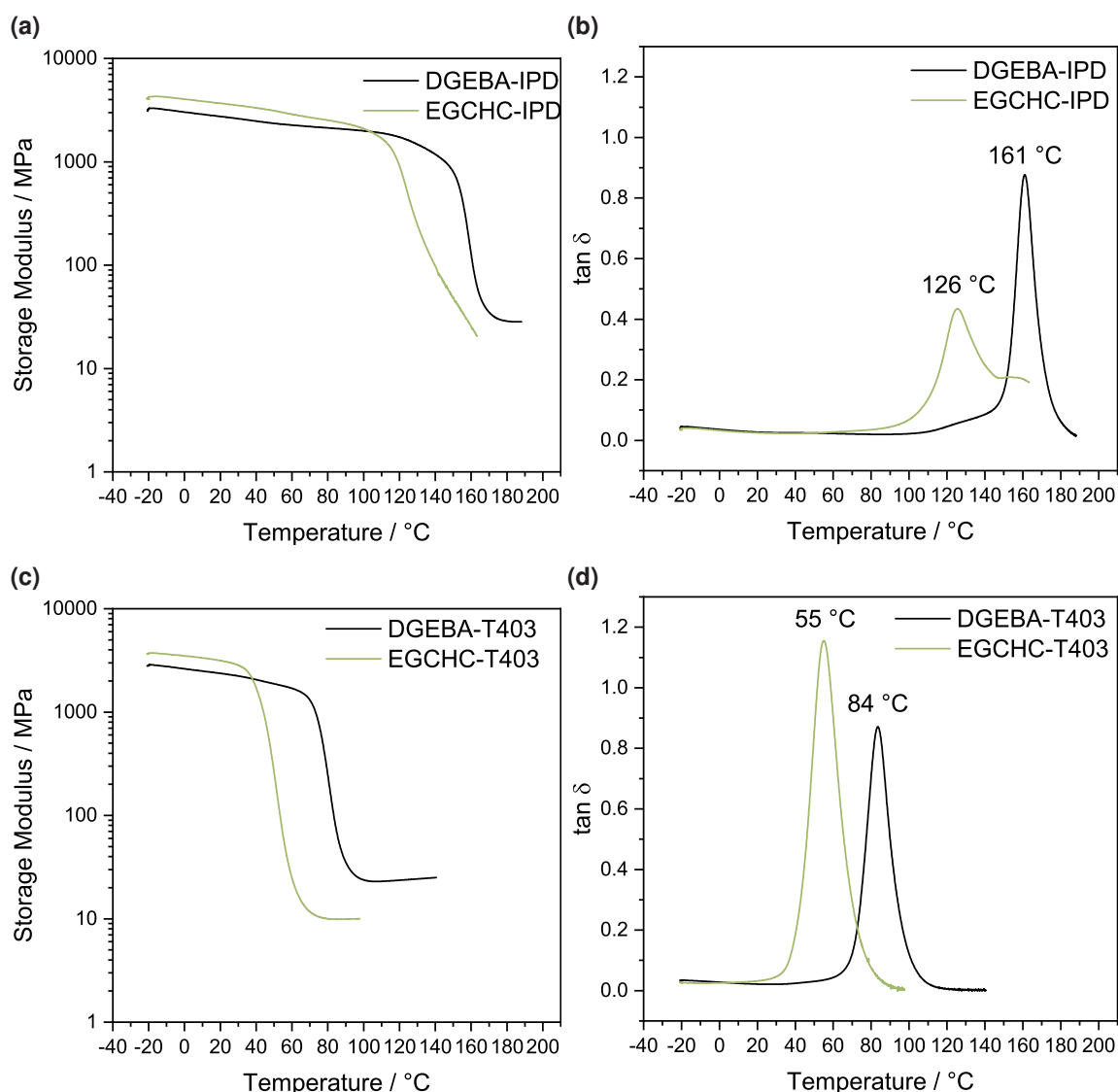
Figure 4.54: a) Storage modulus and b) tan δ of DGEBA/EGCHC cured with IPD. c) Storage modulus and d) tan δ of DGEBA/EGCHC cured with T403. Figures reprinted from Breitsameter *et al.*[251]

the glass transition points of the EGCHC systems turn out to be lower than those of the DGEBA counterparts (Table 4.17). This can be explained by the structural differences of the resins. In contrast to EGCHC, DGEBA has aromatic substructures that can form relatively strong π–π interactions. This leads to the fact that the glassy temperature regime in the EGCHC systems ends at lower temperatures and loses its stiffness faster. Nevertheless, an application of EGCHC at higher temperatures is conceivable since a T_g of 130 °C is present and no significant loss of stiffness is observable in the range of −20 to 100 °C.

Table 4.17: T_g obtained from DMA-measurements for the EGCHC and DGEBA-bases samples. Table adapted from Breitsameter *et al.*[251]

Sample	Glass transition temperature / %
EGCHC-IPD	192.8(6.2)
EGCHC-T403	56.5(1.3)
DGEBA-IPD	161.7(0.4)
DGEBA-T403	82.0(1.2)

4.9.4 Mechanical Properties

Figure 4.55 shows the measured values for tensile strength and tensile modulus of the EGCHC and DGEBA samples. In comparison, EGCHC cured with IPD shows better mechanical properties than the corresponding DGEBA sample. An average maximum tensile modulus of 3965 MPa and an average maximum tensile strength of 76 MPa could be determined for the EGCHC-IPD samples.

The tensile modulus results are consistent with the DMA results of Figure 4.54. The EGCHC systems show higher stiffness than the DGEBA-based specimens, and the IPD-cured specimens are again stiffer than those hardened with T403. The higher E-modulus of EGCHC emphasizes that EGCHC achieves the required mechanical properties to be used in high-performance applications. In comparison, Sika's high-performance epoxy system CR80 has a tensile modulus of 2900 to 3000 MPa.[171] The cured DGEBA specimens fall within this range and are consistent with the literature.[268] The EGCHC-IPD specimens show a relatively high uncertainty in tensile strength, which is related to the rapid setting of the specimens within minutes after mixing at room temperature. This allows only short degassing times of 30 s, which does not allow removing all air inclusions. These voids in the epoxy thermoset specimens affect the tensile strength after curing. However, the average tensile strength of the EGCHC-IPD specimens is still higher than that of DGEBA-IPD, while the EGCHC-T403 specimens perform comparably to the DGEBA samples. Thus, it could be shown that EGCHC can compete with the mechanical properties of DGEBA.
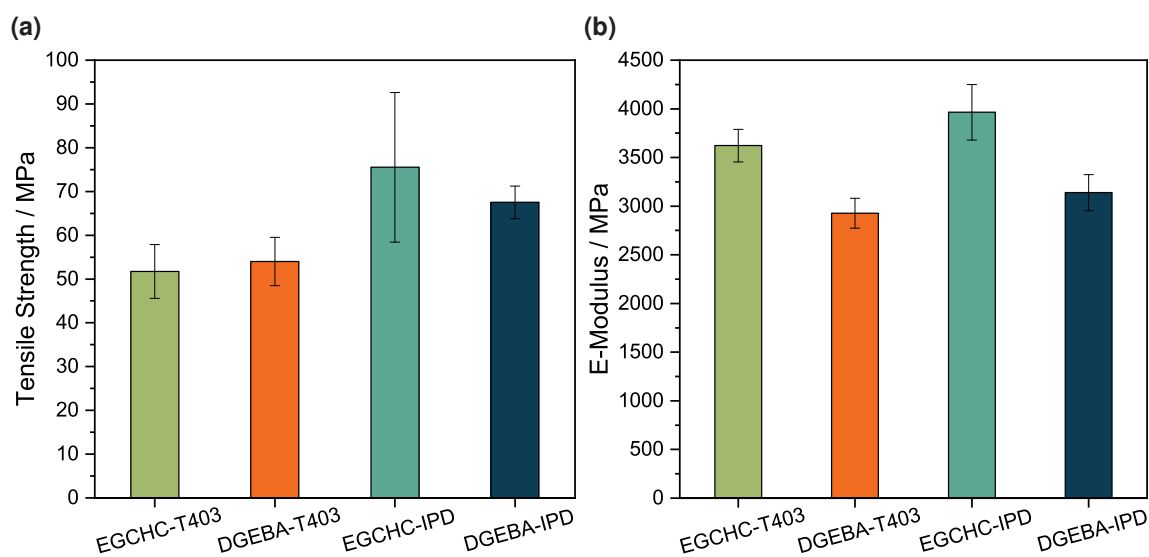
Figure 4.55: a) Tensile strength and b) tensile modulus of EGCHC-IPD, EGCHC-T403, DGEBA-IPD and DGEBA-T403. Figures reprinted from Breitsameter *et al.*[251]

4.9.5 Thermal Stability

As can be seen in the thermal gravimetric analysis in Figure 4.56, degradation of EGCHC starts at a temperature of 203 °C for IPD and 222 °C for T403 hardened samples. DGEBA shows higher thermal stability (around 340 °C). However, the $T5\%$ of both EGCHC cured with IPD and T403 is high enough to withstand temperatures of standard applications. The lower thermal stability results from the ester bonds, which are more prone to pyrolysis than ester bonds in DGEBA resins. Another factor is again the absence of aromatic structures, which contribute with high intermolecular interactions to thermal stability.

4.9.6 Solvolysis of EGCHC-based thermosets

Particularly in the case of fiber-reinforced polymers, the dissolution of the composite materials is of great interest, as this allows the recovery and reuse of the cost-intensive fiber materials.[271,272] The ester bonds in EGCHC already discussed earlier allow in contrast to DGEBA basic hydrolysis. Densely crosslinked materials such as DGEBA-based thermosets are usually only dissolvable under harsh conditions such
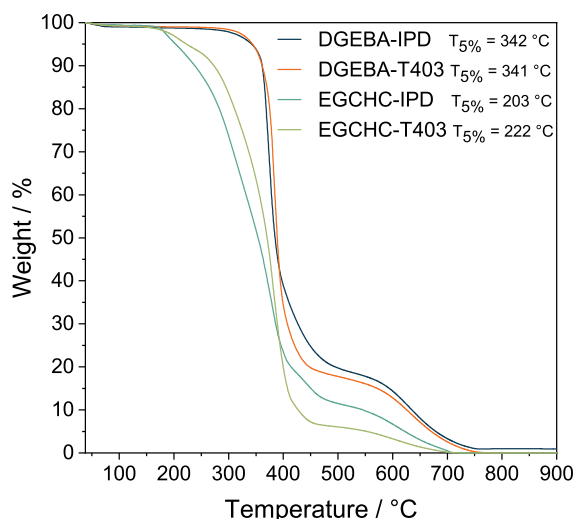
Figure 4.56: TG curves of EGCHC and DGEBA for comparison both cured with IPD or T403. Reprinted from Breitsameter *et al.*[251]

as high temperatures or pressure.[273–275] To investigate the decomposition behavior, EGCHC-based thermoset samples were placed in a 1 M NaOH solution. Weight loss over time was observed at 80, 40 and 30 °C and room temperature. At 80 °C, both samples cured with IPD and Jeffamine T403 completely decomposed within 30 min. At room temperature, EGCHC-T403 decomposed throughout 17 h, and the IPD sample lost 17 % of its original weight at the same time. As can be seen from Figure 4.57, complete solvolysis here takes 4 d. The density of the formed 3D network can explain the different behavior. Jeffamine T403 consists of oxypropylene repeating units in the backbone, resulting in larger gaps in the cured structure. This allows the solvent to penetrate deeper and cleave more ester bonds immediately. On the other hand, the network formed by IPD is denser with fewer degrees of freedom, preventing the solvent from diffusing into the thermoset.
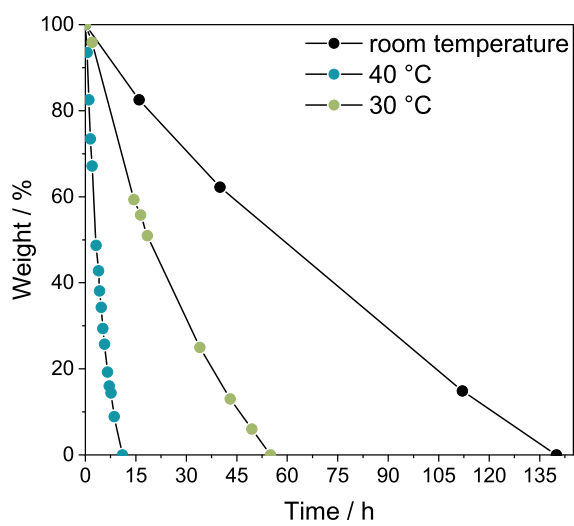
Figure 4.57: Decomposition of EGCHC-IPD in 1 M NaOH at room temperature, 30 and 40 °C. Reprinted from Breitsameter *et al.*[251]

4.10 Estolides from fatty acid polycondensation

4.10.1 Monomer synthesis
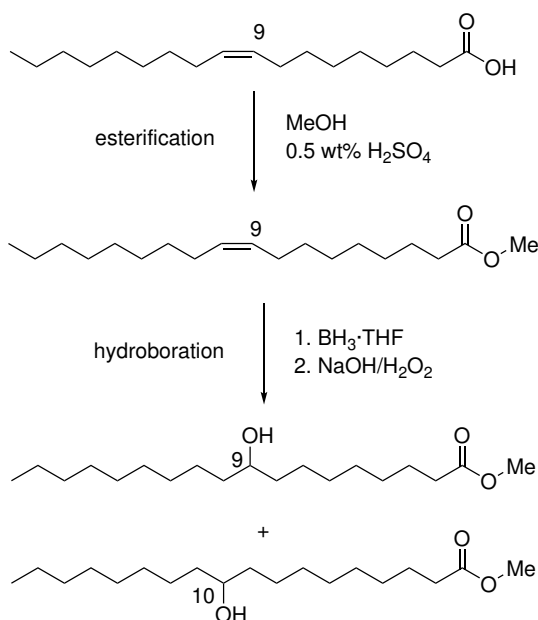
Scheme 20: Synthesis route to methyl-9/10-hydroxystearate by hydroboration of methyl oleate.

For the preparation of estolides, two different C18 fatty acid methyl esters bearing a hydroxy group were used. While 12-hydroxystearic acid (12-HSA) is commercially available, the 9/10-hydroxystearic acid (9/10-HSA) mixture had to be prepared synthetically by a hydroboration reaction of methyl oleate. The use of the methyl esters of the fatty acids is beneficial for the metal-catalyzed polycondensation reaction since that way the by-product water can be avoided. Also, the hydroboration reaction is expected to perform better in the absence of acidic protons from the carboxyl groups. As shown in Scheme 20, oleic acid was esterified with methanol and concentrated sulfuric acid as a catalyst for the synthesis of methyl oleate. The successful methylation can be validated by ^{1}H-NMR (Figure 4.58), the signal at 3.66 ppm represents the methylated carboxyl group. The hydroxy-functionality is introduced *via* hydroboration using $BH_3 \cdot$ thf and subsequent oxidation with sodium hydroxide and hydrogen peroxide. As products are a mixture of methyl hydroxystearic acid with the alcohol at
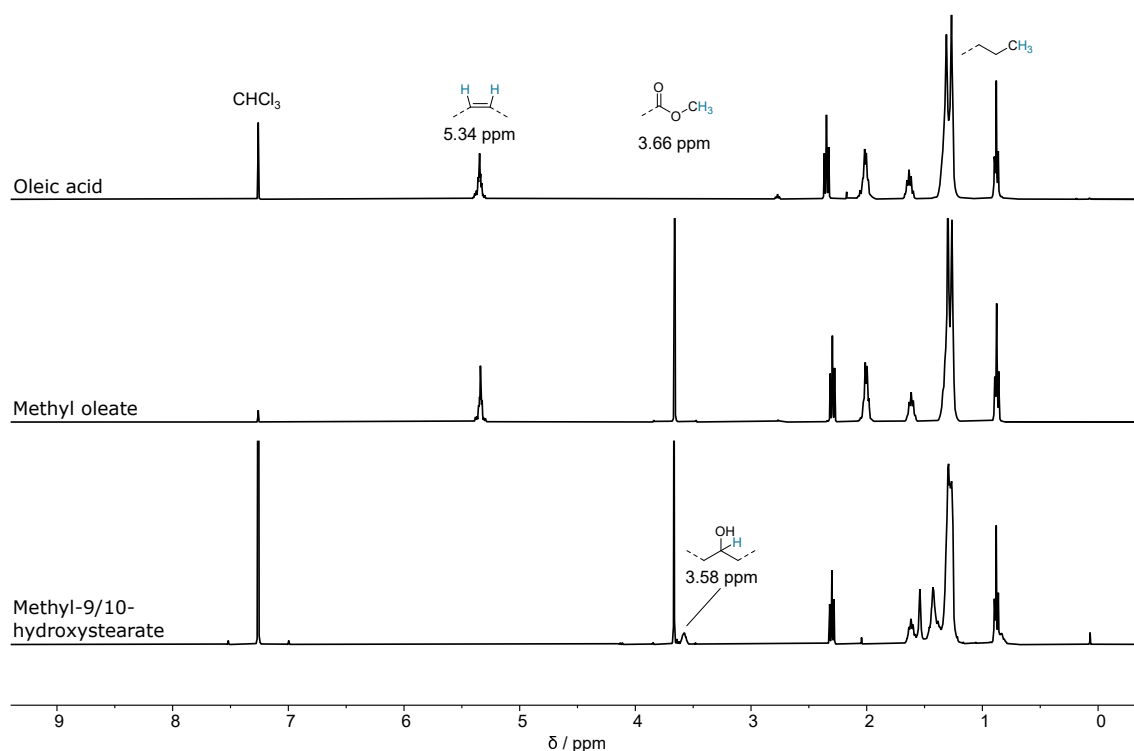
Figure 4.58: ^{1}H-NMR in chloroform-d of oleic acid, methyl oleate and the hydroboration product methyl-9/10-hydroxystearate.

position 9 or 10 (Me-9/10-HSA) since the hydroboration is not regiospecific. In the ^{1}H-NMR-spectrum (Figure 4.58) the signal of the double bond at 5.34 ppm vanishes while the signal of the methine proton at the carbon carrying the alcohol group appears at 3.58 ppm. When analyzing the hydroxylated product by GC-MS (Figure 4.59a), in addition to the product peak at 14.7 min, there is a second peak visible at 12.9 min. This can be identified as stearic acid (C18:0), which is an impurity in the technical grade oleic acid and can be removed by column-chromatography (Figure 4.59b). The regioisomers Me-9-HSA and Me-10-HSA can not be separated in GC-MS and appear as one single peak. Methyl-12-hydroxy stearate (Me-12-HSA) was prepared analog to Me-9/10-HSA.

4.10.2 Estolides from hydroxy stearic acid

First, polycondensation reactions were done with Me-9/10-HSA in a 6.0 g scale and titanium tetra *n*-butoxide as a catalyst at a temperature of 200 °C under dynamic

(a)

(b)
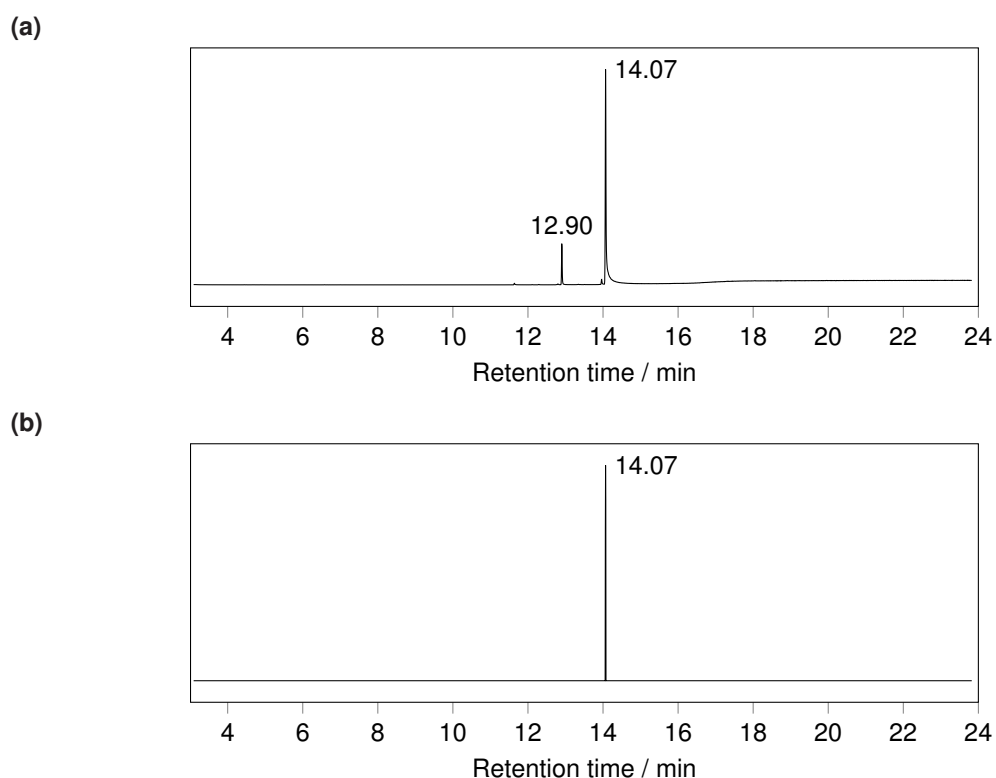
Figure 4.59: GC-MS elugrams a) of the crude product of the hydroboration/oxidation reaction of methyl oleate, b) after purification.

vacuum. The conversion of the monomer can be monitored by ^{1}H-NMR as shown in Figure 4.60. While the signals of the methyl ester protons (3.66 ppm, green) disappear with the ongoing transesterification, the signal of the methine proton (3.58 ppm, green) shifts downfield to 4.85 ppm (light blue) due to the different chemical environment in the ester-bond. This shift can be integrated against the during the reaction unchanged methylene-signal at 0.87 ppm (dark blue). As can be seen in Figure 4.61a, after 22 hours, a high conversion of 95 % is reachable. The influence and effectiveness of Ti(OBu)$_4$ could be shown in an experiment without a catalyst. Here, after 22 hours, only 21 % conversion could be observed. Directly linked to the conversion *via*, the Carothers equation is the degree of polymerization or chain length. Thus, 95 % conversion corresponds mathematically to a degree of polymerization of 20.0. With the relationships just described, viscosity also increases. Also illustrated in Figure 4.61a, kinematic viscosity v is rising and reaches a maximum value of 96 333 cSt. From the flow curves (Figure 4.61b), some conclusions can be drawn regarding the flow behavior of the estolide at different chain lengths. At lower conversions of 70 % ($\bar{X}_n =$
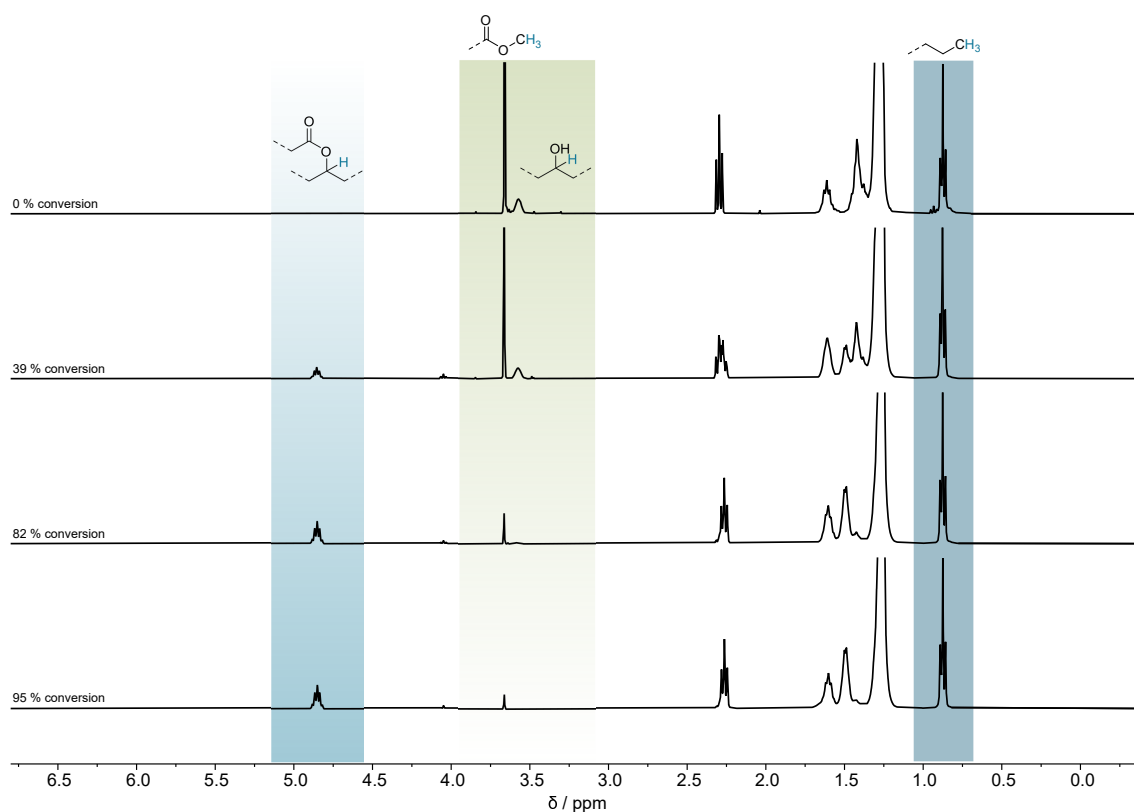
Figure 4.60: Reaction progress in ^{1}H-NMR of the polycondensation of Me-9/10-HSA. Green: disappearing OMe and shifting CH (light-blue) signals integrated against CH$_3$ (dark-blue).

3.4), there is a linear, Newtonian behavior observable in the measured shear rate region. Shear thinning effects occur with increasing chain length; for the highest degree of polymerization, this starts at a shear rate of $100\,\text{s}^{-1}$. This behavior is well-known and described in the literature. At sufficiently high shear rates, polymeric compounds change from their tangled spherical configuration to a stretched, more linear one. This allows the chains to glide past each other better, and the viscosity decreases.[276]

Contrary to the high viscosities achieved in the first experiment, in the following ones with Me-12-HSA, a more common target viscosity of about 700 cSt is aimed at. Additionally, Me-12-HSA is not purified and used containing roughly 20 % methyl stearate as an impurity (Figure A4). A series of 6 polycondensation reactions was carried out to elucidate the relationships between conversion, viscosity, and reaction time for this monomer as well. Several samples were taken during each reaction and analyzed by ^{1}H-NMR spectroscopy and rheology.
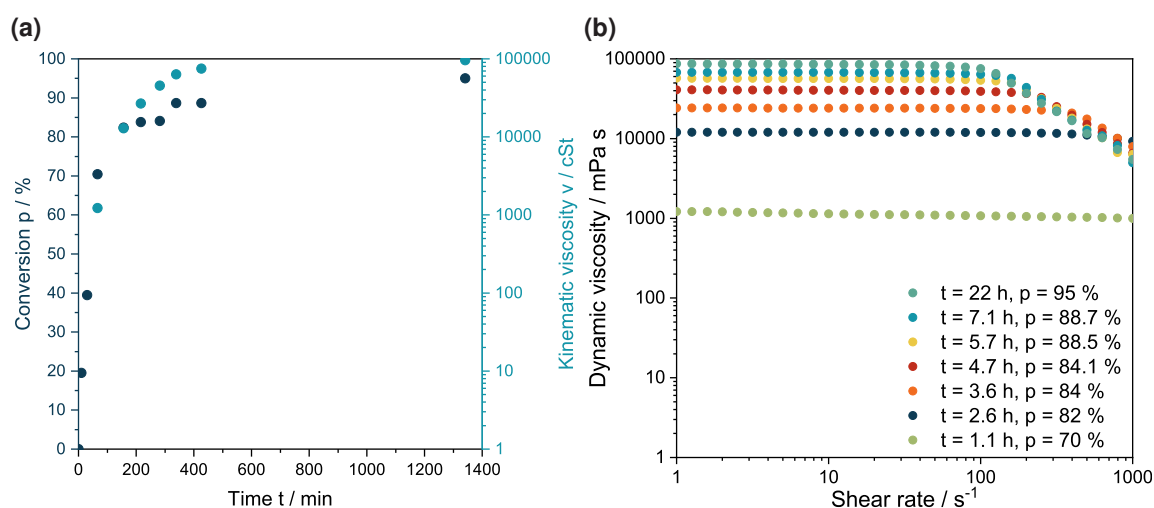
Figure 4.61: a) Conversion and kinematic viscosity against reaction time, b) dynamic viscosity against shear rate of Me-10-HSA estolides.
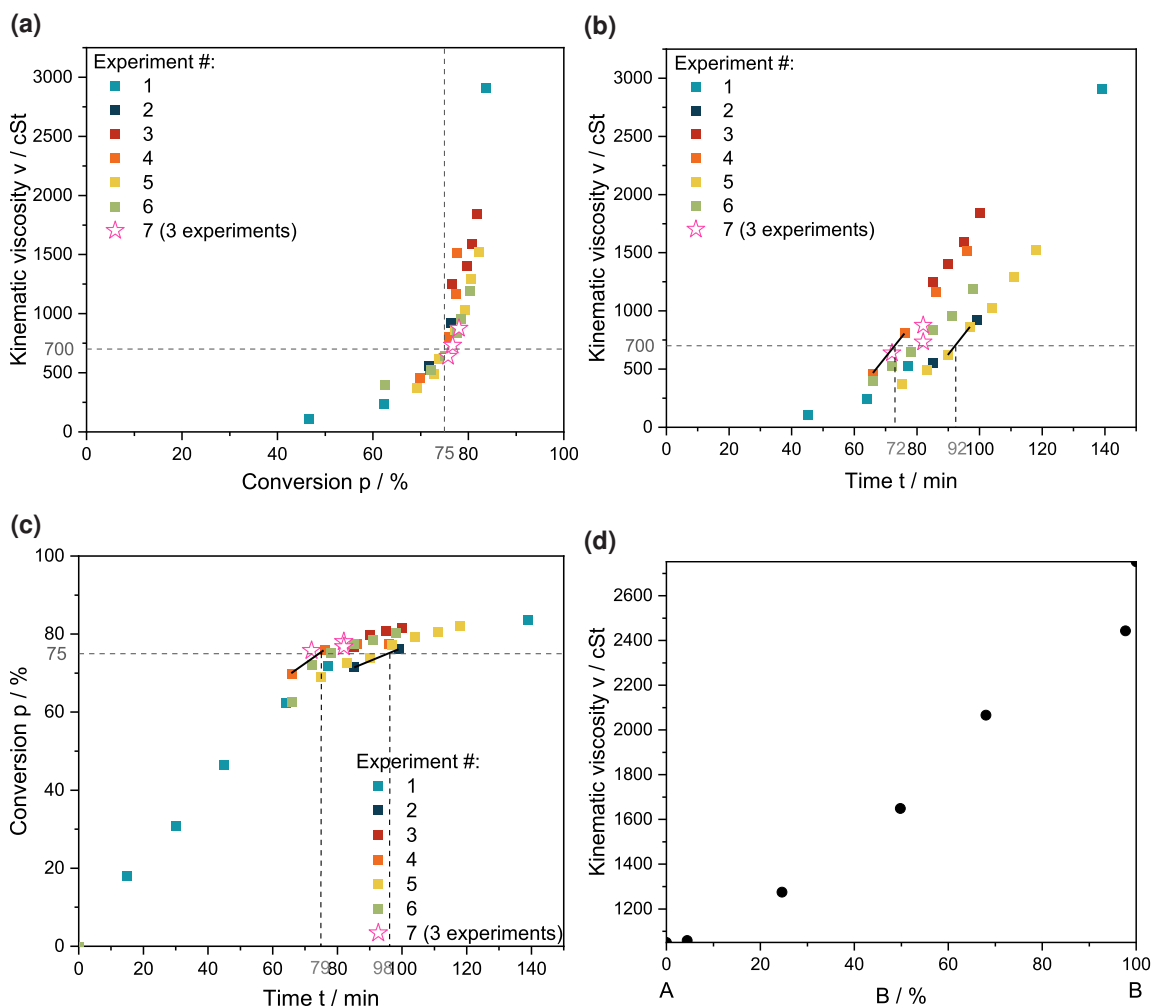
Figure 4.62: Series of polycondensation reactions, correlation of a) viscosity against conversion b) viscosity against time c) conversion against time, d) blend behavior, A = $v_{40\,°C}$ = 2750 cSt, B = $v_{40\,°C}$ = 1050 cSt.

Table 4.18: Three individual experiments to reach the targeted viscosity of 700 cSt. Entries marked with a star in Figure 4.62a, 4.62b, and 4.62c.

#	Reaction time / min	Conversion[a] / %	Kinematic viscosity[b] / cSt
1	72	75.8	639
2	82	78.0	876
3	82	76.7	732

[a] Determined by ^{1}H-NMR,
[b] dynamic viscosity measured at 40 °C, converted to kinematic viscosity with a density of $\rho = 0.9\,\mathrm{kg\,m^{-3}}$.

In Figure 4.62a, the conversion is plotted against the viscosity. The scatter of the measurement points is low here, and the viscosity, therefore, correlates directly with the conversion determined by ^{1}H-NMR. From these data, it can be concluded that the target viscosity of 700 cSt is reached at 75 % conversion. It is striking that, compared with the high conversions for the polycondensations of pure Me-10-HSA, the conversion curve here approaches the mark of approx. 85 %. This can be explained by the impurity Me-12-stearic acid, which lacks hydroxy functionality and thus acts as an end-capping unit. The chain is thereby terminated, and high degrees of polymerization are prevented. A conversion of 85 % equals an $\bar{X}_n$ of 6.7. Plotting the viscosity against time (Figure 4.62b), a clear distribution of the measurement points can be seen. The individual experiments vary in the relevant viscosity range of 700 cSt between 72 and 92 min. The plot of conversion against time (Figure 4.62c) reveals something similar: 75 % conversion is achieved between 78 and 98 min, depending on the experiment. Three further experiments were carried out with the time window determined in this way. The first one was stopped after 72 min, and the two others were terminated after 82 min. The outcome of this experiments is summarized in Table 4.18 and marked with a star (Figure 4.62a, 4.62b, and 4.62c).

The variation in the conversions and viscosities achieved in these approaches can be explained by how the experiments were conducted. Due to the heating phase of the flask, including contents to 200 °C, the reaction start is not precisely defined. The applied vacuum is also subject to non-regulable fluctuations since the pump is a rotary vane pump connected to a Schlenk line. These problems led to the concept of

adjusting the viscosity by blending samples of different viscosities. For this purpose, a low-viscosity sample of 1050 cSt and a higher-viscosity one of 2750 cSt were mixed in different proportions and measured in the rheometer. As can be seen in Figure 4.62d, there is an approximately linear correlation in the viscosities of the blends, with the low-viscosity component appearing to have a slightly greater influence. Also, the samples of Table 4.18 were blended and resulted in a viscosity of 658 cSt. The mathematical average is at 749 cSt, which again indicates the higher influence of the lower viscous parts.

4.10.3 Thermal properties of estolides and purification

Applying estolides as lubricants is interesting because of their thermal properties, such as melting points and degradation behavior. In order to investigate these properties, a sample of Me-12-HSA estolide was prepared with a viscosity of 675 cSt (t = 97 min, p = 76.6 %, $\bar{X}_n$ = 4.3) and analyzed by DSC and TGA. TG-analysis (Figure 4.63a) shows, that the $T_{5\%}$ is at 238 °C and at 311 °C 10 % weight is lost. A DSC-scan (Figure 4.63b) shows a broad melting region between –25 to 2 °C with two peaks at –13 °C and –2.5 °C for the crude Me-12-HSA estolide sample. The second peak and its lower height at –2.5 °C indicates that there is besides the estolide oligomers, a second species is present. This could be confirmed by GPC of the sample (Figure 4.63c). Here, typical for a step-growth polymerization, monomer (Me-12-HSA), dimers, trimers, and tetramers are visible. To narrow the melting range, attempts were made to wash out the low molecular weight compounds. As can be seen in the GPC measurement in Figure 4.63d, mainly mono- and dimers are removed by washing with methanol, while the higher molecular weight oligomers are retained. A new DSC measurement (Figure 4.63b) shows that the melting range visible before washing is reduced to a melting point that is also one degree lower at 14 °C.
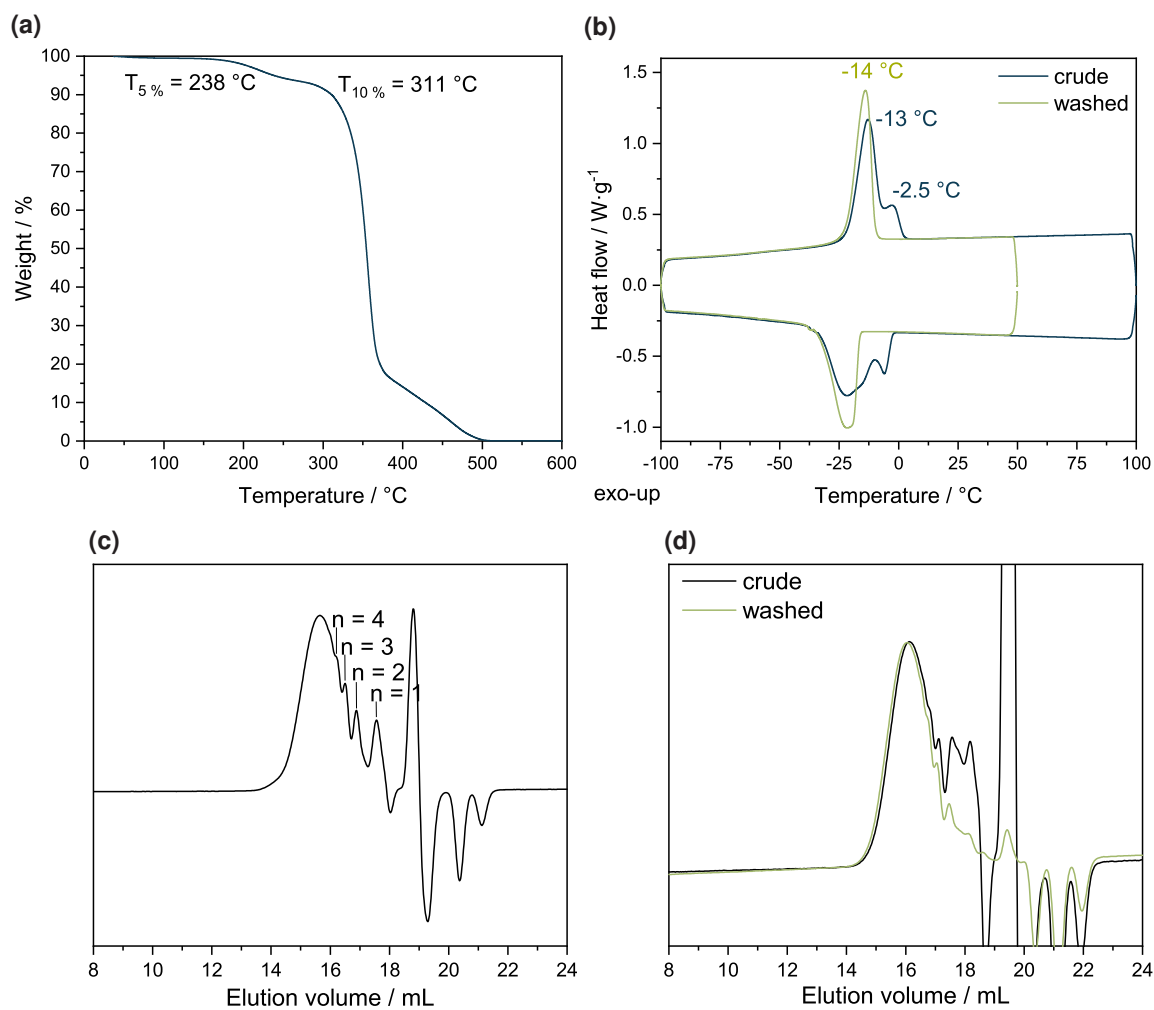
Figure 4.63: a) TG-analysis of the crude Me-12-HSA estolide sample, measured under air, b) DSC-scan of the crude and washed Me-12-HSA estolide sample, c) GPC-trace of the crude Me-12-HSA estolide sample, measured in THF at 30 °C, d) Comparison of GPC-traces before and after washing a estolide sample.

5 Material and methods

5.1 Chemicals

All chemicals were purchased from *Sigma-Aldrich*, *ABCR*, *Fluka*, *TCI Chemicals*, or *Fischer Scientific* and are used without further purification unless otherwise stated. *m*CPBA is bought in a purity of 77 %. 12-Hydroxystearic acid was obtained from *Fuchs Schmierstoffe* GmbH in technical grade. Bio-based air release additive Epinal EL 12.42 was bought from bto epoxy GmbH. Vegetable oils were purchased from local commercial sources and used for epoxidation without prior purification. The acid number of linseed oil was determined to be 0.93 mg KOH per gram following ISO 660.2009 and the iodine value after ISO 3961.2018 to be 186 g(I_2) per 100 g.

Commercially available monomers for polymerization are purified and dried before use. Methyl acrylate and *tert*-butyl acrylate are stirred over CaH_2 at room temperature for several days and distilled prior to use and stored over activated 4 Å molecular sieve. Ammonia for pressurized reactions is obtained from *Westfalen* with a purity of 99.98 % (ammonia 3.8W). Hydrogen for pressurized reactions is obtained from *Westfalen* (H_2 4.6 N). Dry solvents are obtained from an *MBraun* MB-SPS-800 solvent purification system or by drying over activated alumina and stored over activated 3 Å molecular sieve. Dry deuterated solvents are purchased from *Aldrich* and dried over activated 3 Å molecular sieve.

5.2 Devices and analysis

Nuclear magnetic resonance (NMR) spectroscopy. ^{1}H (400 MHz) and ^{13}C (100 MHz) nuclear magnetic resonance experiments were conducted on a *Bruker* AV400 instrument in deuterated chloroform (Sigma-Aldrich, $CDCl_3$, 99.8 atom% D), methylene chloride (Sigma-Aldrich, CD_2Cl_2, 99.9 atom% D), dimethyl sulfoxide (DMSO–d_6), or benzene (C_6D_6) as the solvent at a temperature of 294 K. Chemical shifts were referenced to the solvent proton resonance ($CDCl_3$: 7.26 ppm for ^{1}H-NMR, 77.2 ppm for ^{13}C-NMR; CD_2Cl_2: 5.32 ppm for ^{1}H-NMR, 53.84 ppm for ^{13}C-NMR; DMSO-d_6: 2.50 ppm for ^{1}H-NMR, 39.52 ppm for ^{13}C-NMR), C_6D_6: 7.26 ppm for ^{1}H-NMR, 128.0 ppm for ^{13}C-NMR. Signal multiplicities are abbreviated as following: s – singlet, d – duplet, t – triplet, m – multiplet.

Density functional theory (DFT) calculations. Geometry optimizations were performed using the Gaussian09 software package using the long-range corrected coulomb-attenuated exchange-correlation functional CAM-B3LYP and the basis set DEF2SVP by Sebastian Weißhäupl.

Fiber-spinning, stabilization and carbonization of PAN. All experiments were performed at the Fraunhofer Institute for Applied Polymer Research IAP in Potsdam by Dr André Lehmann and Dr.-Ing. Jens Erdmann. Fibers were spun continuously out of a DMAc solution (17.5 %) and precipitated into a DMAc/H_2O (70:30 v/v) regeneration bath. Spinning parameters were as follows:

Table 5.1: Parameters of the spinning procedure. Process and values by Fraunhofer IAP.

Parameter	Value
Nozzle / n_{hole}/D_{hole}	120/0.06
Precipitation bath	70 % $DMAc_{aq.}$
Temperature precipitation bath / ℃	43
Jet-stretch	0.8
Stretch factor	1.07
Washing medium	$H_2O_{dest.}$
Washing temperature / ℃	60
Drying temperature / ℃	100
Pull-off speed / m min^{-1}	7.6

PAN-fibers were analyzed by tensile testing and REM microscopy. The density of the fibers was calculated from titer ($g\,m^{-1}$) by weighing and cross-sectional area (m^2) by REM. The E-modulus was calculated using the density value of $0.45\,g\,m^{-3}$. The cross-sectional area was determined from the single filament and the average of at least 25 indiviual measurements determined. The diameter was calculated from cross-sectinal area assuming an ideally round cross-section.

Stabilization and carbonization steps were performed in processing lines at Fraunhofer IAP. The stabilization oven consists of three zones reaching up to 300 °C. The low-temperature carbonization furnace is also heated in three zones up to temperatures of 1000 °C. The line is equipped with a continuous thread transport system, a thread tension measuring module and winders. The high-temperature carbonization furnace has six zones with temperatures up to 2000 °C and is equipped with the same continuous thread transporting system. Ultra-high-temperature carbonization was performed in a batch furnace in a retort starting from room temperature to 3000 °C. Analysis of the CF-fibers was performed analogous to PAN.

Differential scanning calorimetry (DSC). DSC measurements were conducted with a TA Instruments Q2000 differential scanning calorimeter under $25\,mL\,min^{-1}$ helium flow. 5 to 9 mg of of substrate (or resin/hardener mixture in the case of epoxy resins) were loaded inside a TZero aluminum pan from TA Instruments. Samples were cooled down at −50 °C and subjected to a heating rate of $10\,K\,min^{-1}$. The onset temperature of the curing enthalpy and the temperature of the maximum of the exothermic peak were determined with the software Universal Analysis.

Dynamic mechanical analysis (DMA). DMA measurements were performed on a DMA Q800 (TA Instruments) under nitrogen atmosphere. TA/ELO samples were measured with a 20 mm 3-point bending clamp. Specimens had dimension of $60 \times 6 \times 2$ mm and were cut lengthwise to obtain the dimensions of $30 \times 6 \times 2$ mm. The samples were dried in a vacuum chamber containing silica balls for three days and then were measured by an oscillating flexural load with an amplitude of 80 μm at a frequency of 10 Hz, a static preload of 0.01 N and a force profile of 125 %. Under the preload, the specimens were equilibrated at −20 °C for 15 min and were then subjected to a

temperature ramp of $1\,\text{K}\,\text{min}^{-1}$ up to $180\,°\text{C}$. For each TA/ELO sample cured with C1 and C2 two specimens were characterized. For EGCHC-samples, measurements were performed with a film tension clamp. After mounting in the clamp, the samples had a free length of approx. $18\,\text{mm}$. The specimens were subjected to an oscillating tensile load at a frequency of $2\,\text{Hz}$, a static preload of $0.01\,\text{N}$ and a force profile of $125\,\%$. The amplitude of the EGCHC/IPD specimens was $3\,\mu\text{m}$ and $2\,\mu\text{m}$ for the specimens hardened with T403. Under load, the samples were equilibrated for $5\,\text{min}$ at $-20\,°\text{C}$ and then heated with a ramp of $2\,\text{K}\,\text{min}^{-1}$. Three specimens were determined for each epoxy system. The glass transition temperature T_g was determined from the peak of the tan δ curve using Universal Analysis software. DMA measurements were performed by Nikita Reinhardt.

Tensile testing. For the tensile tests, dogbone specimens wer cast in a mold and hardened. The specimens were painted wit ha matte acrylic-based paint using an airbrush. First, a white primer was applied in the area important for the measurement, which was then sprayed with black wpeckles. The amount of paint was minimized in order not to influence the underlying stress field. The tensile tests were performed with a universal testing machine Inspekt 100 (Hegewald & Peschke) with screw clamps. The force was measured with a $500\,\text{N}$ load cell. The specimens were testet at a constant loading rate of $0.125\,\text{mm}\,\text{s}^{-1}$. For each EGCHC/IPD and EGCHC/T403 specimen, five tests were performed at a laboratory atomsphere of $21.8\,°\text{C}$ and $33\,\%$ humidity. Deformation was recored using a VCXU-124M camera (Baumer) and a VS-TCM1-130/S telecentric lens (VS Technology). The acquired images were processed with GOM Correlate Professional 2020 software and the tensile modulus was determined from the stress-strain curves in the elongation range between 0.05 to $0.25\,\%$. The tensile strength was also determined from the measurements. Tensile testing experiments were performed by Nikita Reinhardt

Flexural testing. Prior to testing, TA/ELO samples measuring $80 \times 10 \times 4\,\text{mm}$ were dried in a vacuum chamber with silica balls for three days. Three-point flexural testing was performed according to DIN EN ISO 178 on an Inspekt 250 (Hegewald & Peschke). The force was applied with a $500\,\text{N}$ load cell under a constant loading speed

of $2\,\mathrm{mm\,min^{-1}}$ with a span of $64\,\mathrm{mm}$ and the stress/strain curves were recorded. The flexural modulus was determined from the stress/strain curve in the range of a elongation between 0.05 to 0.25 %. The flexural strength and elongation at break were also obtained from these measurements. For each TA/ELO sample, five samples cured with C1 and C2 were tested. The atmosphere in the laboratory during the tests was 21.6 °C with 36 % humidity.

Optical microscopy. Microscopic images were acquired using a BX41M-LED optical microscope (Olympus). TA/ELO specimens were embedded in Sika CR80 epoxy resin in a cylindrical mold and cured at 55 °C for 16 h. The specimens were then polisch with a machine and the surface morphology was observed under the microscope.

Particle size analysis. Particle sizes and their distribution of milled and unprocessed TA were determined using an LS 13 320 laser diffraction particle size analyzer (Beckman Coulter) and the Tornado dry powder system and evaluated using the Mie optical model.

Gel content determination of epoxy thermoset. The gel content of cured epoxy samples was determined by soxleth extraction using methanol (TA/ELO) or acetone (EGCHC) as solvent. After one day of extraction time, the samples were dried in a vacuum oven at 100 °C for 24 h and the mass loss was determined.

Thermogravimetric analysis (TGA). Thermogravimetric analysis experiments were conducted using a TA Instruments Q5000 analyzer. The samples were heated from 30 °C to 600 °C at a rate of $10\,\mathrm{K\,min^{-1}}$ in an argon atmosphere. The weight-loss was analyzed using TA Universal Analysis software.

Attenuated total reflection fourier transformed infrared spectroscopy (ATR-FTIR). ATR-FTIR spectroscopy measurements were performed on a Bruker Vertex70v ATR-IR spectrometer at room temperature in absorption mode. If needed, spectra were converted from absorbance to transmittance by following formula: *Transmittance* = $10^{(2-\%Absorbance)}$. Vibration modes are abbreviated as follwing: ν – streching.

Mass Spectrometry (GC-MS, ESI HRMS). Gas chromatographic/mass spectroscopic analyses (GC-MS) were measured in DCM solutions using an Agilent GC 7890B equipped with HP-5MS UI columns (0.25 mm, 0.25 µm) and an MS 5977A single quadrupole mass detector. Samples were present at a concentration of 0.5 mg mL^{-1}. The temperature range of the chromatography was between 45 °C and 325 °C. Electron-spray high resolution ionization mass spectrometry (ESI HRMS) was measured on a *Thermo Fisher Scientific* Exactive Plus in negative mode in HPLC-grade acetonitrile at a sample concentration of 1.0 ng mL^{-1}.

Size exclusion gel permeation chromatography (GPC). The molar mass distribution and dispersity (*Đ*) of the polymers were determined by size-exclusion chromatography. THF containing 0.22 g L^{-1} 2,6-di-*tert*-butyl-4-methylphenol or DMF containing 25 mmol L^{-1} LiBr was used as the eluent. The polymers were thereby dissolved in the eluent, with a concentration range of 1.0 to 2.0 mg mL^{-1}. Measurements were taken on a PL-GPC 50 Plus by Agilent with an integrated RI unit, two light scattering detectors (15 and 90° and a differential pressure viscosimeter with two PolarGel M colums (Agilent) at 30 °C for DMF as solvent or two MixedC columns (Agilent) at 40 °C for thf. Polystyrene or polymethyl methacrylate served as the standard for the relative molecular weight distribution.

Lyophilization. The samples are dissolved in either ultarpure water or benzene and frozen under constant rotation in liquid nitrogen. For lyophilization, a VaCo 5-II-D from *Zirbus technology GmbH* is applied, the pressure is adjusted to 2 mbar with a condenser temperature of –90 °C.

Rheology. Dynamic viscosities (η) were measured using an *Anton Paar* Modular Compact Rheometer MCR 302 equipped with a *Julabo* CP-200F, a P-PTD200+H-PTD200 measuring cell and a PP25 measuring system. Measurements were conductet in parallel-plate mode with a gap width of 1.0 mm at 40 °C or 100 °C with shear rates $\dot{\gamma}$ ramping up from 1 s^{-1} to $1 \cdot 10^3$ s^{-1}. Kinematic viscosities of estolides were calculated assuming a density ρ of 0.9 kg m^{-3} at 40 °C by the correlation $\nu = \frac{\eta}{\rho}$.

5.3 Experimental procedures

5.3.1 Monomer and polymer synthesis

5.3.1.1 *N,N'*-Dibenzyl acrylamide

In a Schlenk flask, acryloyl chloride (5.60 g, 5.00 mL, 61.87 mmol, 1.0 eq.) and *N,N*-diisorpopylethylamine (8.00 g, 10.52 mL, 61.87 mmol, 1.0 eq.) are added to a solution of dibenzylamine (12.2 g, 11.90 mL, 61.87 mmol, 1.0 eq.) in tetrahydrofuran (200 mL) at a temperature of –15 °C. The reaction mixture is stirred at a temperature of 0 °C for two hours. Then, the solvent is removed *in vacuo*. The solid obtained is then dissolved in ethyl acetate (150 mL) and washed with saturated sodium bicarbonate solution (150 mL), a hydrogen chloride solution (50 mL, 2 M), and a saturated sodium chloride solution (150 mL). Then the crude product is purified and dried by a short column of activate alumina using dry ethyl acetate as a the mobile phase. After removal of the solvent, *N,N'*-dibenzyl acrylamide (10.7 g, 69 %) is obtained as a slightly yellow oil which crystallizes after some time.

^{1}H-NMR (400 MHz, CDCl$_3$): δ [ppm] = 7.42-7.22 (8H, m, CH-aromatic), 7.18 (2H, d, ^3J = 7.4 Hz, CH-aromatic), 6.62 (1H, dd, ^3J = 16.9 Hz, ^3J = 10.4 Hz, acrylic-CH), 6.50 (1H, dd, ^3J = 16.7 Hz, ^2J = 2.3 Hz, acrylic-CH$_2$), 5.74 (1H, dd, ^3J = 10.2 Hz, ^2J = 2.3 Hz, acrylic-CH$_2$), 4.67 (2H, s, NCH$_2$), 4.52 (2H, s, NCH$_2$).

5.3.1.2 Catalytic polymerization procedure Bn$_2$AA

For the polymerization of Bn$_2$AA, 6.75 µmol (1.0 eq.) of the respective catalyst was weighed into a dried screw cap vial and dissolved in 2.5 mL dry solvent (toluene, thf or dichloromethane). Under vigorous stirring the monomer (339 mg, 1.35 mmol, 200 eq.) was dissolved in 2.5 mL dry solvent (toluene, thf or dichloromethane) and added in one portion. The reaction was stirred the desired temperature and the reaction

progress was monitored by ^{1}H-NMR. To terminate the reaction methanol (0.2 mL) was added and the polymer was isolated by precipitation in pentane (15-fold excess).

^{1}H-NMR (400 MHz, CDCl$_3$): δ [ppm] = 1.40—1.80 (m, CH$_2$), 2.32—2.73 (m, CH), 4.37 (s, aryl-CH$_2$), 4.68 (s, aryl-CH$_2$), 7.11—7.59 (m, aryl-CH).

5.3.1.3 Radical polymerization of Bn$_2$AA

Bn$_2$AA (0.678 g, 2.70 mmol, 5 eq.) was dissolved in dry toluene (0.77 to 1.0 mm). The monomer solution was added to AIBN (88.6 mg, 0.54 mmol) and heated to 65 °C to start the reaction. The polymerization was terminated after 1 d using methanol (0.1 mL) and the polymer was isolated by precipitation in a tenfold excess of pentane. The precipitated polymer was separated by centrifugation and dried *in vacuo* at a temperature of 60 °C and a pressure of 0.05 mbar.

Spectroscopic data were analog to the catalytic produce polymer.

5.3.1.4 Polymer analogous deprotection of PBn$_2$AA

Hydrogenation with Pd/C. The hydrogen gas pressure reaction was performed in 50 mL steel reactors equipped with glass inlays. PBn$_2$AA (150 mg, 0.598 mmol, 1.0 eq.) was dissolved in thf (15 mL) and Pd/C (10 wt.%, 1.50 mg, 0.0141 mmol, 0.02 eq.) was added. The reaction was started by heating the reactor up to 50 °C and applying a pressure of 50 bar H$_2$. The reaction was then stirred for three days. After the reactor was vented, the remaining suspension was filtrated and the solvent removed *in vacuo*. The obtained solid was dissolved in chloroform and precipitated in pentane. The precipitate was separated by centrifugation and dried *in vacuo* at a temperature of 60 °C and a reduced pressure of 0.05 mbar. The desired PAA could not be observed by spectroscopic analysis.

Hydrogenation with Pt$_2$O. PBn$_2$AA (5.0 mg, 0.02 mmol, 1.0 eq.) were milled using a ball-mill and suspended with a spade point of Pt$_2$O in water (4 mL). The mixture was stirred under H$_2$-pressure (20 bar) in a steel reactor at 60 °C for 3 d. The suspension was dissolved in toluene, precipitated into pentane (40 mL) and separated by centrifugation. The solid residue was lyophilized over night. ^{1}H-NMR showed no signals of the desired product PAA.

Hydrogenation with Pd/ and acetic acid. PBn$_2$AA 100 mg, 0.40 mmol, 1.0 eq.) were dissolved in thf (2 mL, mixed together with formic acid (9.5 g, 159 mmol) and suspended wit Pd/C (10 wt.%, 10 mg). The reaction mixture was stirred at 60 °C for 3 d. The mixture was precipitated in pentane and the solid separated by centrifugation. The solid was dried *in vacuo* at 60 °C over night. ^{1}H-NMR analysis showed only signals of the starting material PBn$_2$AA.

Deprotection with TFA. PBn$_2$AA (60 mg, 0.24 mmol, 1.0 eq.) was dissolved in chloroform (10 mL) and TFA (10 mL, 130.68 mmol, 544 eq.) and acetic acid (0.53 g, 8.74 mmol, 35 eq.) were added. The reaction mixture was heated to 60 °C for seven days. After this, the mixture was neutralized using a saturated sodium bicarbonate solution. The organic phase was precipitated in cyclohexane and the solid separated by centrifugation. The solid was characterized by ^{1}H-NMR but no hints of the desired product PAA could be found.

Deprotection with TfOH. PBn$_2$AA (50 mg, 0.20 mmol, 1.0 eq.) was dissolved in toluene (3 mL) and TfOH (0.2 mL, 2.27 mmol, 11.5 eq.) were added. The reaction mixture was stirred at 65 °C for 3 d and then neutralized using a saturated sodium bicarbonate solution. After the addition of toluene (20 mL) the solution was washed with water (20 mL). A polymer-like film forms at the phase boundaries of the organic and aqueous phase. This solid is separated and dried in an oven at 60 °C under vacuum overnight. No PAA was identified by ^{1}H-NMR.

Radical deprotection with NBS and AIBN. PBn$_2$AA (152 mg, 0.606 mmol, 1.0 eq.) was dissolved in 15 mL chlorobenzene. BNS (216 mg, 1.21 mmol, 2.0 eq.) and AIBN (40.1 mg, 0.244 mmol, 0.4 eq.) were added to the solution. The reaction mixture was

stirred for three hours at 130 °C. Afterwards, NBS (44 mmol, 0.247 mmol, 0.4 eq.) and AIBN (20.2 mg, 0.123 mmol, 0.2 eq.) were added to the solution, and the reaction was heated overnight. After cooling the mixture to room temperature and filtration, the solvent was removed *in vacuo*. Diethyl ether (10 mL) and water (20 mL) were added and the mixture was stirred for two hours. The phases then were separated and methanol was added to the aqueous phase. The solvent mixture was removed under reduced pressure and a brown solid was observed. In spectroscopic analysis, no hints of the desired product PAA could be found.

5.3.1.5 *N,N'*-Di(*tert*-Butoxycarbonyl)-acrylamide

In a flame dried Schlenk flask, acrylamide (4.0 g, 56.33 mmol, 1.0 eq.) and *N,N'*-dimethylaminopyridine (0.69 g, 5.63 mmol, 0.1 eq.) were dissolved in dry dichloro-metane (300 mL). Di-*tert*-butoxycarbonate (25.8 g, 118.4 mmol, 2.1 eq.) were added and the reaction mixture was stirred one hour at room temperature. After that, the solution was washed with a saturated sodium bicarbonate solution (30 mL) and extracted with dichloromethane (3 × 30 mL). The organic phase was washed again with water (3 × 20 mL) and with a saturated sodium chloride solution (40 mL) and dried over sodium sulfate. The crude product was purified by column chromatography (hexanes / ethyl acetate 9:1). After removal of the solvent the colorless solid was sublimated twice under vacuum at 53 °C to obtain *N,N'*-Di(*tert*-butoxycarbonyl)-acrylamide (3.1 g, 20 %) as a crystalline colorless solid.

^{1}H-NMR (400 MHz, CDCl$_3$): δ [ppm] = 6.98 (1H, dd, J = 17.0, 10.4 Hz, acrylic-CH), 6.48 (1H, dd, J = 17.0, 1.6 Hz, acrylic-CH$_2$), 5.85 (1H, dd, J = 10.4, 1.6 Hz, acrylic-CH$_2$), 1.53 (18H, s, C(CH$_3$)$_3$).

5.3.1.6 Polymerization of Boc$_2$AA

For the polymerization of Boc$_2$AA, 6.75 µmol (1.0 eq.) of the respective catalyst was weighed into a dried screw cap vial and dissolved in 2.5 mL dry solvent (toluene,

thf or dichloromethane). Under vigorous stirring the monomer (367 mg, 1.35 mmol, 200 eq.) was dissolved in 2 mL dry toluene and added in one portion to the catalyst solution. The reaction was stirred the desired temperature and the reaction progress was monitored by ^{1}H-NMR. To terminate the reaction methanol (0.2 mL) was added and the polymer was isolated by precipitation in pentane (15-fold excess).

^{1}H-NMR (400 MHz, CDCl$_3$): δ [ppm] = 3.57 (2H, m, CH$_2$), 2.29 − 1.67 (1H, m, CH), 1.47 (18H, s, Boc-CH$_3$).

5.3.1.7 Deprotection of PBoc$_2$AA

Deprotection with TFA. PBoc$_2$AA (32 mg, 0.12 mmol, 1.0 eq.) was dissolved in chloroform (10 mL) and TFA (20 mL, 259.6 mmol, 2163 eq.) was added. The reaction mixture was heated to 60 °C for seven days. Then, the mixture was neutralized by addition of a saturated sodium bicarbonate solution and the phases were separated. The solvent was removed *in vacuo* and the residue was dissolved in methanol. The resulting sticky, slightly yellow solid was dissolved in DMSO-d6 and analyzed by ^{1}H-NMR, but no signals of PAA could be observed, the high amount of signals indicates decomposition of the polymer.

Deprotection with TfOH. PBoc$_2$AA (24 mg, 0.08 mmol, 1.0 eq.) was dissolved in chloroform (3 mL) and TfOH (0.4 mL, 4.53 mmol, 57 eq.) was added. The reaction mixture was stirred at 60 °C for 4 d after which the solution was neutralized by the addition of a saturated sodium bicarbonate solution. Phases were separated and the organic solvent was removed *in vacuo*. The product only dissolves in DMSO and was precipitated from methanol. After centrifugation and drying in a vacuum oven at 100 °C the solid residue was analyzed by ^{1}H-NMR. No hints of the desired product PAA could be found, the large variety of signals indicates decomposition of the polymer.

5.3.1.8 *N,O*-Bis(trimethylsilyl)-acrylamide

In a flame dried Schlenk flask, acrylamide (10.1 g, 141.8 mmol, 1.0 eq.) were dissolved in dry triethylamine (300 mL) and cooled to 0 °C. With an addition funnel, trimethylsilyl chloride (45.1 g, 374.2 mmol, 2.6 eq.) was added dropwise. After the addition was complete, the raction was heated to 95 °C and stirred over night. After cooling down, the turbid solution was filtrated by the help of a Schlenk-frit and the product was purified by fractional distillation (56 °C, 15 mbar). After Whatman filtration at –50 °C to separate monosilylated acrylamide still present, *N,O*-Bis(trimethylsilyl)-acrylamide (26.65 g, 87 %) was obtained as a colorless liquid.

^{1}H-NMR (400 MHz, CDCl$_3$): δ [ppm] = 5.99 (2H, d, J = 4.9 Hz, acrylilc-CH$_2$), 5.52 (1H, dd, J = 7.4, 4.9 Hz, acrylic-CH), 0.23 (9H, s, Si(CH$_3$)$_3$), 0.14 (9H, s, Si(CH$_3$)$_3$).

5.3.1.9 Radical polymerization of BTSAA

In a pressure Schott flask, the the initiator AIBN (2.22 mg, 0.14 mmol, 0.1 eq.) was dissolved in toluene (2.0 mL) and the reaction solution is heated to 70 °C. To the initiator solution, BTSAA (0.29 g, 1.4 mmol, 1.0 eq.) was added quickly and stirred for 5 h. At the end of the reaction the polymer is precipitated from the reaction solution into a Falcon tube filled with anhydrous pentane (10 mL). The suspension is then centrifuged (4 min, 8000 rpm) and the pentane is decanted. The resulting white product is dried in vacuo.

^{1}H-NMR (400 MHz, CDCl$_3$): δ [ppm] = 2.27 – 1.71 (2H, m, CH$_2$), 1.72 – 1.42 (1H, m, CH), 0.5 – 0.0 (18H, m, –OSi(CH$_3$)$_3$, NSi(CH$_3$)$_3$).

5.3.1.10 Deprotection of PBTSAA

Deprotection of pBTSAA is carried out with a 0.5 M HCl/THF mixture (1:1, v/v, 5 to 10 mL) in methanol. In this process, polyacrylamide precipitates from the acid solution

and is centrifuged at 8000 rpm for two minutes. The solvent is decanted off and the solid is dried *in vacuo*. Polyacrylamide is obtained in quantitative yield.

^{1}H-NMR (400 MHz, CDCl$_3$): δ [ppm] = 2.12 – 2.08 (1H, m, CH), 1.50 -– 1.45 (2H, m, CH$_2$).

5.3.1.11 Triisopropyl((1-methoxy-2-methylprop-1-en-1-yl)oxy)silane ([iPr]SKA)

In a flame dried Schlenk flask, anhydrous tetrahydrofuran (50 mL) and diisoropyl amine (4.2 mL, 30.0 mmol, 1.2 eq.) was charged and cooled to 0 °C. A solution of *n*-butyl lithium (21.2 mL, 27.5 mmol, 1.1 eq., 1.3 M) was added slowly and the reaction mixture was stirred for 30 minutes. Then, the reaction was cooled to –78 °C and methyl isobutyrate (2.87 mL, 25.0 mmol, 1.0 eq.) was added dropwise. After a stirring time of 30 minutes, 1,3-dimethyl-3,4,5,6-tetrahydro-2(1H)-pyrimidinone (4.53 mL, 37.5 mmol, 1.5 eq.) and triisopropylsilyl chloride (6.42 mL, 30.0 mmol, 1.2 eq.) was added and stirred for further 30 minutes at –78 °C. After warming to room temperature, the solvent was removed *in vacuo* and the resulting mixture was diluted with pentane (200 mL) and washed with water (100 mL), saturated copper sulfate (100 mL), saturated sodium bicarbonate (100 mL), and saturated sodium chloride (100 mL). The organic phase was dried over sodium sulfate and after removing the solvent *in vacuo* the crude product was purified by fractional distillation (98 °C, 14 mbar) to result in triisopropyl((1-methoxy-2-methylprop-1-en-1-yl)oxy)silane (5.43 g, 84 %) as a colorless liquid.

^{1}H-NMR (400 MHz, CDCl$_3$): δ [ppm] = 3.55 (3H, s, CH$_3$O), 1.56 (6H, s, (CH$_3$)$_2$C), 1.24–1.12 (3H, m, CHSi), 1.09 (21H, m, ((CH$_3$)$_2$CH)$_3$).

5.3.1.12 Polymerization of methyl acrylate

A typical small-scale polymerization procedure is as follows: methyl acrylate (0.25 mL, 2.77 mmol, 100 eq.) was dissolved in aqueous toluene (2.45 mL). [iPr]SKA (8.0 µL,

2.76 µmol, 1 eq.) was added by a pipette and the polymerization was initiated by the addition of (pentafluorophenyl)bis(triflyl)methane (5.52 µL, 0.55 µmol, 0.02 eq., 0.1 M solution in toluene). The reaction mixture was stirred at room temperature and the reaction progress monitored by ^{1}H-NMR. After the monomer is completely consumed, the reaction is isolated by precipitation in pentane (10-fold excess). Big-scale experiments (100 g) were performed analog in a 2 L Schott-flask in toluene (2 L).

Methyl acrylate:

^{1}H-NMR (400 MHz, CDCl$_3$): δ [ppm] = 6.40 (dd, J = 17.3, 1.5 Hz, 1H), 6.11 (dd, J = 17.3, 10.4 Hz, 1H), 5.82 (dd, J = 10.4, 1.5 Hz, 1H), 3.75 (s, 3H).

Polymethyl acrylate:

^{1}H-NMR (400 MHz, DMSO-d$_6$) 3.65 (3H, s, OMe), 2.32 (1H, m, CH), 1.91 (m, CH$_2$, *threo-meso*), 1.66 (m, CH$_2$, *racemo*), 1.54 (m, CH$_2$, *erythro-meso*).

^{1}H-NMR (400 MHz, CDCl$_3$): δ [ppm] = 3.75 (3H, s, OMe), 2.03 (1H, m, CH), 1.78 (m, CH$_2$, *threo-meso*), 1.53–1.67 (m, CH$_2$, *racemo, erythro-meso*).

^{13}C-NMR (100 MHz, DMSO-d6) 175.0 (m, C=O), 52.0 (m, OMe), 41.5 (m, CH), 35.0 (m, CH$_2$).

Glass transition temperature: T_g = 18 °C.

5.3.2 Polymer analogous conversion of PMA to PAN

5.3.2.1 Conversion of PMA to PAA

Polymethyl acrylate from big-scale polymerization (approx. 100 g) was dissolved in a thf/methanol mixture (2:1 v/v, 2 L) and loaded into a 5 L reactor by Büchi equipped with a mechanical stirring unit and a double jacket which can be cooled or heated by a thermostat. The polymersolution was pressurized with ammonia (8 bar) and heated

to 120 °C which results in an pressure of 20 bar. The reaction progress was monitored by ^{1}H-NMR. After reaching the desired conversion, the reactor is cooled down to room temperature and vented. The solvent was removed *in vacuo* and the resulting polymer was dissolved in water and precipitated from water for purification.

^{1}H-NMR (400 MHz, $CDCl_3$): δ [ppm] = 7.69–6.54 (2H, m, NH_2), 2.11 (1H, m, CH), 1.85–1.30 (2H, m, CH_2).

ATR-IR $\tilde{v}_{max}$ 3331 (v_{as} NH_2), 3192 (v_{as} NH_2), 2931 (v_{as} CH_2), 1654 cm^{-1} (v C=O).

5.3.2.2 Conversion of PAA to PAN

Polyacryl amide (15 g) were dispersed in dmf (600 mL) and DCP (200 mL) were added. The reaction mixture was heated to 60 °C and stirred over night. A clear solution indicates the reaction being complete. The reaction mixture was quenched by pouring it slowly into water (approx. 3 L). After filtration, the filter cake is washed with methanol and the raw product was dried in an vacuum oven at 60 °C for 24 h. The dry polymer was then dissolved in dmf (50 mL) and precipitated in water. After re-filtration and drying, PAN is optained as a white, slightly beige solid.

^{1}H-NMR (400 MHz, $CDCl_3$): δ [ppm] = 3.34–3.01 (H, m, CH), 2.31–1.89 (2H, m, CH_2).

^{13}C-NMR (100 MHz, $CDCl_3$): δ [ppm] = 120.9–118.9 (m, CN), 33.5–32.0 (m, CH), 28.7–26.1 (m, CH_2).

ATR-IR $\tilde{v}_{max}$ 2293 (v_{as} CH_2), 2244 (v C≡N), 1456 (δ CH_2), 1365 (δ_s CH), 1076 (δ C–C), 1036 cm^{-1} (v C–C).

5.3.3 Epoxidation of vegetable oils and their derivatives

5.3.3.1 9,10-Epoxystearic acid

Epoxidation with *m*CPBA Oleic acid (1 g, 3.54 mmol, 1.0 eq.) was dissolved in chloroform (100 mL) and *m*CPBA (1.0 g, 5.8 mmol, 1.6 eq.) was added. The reaction mixture was stirred at room temperature and the reaction progress was monitored by ^{1}H-NMRand was usually completed within 24 hours. The reaction was then terminated by the addition of a sodium bicarbonate solution (5 wt.%, 200 mL). The organic phase was washed with a saturated sodium chloride solution (3 × 200 mL). After drying over sodium sulfate and removing the solvent *in vacuo*, 9,10-epoxystearic acid (1.0 g, 96 %) was obtained as a white solid. Analytic data are in accordance with the literature.[277]

^{1}H-NMR (400 MHz, CDCl$_3$): δ [ppm] = 2.90 (2H, m, epoxy-CH), 2.33 (2H, t, J = 7.14 Hz, CH$_2$COOH), 1.64 (2H, t, J = 7.15 Hz, CH$_2$CH$_2$COOH), 1.56–1.19 (4H, m, CH$_2$CHOCHCH$_2$), 1.40–1.21 (20H, m, alkane-CH$_2$), 3.60 (3H, t, J = 6.65 Hz, CH$_3$).

^{13}C-NMR (100 MHz, CDCl$_3$): δ [ppm] = 179.5, 57.5, 57.4, 34.1, 32.0, 29.7, 29.7, 29.5, 29.4, 29.3, 29.1, 28.0, 27.9, 26.7, 24.8, 22.8, 14.3.

5.3.3.2 9,10-12,13-Diepoxystearic acid

Epoxidation with *m*CPBA. Linoleic acid (10 g, 35.4 mmol, 1.0 eq.) was dissolved in dichloromethane (250 mL) and *m*CPBA (20.0 g, 92.7 mmol, 2.6 eq.) was added. The reaction mixture was stirred at room temperature and the raction progress was monitored by ^{1}H-NMRand was usually complete within 24 hours. The Reaktion was terminated by the addition of a sodium bicarbonate solution (5 wt.%, 350 mL). The organic phase was washed with with a saturated sodium chloride solution (3 × 300 mL). After drying over sodium sulfate and removing the solvent *in vacuo*, the crude product was purified by column chromatography (hexanes / ethyl acetate 4:1) and 9,10-12,13-diepoxystearic acid (2.7 g, 24.4 %) obtained as a white solid.

Epoxidation with Oxone®. Linoleic acid (5 g, 17.8 mmol, 1.0 eq.) was dissolved in acetone (70 mL) and sodium bicarbonate (13.5 g, 160.5 mmol, 9.0 eq.) was added. Oxone® (29.2 g, 46.4 mmol, 2.6 eq.) was dissolved in H_2O (100 mL) and added slowly to the ice-cooled acetone solution. When the addition was complete the reaction mixture was warmed to room temperature and stirred over night. The reaction was then extracted with ethyl acetate (3 × 100 mL) and the organic phase was washed with a saturated sodium chloride solution (200 mL). 9,10-12,13-Diepoxystearic acid (3.74 g, 67 %) was obtained as a white solid.

^{1}H-NMR (400 MHz, $CDCl_3$): δ [ppm] = 3.10 (2H, m, CHOCH), 2.98 (2H, m, CHOCH), 2.35 (2H, t, J = 7.45 Hz, CH_2–COOH), 1.85–1.68 (2H, m, CHOCH2CHO), 1.64 (2H, m, CH_2–CH_2COOH), 1.59–1.23 (19H, m, alkane-CH_2), 0.9 (3H, CH_3).

^{13}C-NMR (100 MHz, $CDCl_3$): δ [ppm] = 178.89, 57.24, 57.14, 56.95, 56.85, 54.53, 54.39, 54.35, 33.95, 31.82, 31.08, 29.38, 29.24, 29.04, 28.01, 27.93, 27.34, 27.05, 26.63, 26.53, 26.39, 26.28, 24.76, 22.71, 14.13.

GC-MS/EI r.t. 14.97 min, m/z = 150.1 (M), 193.0 (M-CH_2).)

5.3.3.3 Methyl oleate

Oleic acid (17.9 g, 57.7 mmol) was dissolved in methanol (50 mL) containing sulfuric acid (0.25 mL, 0.5 vol.%) as catalyst. The reaction mixture was heated to 75 °C and stirred over night. After cooling down, diethyl ether (400 mL) was added and the mixture was neutralized and washed with a saturated sodium bicarbonate solution (300 mL). The aqueous phase was counter-extracted with diethyl ether (200 mL). After drying over sodium sulfate, the solvent was removed *in vacuo* and methyl oleate (15.4 g, 90 %) was obtained as a colorless oil.

^{1}H-NMR (400 MHz, $CDCl_3$): δ [ppm] = 9.18 (2H, s), 5.58 (3H, s), 4.22 (2H, t, J = 7.6 Hz), 3.97 − 3.88 (4H, m), 3.60 − 3.48 (2H, m), 3.20 (20H, d), 2.79 (3H, t)

¹³C-NMR (100 MHz, CDCl₃): δ [ppm] = 174.47, 130.15, 129.90, 51.58, 34.26, 32.06, 29.92, 29.83, 29.67, 29.47, 29.31, 29.28, 29.24, 27.37, 27.31, 25.10, 22.83, 14.26.

GC-MS/EI r.t. 12.8 min, m/z = 296.3 (M), 264.2 (M - CH₃O).

5.3.3.4 Methyl linoleate

Linoleic acid (2.0 g, 7.1 mmol, 1.0 eq.) was dissolved in methanol (10 mL) containing sulfuric acid (1 wt.%) as catalyst and heated to 70 °C. After 4 hours, the reaction mixture was cooled to room temperature and H₂O (20 mL) was added and extracted with diethyl ether (3 × 50 mL). The organic phase was neutralized with a saturated sodium bicarbonate solution and washed with a saturated sodium chloride solution (50 mL). After removing the solvent *in vacuo*, methyl linoleate (1.5 g, 70 %) was obtained as colorless oil. Analytic data are in accordance with the literature.[278]

¹H-NMR (400 MHz, CDCl₃): δ [ppm] = 5.43 – 5.62 (4H, m), 3.66 (3H, s), 2.76 (2H, t, *J* = 5.9 Hz), 2.29 (2H, t, *J* = 7.6 Hz), 2.04 (4H, q, *J* = 6.9 Hz), 1.67 – 1.57 (2H, m), 1.43 – 1.23 (14H, m), 0.87 (3H, t).

¹³C-NMR (100 MHz, CDCl₃): δ [ppm] = 174.41, 130.33, 130.16, 128.17, 128.03, 51.55, 34.22, 31.66, 29.72, 29.48, 29.28, 29.25, 29.22, 27.33, 27.31, 25.75, 25.07, 22.70, 14.19.

GC-MS/EI r.t. 12.8 min, m/z = 294.3 (M), 263.3 (M - CH₃OH)

5.3.3.5 9,10-12,13-Diepoxy methylstearate

Methyl linoleate (5.0 g, 17.0 mmol, 1.0 eq.) was dissolved in acetone (70 mL) and sodium bicarbonate (13.4 g, 159.6 mmol, 9.0 eq.) was added. Oxone® (27.8 g, 44.2 mmol, 2.6 eq.) was dissolved in H₂O (150 mL) and added slowly to the ice-cooled acetone solution. When the addition was complete the reaction mixture was warmed to room temperature and stirred over night. The reaction was then extracted with ethyl acetate

(3 × 250 mL) and the organic phase was washed with a saturated sodium chloride solution (250 mL). 9,18-12,13-Diepoxy methylstearate (5.19 g, 94 %) was obtained as a colorless liquid.

^{1}H-NMR (400 MHz, CDCl$_3$): δ [ppm] = 3.66 (3H, s, OCH$_3$), 3.09 (2H, m,), 2.98 (2H, m,), 2.30 (2H, t, J = 7.5 Hz,), 1.85–1.94 (22H, m, alkane-CH$_2$), 0.9 (3H, t, J = 6.9 Hz, CH$_3$).

^{13}C-NMR (100 MHz, CDCl$_3$): δ [ppm] = 174.40, 57.17, 57.12, 56.89, 56.83, 54.51, 54.49, 54.34, 51.60, 34.20, 31.82, 29.44, 29.30, 29.16, 28.03, 27.96, 27.36, 27.07, 26.67, 26.57, 26.39, 26.28, 25.03, 22.71, 14.13.

GC-MS/EI r.t. 14.8 and 15.0 min (cis/trans-isomers), m/z = 211.1 (M - C$_7$H$_{15}$O), 157.1 (M - C$_{10}$H$_{19}$O$_2$), 55.1 (M - C$_{15}$H$_{27}$O$_4$), 95.1 (M - C$_{11}$H$_{18}$O$_2$).

5.3.3.6 Epoxidation of vegetable oils[182]

The epoxidation of vegetable oils was carried out by the *in-situ* generation of performic acid from formic acid and hydrogen peroxide. This reaction procedure is exemplary for linseed oil but was used analogous for yeast oil, olive oil, canola oil and hempseed oil. A ratio of linseed oil to formic acid to hydrogen peroxide of 1.0:1.0:10 was used. As a reaction vessel, a double-wall 2 L glass reactor connected to a thermostat for cooling or heating, respectively was used. The linseed oil (422 g, 0.479 mol) was loaded into the reactor. Hydrogen peroxide (mL, 4.79 mol, 35 %) was added, and the mixture was stirred with a glass overhead stirrer (400 rpm), and the reactor was cooled to 10 °C. Then, 18.60 mL of formic acid (22.04 g, 0.479 mol) was added dropwise throughout 30 min. The temperature was raised to 50 °C and stirred for 48 h. The epoxidation progress can be followed by ^{1}H-NMR spectroscopy. The reaction mixture was neutralized by addition of a saturated sodium bicarbonate solution (200 mL) after cooling to room temperature and diluted with diethyl ether (200 mL). After washing with a saturated sodium chloride solution, the solvent was removed *in vacuo*. The EEW was estimated to be 140.6 g mol^{-1} resulting from the molecular weight of linseed

oil ($878\,\mathrm{g\,mol^{-1}}$) and approximately 6.2 double bonds per triglyceride determined by ^{1}H-NMR analysis.[279]

5.3.3.7 Milling procedure for tannic acid[182]

TA was milled with in a two-step ball-milling procedure. Before milling, TA was dried in a vacuum oven at 105 °C for 2 h to remove water bound in the biomolecule. The dried powder (100 g) was then loaded into an aluminum container of 1000 mL together with aluminum hydroxide (Al_2O_3) balls (40 pieces with diameter of 10 mm and 40 pieces with a diameter of 5 mm) and placed into a speed mixer (DAC-300 HP, Hauschild GmbH & Co. KG). This way, a pre-milling was performed at a rotation speed of 650 rpm for 3 min in four cycles. Between the cycles, TA was cooled down to room temperature. The gained powder was again dried at 105 °C under vacuum for 2 h to remove all residual bound water and four more milling cycles were performed. The second milling step was conducted with the Al_2O_3-balls in a 3D-shaker mixer (Willy A. Bachofen AG, Switzerland) at 50 rpm for 16 h. Then, the fine TA powder was separated from the balls by sieving through a stainless-steel sieve and once again dried in vacuum for 4 h at 105 °C.

Particle size before milling: D_{25} = 27.3 µm, D_{50} = 50.2 µm, D_{90} = 100.4 µm; after milling: D_{25} = 2.5 µm, D_{50} = 6.6 µm, D_{90} = 35.6 µm.

5.3.3.8 Epoxy sample preparation with epoxidized linseed oil and tannic acid[182]

ELO/TA samples were prepared as follows: ELO (50 g) and the corresponding amount of the molar ratios 0.85, 1.0, 1.15, 1.25, 1.5, 1.75 and 2.0 (exact amounts see Table 4.11) of the milled TA powder and an air release additive (Epinal EL 12.42 by bto epoxy GmbH) were added together in an 500 mL aluminum container. The components in the container were mixed under vacuum in a speed mixer at 600 rpm for 10 min. The mixture was then poured into two different aluminum mold with cavity

dimensions of 60 mm × 6 mm × 2 mm, and 80 mm × 10 mm × 4 mm for DMA or flexural testing, respectively. For easier release of the cured specimens from the molds, Teflon tape was previously laid out in them. The epoxy samples were degassed in a vakuum oven at a temperature of 80 °C and a pressure of 1 mbar for 2 h. Then, the mold was transferred to an oven and cured at two different temperature profiles. C1: 16 h at 90 °C followed by 3 h at 140 °C and C2: 16 h at 120 °C followed by 3 h at 140 °C.

5.3.3.9 Conjugation of linoleic acid

Linoleic acid (0.25 g, 0.89 mmol, 1.0 eq.) was mixed with potassium hydroxide (0.79 g, 7.76 mmol, 8.9 eq.) and ethylene glycol (2.0 mL, 35.8 mmol). The mixture was heated under microwave irradiation and argon atmosphere for 15 min at 160 °C. After the addition of methanol (5 mL) and aqueous hydrogen chloride (20 mL, 3 M), the reaction mixture was extracted with hexanes (5 × 5 mL) and the organic phase was washed with methanol in water (30 vol.%) and with water (30 mL). The organic phase was dried over magnesium sulfate and the solvent was removed *in vacuo*. Conjugated linoleic acid could be isolated as a yellow oil (0.13 g, 52 %).

^{1}H-NMR (400 MHz, CDCl$_3$): δ [ppm] = 6.30 (1H, m, CH-methin), 5.94 (1H, m, CH-methin), 5.65 (1H, m, CH-methin), 5.29 (1H, m, CH-methin), 2.35 (2H, t, CH$_2$COOH), 2.11 (4H, m, CH$_2$–CH=), 1.63 (2H, m, CH$_2$CH$_2$COOH), 1.45 − 1.20 (16H, m, CH$_2$), 0.89 (3H, s, CH$_3$).

5.3.4 Synthesis of EGCHC epoxy monomer[251]

5.3.4.1 Allyl sorbate

Allyl alcohol (200 mL) with a catalytic amount of sulfuric acid (0.5 vol.%, 1.0 mL) was heated to reflux and sorbic acid (50 g, 445.9 mmol) was added. The mixture was

stirred for 24 h. After cooling down the reaction to room temperature a saturated sodium bicarbonate solution was added to neutralize it and the product was extracted with diethyl ether (3 × 200 mL). Then, the combined organic phases were washed with a saturated sodium chloride solution (200 mL) and dried over anhydrous sodium sulfate. The solvent was removed *in vacuo* after filtration and the crude product was purified by distillation (82 °C, 8 mbar). The product allyl sorbate was obtained as a colorless liquid (55.6 g, 82 %).

¹H-NMR (400 MHz, CDCl$_3$): δ [ppm] = 7.27 (m, H4), 6.17 (m, H3), 5.95 (m, H8), 5.80 (d, J = 15.4 Hz, H2), 5.27 (m, H5/H9), 4.65 (m, H7), 1.86 (d, J = 5.7 Hz, H1).

¹³C-NMR (100 MHz, CDCl$_3$): δ [ppm] = 167.00 (C6), 145.46 (C4), 139.65 (C2), 132.54 (C8), 129.88 (C3), 118.37 (C5), 118.07 (C9), 64.99 (C7), 18.75 (C1).

5.3.4.2 Allyl-7-methyl-1,3-dioxo-1,3,3a,4,7,7a-hexahydroisobenzofuran-4-carboxylate (AHIBC)

To maleic anhydride (26.3 g, 268.08 mmol, 1.02 eq.) dissolved in toluene (26 mL, 10 mol dm^{-3} solution) was added allyl sorbate (40 g, 262.82 mmol, 1.0 eq.) under vigorous stirring. The reaction is strongly exothermic, heating was interrupted to prevent overheating. The reaction progress was monitored by ¹H-NMR and was usually finished after 2.5 h. The crude product was crystallized by cooling down the reaction mixture to 0 °C and for purification the crude product was washed with cold methanol. After removing the residual solvent *in vacuo*, the product allyl 7-methyl-1,3-dioxo-1,3,3a,4,7,7a-hexahydroisobenzofuran-4-carboxylate (AHIBC) was obtained as a white, crystalline solid (56.4 g, 84 %).

¹H-NMR (400 MHz, CDCl$_3$): δ [ppm] = 6.47 (1H, dt, J = 9.49, 3.32 Hz, H3), 5.98 (1H, m, J = 16.61, 10.38, 5.98 Hz, H12), 5.86 (1H, dt, J = 9.40, 3.24 Hz, H2), 5.4 − 5.2 (2H, m, H13), 4.76 (2H, dt, J = 6.09, 1.32 Hz, H11), 4.02 (1H, dd, J = 9.78, 5.55 Hz, H5), 3.39 (1H, dd, J = 9.79, 7.82 Hz, H6), 3.19 (1H, m, H4), 2.47 (1H, m, H1), 1.43 (3H, d, J = 7.34 Hz, H9).

13C-NMR (100 MHz, CDCl$_3$): δ [ppm] = 171.3 (C7), 170.3 (C8), 169.2 (C10), 134.8 (C2), 131.7 (C12), 127.0 (C3), 119.1 (C13), 66.4 (C11), 44.6 and 44.5 (C5 and C6), 40.1 (C4), 30.8 (C3), 16.4 (C9).

ATR-IR $\tilde{v}_{max}$ 2975, 2938, 2881, 1846, 1768, 1716, 1648, 1455, 1426, 1391, 1363, 1329, 1302, 1260, 1227, 1196, 1141, 1084, 1066, 1052, 1030, 950, 922, 904, 884, 817, 781, 747, 712 cm^{-1}.

EA Found: C, 62.08; H, 5.63. C$_{13}$H$_{14}$O$_5$ requires C, 62.39; H, 5.64 %.

HRMS (ESI) calculated C$_{13}$H$_{15}$O$_5$ [M + H$^+$] 251.0914, found 251.0912.

GC-MS/EI r.t. = 11.653 min, m/z = 150.1 (M), 193.0 (M - CH$_2$–CH–CH$_2$–O), 165 (M - CH$_2$–CH–CH$_2$–O–CO).

T_m = 88.6 °C.

5.3.4.3 Triallyl-6-methylcyclohex-4-ene-1,2,3-tricarboxylate (TACHC)

AHIBC (40 g, 159.84 g) was dissolved in allyl alcohol (190 mL). After addition of a catalytic amount of sulfuric acid (0.5 vol.%, 0.9 mL) the mixture was stirred under reflux and the reaction progress was monitored by ^{1}H-NMR The reaction was usually complete within 24 h. After the mixture had cooled to room temperature it was diluted with diethyl ether (100 mL), neutralized and washed by addition of saturated sodium bicarbonate solution (3 × 200 mL). The organic phase was washed with saturated sodium chloride solution (200 mL) and the united aqueous phases were extracted once with diethyl ether (200 mL). After drying the organic phases over sodium sulphate and filtration the solvent was removed *in vacuo*. The crude product was purified by column chromatography (1:6 EtOAc/hexanes) and the product triallyl-6-methylcyclohex-4-ene-1,2,3-tricarboxylate (TACHC) was obtained as a colorless oil (45.2 81 %).

¹H-NMR (400 MHz, CDCl$_3$): δ [ppm] = 6.09 (1H, m, H3), 5.90 (3H, m, H12, H12', H12"), 5.65 (1H, m, H2), 5.38 – 5.16 (6H, m, H13, H13', H13"), 4.58 (6H, m, H11, H11', H11"), 3.55 (1H, m, H5), 3.45 (1H, m, H6), 3.11 (1H, m, H4), 2.64 (1H, m, H1), 1.06 (3H, d, J = 7.36 Hz, H9).

¹³C-NMR (100 MHz, CDCl$_3$): δ [ppm] = 171.8, 171.4 and 170.73 (C10, C7 and C8), 132.5, 132.4, 132.1, 132.0 (C12, C12', C12" and C2), 122.9 (C3), 118.5, 118.4 and 118.4 (C13, C13', C13"), 65.8, 65.7 and 65.3 (C11, C11', C11"), 43.5 (C6), 42.3 and 42.1 (C4, C5), 32.2 (C1), 17.2 (C9).

ATR-IR $\tilde{v}_{max}$ 3455, 2940, 2882, 1730, 1649, 1454, 1379, 1310, 1169, 1094, 1061, 911, 927, 833, 720 cm^{-1}.

EA Found: C, 65.22; H, 6.88. C$_{19}$H$_{24}$O$_6$ requires C, 65.50; H, 6.94 %.

HRMS (ESI) calculated C$_{19}$H$_{24}$O$_6$Na [M + Na$^+$] 371.1471, found 371.1451.

5.3.4.4 1,2-Epoxy-6-methyl-triglycidyl-3,4,5-cyclohexanetricarboxylate (EGCHC)

Epoxidation with *m*CPBA. TACHC (40 g, 114.81 mmol, 1.0 eq.) was dissolved in dichloromethane (500 mL) and *m*CPBA (158.5 g, 918.5 mmol, 8.0 eq.) was added. The suspension was stirred at room temperature and the reaction progress was monitored by ¹H-NMR. After 48 h no residual signals of the double bond were left and the reaction was terminated by the addition of potassium carbonate (200 g) to deactivate remaining *m*CPBA. The resulting solids were separated by filtration and the organic phase was washed with a sodium thiosulfate solution (300 mL, 10 wt.%), water (200 mL), and a saturated sodium chloride solution (200 mL). After drying the organic phase over sodium sulphate and removing the solvent *in vacuo*, 1,2-epoxy-6-methyl-triglycidyl-3,4,5-cyclohexanetricarboxylate (EGCHC) was obtained as as colorless viscous oil (36.9 g, 78 %).

Epoxidation with Oxone®. TACHC (0.943 g, 2.71 mmol, 1.0 eq.) was dissolved in acetone (200 mL). Sodium bicarbonate (27.5 g, 446.0 mmol, 165 eq.) was suspended in water (90 mL) and added to the acetone solution. The mixture was cooled to 0 °C in an ice bath and Oxone® (50.0 g, 81.2 mmol, 30 eq.) dissolved in water (170 mL) was added drop wise over a period of 30 min. After stirring the reaction for 3 d at room temperature, the mixture was extracted with ethyl acetate (3 × 100 mL) and the combined organic phases were washed by a saturated sodium chloride solution. After drying over sodium sulfate the solvent was removed *in vacuo*. EGCHC was obtained as a colorless viscous oil (0.338 g, 30 %).

¹H-NMR (400 MHz, CDCl$_3$): δ [ppm] = 4.45 - 4.0 (3H, m, H11, H11', H11"), 3.93 (1H, m, H3), 3.76 (3H, m, H11, H11', H11"), 3.35 (1H, m, H4), 3.28 (1H, m, H5), 3.13 (3H, m, H12, H12', H12"), 2.97 (1H, m, H2), 2.93 (1H, m, H6), 2.80 - 2.73 (3H, m, H13, H13', H13"), 2.60 – 2.54 (3H, m, H13, H13', H13"), 2.38 (1H, q, H1), 1.06 (3H, m, H9).

¹³C-NMR (100 MHz, CDCl$_3$): δ [ppm] = 172.6, 172.0 and 169.8 (C10, C7 and C8), 65.9 (C11, C11', C11"), 56.8 (C3), 53.6 (C2), 49.2 – 48.9 (C12, C12', C12"), 44.8 – 44.5 (C13, C13', C13"), 41.5 (C4), 40.9 (C6), 39.6 (C5), 30.9 (C1), 14.8 (C9).

ATR-IR $\tilde{v}_{max}$ 2950, 1729, 1434, 1385, 1348, 1304, 1256, 1199, 1179, 1078, 1045, 1012, 940, 905, 840, 762, 738 cm^{-1}.

EA Found: C, 55.12; H, 8.87. C$_{19}$H$_{24}$O$_{10}$ requires C, 55.12; H, 8.83 %.

HRMS (ESI) calculated C$_{19}$H$_{24}$O$_{10}$Na [M + Na$^+$] 435.1267, found 435.1249.

5.3.4.5 EGCHC/DGEBA curing sample preparation

Samples for curing EGCHC and DGEBA were prepared as following: EGCHC/DGEBA (2 g) and the corresponding amount of the curing agent IPD or Jeffamine T403 (Table 4.14) were mixed in a 20 mL screw cap vial with a septum using a Classic Advanced Vortex Mixer (Velp Scientifica) with 30 000 rpm for 1 min. The samples

were degassed *in vacuo*for 3 min to remove trapped air. EGCHC-IPD samples were degassed for 30 s only as it cures comparably fast (setting under 4 min). The mixtures were then poured into the cavities of a silicone mold. Sample dimensions for DMA were 30 mm × 5 mm × 1 mm and for tensile testing the dogbone shape 1BB according to ISO 527-2 with a length of 30 mm and a thickness of 1 mm. For a flat surface finish a glass plate coated with a mold release agent was laid on the silicone mold. The samples were cured in an oven at the temperatures and durations given in Table 4.15. As post-processing the edges of the samples were wet-polished with sandpaper for a smooth surface.

5.3.5 Estolides

5.3.5.1 Methyl-9/10-hydroxystearic acid

Methyl oleate (16.7 g, 56.5 mmol) was dissolved in dry tetrahydrofuran (90 mL) and cooled by the help of an ice-bath. Borane-THF-complex (34 mL, 33.9 mmol, 1 M, 0.6 eq.) was added slowly and the solution was stirred over night at room temperature. Then, water (40 mL) was added and the reaction mixture was again cooled to 0 °C. A sodium hydroxide solution (30 mL, 3 M) was added slowly followed by hydrogen peroxide (70 mL). After reacting for one more hour the phases were separated and the organic phase was washed with water (70 mL) and a saturated sodium chloride solution (70 mL). The organic layer was dried over sodium sulfate and the solvent removed *in vacuo*. The crude product was purified by column chromatorgaphy (hexanes / ethyl acetate 6:1) and methyl-9/10-hydroxystearic acid was obtained as a waxy, colorless solid.

^{1}H-NMR (400 MHz, CDCl$_3$): δ [ppm] = 3.67 (3H, s, COOCH$_3$), 3.58 (1H, s, CH), 2.30 (2H, t, ^3J = 7.5 Hz, CH$_2$), 1.62 (2H, m, CH$_2$), 1.54 (2H, s, CH$_2$), 1.43 (4H, m, CH$_2$), 1.28 (20H, m, CH$_2$), 0.87 (3H, s, CH$_3$).

GC-MS/EI r.t. 14.2 min, m/z = 297.3 (M - OH), 155.1 (M - C$_9$H$_{19}$O$_2$).

5.3.5.2 Methyl-12-hydroxystearic acid

12-Hydroxystearic acid (30 g, 99.8 mmol) was dissolved in methanol (50 mL) containing sulfuric acid (0.3 mL, 0.6 vol.%) as catalyst. The reaction mixture was heated to 75 °C and stirred over night. After cooling down, diethyl ether (400 mL) was added and the mixture was neutralized and washed with a saturated sodium bicarbonate solution (300 mL). The aqueous phase was counter-extracted with diethyl ether (200 mL) and the organic phase washed with water (200 mL) and a saturated sodium chloride solution (200 mL). After removing the solvent *in vacuo*, methyl-12-hydroxystearic acid (28.2 g, 90 %) was obtained as a waxy, slightly yellow solid.

^{1}H-NMR (400 MHz, CDCl$_3$): δ [ppm] = 3.65 (3H, s, OCH$_3$), 3.56 (1H, m, HCOH), 2.28 (2H, t, J = 7.6 Hz, CH$_2$CO), 1.60 (2H, m, CH$_2$CH$_2$CO), 1.49–1.16 (27H, m, alkyl-CH$_2$), 0.86 (3H, m, CH$_3$).

5.3.5.3 General procedure polycondensation

Hydroxystearate (Me-10/9-HSA or Me-12-HSA) was charged in a three-necked flask equipped with a vacuum-tight overhead stirrer and a vacuum receiver adapter and placed in an oil-bath (see Figure A40). Titanium tetra *n*-butoxide (1.0 mol %) was added as a catalyst and the mixture was heated under stirring (400 rpm) to 200 °C under dynamic vacuum. Samples of 0.4 mL were taken by the help of a syringe to monitor the reaction progress by ^{1}H-NMR and rheology measurements.

6 Summary and Outlook

In the use and production of polymeric compounds, criteria such as synthesis starting from biomolecules and degradability after reaching the end-of-life phase are becoming increasingly important. These issues are also of great interest for carbon fiber composites (CFRPs), for example to reduce the carbon footprint of the aerospace industry already during the construction of the aircraft. In this work, the components of CFRPs (carbon fiber and epoxy resin matrices) as well as the required chemical feedstocks are optimized with respect to "greener" syntheses and bio-based nature.

For the precursor polyacrylonitrile, which is commonly used for the production of carbon fibers, different approaches *via* a polymer analog synthesis route are pursued. Polymer-analogous reactions allow the substitution of petroleum-based acrylonitrile as the starting material for carbon fiber synthesis to alternative monomers derived from biogenic sources. For the polymer of methyl acrylate, the proof of principle was already provided in previous work in a two-step, polymer-analogous route *via* the intermediate stage polyacrylamide. Various approaches exist for synthesizing acrylic monomers from biogenic glycerol. In addition to methyl acrylate, the monomers *N,N'*-dibenzylacrylamide, *N,N'*-di(*tert*-butoxycarbonyl)-acrylamide and *N,O*-bis(trimethylsilyl)-acrylamide are identified as potential candidates for polymer analog conversion toward polyacrylonitrile. All monomers are first tested for their polymerizability with various rare earth-based organometallic catalyst systems, and defined polymers with controllable molecular masses and narrow molecular mass distributions were achievable especially with the benzyl-protected acrylamide derivative with yttrium and lutetium-based catalysts. In contrast, polymerization of the *tert*-butoxycarbonyl protected acrylamide was difficult to control because side reactions

can be entered at the carbonyl functionalities of the side chain. The polymerization reactions take long time to achieve high conversions and yield comparatively low molecular weights. The same applies to the molecule equipped with trimethylsilyl groups. Here, the catalyst is presumably deactivated by silylation, which prevents catalytic polymerization. Subsequently, in the case of polymethyl acrylate, the reactions to polyacrylonitrile are scaled up to the multigram scale. Since dehydration could not be successfully performed on higher molecular weight PAA – presumably due to solubility problems – a screening of different polar and aprotic solvent mixtures could be a viable addition to the experiments performed. Spinning, stabilization, and carbonization trials conducted by Fraunhofer IAP demonstrated the potential of PAM-PAN as a precursor for carbon fiber production. It could be shown that the polymer can be transferred from a spinning solution into fibers. However, the low molecular weight of the polymer severely limits the process capability since stretching of the sample is not possible, and the fibers thus do not have good orientation along the fiber direction and show inhomogeneities. Nevertheless, the PAM-PAN fibers could be partially carbonized continuously and successfully converted into CF. The problems associated with the low molecular weight could be solved by optimizing the PAM described earlier. In addition, Fraunhofer IAP sees room for optimization in the spinning process, which could also result in more homogeneous fibers. Different PAN samples would be necessary for this.

For the other polymers mentioned, the cleavage of the benzyl, *tert*-butoxycarbonyl, and trimethylsilyl protecting groups is investigated. The cleavage reactions were unsuccessful, only the polymer analog deprotection of the trimethylsilyl groups could be reproduced according to the literature and the polyacrylamide thus obtained could be successfully converted to polyacrylonitrile. Further experiments on the deprotection of PBn$_2$AA should be conducted since the controlled polymerization of the monomer makes the polymer still an interesting candidate for the PAM toward PAN.

Unsaturated triglycerides or the free fatty acids were identified as the starting material for biobased epoxy resins. Epoxidation of these could be accomplished by the *Prilezhaev* method using peracids as well as potassium peroxomonosulfate

(Oxone®). Vegetable oils are known to have disadvantages when used as epoxy resins due to their aliphatic nature and the absence of rigid aromatic structures. These structural conditions lead to comparatively weak mechanical and thermal properties after reaction with a curing agent. In this work, however, it was shown that tannic acid is an outstanding curing agent for epoxidized linseed oil. With a flexural modulus of 2986 MPa, it shows comparable flexibility to that of commercial petroleum-based epoxy resins. In addition, a high T_g of 147 °C and a flexural strength of 72 MPa were observed. The high stiffness and aromatic structures in TA contribute to the high mechanical properties of the cured TA/ELO thermoset. Due to the fact that the particle size of TA was significantly reduced by a two-step painting process, a homogeneous dispersion of the curing agent in ELO is possible, resulting in a fully bio-based thermoset with high material properties. Due to steric hindrance and the lower reactivity of the phenolic groups of tannic acid compared to, for example, amine hardeners, an excess of tannic acid is necessary and a curing procedure of 16 h at 120 °C + 3 h at 140 °C is required to crosslink the material and achieve stiffness. Too high excess of tannic acid has a negative effect on the thermal stability of the cured thermoset, but the decomposition temperature is high enough for most applications. In the future, it is thus conceivable that the system represents a serious alternative to petroleum- and bisphenol-A-based thermoset. Here, future work could address further optimization of the curing process and adapt it more for industrial processes. In order to make the hardening process shorter and thus more energy-efficient, the use of catalysts is conceivable and should be part of further experiments. Also testing of the thermoset in combination with carbon or bio-based fibers would round off the work and pave the way towards bio-based composite materials.

Another approach toward high-performance, greener epoxy resins was pursued in the synthesis of a novel, highly functionalized molecule. In a four-step reaction sequence starting with the esterification of sorbic acid with allyl alcohol and proceding with a Diels-Alder reaction forming a six-membered ring provides bioavailable starting material and high atom efficiency. After the introduction of further allyl functionalities and epoxidizing the double bonds, EGCHC could be prepared. Due to the high number of four epoxy groups, the resin shows high tensile modulus and tensile strength

values after curing with standard amine curing agents. It could be demonstrated that the EGCHC samples can compete with the mechanical properties of DGEBA-based systems. When cured with IPD, better mechanical properties and higher T_gs up to126 °C were observed compared to Jeffamine T-403 (55 °C). In addition, the ester bonds allow solvolytic decomposition in NaOH at mild conditions. This is interesting for the application in composite materials, since the fibers used can be recovered after reaching end-of-life. For this purpose, it would be interesting to produce EGCHC composite materials with fibers and conduct studies on their performance. Part of the further work here could also be experiments on the recovery of the fibers after solvolysis. Because of the fast setting of EGCHC experiments on the adhesion on different substrate could reveal an possible application as two component adhesive.

The last part of the work dealt with the synthesis of fatty acid-based lubricants, so-called estolides. Here, the monomer methyl-10-hydroxystearate was first synthesized and purified starting from oleic acid. In the subsequent polycondensation reactions, the bifunctional monomers were converted to oligomeric compounds in the presence of a titanium catalyst. In particular, the relationships between conversion, viscosity, and time were the focus of the work in order to achieve the targeted viscosity of about 700 cSt. Finally, after investigations on the purification of the estolide samples, the thermal properties of the obtained lubricants were analyzed. A melting point of –14 °C and a temperature stability up to 238 °C could be determined. Regarding estolides, end-group functionalization with commonly used alcohols is an interesting starting point for investigations to further fine-tune thermal properties of bio-based lubricants.

Literature

[1]   T. A. Ewing, N. Nouse, M. van Lint, J. van Haveren, J. Hugenholtz, D. S. van Es, *Green Chemistry* **2022**, *24*, 6373–6405.

[2]   Anders Södergård, Mikael Stolt in *Poly(Lactic Acid)*, John Wiley & Sons, Ltd, **2010**, pp. 27–41.

[3]   K. J. Jem, B. Tan, *Advanced Industrial and Engineering Polymer Research* **2020**, *3*, 60–70.

[4]   B. L. C. Cunha, J. O. Bahú, L. F. Xavier, S. Crivellin, S. D. A. de Souza, L. Lodi, A. L. Jardini, R. M. Filho, Schiavon, Maria I. R. B., V. O. C. Concha, P. Severino, E. B. Souto, *Bioengineering (Basel Switzerland)* **2022**, *9*, DOI `10.3390/bioengineering9040164`.

[5]   S. Mecking, *Philosophical transactions. Series A Mathematical physical and engineering sciences* **2020**, *378*, 20190266.

[6]   J. Phillips, Visualising a year's production of palm oil, (Ed.: China Dialogue), **2020**, `https://chinadialogue.net/en/food/visualising-a-years-production-of-palm-oil/` (visited on 03/28/2023).

[7]   M. A. Masri, D. Garbe, N. Mehlmer, T. B. Brück, *Energy & Environmental Science* **2019**, *12*, 2717–2732.

[8]   J. Lorenzen, N. Igl, M. Tippelt, A. Stege, F. Qoura, U. Sohling, T. Brück, *Bioprocess and Biosystems Engineering* **2017**, *40*, 911–918.

[9]   G. A. Reinhardt, D. Paulsch, H. Keller, *Chemie Ingenieur Technik* **2013**, *85*, 313–317.

[10] M. Minus, S. Kumar, *JOM* **2005**, *57*, 52–58.

[11] L. H. Peebles, *Carbon Fibers: Formation, Structure, and Properties*, First edition, CRC Press, Boca Raton, FL, **1994**.

[12] M. Sauer, D. Schüppel, Market Report 2021: The Global Market for Carbon Fibers and Carbon Composites, Berlin, **2022**.

[13] H. T. Hwang, A. Varma, *Current Opinion in Chemical Engineering* **2014**, *5*, 42–48.

[14] R. Saidur, M. R. Islam, N. A. Rahim, K. H. Solangi, *Renewable and Sustainable Energy Reviews* **2010**, *14*, 1744–1762.

[15] J. Zhang, V. S. Chevali, H. Wang, C.-H. Wang, *Composites Part B: Engineering* **2020**, *193*, 108053.

[16] X. Huang, *Materials* **2009**, *2*, 2369–2403.

[17] S.-J. Park, *Carbon Fibers*, *Vol. 210*, Springer Singapore, Singapore, **2018**.

[18] P. Morgan, *Carbon fibers and their composites*, Taylor & Francis, Boca Raton et al., **2005**.

[19] Q.-Y. Wu, X.-N. Chen, L.-S. Wan, Z.-K. Xu, *The journal of physical chemistry. B* **2012**, *116*, 8321–8330.

[20] D. D. L. Chung, *Carbon fiber composites*, Butterworth-Heinemann, Boston, **1994**.

[21] H. Khayyam, R. N. Jazar, S. Nunna, G. Golkarnarenji, K. Badii, S. M. Fakhrhoseini, S. Kumar, M. Naebe, *Progress in Materials Science* **2020**, *107*, 100575.

[22] E. Frank, F. Hermanutz, M. R. Buchmeiser, *Macromolecular Materials and Engineering* **2012**, *297*, 493–501.

[23] R. C. Houtz, *Textile Research Journal* **1950**, *20*, 786–801.

[24] W. J. Burlant, J. L. Parsons, *Journal of Polymer Science* **1956**, *22*, 249–256.

[25] E. M. La Combe, *Journal of Polymer Science* **1957**, *24*, 152–154.

[26] N. Grassie, J. N. Hay, I. C. McNeill, *Journal of Polymer Science* **1958**, *31*, 205–206.

[27] J. Schurz, *Journal of Polymer Science* **1958**, *28*, 438–439.

[28] A. E. Standage, R. D. Matkowsky, *European Polymer Journal* **1971**, *7*, 775–783.

[29] A. Konkin, W. Watt in *Strong Fibers*, (Eds.: W. Watt, B. Perov), Elsevier Science Publishers, Amsterdam, The Netherlands, **1985**, pp. 241–273, 275–325, 327–387.

[30] T. Takahagi, I. Shimada, M. Fukuhara, K. Morita, A. Ishitani, *Journal of Polymer Science Part A: Polymer Chemistry* **1986**, *24*, 3101–3107.

[31] E. Fitzer, D. J. Müller, *Carbon* **1975**, *13*, 63–69.

[32] E. Fitzer, W. Frohs, M. Heine, *Carbon* **1986**, *24*, 387–395.

[33] A. Ju, S. Guang, H. Xu, *Carbon* **2013**, *54*, 323–335.

[34] G. T. Sivy, M. M. Coleman, *Carbon* **1981**, *19*, 137–139.

[35] N. Yusof, A. F. Ismail, *Journal of Analytical and Applied Pyrolysis* **2012**, *93*, 1–13.

[36] *Ceramic matrix composites: Fiber reinforced ceramics and their applications*, (Ed.: W. Krenkel), Wiley-VCH, Weinheim, **2008**.

[37] E. Fitzer, K.-H. Kochling, H. P. Boehm, H. Marsh, *Pure and Applied Chemistry* **1995**, *67*, 473–506.

[38] Type of Carbon Fiber Products and their Special Features, **2022**, `https://www.carbonfiber.gr.jp/english/material/type.html` (visited on 01/09/2023).

[39] Y. Xu, Y. Liu, S. Chen, Y. Ni, *BioResources* **2020**, *15*, 7234–7259.

[40] American Chemical Society National Historic Chemical Landmarks, Sohio Acrylonitrile Process, **2007**, `http://www.acs.org/content/acs/en/education/whatischemistry/landmarks/acrylonitrile.html` (visited on 01/23/2023).

[41] E. M. Karp, T. R. Eaton, V. Sànchez I Nogué, V. Vorotnikov, M. J. Biddy, E. C. D. Tan, D. G. Brandner, R. M. Cywar, R. Liu, L. P. Manker, W. E. Michener, M. Gilhespy, Z. Skoufa, M. J. Watson, O. S. Fruchey, D. R. Vardon, R. T. Gill, A. D. Bratis, G. T. Beckham, *Science (New York N.Y.)* **2017**, *358*, 1307–1310.

[42] J. R. Hopper, C. L. Yaws, T. C. Ho, M. Vichailak, *Waste Management* **1993**, *13*, 3–14.

[43] J.-L. Dubois, US20100048850A1, **2010**.

[44] M. O. Guerrero-Pérez, M. A. Bañares, *ChemSusChem* **2008**, *1*, 511–513.

[45] C. Liebig, S. Paul, B. Katryniok, C. Guillon, J.-L. Couturier, J.-L. Dubois, F. Dumeignil, W. F. Hoelderich, *Applied Catalysis B: Environmental* **2013**, *132-133*, 170–182.

[46] American Chemical Society National Historic Chemical Landmarks, High Performance Carbon Fibers, **2003**, `https : / / www . acs . org / education / whatischemistry/landmarks/carbonfibers.html` (visited on 01/15/2023).

[47] A. Milbrandt, S. Booth, Carbon Fiber from Biomass, NREL/TP-6A50-66386, Clean Energy Manufacturing Analysis Center, Golden, Colorado, USA, **2016**.

[48] R. K. Grasselli, F. Trifirò, *Topics in Catalysis* **2016**, *59*, 1651–1658.

[49] J. Le Nôtre, E. L. Scott, M. C. R. Franssen, J. P. M. Sanders, *Green Chemistry* **2011**, *13*, 807.

[50] *Handbook of heterogeneous catalysis*, 2nd ed., (Eds.: G. Ertl, H. Knözinger, F. Schüth, J. Weitkamp), Wiley-VCH, Weinheim, **2008**.

[51] J. L. Callahan, R. K. Grasselli, E. C. Milberger, H. A. Strecker, *Product R&D* **1970**, *9*, 134–142.

[52] J. Akhavan, *The chemistry of explosives*, 2nd ed., Royal Society of Chemistry, Cambridge, **2004**.

[53] P. Theato, H.-.-A. Klok, *Functional Polymers by Post–Polymerization Modification*, Wiley, **2012**.

[54] A. G. Day, C. Goodyear, *Gum-elastic and its varieties : with a detailed account of its applications and uses, and of the discovery of vulcanization*, Published for the author, New Haven, Conn., **1853**.

[55] A. Y. CORAN in *Science and Technology of Rubber*, (Eds.: J. E. Mark, B. Erman, F. R. Eirich), Elsevier, **1994**, pp. 339–385.

[56] G. Camino, M. Guaita, A. Priola, *Polymer Degradation and Stability* **1985**, *12*, 241–247.

[57] W. S. Lyoo, H. W. Lee, *Colloid and Polymer Science* **2002**, *280*, 835–840.

[58] A. P. Kharitonov, *Progress in Organic Coatings* **2008**, *61*, 192–204.

[59]   J. M. Breitsameter, Master Thesis, Technische Universität München, München, **2019**.

[60]   W. Schmidt, Master Thesis, Technische Universität München, München, **2018**.

[61]   X. Li, Y. Zhang, *ACS Catalysis* **2016**, *6*, 143–150.

[62]   C. Guillon, C. Liebig, S. Paul, A.-S. Mamede, W. F. Hölderich, F. Dumeignil, B. Katryniok, *Green Chemistry* **2013**, *15*, 3015.

[63]   J. K. Thottathil, J. L. Moniot, R. H. Mueller, M. K. Y. Wong, T. P. Kissick, *The Journal of Organic Chemistry* **1986**, *51*, 3140–3143.

[64]   A. Abiko, J. C. Roberts, T. Takemasa, S. Masamune, *Tetrahedron Letters* **1986**, *27*, 4537–4540.

[65]   S. Goldschmidt, P. Askenasy, H. Grimm, *Berichte der deutschen chemischen Gesellschaft (A and B Series)* **1934**, *67*, 202–213.

[66]   S. Mannam, G. Sekar, *Tetrahedron Letters* **2008**, *49*, 2457–2460.

[67]   G. Qian, R. Zhao, G. Lu, Y. Qi, J. Suo, *Synthetic Communications* **2004**, *34*, 1753–1758.

[68]   D. Kim, W. Lee, H. Hyon-Bae, J. Soyi, Y. Choi, KR20170001088 (A), **2017**.

[69]   R. L. Oliveira, P. K. Kiyohara, L. M. Rossi, *Green Chemistry* **2009**, *11*, 1366.

[70]   J. Kankaanpää, E. Elovaara, K. Hemminki, H. Vainio, *Toxicology Letters* **1979**, *4*, 93–96.

[71]   Y.-m. Liang, Q.-h. Xu, X.-l. Wu, Y.-x. Ma, *Journal of Chemical Research* **2004**, *2004*, 226–227.

[72]   K. Lowpetch, D. W. Young, *Organic & biomolecular chemistry* **2005**, *3*, 3348–3356.

[73]   Y. Wang, Z. Wu, H. Yu, S. Han, Y. Wei, *Green Chemistry* **2020**, *22*, 3150–3154.

[74]   W. J. Brittain, *Rubber Chemistry and Technology* **1992**, *65*, 580–600.

[75]   Y.-C. Wang, H. Morawetz, *Journal of the American Chemical Society* **1976**, *98*, 3611–3615.

[76]   A. S. Norgren, S. Zhang, P. I. Arvidsson, *Organic Letters* **2006**, *8*, 4533–4536.

[77] S. Hoque, N. N. Dass, K. G. Bhattacharyya, N. S. Sarma, *Molecular Crystals and Liquid Crystals* **2014**, *592*, 149–162.

[78] M. Movsisyan, T. S. A. Heugebaert, B. I. Roman, R. Dams, R. van Campenhout, M. Conradi, C. V. Stevens, *Chemistry (Weinheim an der Bergstrasse Germany)* **2018**, *24*, 11779–11784.

[79] T. Yamate, H. Suzuki, T. Fujiwara, T. Yamaguchi, M. Akazome, *Advanced Materials Letters* **2018**, *9*, 1–.

[80] T. Yamate, WO2018070079, **2018**.

[81] M. B. Larsen, S. E. Herzog, H. C. Quilter, M. A. Hillmyer, *ACS Macro Letters* **2018**, *7*, 122–126.

[82] L. Birkofer, A. Ritter, W. Gießler, *Angewandte Chemie* **1963**, *75*, 93–94.

[83] A. Dasgupta, S. Sivaram, *Macromolecules* **1994**, *27*, 1665–1667.

[84] O. W. Webster, US4681918 (A), **1987**.

[85] F. P. Boettcher, I. B. Dicker, R. C. Ebersole, W. R. Hertler, US4940760 (A), **1990**.

[86] O. W. Webster, W. R. Hertler, D. Y. Sogah, W. B. Farnham, T. V. RajanBabu, *Journal of the American Chemical Society* **1983**, *105*, 5706–5708.

[87] O. W. Webster, *Journal of Polymer Science Part A: Polymer Chemistry* **2000**, *38*, 2855–2860.

[88] R. P. Quirk, J. Ren, *Macromolecules* **1992**, *25*, 6612–6620.

[89] A. H. E. Mueller, *Macromolecules* **1994**, *27*, 1685–1690.

[90] Y. Chen, T. Kakuchi, *Chemical record (New York N.Y.)* **2016**, *16*, 2161–2183.

[91] K. Takada, K. Fuchise, Y. Chen, T. Satoh, T. Kakuchi, *Journal of Polymer Science Part A: Polymer Chemistry* **2012**, *50*, 3560–3566.

[92] K. Takada, T. Ito, K. Kitano, S. Tsuchida, Y. Takagi, Y. Chen, T. Satoh, T. Kakuchi, *Macromolecules* **2015**, *48*, 511–519.

[93] K. Fuchise, R. Sakai, T. Satoh, S.-i. Sato, A. Narumi, S. Kawaguchi, T. Kakuchi, *Macromolecules* **2010**, *43*, 5589–5594.

[94] D. Y. Sogah, W. R. Hertler, O. W. Webster, G. M. Cohen, *Macromolecules* **1987**, *20*, 1473–1488.

[95] H. Yasuda, H. Yamamoto, K. Yokota, S. Miyake, A. Nakamura, *Journal of the American Chemical Society* **1992**, *114*, 4908–4910.

[96] H. Yasuda, E. Ihara, *Macromolecular Chemistry and Physics* **1995**, 2417–2441.

[97] H. Yasuda, *Journal of Organometallic Chemistry* **2002**, *647*, 128–138.

[98] T.-Q. Xu, G.-W. Yang, X.-B. Lu, *ACS Catalysis* **2016**, *6*, 4907–4913.

[99] H. Kaneko, H. Nagae, H. Tsurugi, K. Mashima, *Journal of the American Chemical Society* **2011**, *133*, 19626–19629.

[100] C.-X. Cai, L. Toupet, C. W. Lehmann, J.-F. Carpentier, *Journal of Organometallic Chemistry* **2003**, *683*, 131–136.

[101] P. T. Altenbuchner, B. S. Soller, S. Kissling, T. Bachmann, A. Kronast, S. I. Vagin, B. Rieger, *Macromolecules* **2014**, *47*, 7742–7749.

[102] F. Adams, M. R. Machat, P. T. Altenbuchner, J. Ehrmaier, A. Pöthig, T. N. V. Karsili, B. Rieger, *Inorganic chemistry* **2017**, *56*, 9754–9764.

[103] E. Ihara, M. MORIMOTO, H. Yasuda, *Proceedings of the Japan Academy Series B* **1995**, *71*, 126–131.

[104] E. Y.-X. Chen, *Chemical reviews* **2009**, *109*, 5157–5214.

[105] J. B. Brenneman, J. D. Ginn, C. R. Sarko, J. Westbrook, Z. Zhang, M. Yu, T. D. Hopkins, M. D. Lowe, WO2016014463 (A1), **2016**.

[106] P. G. M. Wuts, T. W. Greene, *Greene's protective groups in organic synthesis*, 4. ed., Wiley, Hoboken, **2007**.

[107] M. D. Alexander, J. J. Mcdonald, Y. Ni, D. Niu, R. C. Petter, L. Qiao, J. Singh, T. Wang, Z. Zhu, WO2014149164 (A1), **2014**.

[108] C. Cheng, J. Sun, L. Xing, J. Xu, X. Wang, Y. Hu, *The Journal of Organic Chemistry* **2009**, *74*, 5671–5674.

[109] S. A. Yakukhnov, V. P. Ananikov, *Advanced Synthesis & Catalysis* **2019**, *361*, 4781–4789.

[110] Y. Yamamoto, E. Shimizu, K. Ban, Y. Wada, T. Mizusaki, M. Yoshimura, Y. Takagi, Y. Sawama, H. Sajiki, *ACS omega* **2020**, *5*, 2699–2709.

[111] A. David, A. M. Vannice, *Journal of Catalysis* **2006**, *237*, 349–358.

[112] K. Dong, Y. Chen, Y. Zhang, C. Sun, S. Pang, *Journal of Energetic Materials* **2017**, 1–9.

[113] H. T. Hwang, J. R. Martinelli, R. Gounder, A. Varma, *Chemical Engineering Journal* **2016**, *288*, 758–769.

[114] M. Studer, H.-U. Blaser, *Journal of Molecular Catalysis A: Chemical* **1996**, *112*, 437–445.

[115] K. Okano, K.-i. Okuyama, T. Fukuyama, H. Tokuyama, *Synlett* **2008**, *2008*, 1977–1980.

[116] E. Paliakov, L. Strekowski, *Tetrahedron Letters* **2004**, *45*, 4093–4095.

[117] T. WATANABE, Nishiuran, Michiko, Takahasi, Hiroyuki, T. USUI, I. KAMIYAMA, N. MOCHIZUKI, K. NORITAKE, Y. YOKOYAMA, Y. MURAKAMI, *Chemical and Pharmaceutical Bulletin* **1991**, *39*, 1152–1156.

[118] P. Kowalski, Z. Majak, T. Kowalska, *Chemistry of Heterocyclic Compounds* **1998**, *34*, 740–741.

[119] C.-Y. Chern, Y.-P. Huang, W. M. Kan, *Tetrahedron Letters* **2003**, *44*, 1039–1041.

[120] S. Richard Baker, A. F. Parsons, M. Wilson, *Tetrahedron Letters* **1998**, *39*, 331–332.

[121] F. X. Webster, J. G. Millar, R. M. Silverstein, *Tetrahedron Letters* **1986**, *27*, 4941–4944.

[122] R. M. Williams, B. H. Lee, M. M. Miller, O. P. Anderson, *Journal of the American Chemical Society* **1989**, *111*, 1073–1081.

[123] A. Pingoud, C. Urbanke, *Arbeitsmethoden der Biochemie: Enthält 50 Tabellen*, de Gruyter, Berlin, **1997**.

[124] T. W. Greene, P. G. M. Wuts, *Protective Groups in Organic Synthesis*, John Wiley & Sons, Inc, New York, USA, **1999**.

[125] L. A. Carpino, *Accounts of Chemical Research* **1973**, *6*, 191–198.

[126] S. Calimsiz, M. A. Lipton, *The Journal of Organic Chemistry* **2005**, *70*, 6218–6221.

[127] J. A. Stafford, M. F. Brackeen, D. S. Karanewsky, N. L. Valvano, *Tetrahedron Letters* **1993**, *34*, 7873–7876.

[128] M. Inoue, H. Sakazaki, H. Furuyama, M. Hirama, *Angewandte Chemie (International ed. in English)* **2003**, *42*, 2654–2657.

[129] Z.-Y. Wei, E. E. Knaus, *Tetrahedron Letters* **1994**, *35*, 847–848.

[130] G. Casiraghi, F. Ulgheri, P. Spanu, G. Rassu, L. Pinna, G. G. Fava, M. B. Ferrari, G. Pelosi, *Journal of the Chemical Society Perkin Transactions 1* **1993**, 2991.

[131] J. N. Hernández, M. A. Ramírez, V. S. Martín, *The Journal of Organic Chemistry* **2003**, *68*, 743–746.

[132] J. G. Siro, J. Martín, J. L. García-Navío, M. J. Remuiñan, J. J. Vaquero, *Synlett* **1998**, *1998*, 147–148.

[133] S. R. Dandepally, A. L. Williams, *Tetrahedron Letters* **2009**, *50*, 1071–1074.

[134] E. J. Corey, B. B. Snider, *Journal of the American Chemical Society* **1972**, *94*, 2549–2550.

[135] J. A. Marshall, M. P. Bourbeau, *The Journal of Organic Chemistry* **2002**, *67*, 2751–2754.

[136] D. T. Hurst, A. G. McInnes, *Canadian Journal of Chemistry* **1965**, *43*, 2004–2011.

[137] G. L. Bundy, D. C. Peterson, *Tetrahedron Letters* **1978**, *19*, 41–44.

[138] S. Hanada, Y. Motoyama, H. Nagashima, *European Journal of Organic Chemistry* **2008**, 4097–4100.

[139] N. Prileschajew, *Berichte der deutschen chemischen Gesellschaft* **1909**, *42*, 4811–4815.

[140] A. R. Katritzky, *Handbook of Heterocyclic Chemistry*, 3rd ed., Elsevier, London, **2010**.

[141] M. Dornbusch in *Epoxy Resins*, (Eds.: M. Dornbusch, U. Christ, R. Rasing), European Coatings LIBRARY, Vincentz Network, Hannover, **2016**, pp. 21–100.

[142] N. B. Chapman, N. S. Isaacs, R. E. Parker, *Journal of the Chemical Society (Resumed)* **1959**, 1925.

[143] R. E. Parker, N. S. Isaacs, *Chemical Reviews* **1959**, *59*, 737–799.

[144] K. Sung, *Canadian Journal of Chemistry* **2000**, *78*, 562–567.

[145] H. K. Sheikh, T. Arshad, M. Merajoddin, Z. S. Mohammad, R. Usman, M. M. Hasan, *pakistan journal of pharmaceutical sciences* **2020**, *33*, 2017–2021.

[146] Propylene oxide: from a gap of 467,000 tons to self-sufficiency is just around the corner, **2021**, `https://www.echemi.com/cms/257860.html` (visited on 01/23/2023).

[147] T. A. Nijhuis, M. Makkee, J. A. Moulijn, B. M. Weckhuysen, *Industrial & Engineering Chemistry Research* **2006**, *45*, 3447–3459.

[148] L. Krähling, J. Krey, G. Jakobson, J. Grolig, L. Miksche in *Ullmann's encyclopedia of industrial chemistry*, *Vol. 29*, Wiley-VCH, Weinheim and Wiley online library, **2010**, p. 466.

[149] M. R. Monteiro, C. L. Kugelmeier, R. S. Pinheiro, M. O. Batalha, A. Da Silva César, *Renewable and Sustainable Energy Reviews* **2018**, *88*, 109–122.

[150] B. M. Bell, J. R. Briggs, R. M. Campbell, S. M. Chambers, P. D. Gaarenstroom, J. G. Hippler, B. D. Hook, K. Kearns, J. M. Kenney, W. J. Kruper, D. J. Schreck, C. N. Theriault, C. P. Wolfe, *CLEAN - Soil Air Water* **2008**, *36*, 657–661.

[151] Y. Meng, F. Taddeo, A. F. Aguilera, X. Cai, V. Russo, P. Tolvanen, S. Leveneur, *Catalysts* **2021**, *11*, 765.

[152] *Name reactions for functional group transformations*, (Eds.: J. J. Li, E. J. Corey), Wiley-Interscience, Hoboken, N.J., **2007**.

[153] L. Charbonneau, X. Foster, S. Kaliaguine, *ACS Sustainable Chemistry & Engineering* **2018**, *6*, 12224–12231.

[154] L. Charbonneau, X. Foster, D. Zhao, S. Kaliaguine, *ACS Sustainable Chemistry & Engineering* **2018**, *6*, 5115–5121.

[155] S. E. Denmark, D. C. Forbes, D. S. Hays, J. S. DePue, R. G. Wilde, *The Journal of Organic Chemistry* **1995**, *60*, 1391–1407.

[156] H. M. Ferraz, R. M. Muzzi, T. de O. Vieira, H. Viertler, *Tetrahedron Letters* **2000**, *41*, 5021–5023.

[157] A. González-Benjumea, G. Marques, O. M. Herold-Majumdar, J. Kiebist, K. Scheibner, J. C. Del Río, A. T. Martínez, A. Gutiérrez, *Frontiers in bioengineering and biotechnology* **2020**, *8*, 605854.

[158] R. R. C. Monteiro, P. J. M. Lima, B. B. Pinheiro, T. M. Freire, L. M. U. Dutra, P. B. A. Fechine, L. R. B. Gonçalves, M. C. M. de Souza, J. C. S. Dos Santos, R. Fernandez-Lafuente, *International journal of molecular sciences* **2019**, *20*, DOI 10.3390/ijms20164018.

[159] A. S. Bajwa, S. Sathaye, V. M. Kulkarni, A. V. Patwardhan, *Asia-Pacific Journal of Chemical Engineering* **2016**, *11*, 314–322.

[160] T. Katsuki, K. B. Sharpless, *Journal of the American Chemical Society* **1980**, *102*, 5974–5976.

[161] W. Zhang, J. L. Loebach, S. R. Wilson, E. N. Jacobsen, *Journal of the American Chemical Society* **1990**, *112*, 2801–2803.

[162] R. Irie, K. Noda, Y. Ito, N. Matsumoto, T. Katsuki, *Tetrahedron: Asymmetry* **1991**, *2*, 481–494.

[163] T. Linker, *Angewandte Chemie International Edition* **1997**, *36*, 2060–2062.

[164] F.-L. Jin, X. Li, S.-J. Park, *Journal of Industrial and Engineering Chemistry* **2015**, *29*, 1–11.

[165] X. M. Chen, B. Ellis in *Chemistry and Technology of Epoxy Resins*, Springer, Dordrecht, **1993**, pp. 303–325.

[166] H. Jin, G. M. Miller, S. J. Pety, A. S. Griffin, D. S. Stradley, D. Roach, N. R. Sottos, S. R. White, *International Journal of Adhesion and Adhesives* **2013**, *44*, 157–165.

[167] C.-H. Park, S.-W. Lee, J.-W. Park, H.-J. Kim, *Reactive and Functional Polymers* **2013**, *73*, 641–646.

[168] X. Wang, W. Guo, L. Song, Y. Hu, *Composites Part B: Engineering* **2019**, *179*, 107487.

[169] H. Q. Pham, M. J. Marks in *Ullmann's encyclopedia of industrial chemistry*, Wiley-VCH, Weinheim and Wiley online library, **2010**.

[170] N. J. Jin, J. Yeon, I. Seung, K.-S. Yeon, *Construction and Building Materials* **2017**, *156*, 933–943.

[171] Sika Deutschland GmbH, Biresin CR80 Composite resin system, **2021**, `https://industry.sika.com/content/dam/dms/global-industry/m/Biresin-CR80-SikaBiresin-CH80-2-New.pdf` (visited on 01/17/2022).

[172] H. Sukanto, W. W. Raharjo, D. Ariawan, J. Triyono, M. Kaavesina, *Open Engineering* **2021**, *11*, 797–814.

[173] E. Bodnar, P. Taylor, *Pigment & Resin Technology* **1986**, *15*, 10–15.

[174] H. Yan, C. Lu, D. Jing, X. Hou, *Polymer Degradation and Stability* **2013**, *98*, 2571–2582.

[175] M. J. Yoo, S. H. Kim, S. D. Park, W. S. Lee, J.-W. Sun, J.-H. Choi, S. Nahm, *European Polymer Journal* **2010**, *46*, 1158–1162.

[176] J.-E. Ehlers, N. G. Rondan, L. K. Huynh, H. Pham, M. Marks, T. N. Truong, *Macromolecules* **2007**, *40*, 4370–4377.

[177] H. F. Mark, N. M. Bikales, C. G. Ovenberger, G. Menges in *Encyclopedia of polymer science and engineering*, (Ed.: H. F. Mark), A Wiley-Interscience publication, Wiley, New York, **1985**.

[178] M. Korey, G. P. Mendis, J. P. Youngblood, J. A. Howarter, *Journal of Polymer Science Part A: Polymer Chemistry* **2018**, *56*, 1468–1480.

[179] M. Qi, Y.-J. Xu, W.-H. Rao, X. Luo, L. Chen, Y.-Z. Wang, *RSC Advances* **2018**, *8*, 26948–26958.

[180] Y.-O. Kim, J. Cho, H. Yeo, B. W. Lee, B. J. Moon, Y.-M. Ha, Y. R. Jo, Y. C. Jung, *ACS Sustain. Chem. Eng. (ACS Sustainable Chemistry & Engineering)* **2019**, *7*, 3858–3865.

[181] M. Shibata, N. Teramoto, K. Makino, *J. Appl. Polym. Sci. (Journal of Applied Polymer Science)* **2011**, *120*, 273–278.

[182] N. Reinhardt, J. M. Breitsameter, K. Drechsler, B. Rieger, *Macromolecular Materials and Engineering* **2022**, *307*, 2200455.

[183] K. Dušek in *Epoxy resins and composites*, (Eds.: K. Dušek, K. Dušek), Advances in Polymer Science, Springer, Berlin, **1986**, pp. 1–59.

[184] E. A. Baroncini, S. Kumar Yadav, G. R. Palmese, J. F. Stanzione, *J. Appl. Polym. Sci. (Journal of Applied Polymer Science)* **2016**, *133*, 44103.

[185] *Advances in Molecular Toxicology*, (Eds.: J. C. Fishbein, J. M. Heilman), Elsevier, **2015**.

[186] K. Hąc-Wydro, K. Połeć, M. Broniatowski, *J. Mol. Liq. (Journal of Molecular Liquids)* **2019**, *289*, 111136.

[187] K.-A. Hwang, K.-C. Choi in *Advances in Molecular Toxicology*, *Vol. 9*, (Eds.: J. C. Fishbein, J. M. Heilman), Elsevier, **2015**, pp. 1–33.

[188] M. R. Loos, L. A. F. Coelho, S. H. Pezzin, S. C. Amico, *Polímeros* **2008**, *18*, 76–80.

[189] R. A. Nowak, F. Koohestani, J. Bi, P. Mehrotra, F. S. Mesquita, F. Masoud, S. A. Machado, *Comprehensive Toxicology (Second Edition)* **2010**, 499–522.

[190] M. Fache, B. Boutevin, S. Caillol, *Green Chemistry* **2016**, *18*, 712–725.

[191] J. Ding, O. u. Rahman, W. Peng, H. Dou, H. Yu, *Applied Surface Science* **2018**, *427*, 981–991.

[192] D. Santiago, D. Guzmán, X. Ramis, F. Ferrando, À. Serra, *Polymers* **2019**, *12*, 44.

[193] J. Xin, M. Li, R. Li, M. P. Wolcott, J. Zhang, *ACS Sustainable Chemistry & Engineering* **2016**, *4*, 2754–2761.

[194] J. Xin, P. Zhang, K. Huang, J. Zhang, *RSC Advances* **2014**, *4*, 8525.

[195]   T. Koike, *Polymer Engineering & Science* **2012**, *52*, 701–717.

[196]   D. Fourcade, B. S. Ritter, P. Walter, R. Schönfeld, R. Mülhaupt, *Green Chemistry* **2013**, *15*, 910.

[197]   Z. Rapi, B. Szolnoki, P. Bakó, P. Niedermann, A. Toldy, B. Bodzay, G. Keglevich, G. Marosi, *European Polymer Journal* **2015**, *67*, 375–382.

[198]   P. Niedermann, G. Szebenyi, A. Toldy, *Express Polymer Letters* **2015**, *9*, 85–94.

[199]   J. Łukaszczyk, B. Janicki, M. Kaczmarek, *European Polymer Journal* **2011**, *47*, 1601–1606.

[200]   M. Chrysanthos, J. Galy, J.-P. Pascault, *Polymer* **2011**, *52*, 3611–3620.

[201]   G. M. Lari, G. Pastore, C. Mondelli, J. Pérez-Ramírez, *Green Chemistry* **2018**, *20*, 148–159.

[202]   S. M. Danov, O. A. Kazantsev, A. L. Esipovich, A. S. Belousov, A. E. Rogozhin, E. A. Kanakov, *Catalysis Science & Technology* **2017**, *7*, 3659–3675.

[203]   N. W. Manthey, F. Cardona, G. Francucci, T. Aravinthan, *J. Compos. Mater. (Journal of Composite Materials)* **2014**, *48*, 1611–1622.

[204]   R. Mustapha, A. R. Rahmat, R. Abdul Majid, S. N. H. Mustapha, *Polym. -Plast. Technol. Mater. (Polymer-Plastics Technology and Materials)* **2019**, *58*, 1311–1326.

[205]   A. Campanella, M. A. Baltanás, M. C. Capel-Sánchez, J. M. Campos-Martín, J. L. G. Fierro, *Green Chem* **2004**, *6*, 330–334.

[206]   S. G. Tan, W. S. Chow, *J Am. Oil Chem. Soc. (Journal of the American Oil Chemists' Society)* **2011**, *88*, 915–923.

[207]   T. S. Omonov, J. M. Curtis, *J. Appl. Polym. Sci. (Journal of Applied Polymer Science)* **2014**, *131*, n/a–n/a.

[208]   N. R. Paluvai, S. Mohanty, S. K. Nayak, *Polym. Plast. Technol. Eng. (Polymer-Plastics Technology and Engineering)* **2014**, *53*, 1723–1758.

[209]   M. D. Samper, R. Petrucci, L. Sánchez-Nacher, R. Balart, J. M. Kenny, *Compos. B. Eng. (Composites Part B: Engineering)* **2015**, *71*, 203–209.

[210] N. Boquillon, C. Fringant, *Polymer* **2000**, *41*, 8603–8613.

[211] J.-M. Pin, N. Sbirrazzuoli, A. Mija, *ChemSusChem* **2015**, *8*, 1232–1243.

[212] A. Todorovic, K. Resch–Fauster, A. R. Mahendran, G. Oreski, W. Kern, *J. Appl. Polym. Sci. (Journal of Applied Polymer Science)* **2021**, *138*, 50239.

[213] S.-G. Hong, C.-S. Wu, *Thermochim. Acta (Thermochimica Acta)* **1998**, *316*, 167–175.

[214] O. Vryonis, T. Andritsch, A. S. Vaughan, P. L. Lewin, *IEEE Conference on Electrical Insulation and Dielectric Phenomenon (CEIDP)* **2017**, 509–512.

[215] K. Qiu, R. Tannenbaum, K. I. Jacob, *Polym. Eng. Sci. (Polymer Engineering & Science)* **2021**, *61*, 1281–1294.

[216] M. Shibata, K. Nakai, *Journal of Polymer Science Part B: Polymer Physics* **2010**, *48*, 425–433.

[217] Y. Endo, T. Takeyama, S. Yanagisawa, US 9428606B2.

[218] T. A. Isbell, S. C. Cermak, *Journal of the American Oil Chemists' Society* **2002**, *79*, 1227–1233.

[219] T. Romsdahl, A. Shirani, R. E. Minto, C. Zhang, E. B. Cahoon, K. D. Chapman, D. Berman, *Scientific Reports* **2019**, *9*, 11711.

[220] Y. Chen, G. Biresaw, S. C. Cermak, T. A. Isbell, H. L. Ngo, L. Chen, A. L. Durham, *Journal of the American Oil Chemists' Society* **2020**, *97*, 231–241.

[221] S. S. Gupta, T. P. Hilditch, J. P. Riley, *Journal of the Science of Food and Agriculture* **1951**, *2*, 245–251.

[222] A. K. Maskaev, N. K. Man'kovskaya, I. V. Lend'el, V. T. Fedorovskii, E. I. Simurova, V. N. Terent'eva, *Chemistry and Technology of Fuels and Oils* **1971**, *7*, 109–112.

[223] S. Prem, C. P. O. Helmer, N. Dimos, S. Himpich, T. Brück, D. Garbe, B. Loll, *Microbial Cell Factories* **2022**, *21*, 58.

[224] J. P. Wiegner, V. Voerckel, D. Runkel, R. Eckert, US2012316316 (A1), **2012**.

[225] W. H. Carothers, *Transactions of the Faraday Society* **1936**, *32*, 39.

[226] S. C. Cermak, T. A. Isbell, *Industrial Crops and Products* **2002**, *16*, 119–127.

[227] A. Buchter, H. Peter, *Giornale italiano di medicina del lavoro* **1984**, *6*, 83–86.

[228] J. M. Birmingham, G. Wilkinson, *Journal of the American Chemical Society* **1956**, *78*, 42–44.

[229] S. Salzinger, B. Rieger, *Macromolecular rapid communications* **2012**, *33*, 1327–1345.

[230] M. Weger, Dissertation, Technische Universität München, München, **2019**.

[231] G. Miyake, L. Caporaso, L. Cavallo, E. Y.-X. Chen, *Macromolecules* **2009**, *42*, 1462–1471.

[232] T. Kodaira, H. Tanahashi, K. Hara, *Polymer Journal* **1990**, *22*, 649–659.

[233] J. F. Klebe, H. Finkbeiner, D. M. White, *Journal of the American Chemical Society* **1966**, *88*, 3390–3395.

[234] B. de Falco, V. Lanzotti, *Phytochemistry Reviews* **2018**, *17*, 951–972.

[235] M. Kränzlein, Masters Thesis, Technische Universität München, München, **2019**.

[236] G. M. Diamond, R. F. Jordan, J. L. Petersen, *Journal of the American Chemical Society* **1996**, *118*, 8024–8033.

[237] Y. Ning, E. Y.-X. Chen, *Journal of the American Chemical Society* **2008**, *130*, 2463–2465.

[238] S. Sunil, J. K. Abhilas, A. Kumar, H. K. Shukla in INTERNATIONAL CONFERENCE ON INVENTIVE MATERIAL SCIENCE APPLICATIONS : ICIMA 2019, AIP Publishing, **2019**, p. 020018.

[239] J. Erdmann, private interview, **2023**.

[240] G. Maerker, E. T. Haeberer, S. F. Herb, *Journal of the American Oil Chemists' Society* **1966**, *43*, 505–508.

[241] L. Ricciotti, G. Roviello, O. Tarallo, F. Borbone, C. Ferone, F. Colangelo, M. Catauro, R. Cioffi, *International journal of molecular sciences* **2013**, *14*, 18200–18214.

[242]   L. Shechter, J. Wynstra, *Industrial & Engineering Chemistry* **1956**, *48*, 86–93.

[243]   S. Ebnesajjad, *Surface Treatment of Materials for Adhesive Bonding*, 2nd ed., William Andrew, Norwich, **2014**.

[244]   M. R. M. Hafiezal, A. Khalina, Z. A. Zurina, M. D. M. Azaman, Z. M. Hanafee, *Journal of Composites Science* **2019**, *3*, 6.

[245]   A. Campanella, M. Zhan, P. Watt, A. T. Grous, C. Shen, R. P. Wool, *Compos. - A: Appl. Sci. Manuf. (Composites Part A: Applied Science and Manufacturing)* **2015**, *72*, 192–199.

[246]   F. C. Fernandes, K. Kirwan, P. R. Wilson, S. R. Coles, *Green Mater. (Green Materials)* **2018**, *6*, 38–46.

[247]   X. Feng, J. Fan, A. Li, G. Li, *ACS Sustain. Chem. Eng. (ACS Sustainable Chemistry & Engineering)* **2020**, *8*, 874–883.

[248]   J. Lange, N. Altmann, C. Kelly, P. Halley, *Polymer* **2000**, *41*, 5949–5955.

[249]   A. Shrivastava, *Introduction to Plastics Technology*, William Andrew, Saint Louis, **2018**.

[250]   F. I. Altuna, V. Pettarin, R. J. J. Williams, *Green Chemistry* **2013**, *15*, 3360.

[251]   J. M. Breitsameter, N. Reinhardt, M. Feigel, O. Hinrichsen, K. Drechsler, B. Rieger, *Macromolecular Materials and Engineering* **2022**, *308*, 202300068.

[252]   B. M. Trost, U. Kazmaier, *Journal of the American Chemical Society* **1992**, *114*, 7933–7935.

[253]   C. Guo, X. Lu, *Journal of the Chemical Society Perkin Transactions 1* **1993**, 1921–1923.

[254]   S. F. Martin, S. A. Williamson, R. P. Gist, K. M. Smith, *The Journal of Organic Chemistry* **1983**, *48*, 5170–5180.

[255]   P. Klán, P. Beňovský, *Monatshefte für Chemie / Chemical Monthly* **1992**, *123*, 469–471.

[256]   A. W. Hofmann, *Justus Liebigs Annalen der Chemie* **1859**, *110*, 129–140.

[257]   J. D. Piper, P. W. Piper, *Comprehensive Reviews in Food Science and Food Safety* **2017**, *16*, 868–880.

[258] V. Canale, L. Tonucci, M. Bressan, N. d'Alessandro, *Catalysis Science & Technology* **2014**, *4*, 3697–3704.

[259] Europena Chemicals Agency, Ed., Substance Information - ECHA: Maleic anhydride, **2022**, `https://echa.europa.eu/de/substance-information/-/substanceinfo/100.003.247` (visited on 07/13/2022).

[260] M. Moreno, M. V. Gomez, C. Cebrian, P. Prieto, A. de La Hoz, A. Moreno, *Green Chemistry* **2012**, *14*, 2584.

[261] G. Østergaard, E. Nielsen, O. Ladefoged, *Evaluation of health hazards by exposure to maleic anhydride and proposal of a health-based quality criterion for ambient air*, The Danish Environmental Protection Agency, Copenhagen, **2013**.

[262] K. Lohbeck, H. Haferkorn, W. Fuhrmann, N. Fedtke, *Ullmann's Encyclopedia of Industrial Chemistry* **2000**, DOI `10.1002/14356007.a16{\_}053`.

[263] Z. Du, J. Ma, F. Wang, J. Liu, J. Xu, *Green Chemistry* **2011**, *13*, 554.

[264] H. Guo, G. Yin, *The Journal of Physical Chemistry C* **2011**, *115*, 17516–17522.

[265] S. Shi, H. Guo, G. Yin, *Catalysis Communications* **2011**, *12*, 731–733.

[266] H. Choudhary, S. Nishimura, K. Ebitani, *Applied Catalysis A: General* **2013**, *458*, 55–62.

[267] C. Aouf, J. Lecomte, P. Villeneuve, E. Dubreucq, H. Fulcrand, *Green Chemistry* **2012**, *14*, 2328.

[268] H. Cai, P. Li, G. Sui, Y. Yu, G. Li, X. Yang, S. Ryu, *Thermochimica Acta* **2008**, *473*, 101–105.

[269] E. Ernault, PhD thesis, Arts et Métiers, Paris, **2016**.

[270] E. Darroman, N. Durand, B. Boutevin, S. Caillol, *Progress in Organic Coatings* **2016**, *91*, 9–16.

[271] B. A. Miller-Chou, J. L. Koenig, *Progress in Polymer Science* **2003**, *28*, 1223–1270.

[272] X. Kuang, Q. Shi, Y. Zhou, Z. Zhao, T. Wang, H. J. Qi, *RSC advances* **2018**, *8*, 1493–1502.

[273] L. Henry, A. Schneller, J. Doerfler, W. M. Mueller, C. Aymonier, S. Horn, *Polymer Degradation and Stability* **2016**, *133*, 264–274.

[274] R. Morales Ibarra, M. Sasaki, M. Goto, A. T. Quitain, S. M. García Montes, J. A. Aguilar-Garib, *Journal of Material Cycles and Waste Management* **2015**, *17*, 369–379.

[275] R. Piñero-Hernanz, J. García-Serna, C. Dodds, J. Hyde, M. Poliakoff, M. J. Cocero, S. Kingman, S. Pickering, E. Lester, *The Journal of Supercritical Fluids* **2008**, *46*, 83–92.

[276] P. Liu, J. Lu, H. Yu, N. Ren, F. E. Lockwood, Q. J. Wang, *The Journal of chemical physics* **2017**, *147*, 084904.

[277] T. Hayes, Y. Hu, S. A. Sanchez-Vazquez, H. C. Hailes, A. E. Aliev, J. R. G. Evans, *Journal of Polymer Science Part A: Polymer Chemistry* **2016**, *54*, 3159–3170.

[278] M. Lin, F. Ye, F. Yun, Study on Preparation of Conjugated Linoleic Acids with Alkaly Catalyst from Natural Unsaturated Fatty Acid Methyl Esters, (Ed.: MOE Key Laboratory of Food Colloids and Biotechnology), Wuxi.

[279] P. J. Gay, *J. Soc. Chem. Ind. (Journal of the Society of Chemical Industry)* **1933**, *52*, 703–705.

List of Figures

List of Schemes

List of Tables

Appendix

Figure A1: ^{1}H-NMR in chloroform-d of triisopropyl((1-methoxy-2-methylprop-1-en-1-yl)oxy)silane ($^{i\mathrm{Pr}}$SKA).

Figure A2: ^{1}H-NMR in chloroform-d the reaction of conjugated linoleic acid with maleic anhydride.
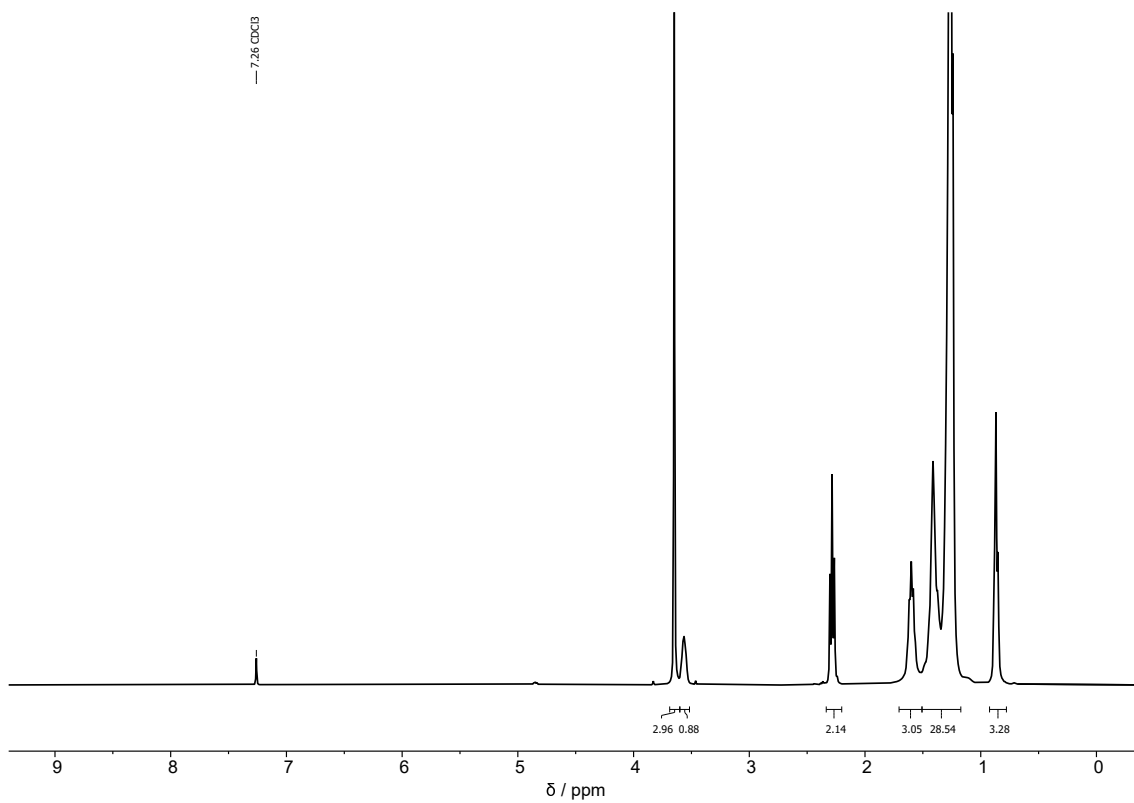
Figure A3: ^{1}H-NMR in chloroform-d of methylated 12-hydroxystearic acid (methyl-12-hydroxystearate).
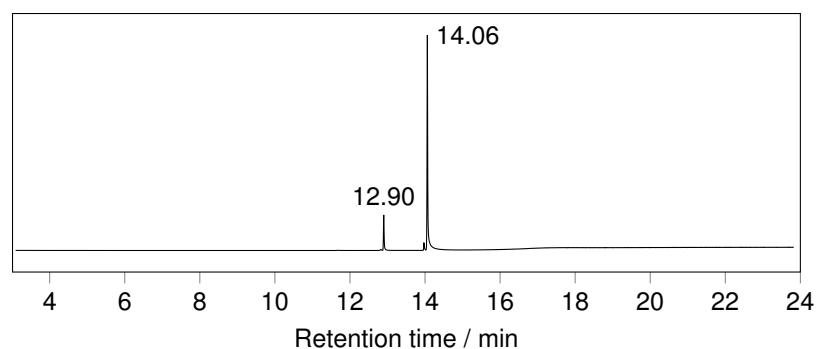
Figure A4: GC-MS elugram of methylated 12-hydroxystearic acid (methyl-12-hydroxystearate). R.t = 12.90 min: stearic acid, r.t. = 14.06 min: Me-12-HSA.

(a)

(b)
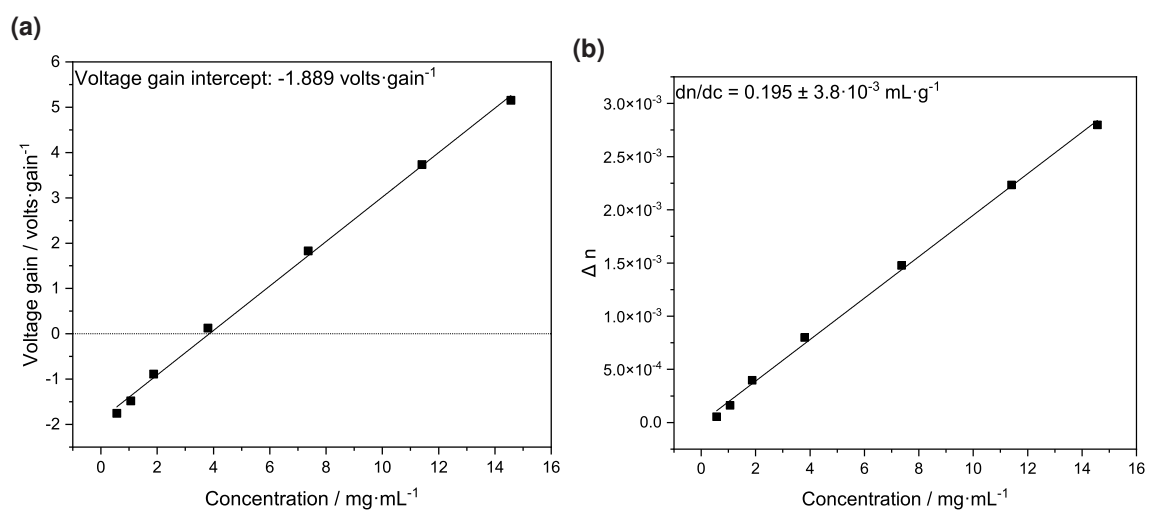
Figure A5: Refractive index increment determination of pBn2AA in tetrahydrofuran, a) voltage gain per concentration, b) Δn per concentration. dn/dc = 0.005 28 mL g^{-1}.
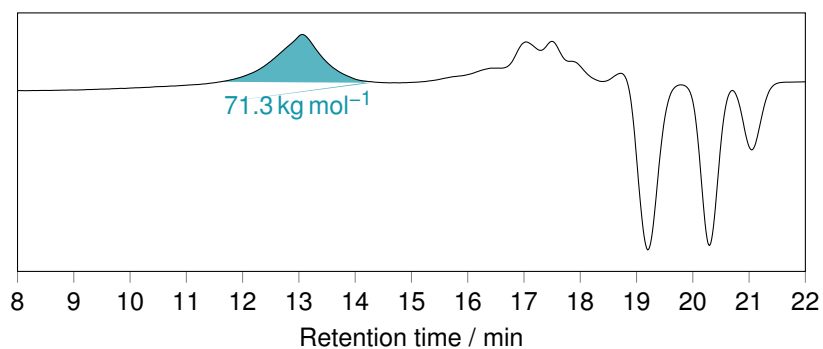
Figure A6: SEC-GPC trace of Boc$_2$AA polymerized with catalyst Ib (Table 4.3).
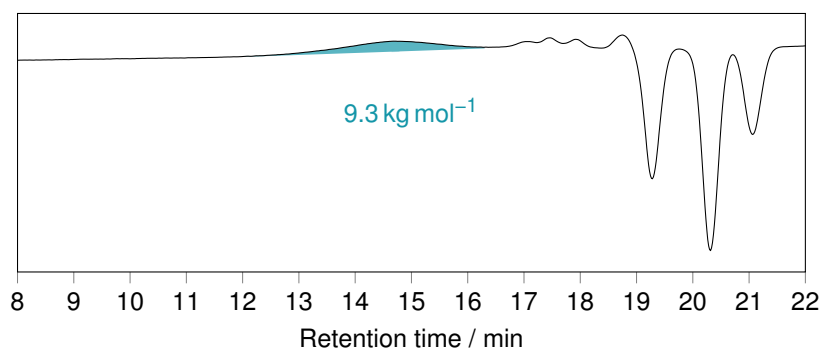
Figure A7: SEC-GPC trace of Boc$_2$AA polymerized with catalyst VII (Table 4.3).
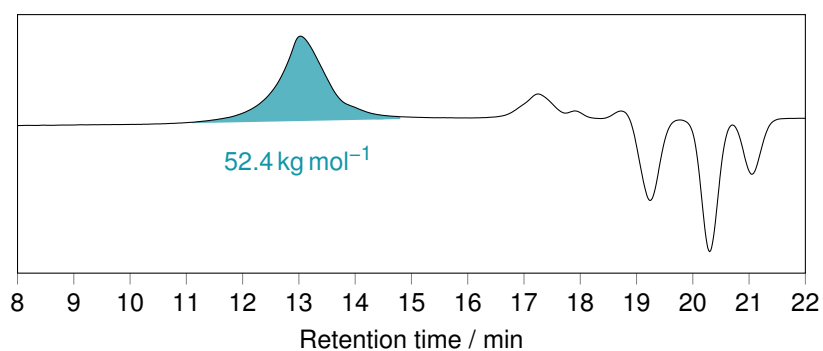
Figure A8: SEC-GPC trace of Boc$_2$AA polymerized with catalyst VIII (Table 4.3).
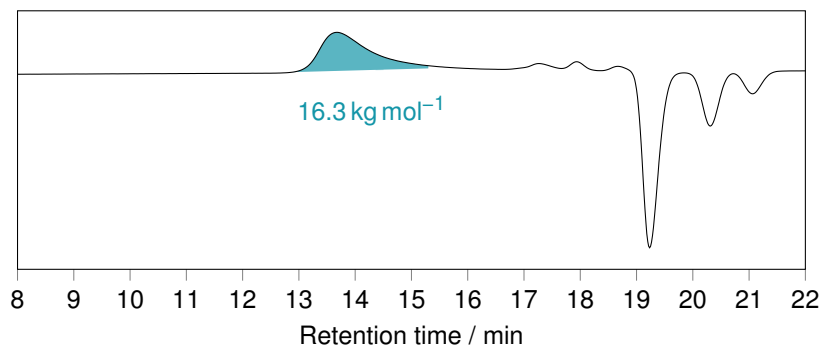
Figure A9: SEC-GPC trace of Boc$_2$AA polymerized with catalyst (Table 4.3).
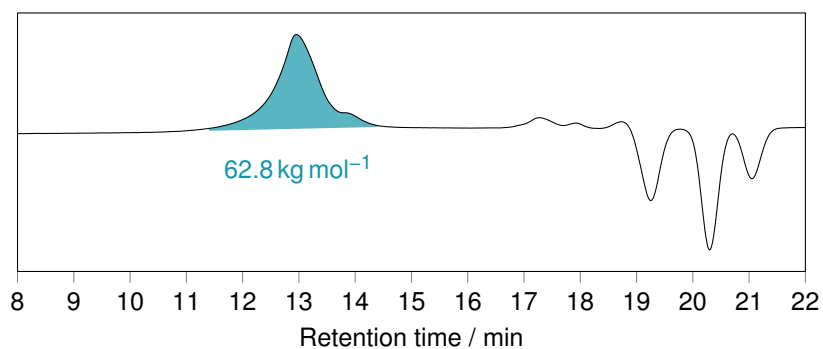
Figure A10: SEC-GPC trace of Boc$_2$AA polymerized with catalyst (Table 4.3).
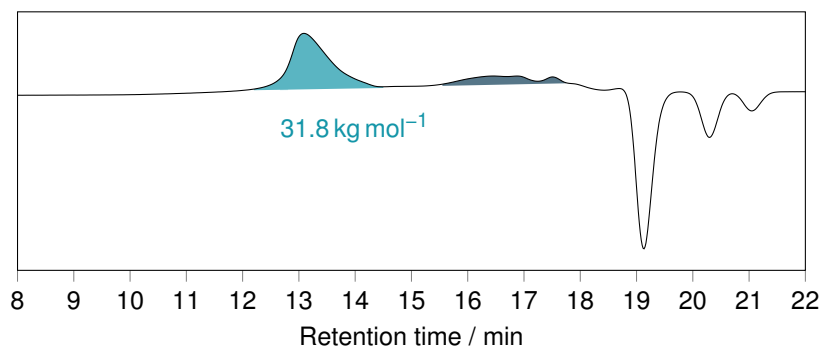
Figure A11: SEC-GPC trace of Boc$_2$AA polymerized with catalyst (Table 4.3).
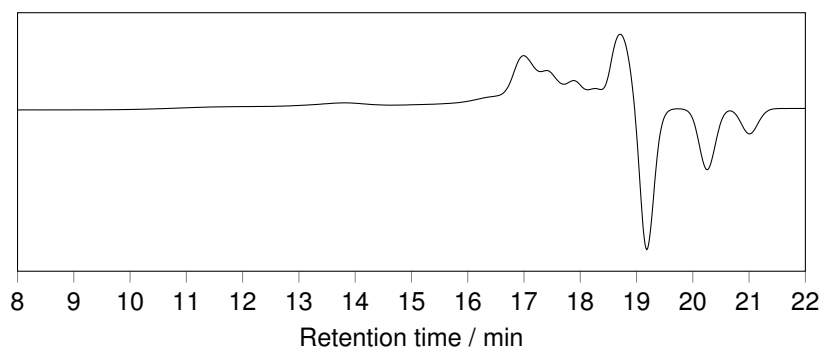
Figure A12: SEC-GPC trace of Boc$_2$AA polymerized with catalyst (Table 4.3).
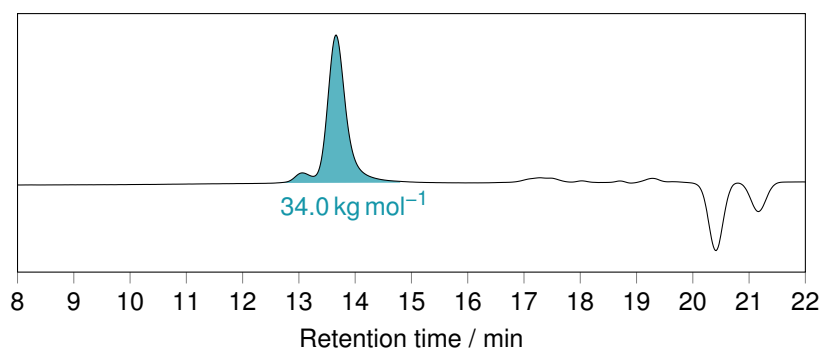
Figure A13: SEC-GPC trace of *t*BuA polymerized with catalyst Cp$_2$*YMe.

(a)

(b)
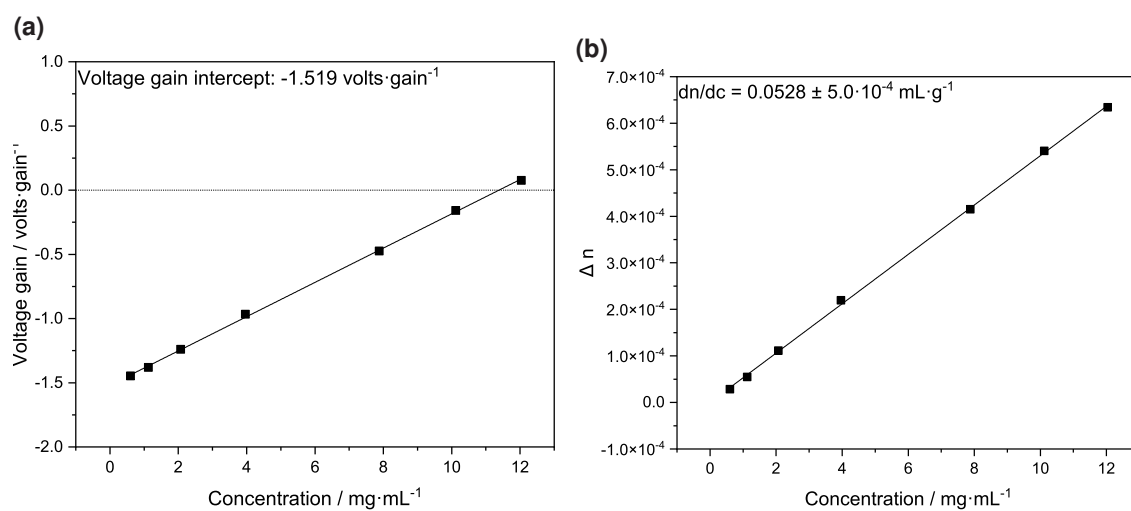
Figure A14: Refractive index increment determination of pMA in *N,N'*-dimethylformamide containing LiBr, a) voltage gain per concentration, b) Δn per concentration. $dn/dc = 0.195 \, \text{mL} \, \text{g}^{-1}$.
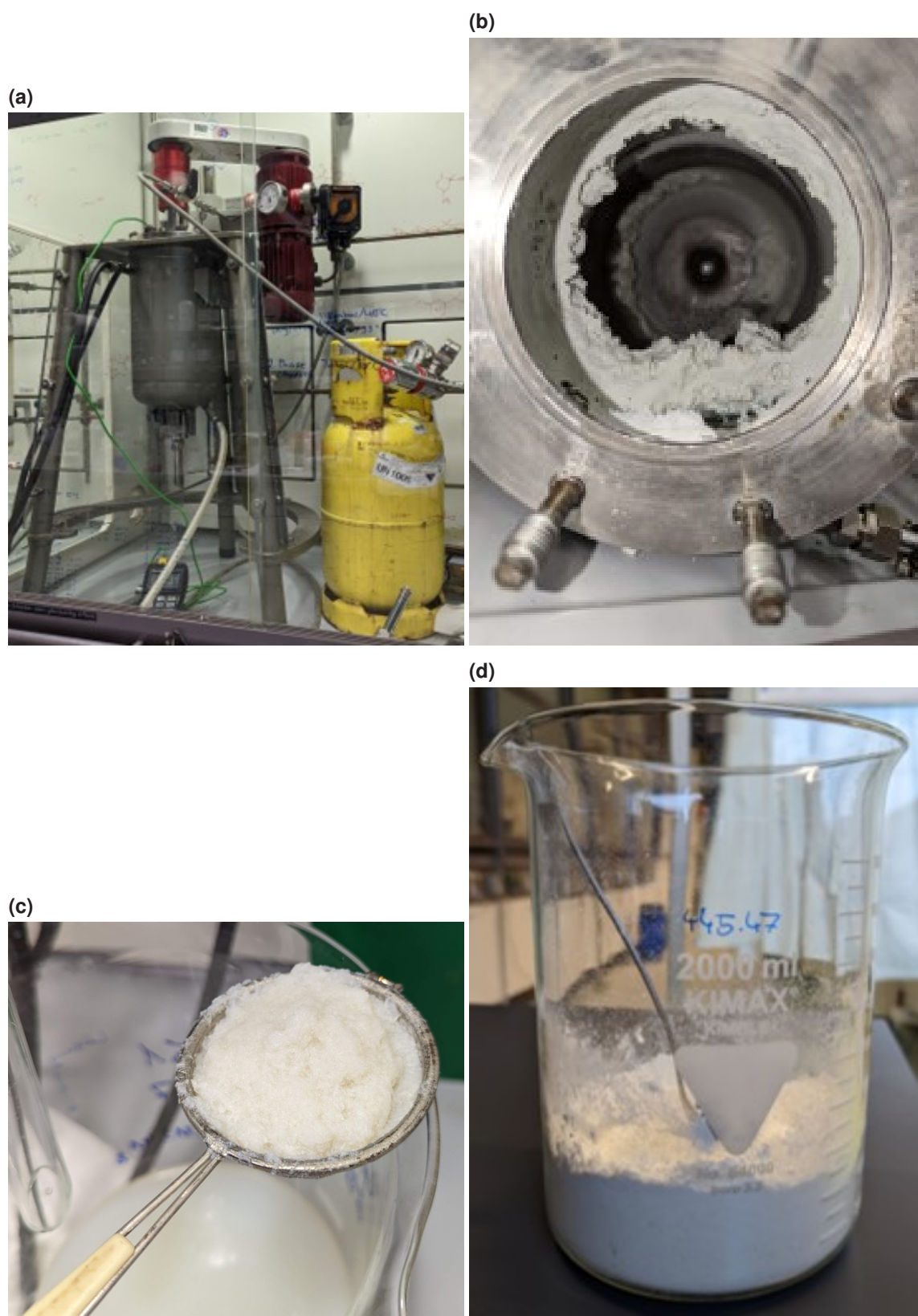
Figure A15: a) Reactor setup used for the amidation reaction, b) precipitated PAA inside the reactor, c) skimming of the reprecipitated polymer wit ha tea strainer, d) isolated PAA.
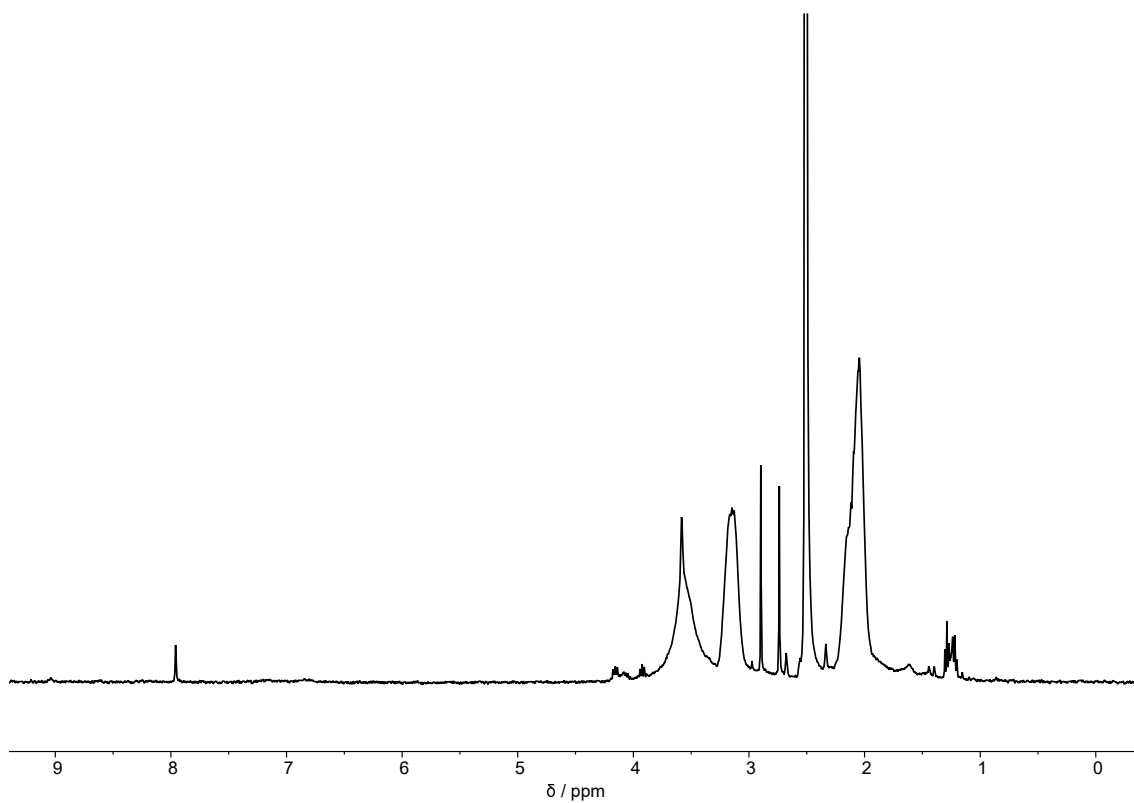
Figure A16: ^{1}H-NMR of the the upscaling dehydration experiment of PAA in DMSO-d$_6$ as solvent (Table 4.8, entry 8).
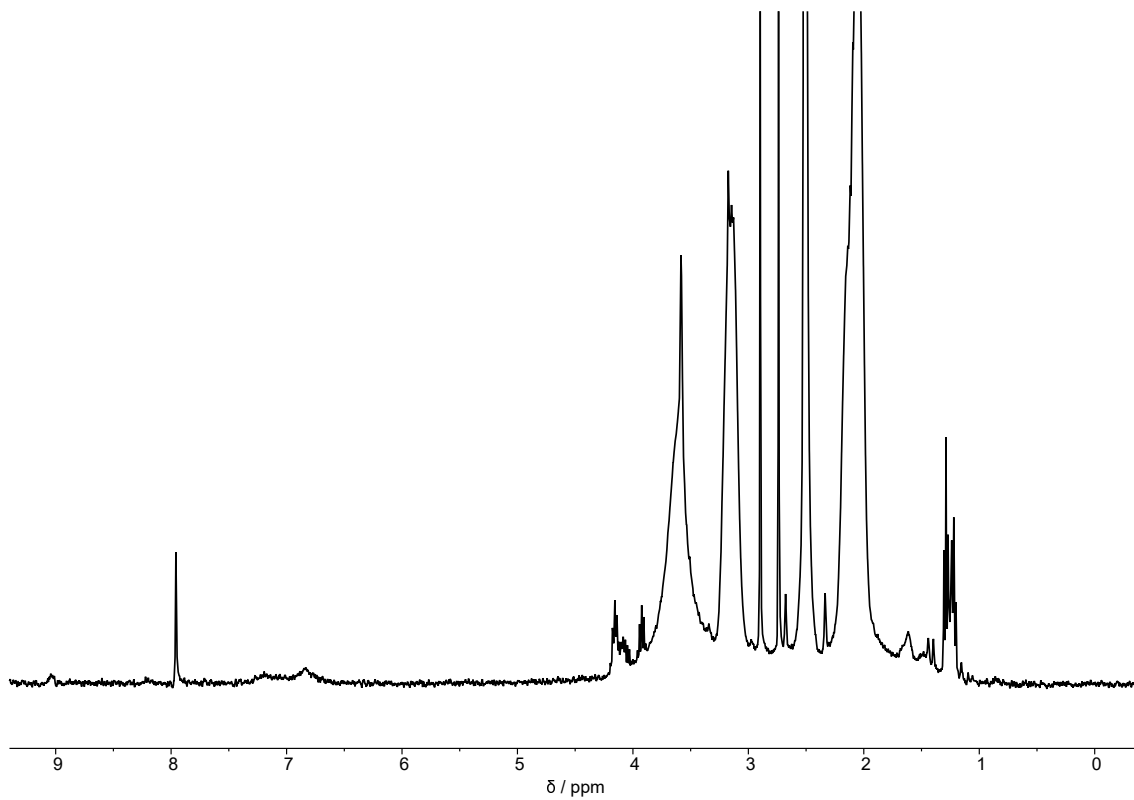
Figure A17: ^{1}H-NMR of the the upscaling dehydration experiment of PAA in DMSO-d$_6$ as solvent (Table 4.7, entry 9).
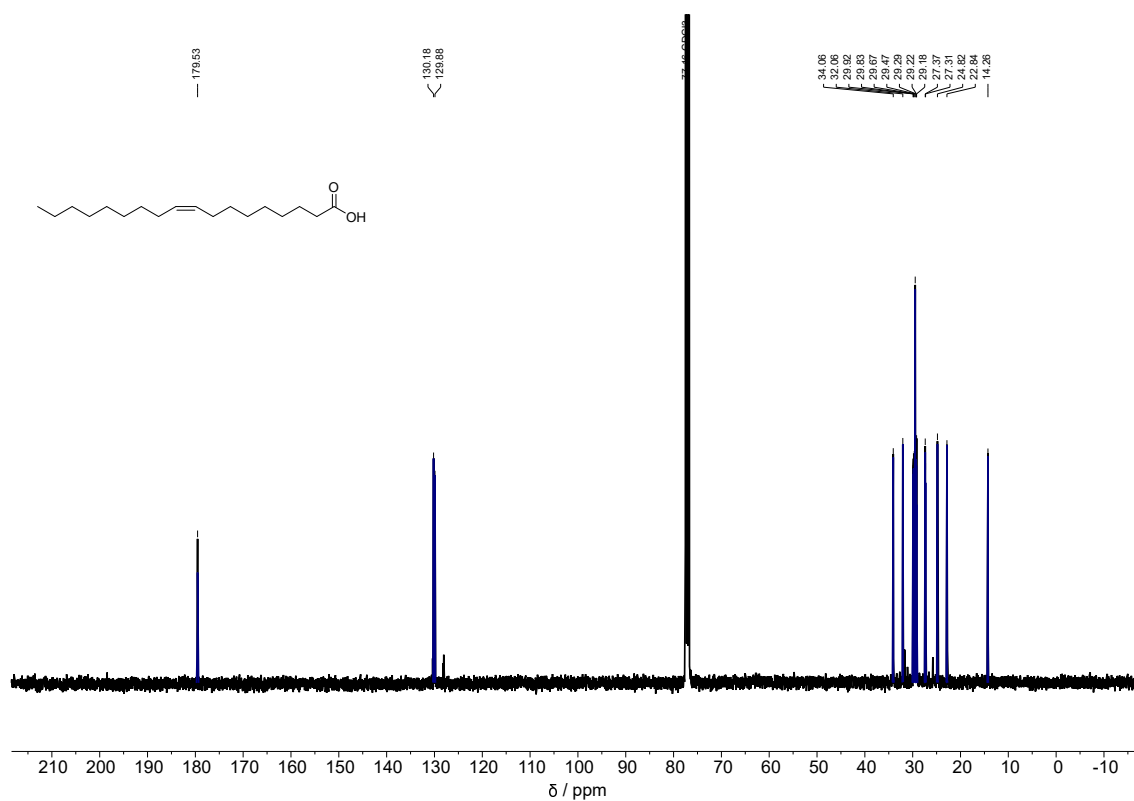
Figure A18: ^{13}C-NMR of oleic acid in chloroform-d as solvent.
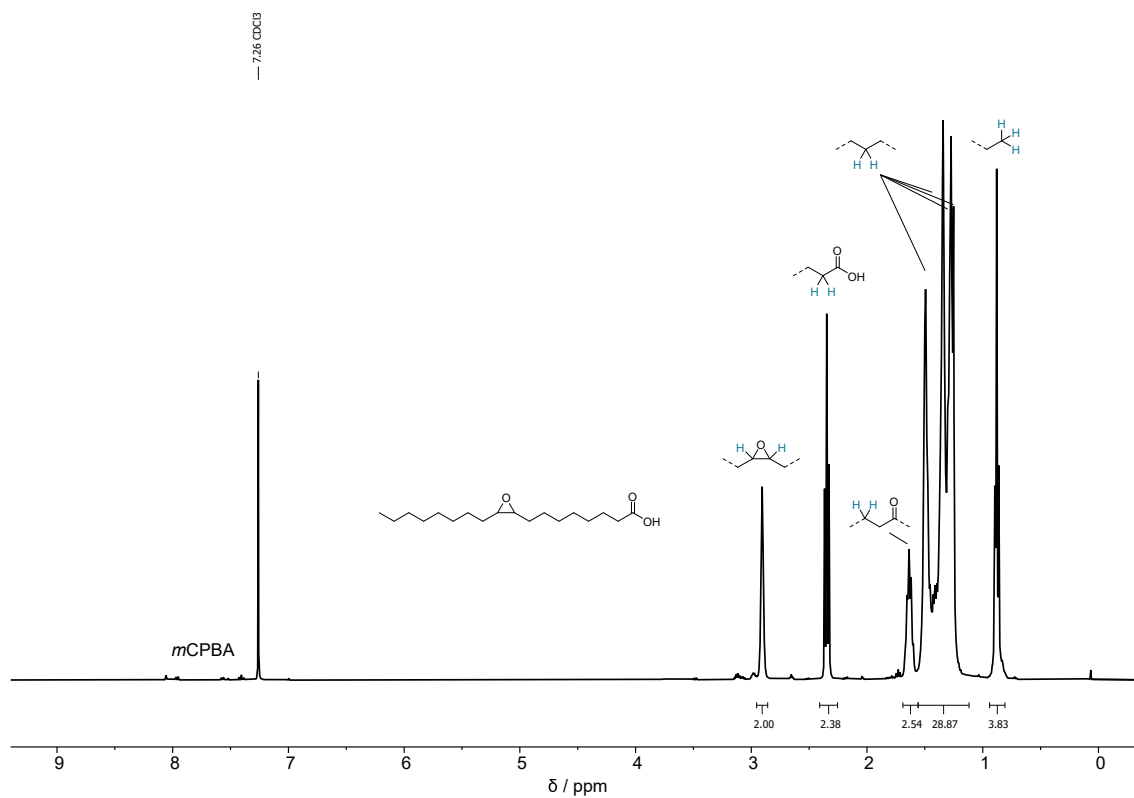
Figure A19: ^{1}H-NMR of epoxidized oleic acid (9,10-epoxystearic acid) in chloroform-d as solvent.
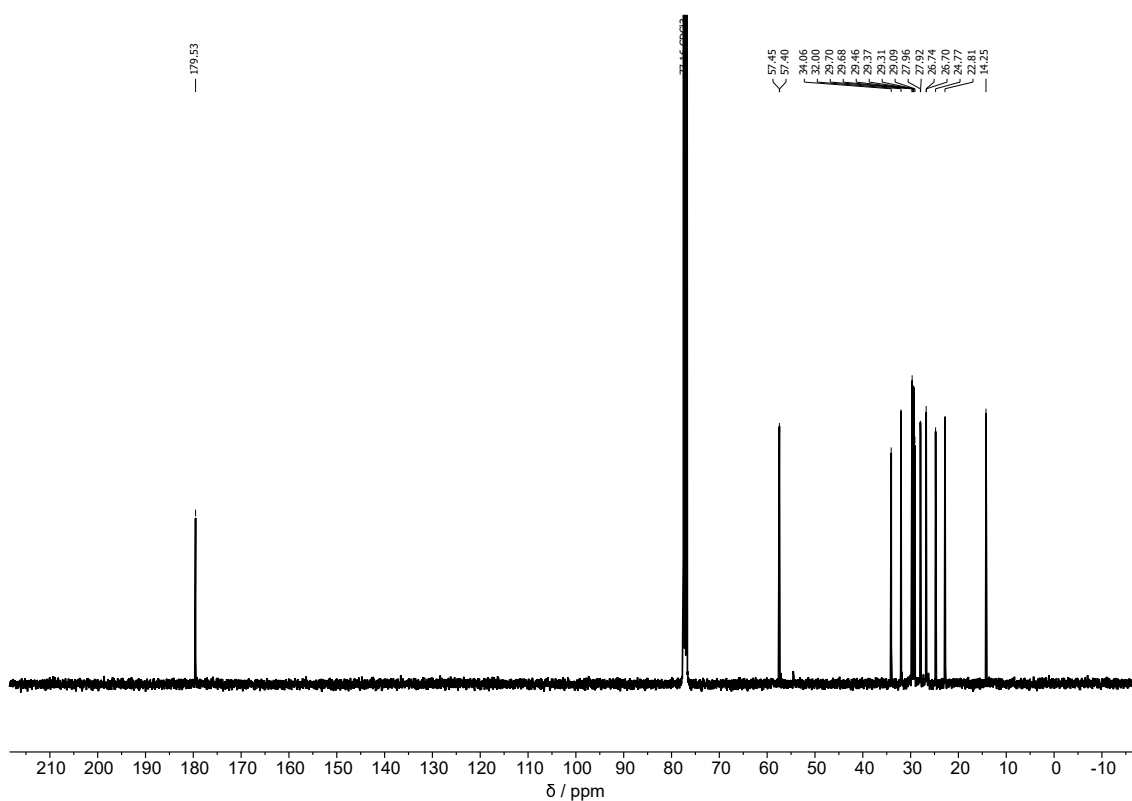
Figure A20: ^{13}C-NMR of epoxidized oleic acid (9,10-epoxystearic acid) in chloroform-d as solvent.
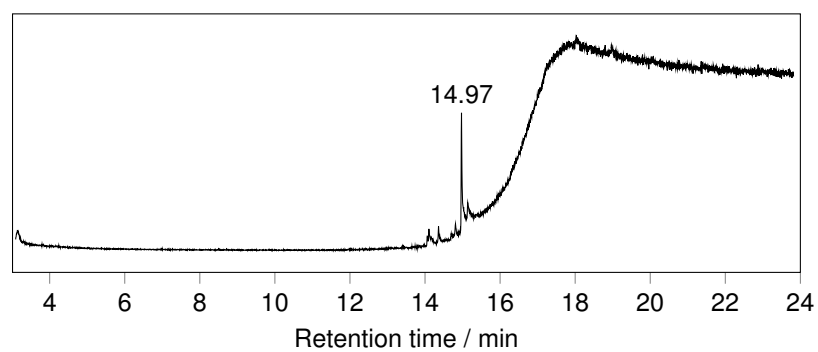
Figure A21: GC-MS elugram of epoxidized linoleic acid (9,10-12,13-diepoxystearic acid). R.t = 14.97 min.
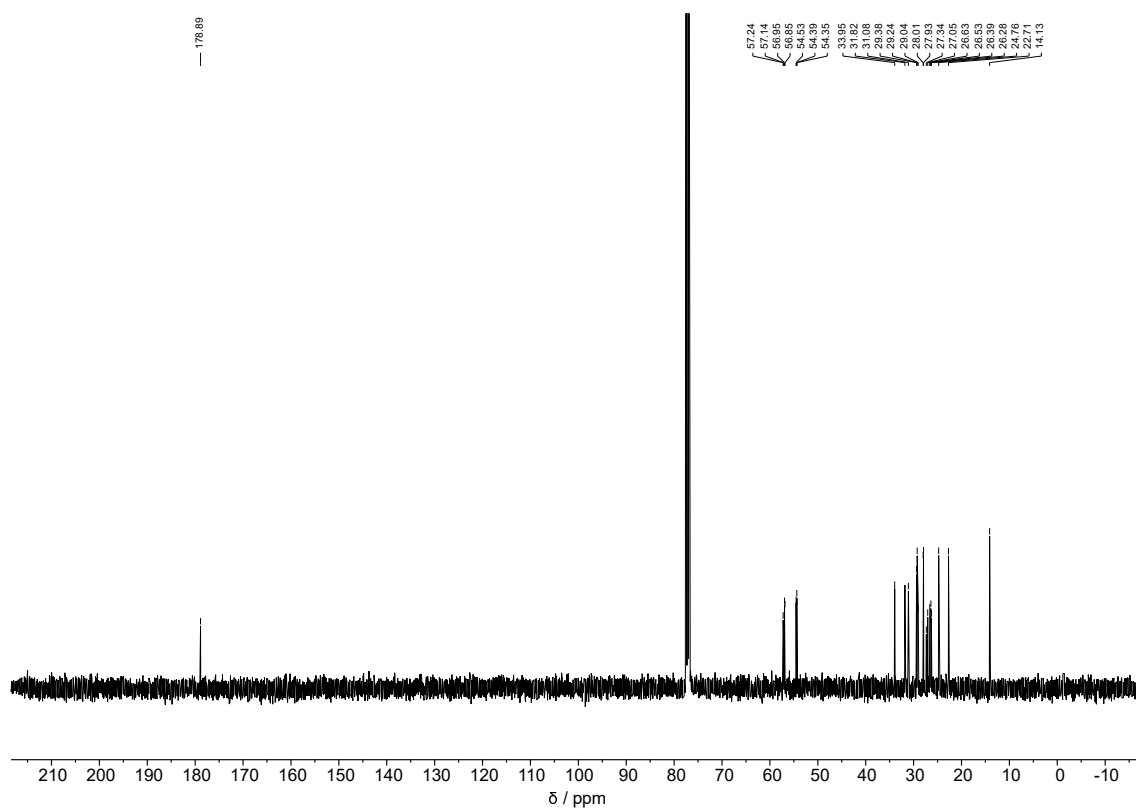
Figure A22: ^{13}C-NMR of epoxidized linoleic acid (9,10-12,13-diepoxystearic acid) in chloroform-d as solvent.
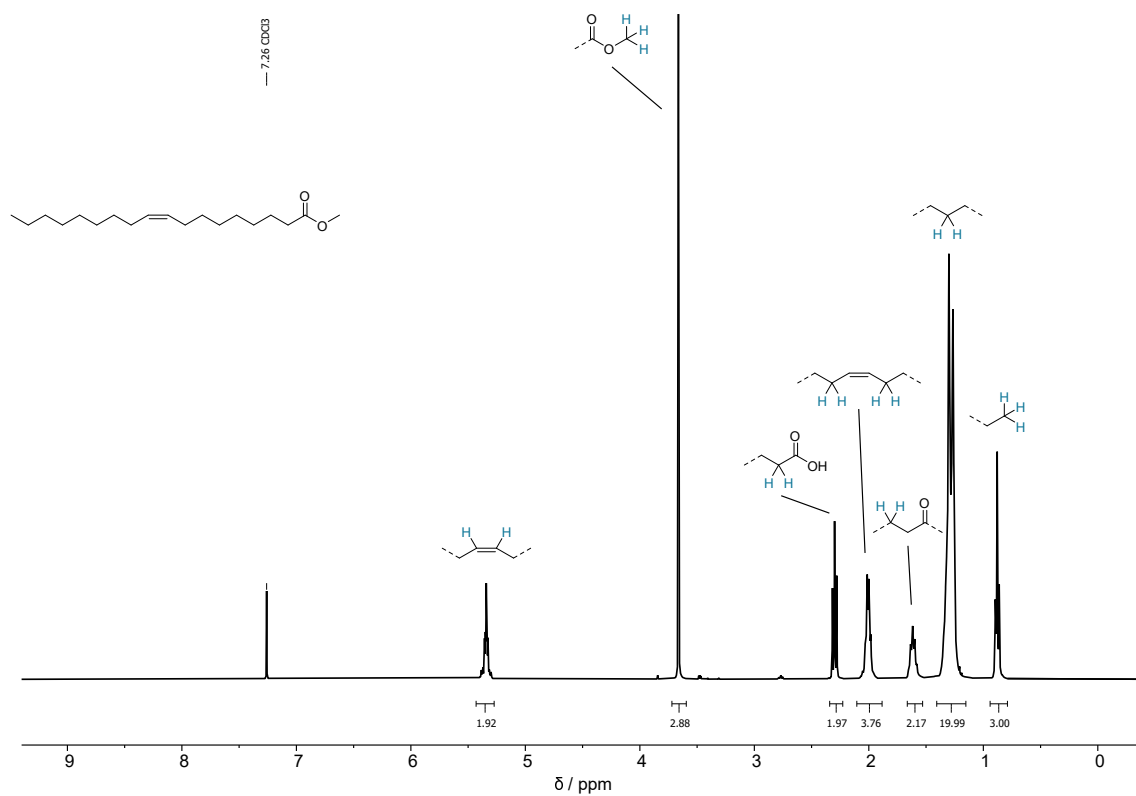
Figure A23: ^{1}H-NMR of methylated oleic acid (methyl oleate) in chloroform-d as solvent.
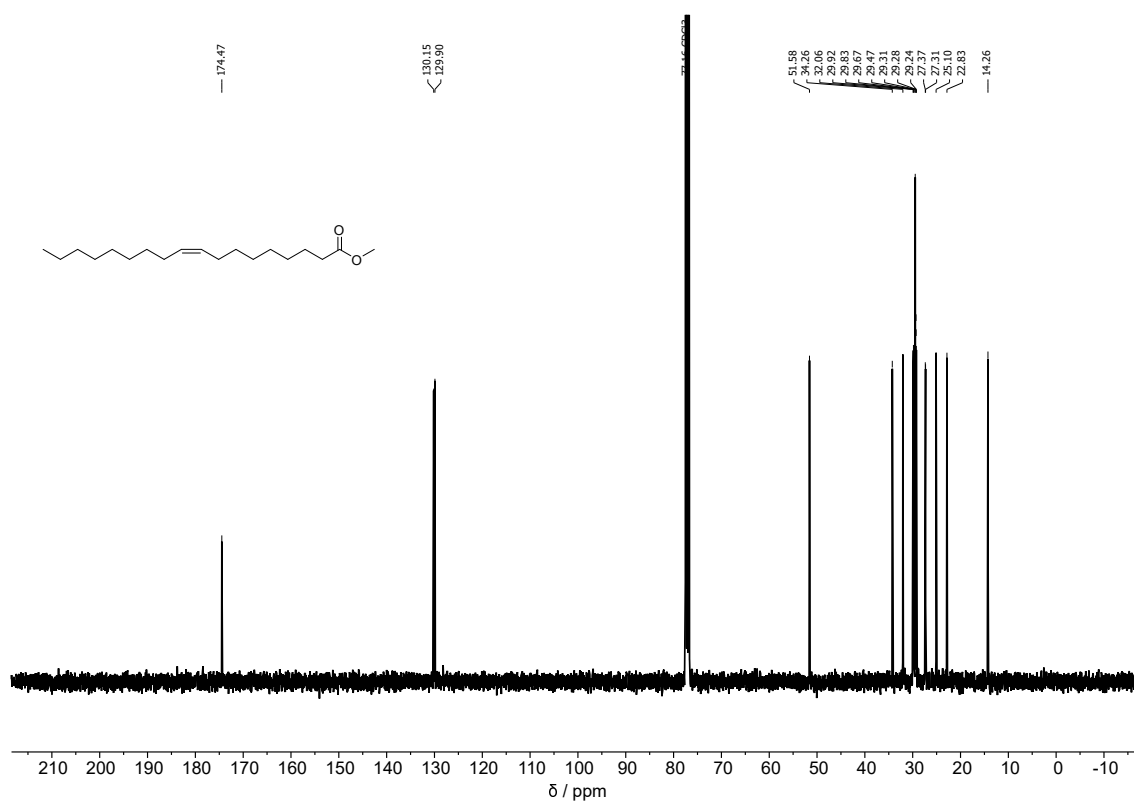
Figure A24: ^{13}C-NMR of methylated oleic acid (methyl oleate) in chloroform-d as solvent.
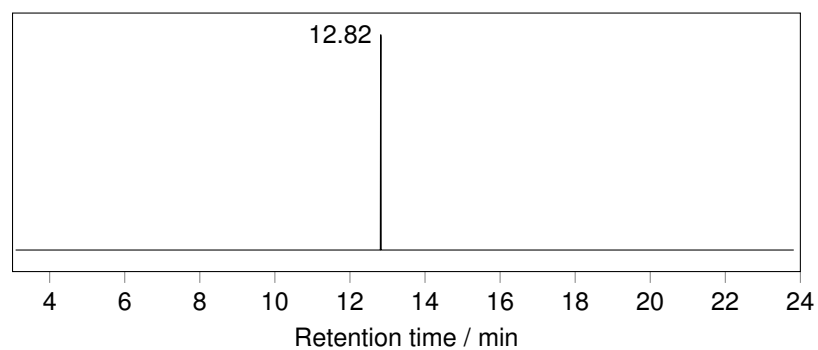
Figure A25: GC-MS elugram of methylated oleic acid (methyl oleate). R.t = 12.82 min.

Figure A26: ^{1}H-NMR of methylated linoleic acid (methyl linoleate) in chloroform-d as solvent.

Figure A27: ^{13}C-NMR of methylated linoleic acid (methyl linoleate) in chloroform-d as solvent.
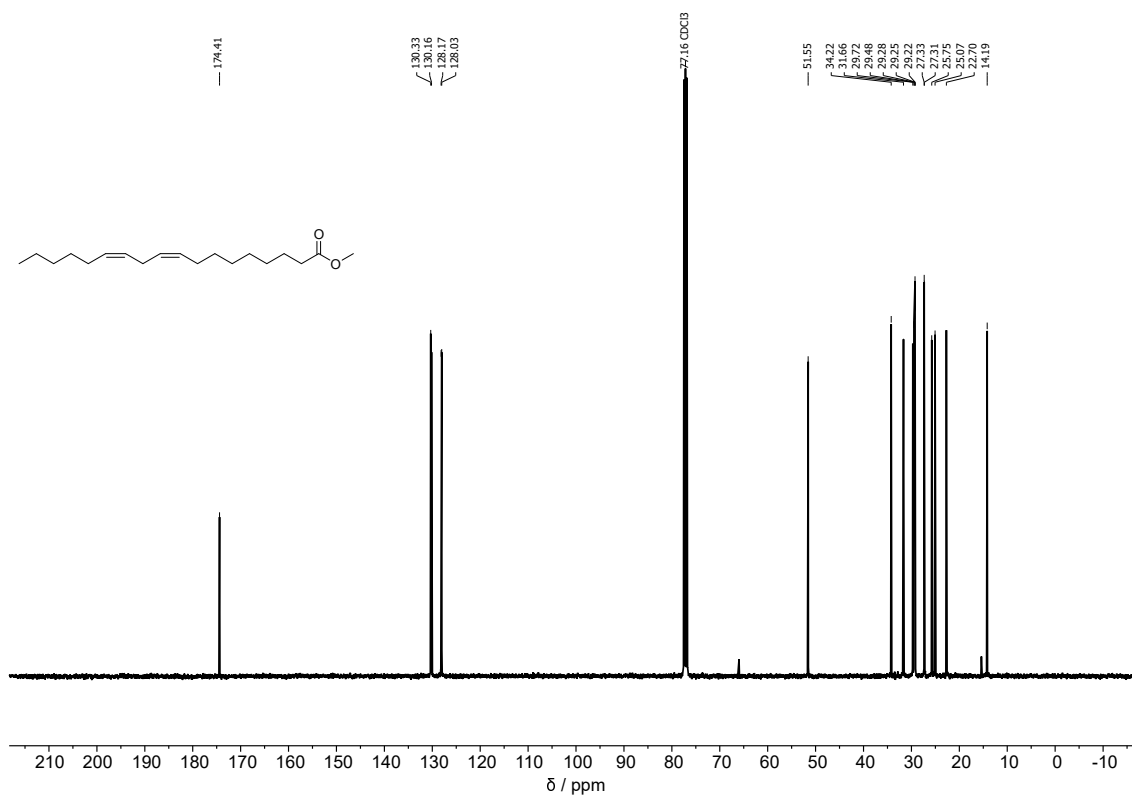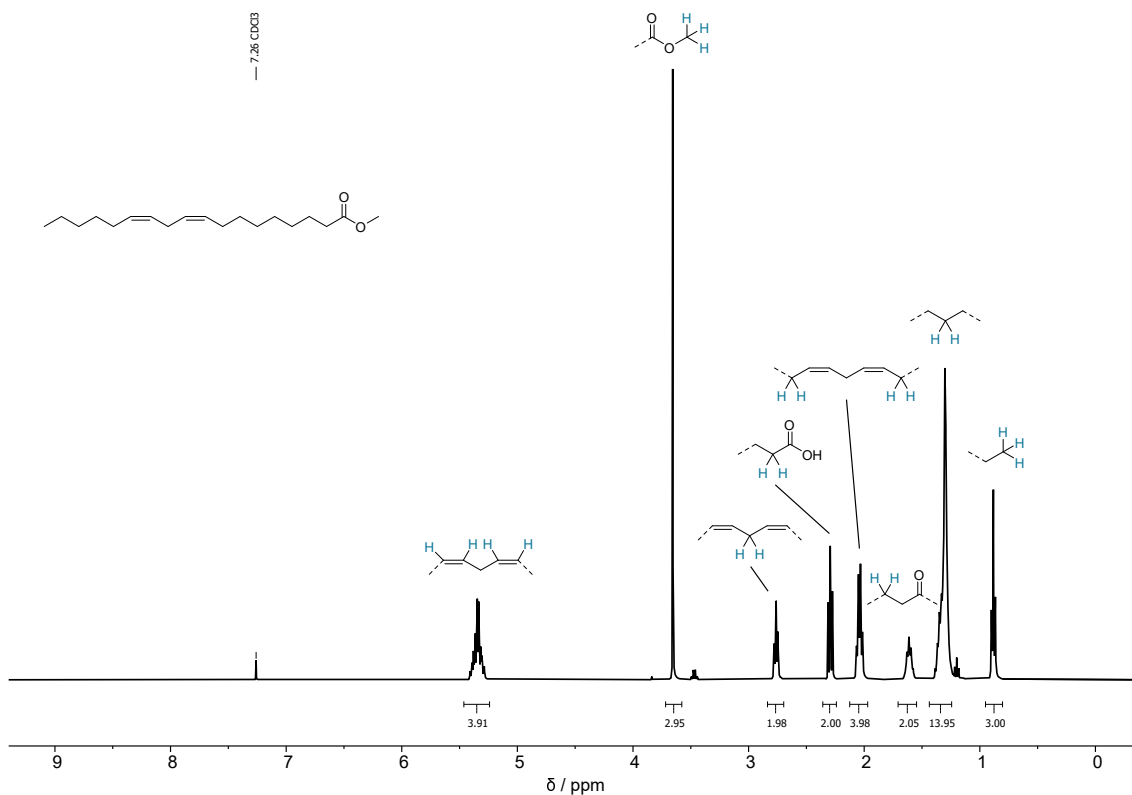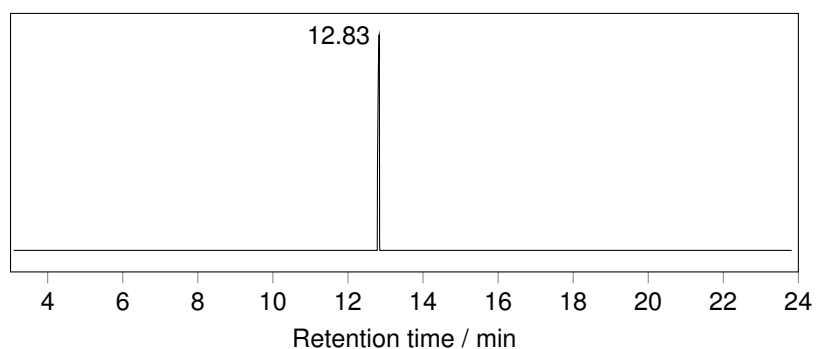
Figure A28: GC-MS elugram of methylated linoleic acid (methyl linoleate). R.t = 12.83 min.
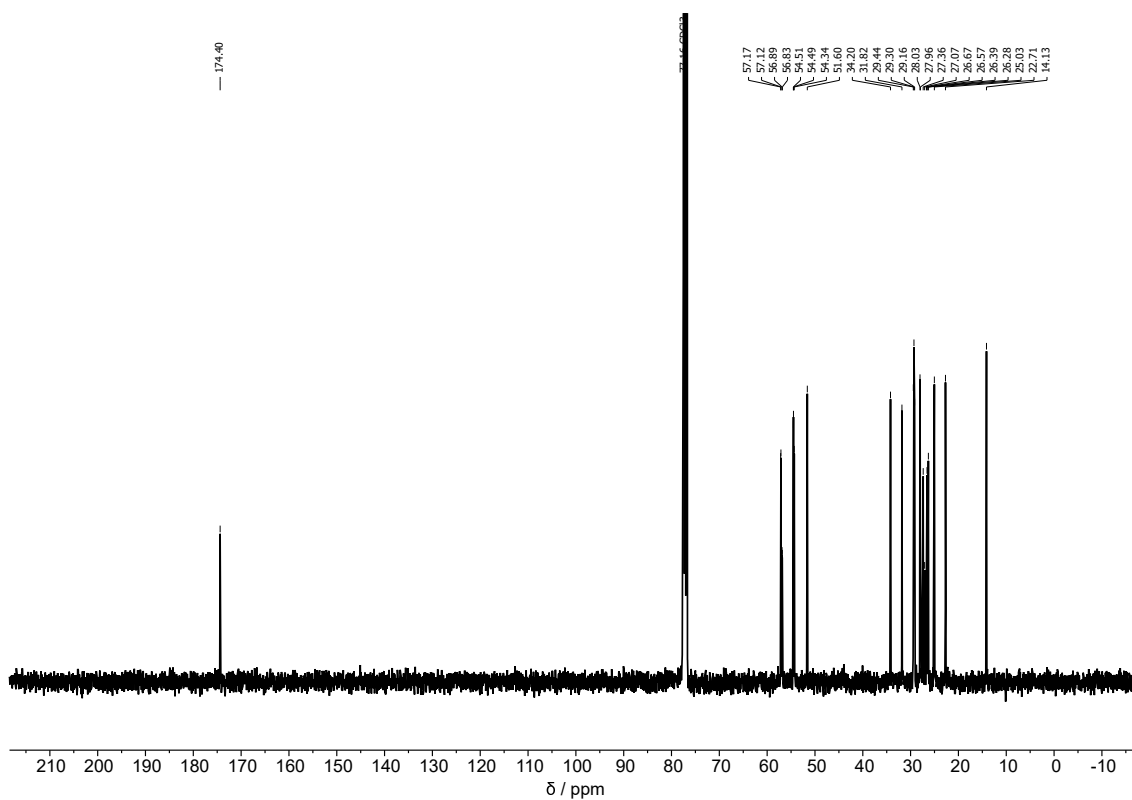
Figure A29: ^{13}C-NMR of epoxidized methyl linoleate (9,10-12,13-diepoxy methyl-stearate) in chloroform-d as solvent.
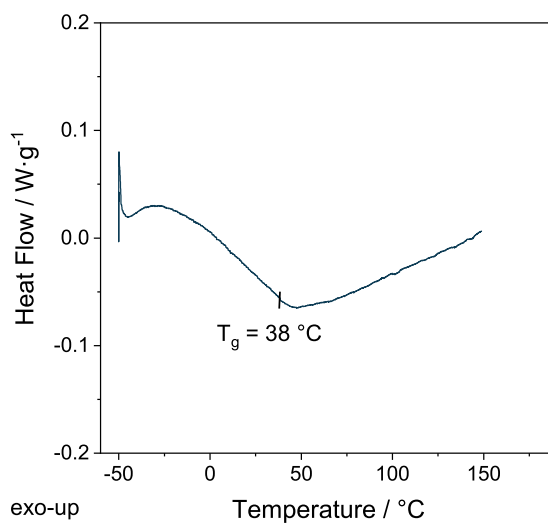
Figure A30: DSC-scan of DESMe cured with IPD, T_g = −38 °C.
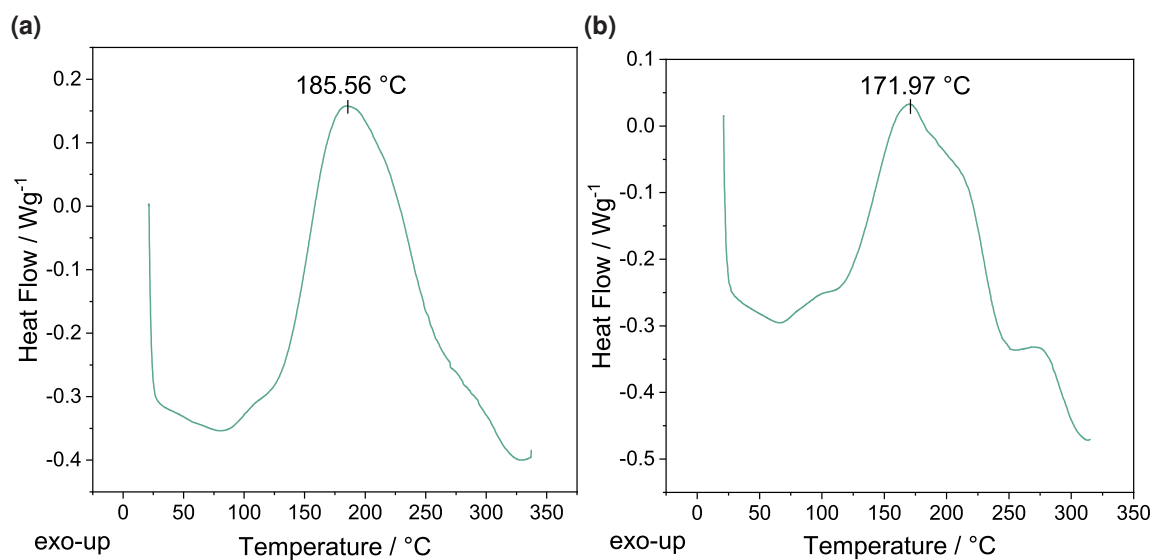
Figure A31: a) DSC-scan of the sample TA/ELO 1.0, b) DSC-scan of the sample TA/ELO 2.0. Figures adapted from Reinhardt *et al.*.[182]
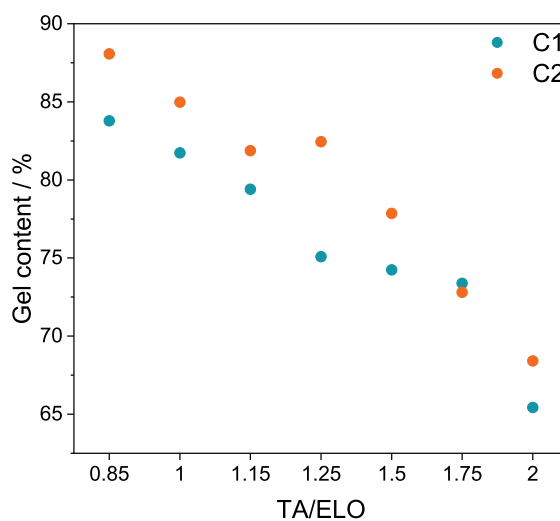
Figure A32: Gel content measurements of TA/ELO samples cured with condition C1 and C2. Adapted from Reinhardt *et al.*[182]
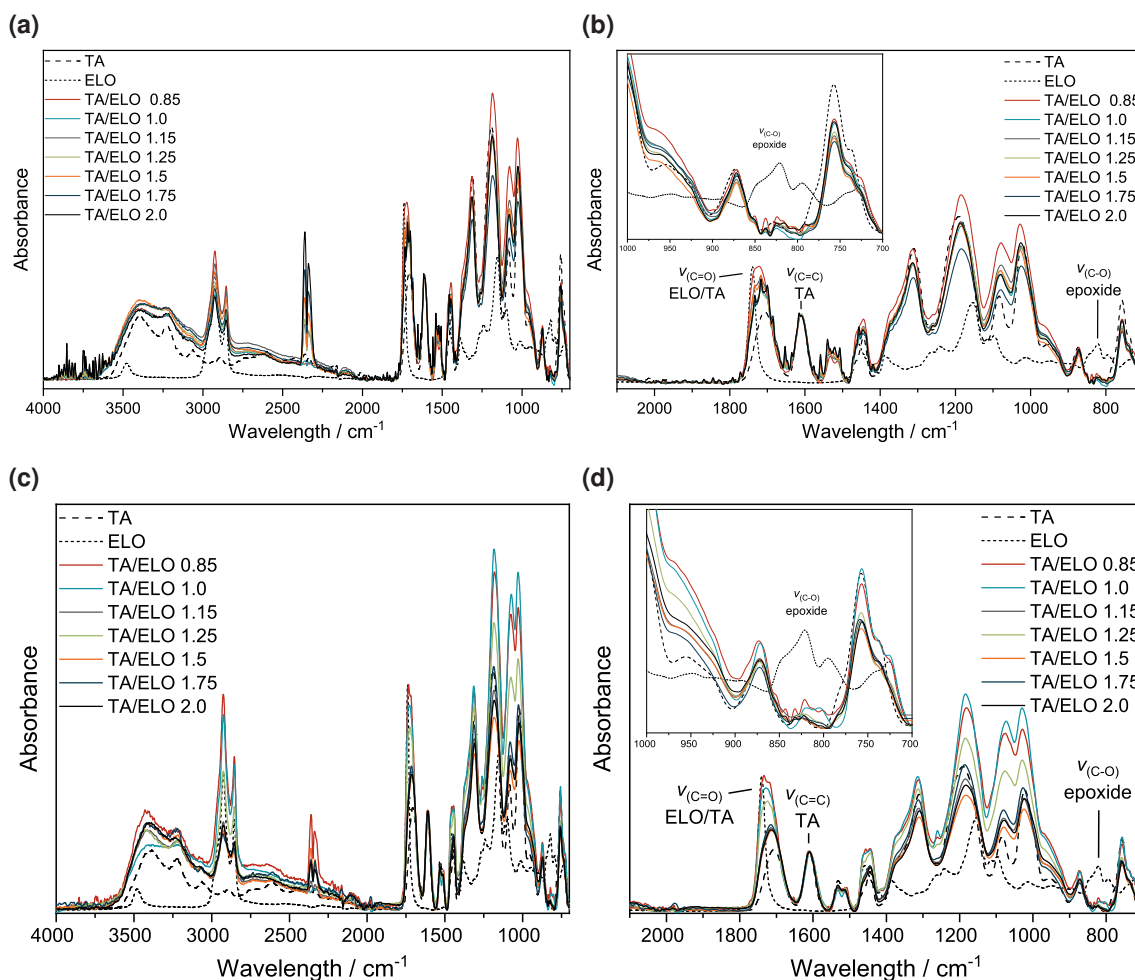
Figure A33: ATR-IR measurements of TA/ELO samples cured with a and b) C1, c and d) C2. Signals normalized to the C=C vibration of TA ($1610\,cm^{-1}$). Signal of the C–O epoxide vibration at $820\,cm^{-1}$. Figures reprinted from Reinhardt *et al.*[182]
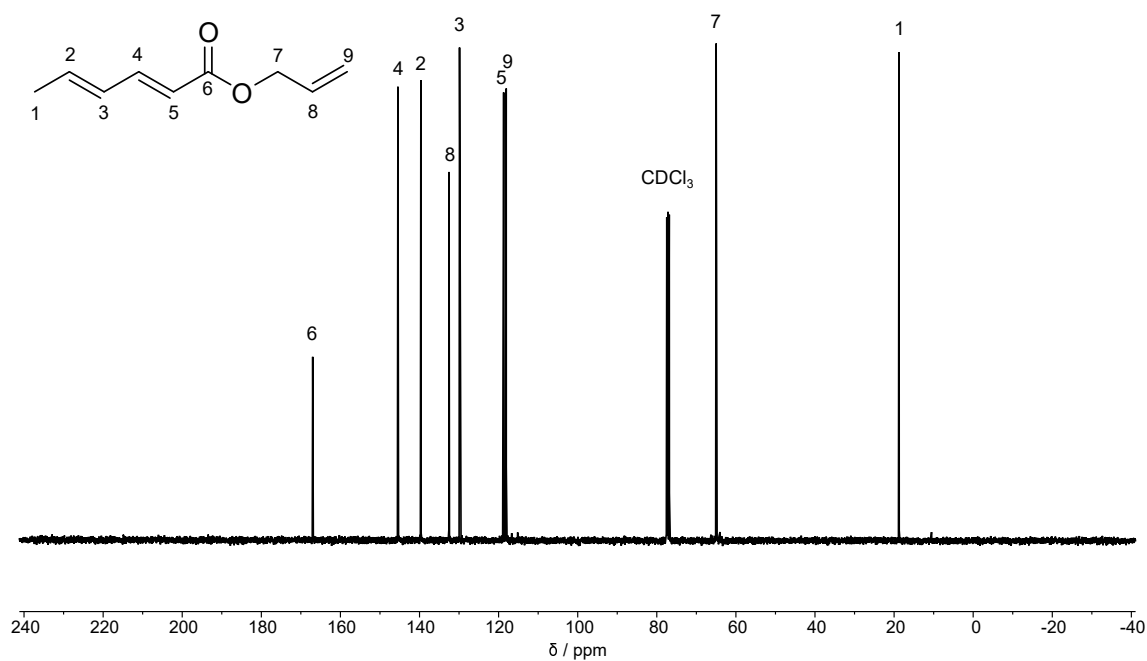
Figure A34: ^{13}C-NMR of allyl sorbate in chloroform-d as solvent. Reprinted from Breitsameter *et al.*[251]
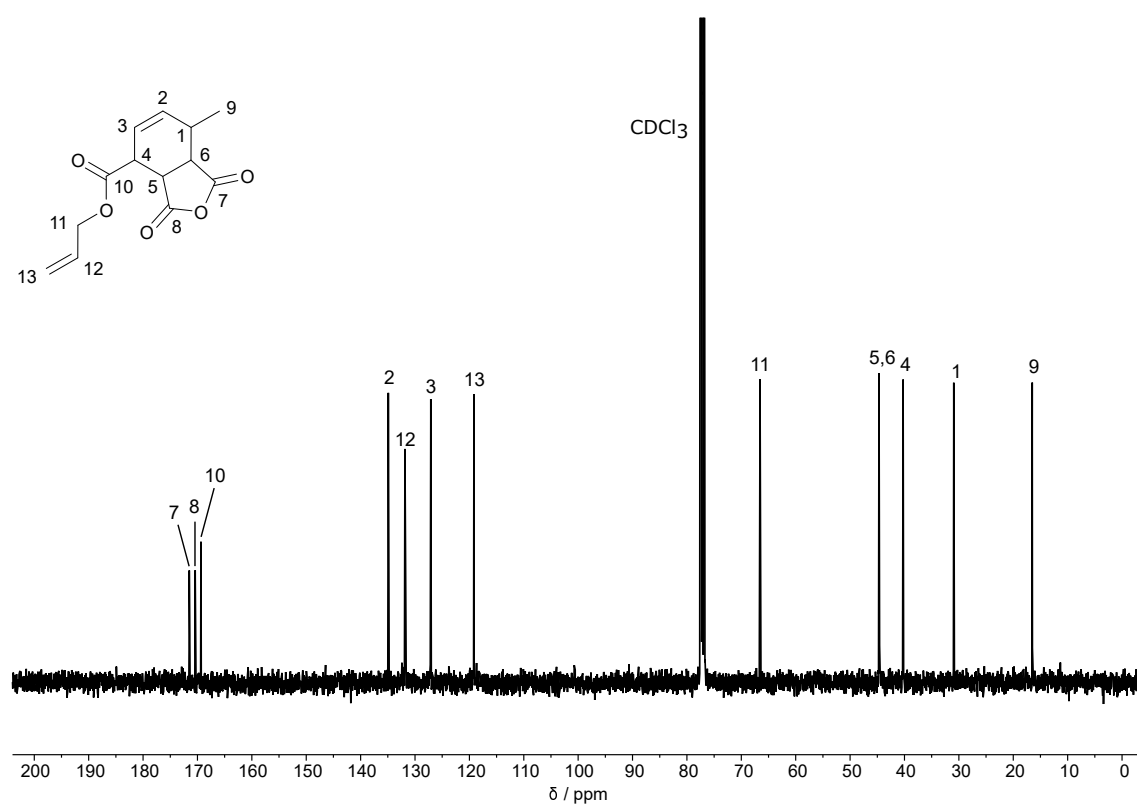

Figure A35: ^{13}C-NMR of AHIBC in chloroform-d as solvent. Reprinted from Breitsameter *et al.*[251]
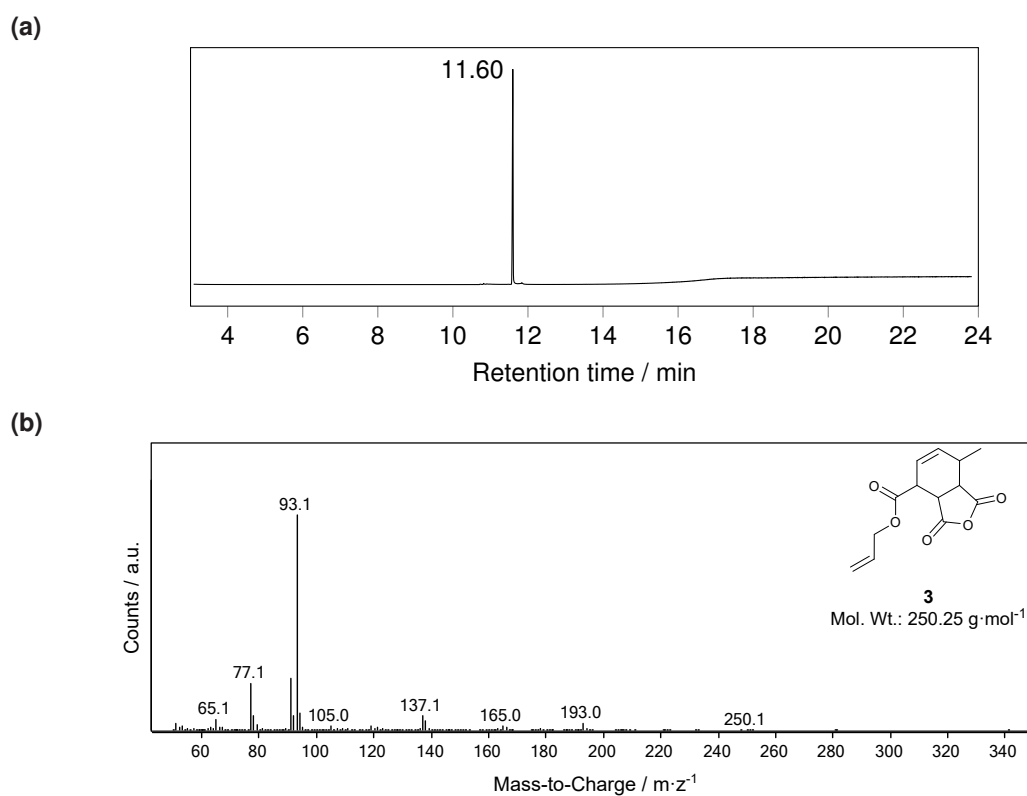
(a)

(b)

Figure A36: a) GC elugram of AHIBC. R.t = 11.60 min, b) Mass spectrum of AIBC. Figures adopted from Breitsameter *et al.*[251]

Figure A37: ^{13}C-NMR of TACHC in chloroform-d as solvent. Reprinted from Breitsameter *et al.*[251]

(a)

(b)

Figure A38: a) GC elugram of TACHC. R.t = 13.22 min, b) Mass spectrum of TACHC. Figures adopted from Breitsameter *et al.*[251]

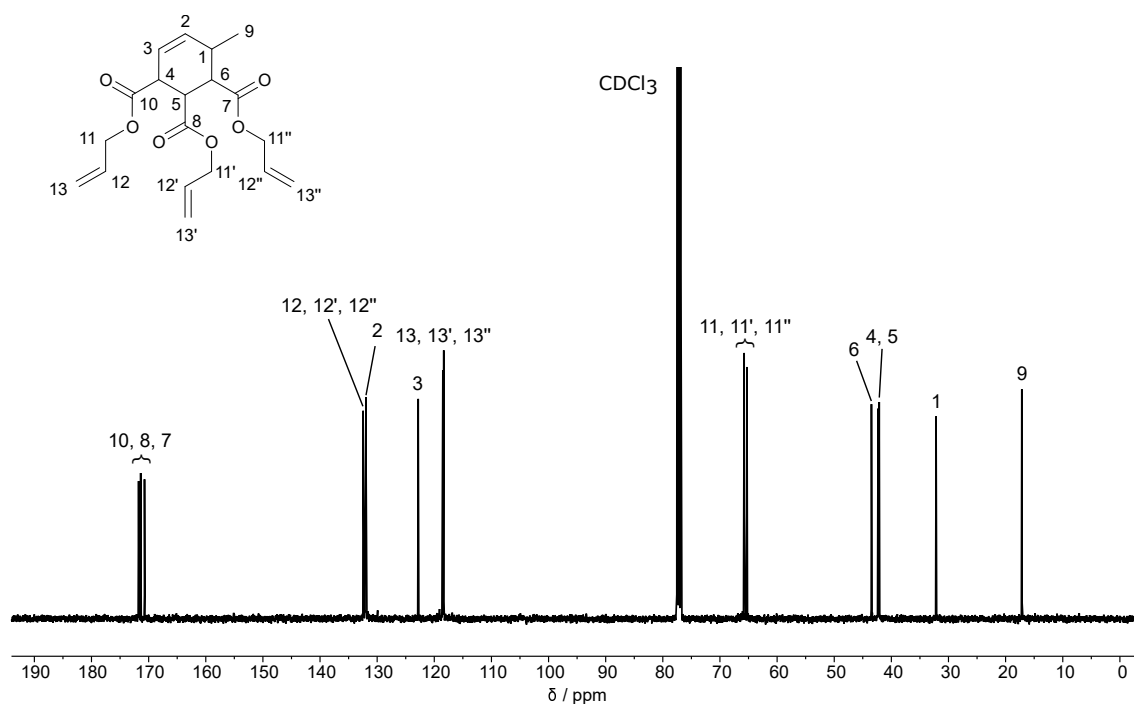**Figure A39:** ^{13}C-NMR of EGCHC in chloroform-d as solvent. Reprinted from Breitsameter *et al.*[251]
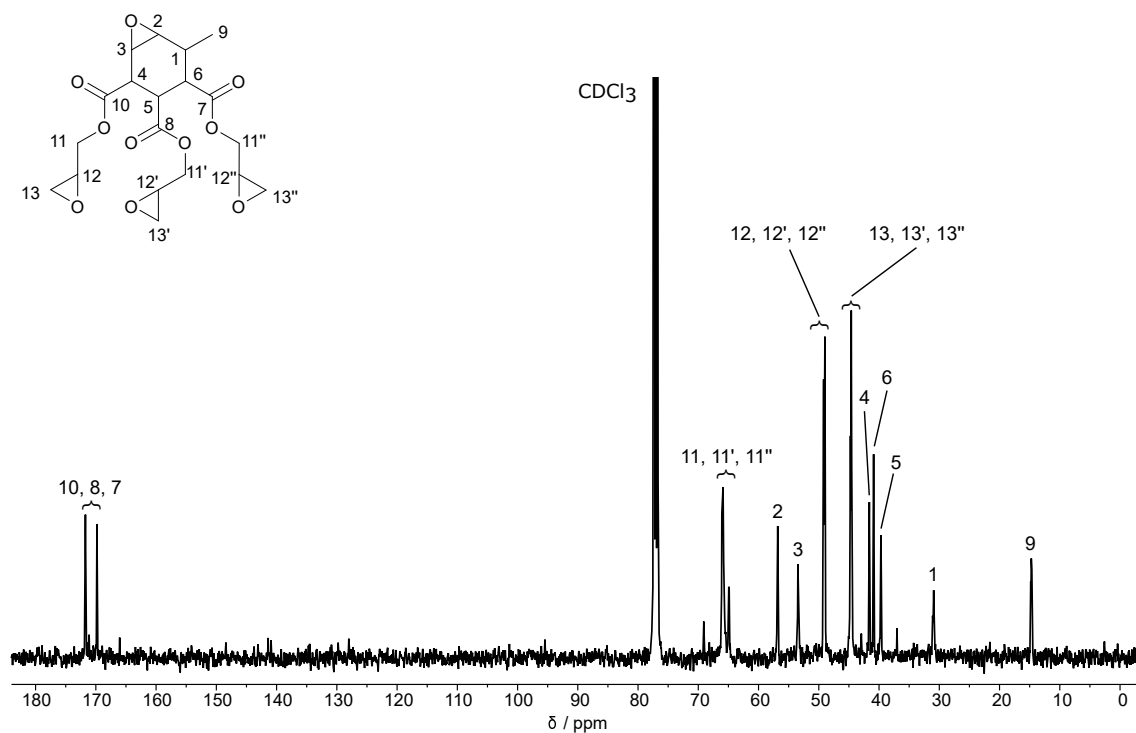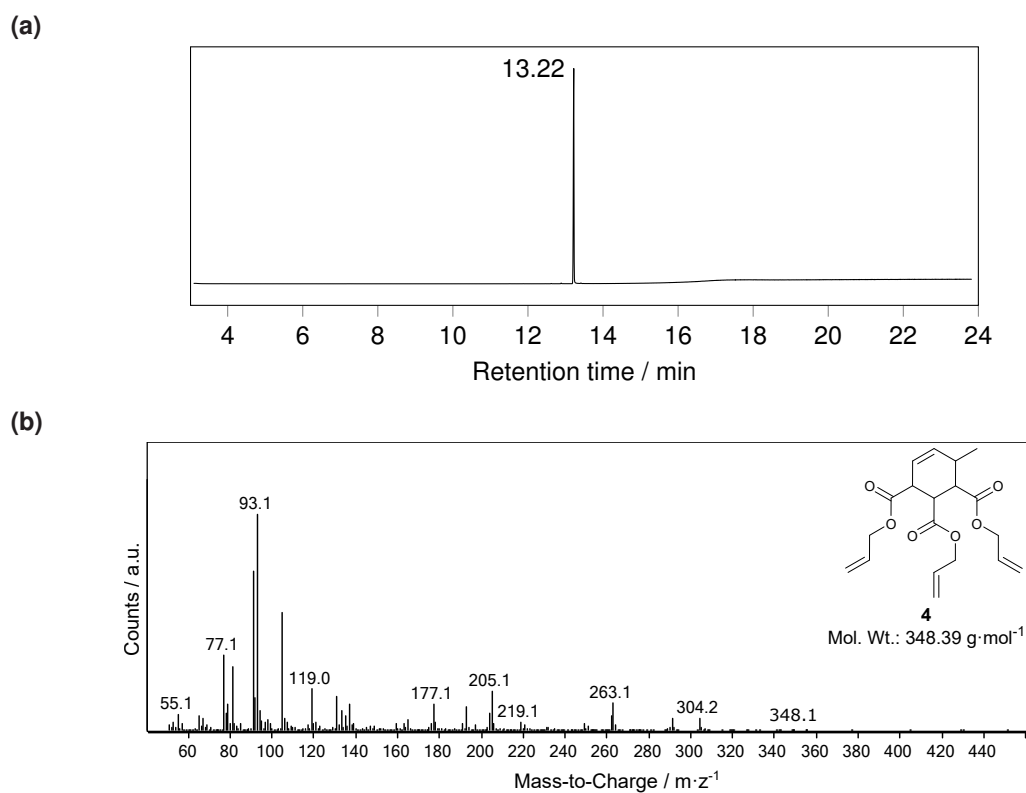
Figure A40: Reactor setup for polycondensation reactions. Three necked flask with vacuum-tight overhead stirrer and a vacuum receiver connector.

Figure A41: Glass reactor used for synthesizing epoxidized vegetable oils with formic acid and hydrogen peroxide.